# Revista Română de Inginerie Civilă

**Indexată în bazele de date internationale (BDI)**

**ProQuest, INSPEC, EBSCO**

**INDEX COPERNICUS, ULRICH'S şi JOURNALSEEK**

**Volumul 12 (2021), Numărul 1**

**MATRIX ROM**
**OP CHIAJNA CP 2**
**077040 – ILFOV**
**Tel. 021 4113617 Fax. 021 4114280**
**e-mail: office@matrixrom.ro**
**www.matrixrom.ro**



**Romanian Journal of Civil Engineering is founded, published and funded by publishing house MATRIX ROM**
**Executive Director: mat. Iancu ILIE**

Online edition ISSN 2559-7485
Print edition ISSN 2068-3987; ISSN-L 2068-3987

# Experimental analysis of the noise produced by burners inside a boiler plant in an educational building

Catalin Bailescu, Vlad Iordache

Technical University of Civil Engineering of Bucharest, Romania
124 Bdul Lacul Tei, Bucharest, 020396
*E-mail: catalin.bailescu@gmail.com*
*E-mail: viordach@yahoo.com*

DOI: 10.37789/rjce.2021.12.1.1

**Abstract.** *One of the most important parameters of comfort in a building is acoustic comfort for which designer engineer typically given little or no attention during project planning and design. The purpose of this article is to highlight the noise produced by boilers in a technical room of a faculty in Romania. Different measurements were performed for the gas flow and noise level in the boiler room. The measurements resulted in several values of the noise level for different thermal loads of the boilers. The result obtained confirm that noise level depends on the thermal load and that increase of thermal load is directly proportional to the noise level inside the plant room. After the measurements, the values of the noise level were processed and compared with literature predicted values and the maximum limit values from the Romanian norm. The results of this article highlighted the noise produced in a technical space of a modern power plant, correctly installed and calibrated. This study can by used by design engineers and all participants in designing and installing equipment in a new educational building, but also in an existing building to meet the comfort conditions of the students.*
***Key words:*** *acoustic comfort, noise level, faculty, measurements, boiler plant*

## 1. Introduction

Beside the already recognized indoor comfort categories (thermal, illumination, pollution), the acoustic comfort becomes an increasingly important aspect nowadays both nationally and internationally.
As a result, national standards have been adopted in several countries by setting maximum noise levels for different environments. These standards vary from one country to another and in the United States have been imposed in the form of recommendations [3], guidelines [4] or statutory requirements [5]. In the European Community the limits of noise level are imposed by mandates regulations of noise exposure [6] and noise evaluation standard [7].
In Romania, the acoustics norm in constructions and urban areas [8] prescribes admissible limits established considering the appropriate climate specific to the use and the indoor destination of the space.
Because road traffic noise is considered the main source of loss of environmental and life in a metropolis [10] much of previous studies on acoustic comfort has been

focused on road, rail, and air traffic [11-13]. However achieving acoustical comfort in buildings, it is not just about reducing this type of noise, because in several previous studies [14-15] has been reported that in residential building an important source of acoustic discomfort is noise from boiler plant. The noise prediction from technical room is an important consideration in the design stage, operation, and construction of all buildings.
In [9] two methods of predicting the noise level in the technical spaces are proposed. The first model [1] established by Cyssau in 1997 shows a formula established following a study of a 145 database of thermal power plants under 16MW designed to present the relationship between the noise level of thermal power plants and their thermal power:

$$L_p = 10 \cdot \log_{10}(P) + 55 \quad (1)$$

where:
Lp, dB, is sound pressure level and
P, kW, is real thermal power for 60 seconds.

This prediction model is characterized by a 10 [dBA] error. Another method [2] predicts the noise level inside thermal plants as a function of both the thermal power and the volume of the thermal plant:

$$L_p = 16 \log Q - 10 \log V + 54 \ [\text{dBA}] \quad (2)$$

which is characterized by a 5 [dBA] error, and where:
Lp, dB, is sound pressure level
Q, kW, is the real thermal power for 60 seconds,
V, $m^3$, is the room volume.

These noise prediction models are characterized by large errors and rises questions regarding their suited for today's thermal equipment. In this analysis we will analyse if these models are adapted to today's boiler plant equipment or it is necessary to create a new prediction model of noise level for design stage.
The study follows an experimental approach. Simultaneous measurements of thermal power and the noise level were recorded in order to understand the relationship between the noise level and the thermal power generated inside the thermal plant. The noise level ware recorded for different operation status of the boilers (different thermal loads) and was compared to the value required by Romanian norm [8] and the prediction methods [1],[2].
The paper presents the experimental results of noise level inside one a technical room, the recordings database, results, and discussions.

## 2. Experiments

The measurements were carried out by a team of three people: one person registers the gas index, another one operates the boiler automation, and the third person carries out the noise measurements.
The analysed thermal plant is a stand-alone building located on demi basement of a Faculty of Geodesy of Technical University of Construction (Fig.1a) in Bucharest town, Romania. It has a 4.8MW thermal power capacity and serves a group of five faculties and annexes.
The thermal plant room is rectangular shaped (dimensions: 12.46m long, 10.96m wide and 4.84m height, volume 660.96 $m^3$.) (Fig.1c). The walls of the boiler plant are made of brick, hardwood, and the tiled floor. Hard surfaced of this boiler room will have a longer reverberation time than rooms finished with sound absorbing materials. The immediate effect of multiple reflections is an increase in the sound intensity caused by the reflections. A fireman will hear the direct sound arriving at the ear along with all of the multiple sound wave reflections.
The thermal plant has three 1480KW Prextherm RSW and one 399KW Prextherm RSW. The burners of these boilers are of the RBL type RS190 with two power stages of 470-2290KW, respectively RBL type R38 with two power stages of 105-440KW
In the boiler assembly we find 12 Grundfoss pumps MG90LA4, two heat exchangers with plates, 2 buffer tank.

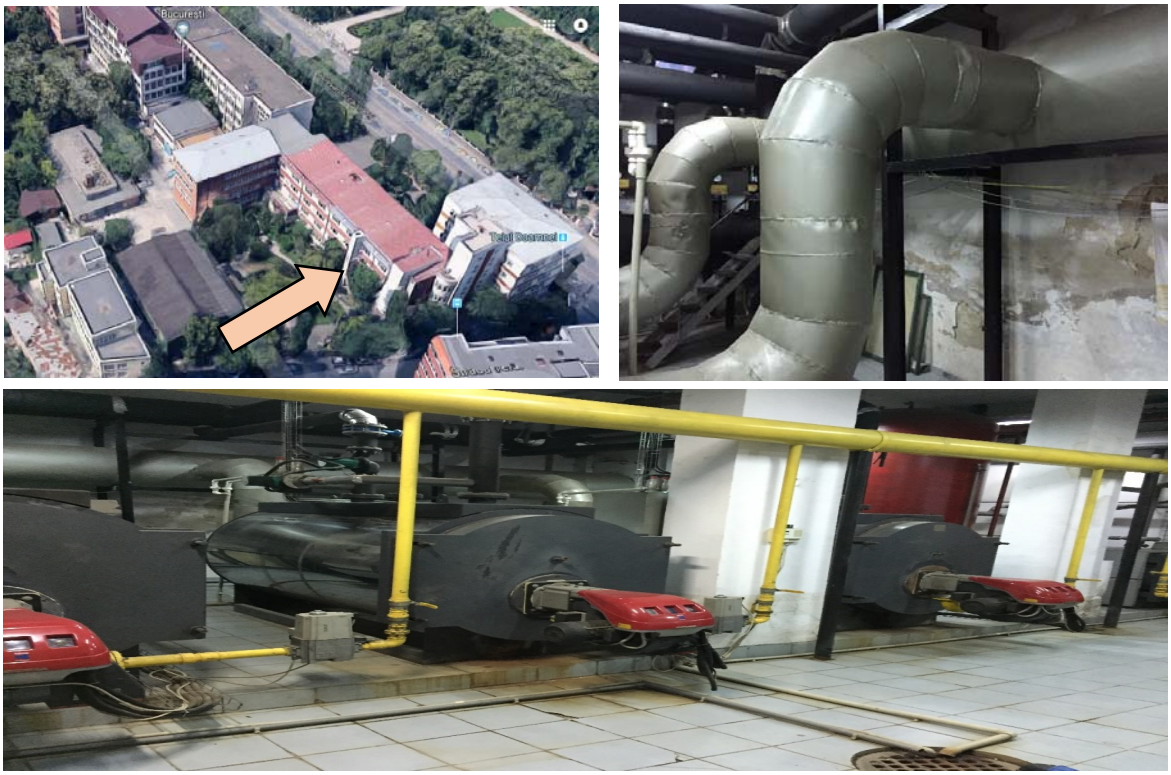

Fig.1 - Thermal plant. a) Boiler plant location b) Photo inside the thermal plant,
c) Noise protection solution for the chimney

The boiler chimney (Fig.1b) is made of metallic material, insulated with mineral wool and covered with gypsum. The boilers are placed on puffers and their own foundation. The three burners do not have sound absorption housing, and the pipe connections are made by metal bracelets. The heating installation does not have flexible connections to ducts of the boiler (thermal / gas / fluid). There is no other noise protection like sound attenuator at chimney (in pipe or in quarter-wave) or walls captured with mineral wool or/and plasterboard.

Five types of measurements were made for each thermal power plant:

• dimensions (room, equipment, windows, doors, chimney).

• gas pressure and temperature. pg=0.03 [bar]; Tg [oC];

• reverberation time inside the thermal plant (EDT, T20, T30);

• sound pressure level ,Lp [dB], and global weighted sound pressure level, LAeq [dBA] for all audible spectrum octaves 16Hz, 31.5Hz, 63Hz, 125Hz, 250Hz, 500Hz, 1000Hz, 2000Hz, 4000Hz, 8000Hz

• gas consumption for each thermal power: two indexes and time period

The burner stage control was set using the boiler control panel by selecting the desired step, as shown below. A number of 12 operating condition of the boiler are presented in Table 1. The first case is the situation where no equipment is working. These boilers have a circulating pump, which circulate water within the boiler to enhance boiler operation. To analyze the noise produced by these equipment, the burners of boilers were switched off. Cases 2-12 are situations in which burner operate simultaneously, at different power stages.

*Table 1*

**Operating condition of the boiler**

| Case [-] | Boilers pump [-] | Burner1 [-] | Burner2 [-] | Burner3 [-] | Burner4 [-] |
|---|---|---|---|---|---|
| 1 | OFF | OFF | OFF | OFF | OFF |
| 2 | OFF | STAGE 1 | OFF | OFF | OFF |
| 3 | ON | STAGE 2 | OFF | OFF | OFF |
| 4 | ON | OFF | OFF | STAGE 1 | OFF |
| 5 | ON | OFF | OFF | STAGE 2 | OFF |
| 6 | ON | STAGE 1 | OFF | STAGE 2 | OFF |
| 7 | ON | STAGE 2 | OFF | STAGE 2 | OFF |
| 8 | ON | STAGE 1 | OFF | STAGE 1 | OFF |
| 9 | ON | STAGE 1 | STAGE 2 | OFF | OFF |
| 10 | ON | STAGE 1 | STAGE 2 | STAGE 1 | OFF |
| 11 | ON | STAGE 2 | STAGE 2 | STAGE 2 | OFF |
| 12 | ON | STAGE 2 | STAGE 2 | STAGE 2 | STAGE 2 |

For the fuel consumption measurement, the initial and final index of gas meter was recorded for a period of 1 min. During this time the noise measurements were made inside the technical space. Before the actual measurements began, the gas temperature and pressure were recorded (Fig.2).

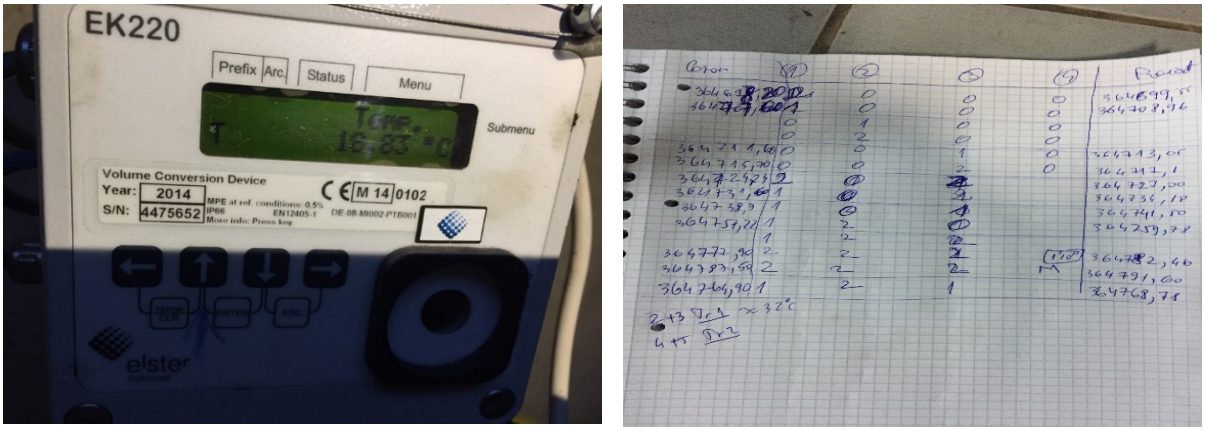


Fig.2 - Reading of gas index b) gas parameter

The measurement of the noise level was carried with a 2250 sound meter from Bruel&Kjaer. The point from which the measurements were made is represented in Fig.3 with blue. This point was situated at the heights that the [9] standard established. The noise measurement was recorded at 1-meter distance from the burner, measured according to the norms. With red dot are the two main noise sources of the technical space (the two boilers burners that were on).

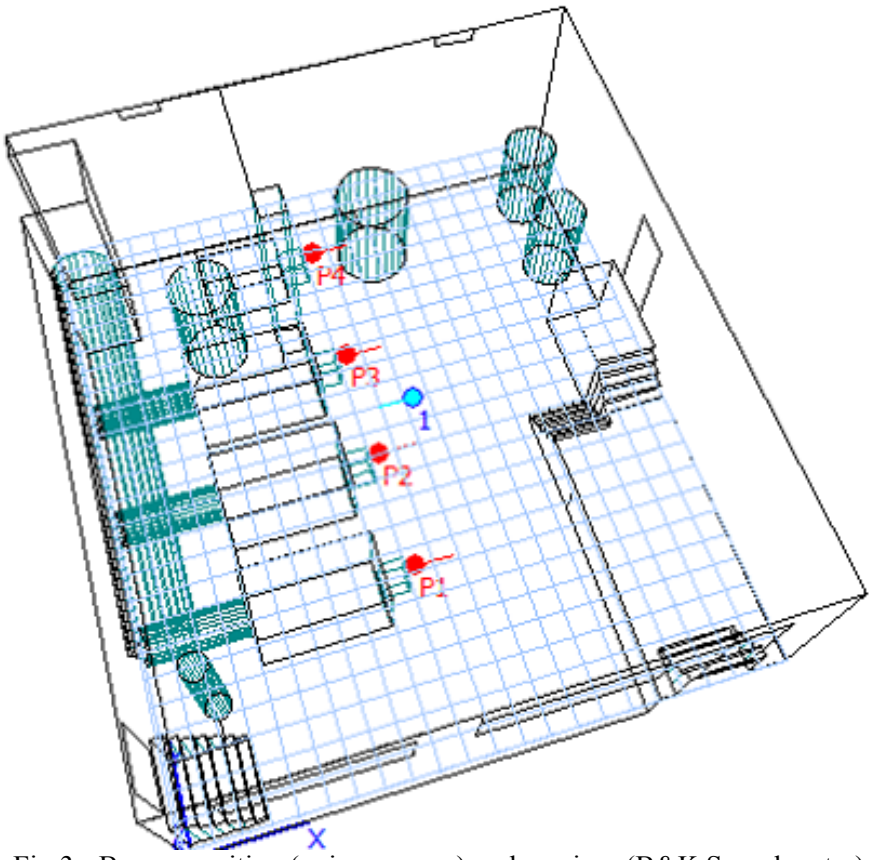


Fig.3 - Burner position (noise sources) and receiver (B&K Sound meter)

The reverberation time was also measured using the same sound meter and a noise source, we record the decay curves for all frequency bands and the reverberation time is calculated by means of the sound meter software for all frequencies.

## 3 The database and results

The gas measurements and the real thermal power are presented in Table 2, calculated based on the gas consumption, which is the difference between the final index and the initial reading from the gas meter by one of the participants in the experiment.

*Table 2*

**Gas consumption and parameters**

| Case [-] | Initial Index [$m^3$] | Final Index [$m^3$] | Consumption [$m^3$] | $\Phi_{burner}$ [kW] |
|---|---|---|---|---|
| 1 | 364698.20 | 364698.20 | 0.00 | 0.00 |
| 2 | 367707.60 | 364708.96 | 1.36 | 794.00 |
| 3 | 364698.20 | 364699.55 | 1.35 | 787.00 |
| 4 | 364711.60 | 364713.05 | 1.45 | 847.00 |
| 5 | 364715.70 | 364717.10 | 1.40 | 818.00 |
| 6 | 364731.60 | 364734.18 | 2.58 | 1507.00 |
| 7 | 364724.24 | 364727.00 | 2.76 | 1612.00 |
| 8 | 364738.70 | 364741.00 | 2.80 | 1636.00 |
| 9 | 364757.22 | 364759.78 | 2.56 | 1495.00 |
| 10 | 364764.90 | 364768.78 | 3.88 | 2266.00 |
| 11 | 364777.90 | 364777.90 | 4.56 | 2664.00 |
| 12 | 364787.50 | 364787.60 | 4.10 | 2395.00 |

The following formula was used to determine the actual thermal load of the boiler:

$$\Phi_{burner} = \frac{I_F - I_I}{60} \cdot \frac{p_g + p_0}{p_0} \cdot \frac{T_0}{T_g} \cdot H_i \quad (3)$$

where:

$\Phi_{burner}$, kW, is real thermal power for 60 seconds;

$I_F$, $m^3$, and $I_I$, $m^3$, are the final index and initial read recording from the gas meter;

$H_{I\,comb}$, kJ/$m^3$N, is the low fuel calorific value, $H_{Icomb}$=35371.70 [kJ/$m^3$N];

$p_o$, bar, is the atmospheric pressure, $p_o$=1.01325 [bar]

$T_0$, K, is the gas temperature under normal conditions, $T_0$=273.15 [K]

Pg, bar, is the measured gas pressure,

Tg, K, is the measured temperature of methane gas

It can be seen from the Fig.4 that the noise level for the situation where pumps works (yellow) works is below 62dB for each frequency. After starting burners, the noise level increases above 73dB at 1000Hz and is directly proportional to the thermal load. However, the norm is not exceeded for any of the operating scenarios.

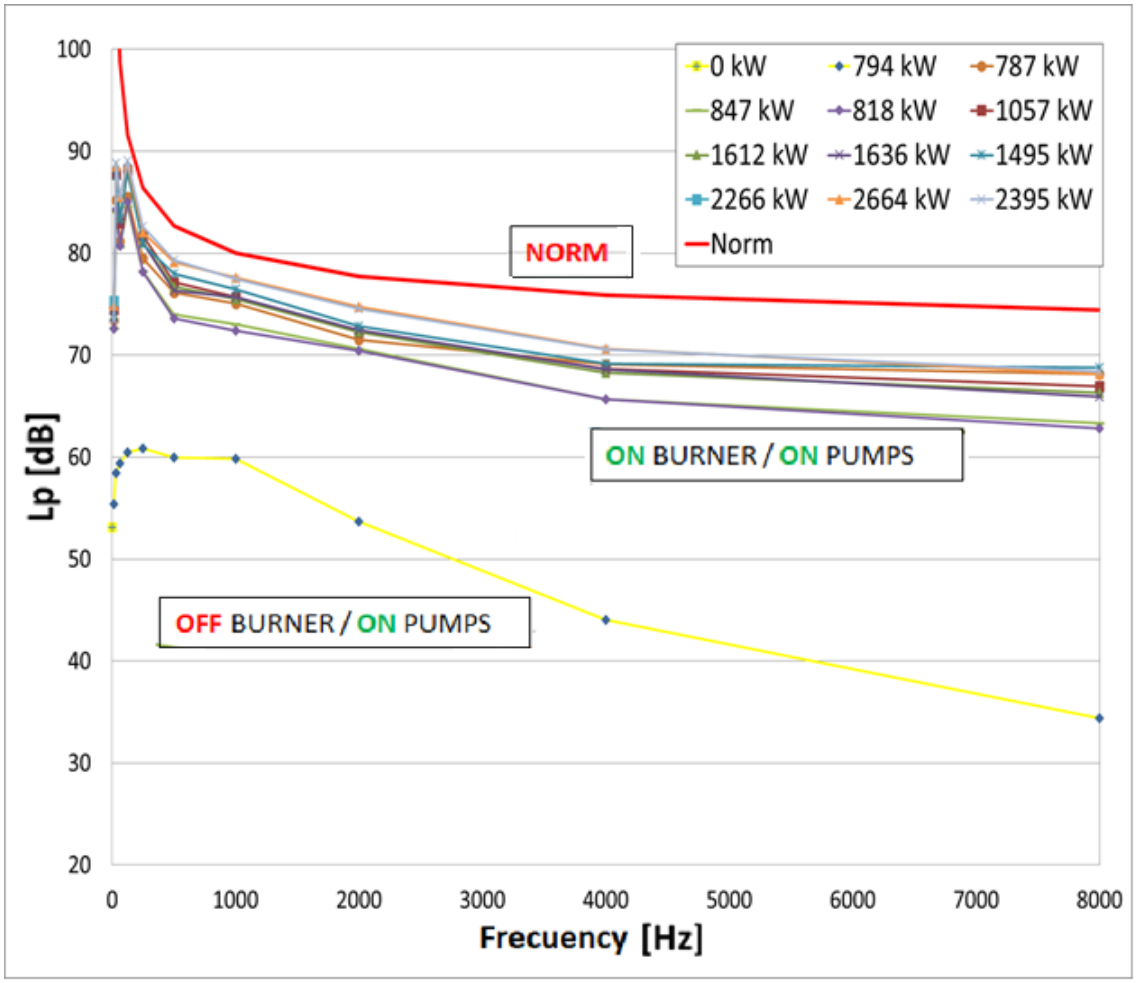


Fig.4 - Comparison between noise level on each frequency and Cz80 from norms

It is noticed that the noise level has different values depending on the frequencies. Another observation is that for higher frequencies the measurements of noise level have higher values compared to the low frequency noise level. From medium to high frequencies the noise level has a downward trend. There is a difference of up to 20dB for the noise level measured at 1000Hz compared to the noise level at 8000Hz.

Another noise level measurement collected was noise level, measured using the filter specified as the A-curve. In the Fig.5 has been compared global noise levels weighted after curve A for all 12 operating situations with the noise value from technical data sheet of boiler and the value imposed by [8].

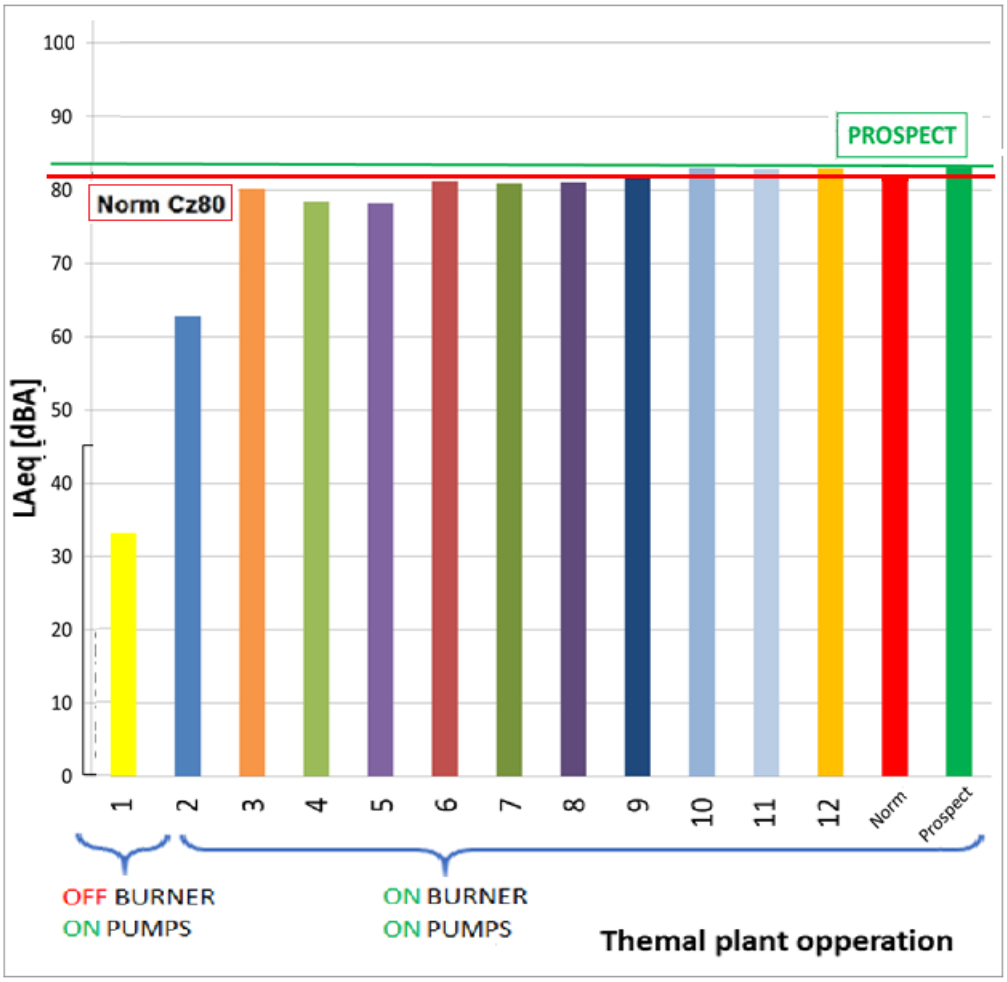


Fig.5 - Comparison between global weight equivalent noise level, boiler data sheet and Cz80 from norms

It is noticed that measurements for all operating conditions of the boilers don't exceed the value indicated from datasheet but is higher than 82 dB(A) from norm [8]. The conclusion is that this thermal plant needs an acoustic refurbishment to full fill today's acoustic norms because the equivalent noise level is higher than the values from the norm.

In the figures below, the dependence between the noise level for each frequency and the thermal load of the burner will be studied. From Fig.6a it is observed that at low frequency the noise level has value between 63 dB and 83 dB. An increasing tendency is observed in both graphs, thus validating the prediction models [1] and [2], which have as main parameter for predicting noise level the thermal load. The same increasing trend is also noticeable in Fig.6b. For average frequencies, the noise level is between 60 dB and 79dB. At all frequencies, the noise level is not well fitted.

The coefficient of determination, R2, is represented in Fig.6 and this value is used to analyse how differences in one variable can be explained by a difference in a second variable. Subsequently, R is calculated and corresponds to correlation coefficients, but for nonlinear variation tendencies.

In acoustics, phenomena vary depending on the frequencies studied, so the rules are broken down at each frequency. And in this study, we looked at the dependence between Lp and Φburner for different frequencies.

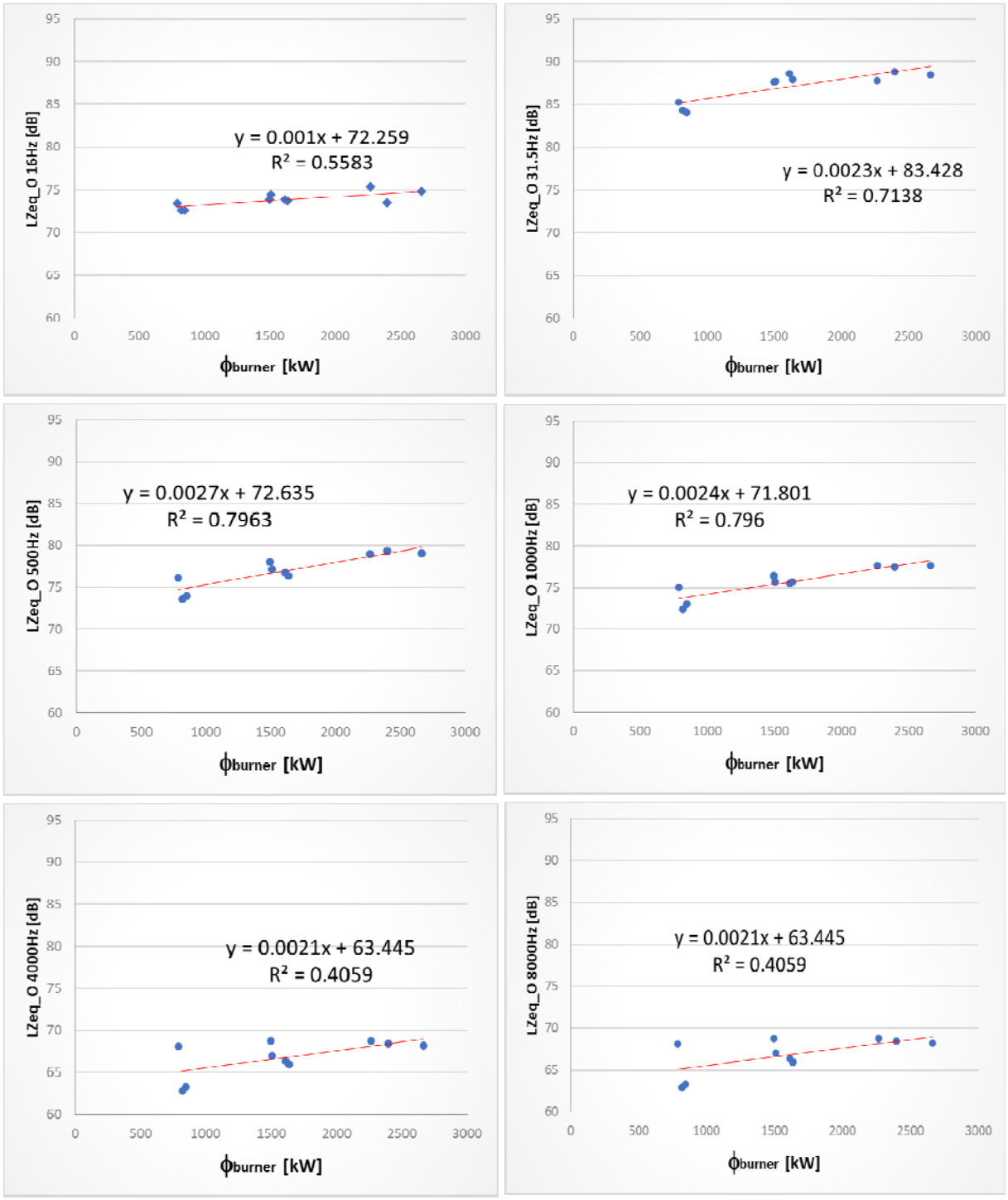


Fig.6 - Recorded sound pressure level based on thermal power for a) low frequencies (16Hz, 31.5Hz); b) medium frequencies (500Hz, 1000Hz) and c) high frequencies (4000Hz, 8000Hz)

Fig.7 depicts the relationship between equivalent noise level (LAeq) and thermal power Φburner. From this graph we can see the increasing tendency of the equivalent noise level depending on the thermal load of the boiler. This increase validates the prediction models from the literature, which have their component and thermal load, as the main parameter.

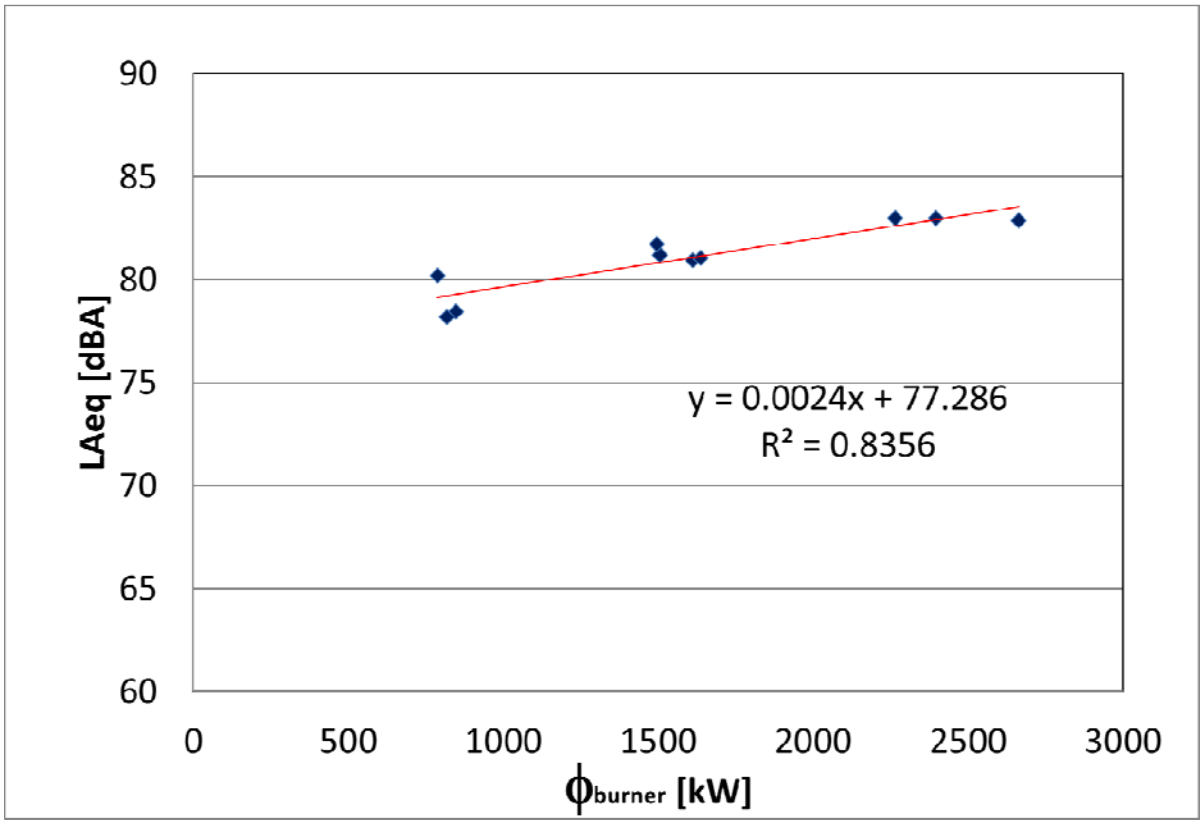


Fig.7 - Equivalent noise level based on actual thermal power, equation and R2

Further, we study the adaptability of predictive models of noise level for the analysed thermal plant. Cyssau's model [1], as well as Hamayon's model [2], predicts the global weighted equivalent noise level. These values were compared with the measurements obtained during the experiment to highlight if the errors of the two models are centred in 0 and if they are adapted for modern thermal power plants and new equipment.

Compared to our measurements, Cyssau's model [1] has an error between 11 dBA (for 2000kW) and 13 dBA (for 700 kW), higher than 10 dBA declared by the author (Fig.8). The errors of the Cyssau's model compared to our experimental data are not centred in zero. We conclude that Cyssau's model is not suited for today's thermal powers and for the new thermal generation equipment.

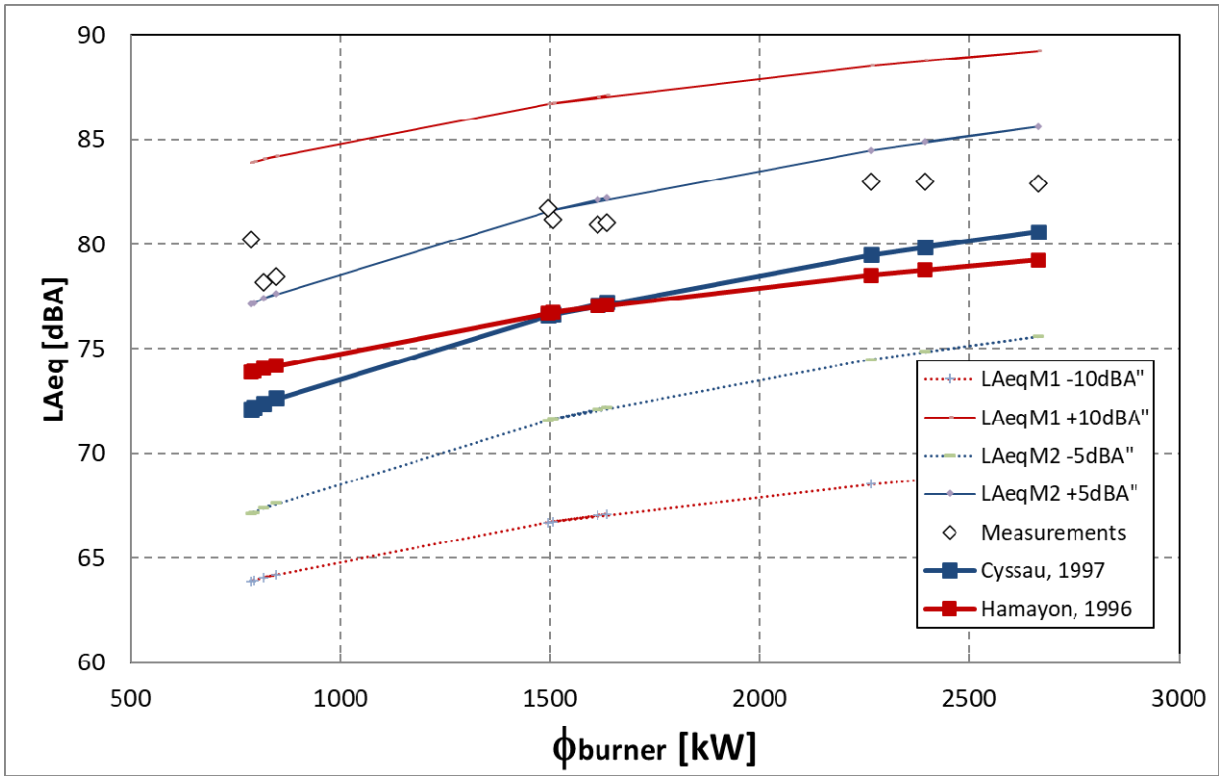


Fig.8 - Comparison between measured and predicted noise level values, Cyssau [1] and Hamayon[2]

Hamayon's model [2] present slightly higher errors: between 15 dBA (for 800kW) and 10 dBA (for 2000kW), higher than 5dBA declared by the author. The graph from Fig.8 shows that Hamayon's model predicts lower noise levels than those measured for 8 different thermal powers, and the lower and upper limit of its error is far from the measurements made during the experiment. Similar to Cyssau's model, Hamayon's model present errors that are not centred in zero. In conclusion Hamayon's model is not suited either, for today's thermal powers and for the new thermal generation equipment.

Therefore there is need for an adaptation of the noise prediction models to today's thermal conditions (larger thermal power stations, noisier equipment and automation control).

## 4. Conclusions

There is a reasonable consensus that the equipment that produces a high noise level in a thermal plant is the burner, and not pumps or other components of the heating system.

From the analyzes made in comparison with the datasheet, there were revealed that they produce a lot of noise but do not exceed the values given by the producer of the burner, which indicate a correct operation of the equipment. Also in this study were highlighted that the measurements of the noise levels exceed the maximum value indicated in the norm [8]. Out of the 11 operating situations of the burners in 4 were

found exceedances of the value of 82dBA. For case 12, the highest noise level was recorded, with 2dBA higher than the value imposed by the norm.
The increasing tendency of the equivalent noise level depending on the thermal load of the boiler is another very useful conclusion for designers to estimating the noise level. So when a building requires a higher installed thermal load, designers need to take into consideration the higher equivalent noise level generated in the thermal plant room in order to ensure the comfort parameters indoors.
The acuracy of the existing prediction models of the noise level inside the thermal plant room, is higher than the error characterizing the models. Therefore there is need for an adaptation of the noise prediction models to today's thermal conditions (larger thermal power stations, noisier equipment, and automation control). New prediction model should be based on new experimental campaign for the new type of thermal plants and the new installed equipment.

## Reference

[1] Cyssau, R., Palenzuela, D. & Francoise E. (1997). **Bruit des equipments. Collection des guides de l'AICVF**. France: Ed PYC Edition livres

[2] Hamayon, L. (2001). **Reussir l'acoustique d'un batiment**. France: Ed. Le Montieur

[3] United States Building Council (2009). LEED™, Guide of reference, Version: 3.0. USA: Ed. USBC.

[4] American National Standard Acoustical Performance Criteria (2002). Performance Criteria, Design. Requirements, and Guidelines for Schools. ASA S12.60 PART 1. USA

[5] Ocupational Safety and Health Standards (2003). Occupational noise exposure. 29 CFR 1910.25. USA

[6] European Parliament and of the Council (2003). Directive 2003/10/CE on the minimum health and safety requirements regarding the exposure of workers to the risks arising from physical agents. Eurpean Union: Ed. European Parliament and of the Council

[7] International Organization for Standardization (2009). Acoustics- Determination of occupational noise exposure- Engineering method. EN ISO 9612:2009, Switzerland

[8] Monitorul oficial al Romaniei (2012). Normativ privind acustica în construcţii şi zone urbane C125-2013. Romania: Guvernul Romaniei. Ministrul dezvoltării regionale şi turismului. (romanian)

[9] International Organization for Standardization. (2017). Acoustics - Description, measurement and assessment of environmental noise - Part 2: Determination of sound pressure levels. ISO 1996-2:2017. USA

[10] Vianna, K., Cardoso, M. & Rodrigues, R. (2015). Noise pollution and annoyance: An urban soundscapes study, Noise Health. 17(76): 125–133. doi: 10.4103/1463-1741.155833
[11] Tandel, B.N, & Jem, M. (2013). Assessment and Mlr Modelling Of Urban Traffic Noises at Major Arterial Roads of Surat. Journal of Environmental Research and Development. 2013; 7(4A):1703-1709.

[12] Méline, J., Van Hulst, A., Thomas, F., Karusisi, N & Chaix, B. (2013). Transportation noise and annoyance related to road traffic in the French RECORD study. Int J Health Geogr. 2013;12:44.

[13] Brambilla, G., Gallo. V, & Zambon. G. (2013). The Soundscape quality in some urban parks in Milan, Italy. Int J Environ Res Public Health. 2013;10:2348–6

[14] Iordache, V. & Catalina, T. (2013). Experimental investigation on the sound pressure level for a high thermal capacity burner during a running cycle. JOURNAL Applied Acoustics, Volume: 74 Issue: 5 Pages: 708-717

[15] Tacutu, L., Pocola, A., Balan, M. & Iordache, V. (2017). Acoustic measurements for two configurations of acoustic casings with applications on ambient noise pollution, Conference: 8th International Conference on ENERGY and ENVIRONMENT (CIEM). 19-20 October 2017 (pp. 129-133). Bucharest, Romania: International Conference on Energy and Environment.

# Evaluation of the potential of natural ventilation in different Algerian climates.

Meriem Mezouari [1], Naima Fezzioui [1], Mohamed El-mir [2], Roulet Claude-Alain [3]

[1] Laboratory of Mechanical Structures « LMS »
University of TAHRI Mohammed Bechar, Algeria
*Meriem.m82@live.fr*

[2] Energy Laboratory in Arid Zones ENERGARID
University of TAHRI Mohammed Bechar, Algeria
*mir0562@yahoo.fr*

[3]École Polytechnique Fédérale de Lausanne EPFL
*Claude.roulet@epfl.ch*

DOI: 10.37789/rjce.2021.12.1.2

**Abstract.***The purpose of our research is to test the effectiveness of some basic configurations of natural ventilation on the thermal comfort of occupants for different climates. The study focuses on the Algerian climate. Seven cities were selected from the new climate zoning of Algeria proposed by [1]. To evaluate the potential of the selected configurations and given the diversified nature of the Algerian climate, the study will focus on the mid-season period that includes the months of May September and October and the summer season for the months of June, July and August. The study was carried out through numerical simulations using the TRNSYS software coupled with the COMIS aeraulic software.*
*The results of the simulations showed the contribution of natural chimney ventilation caused by the stairwell to improve occupant comfort Its integration, however, requires a judicious and permanent control to guard against the falls of temperatures or the risks of overheating.*

**Keywords:** Algerian climate; natural ventilation, thermal comfort; TRNSYS- COMIS.

## 1. Introduction

The building sector is the largest consumer of energy, criteria used for heating, ventilation and air-conditioning (HVAC) systems have been found to account for almost 60% of the global energy consumption of the building sector [2].

The energy demand for buildings is growing steadily and may exceed 64% of energy consumption by 2100 [3]. The energy used for cooling takes an increasing part in the energy balance especially in the Mediterranean climate, due to the increasing use of mechanical conditioning devices [4]. Due in particular of climate change and global warming [5]. More, it is necessary to emphasize that concrete is the most used material in the construction of buildings.in the world. Thermal energy absorbed on hot days does not have enough time to dissipate at night. Also air conditioning is necessary to keep the occupants comfortable and therefore contributes to the increase in energy costs [6].

To remedy this situation, several authors have looked into passive cooling techniques which make it possible to reduce the level of consumption observed and to achieve an acceptable level of thermal comfort. Among these techniques, natural ventilation has been widely studied numerically by The Computational Fluid Dynamic (CFD): [7] examined natural ventilation for underground constructions in Spain. [8] Looked at the methodology and case study of optimizing the building's natural ventilation thanks to the simulation of the CFD wind environment in three aspects, namely site planning, building shape and building envelope, in order to propose ideas to remedy the inadequacy and the weak synergy between architectural design and technological analysis. [9] Used the unstable RNG k-ε model to determine the air flow around and inside the building. [10] Studied

The potential of natural ventilation in a traditional Iranian CFD strategy. [11] Assessed the air flow in a traditional building fitted with a bilateral Wind catcher using the standard turbulence model (k-ε). Ventilation has also proven its role in preserving the durability of building structures, indeed, the rate of condensation which can take place in winter in certain buildings contributes to the creation of building pathologies and to the degradation of its structure [12,13]. Other research has also shown that it is beneficial to use natural ventilation in an enclosed space for a humid climate for three reasons: promoting thermal comfort, air purification inside the building and lower energy consumption [10]. In addition natural ventilation intervenes in the reduction of carbon emissions [14] and energy costs, which increase by 40% for air-conditioned buildings compared to naturally ventilated buildings [15]. Algeria is no exception. The nature of its climate requires the use of air conditioning even in mid-season for the hot and dry climate and summer period for the semi-arid continental climate and high plateaus where the inhabitants are forced to use air conditioners, as indicated on the balance sheet of SONELGAZ [national electricity and gas company].

To remedy this situation in Algeria, several studies have been carried out on natural ventilation, among them that relating to the circulation of air which proved that this last strongly depends on the opening and their dimensions (windows, doors, orifices) and their location in the rooms [16-17]. More [18] have studied by digital analysis the

impact of natural night ventilation in summer in a hot and dry climate in the east of Algeria by coupling between TRNSYS and CONTAM. Their results show the effectiveness of window dimensions in improving this ventilation.

Finally, the aim of our research work is to examine the contribution of natural ventilation on thermal comfort for basic configurations in different climates of Algeria.

## 2. Climate

The climate has a major impact on thermal comfort and on the energy consumption of buildings. Energy codes and standards are based on a clear definition of climate zones to meet the needs of manufacturers. Algeria which covers an area of 2,381,741 km2, has known three climatic zoning classifications: in 1962, 1984 and in 2015. The latter was developed in the work of [1] and is based on the analysis of climate data recorded by 60 weather stations over the period 1999 to 2008, by defining the Climate Zoning maps according to the thermal energy costs necessary for heating and cooling.

Starting from the fact that heating costs less in Algeria than air conditioning which is done by the use of electricity, the authors have come up with two maps as shown below: a map of the climatic zones of Algeria: for heating (A) and for cooling (B). Another map of climatic zones has been drawn up based on energy consumption costs. The latter will be used for the selection of the cities studied.

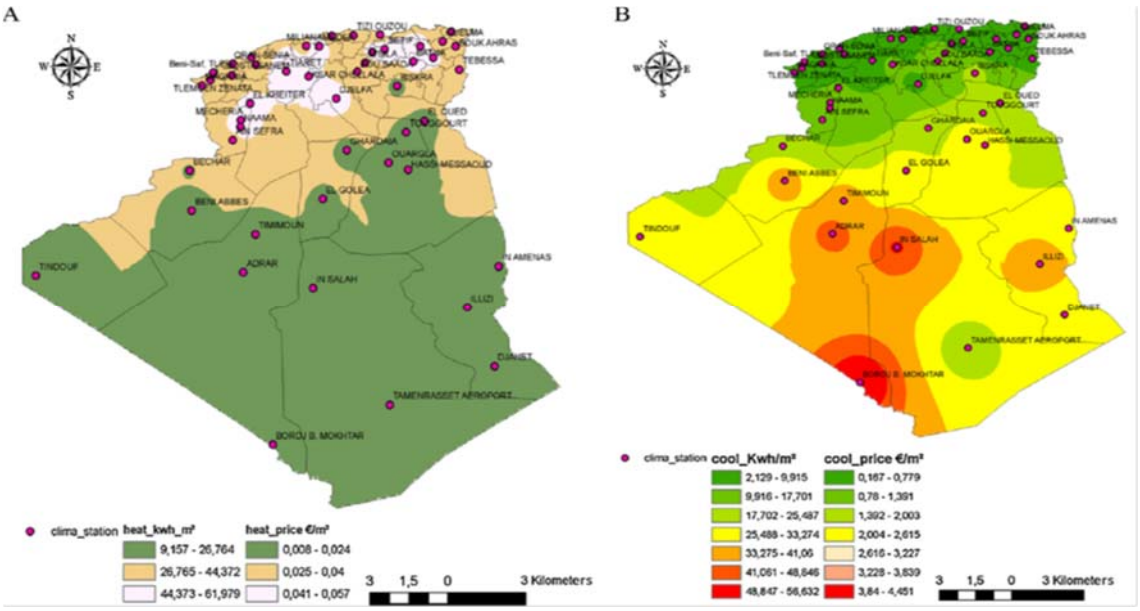


Fig. 1. Map of the climatic zones of Algeria: (A) for heating; (B) for cooling [1].

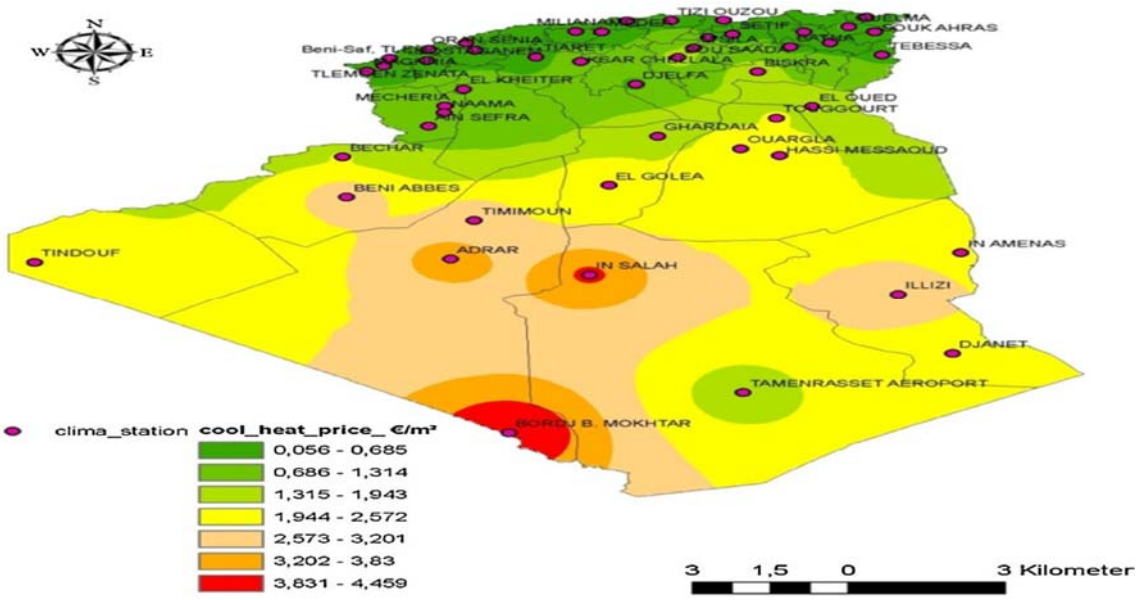


Fig. 2. Climate zones in Algeria according to energy consumption costs [1].

Several previous works have shown that the aridity of the Saharan climate requires the use of air conditioning in summer [19,20], and that achieving optimal comfort during this period really requires the combination of several passive cooling strategies. According to The psychrometric diagram for the city of Hassi Messaoud (Figure 3), the hottest and driest months are 2/3 of May as well as June to September, for this the solar control, the thermal mass effect (thermal inertia), and especially an evaporative cooling and night ventilation are the strategies recommended for this period in order to reintegrate summer comfort [21].

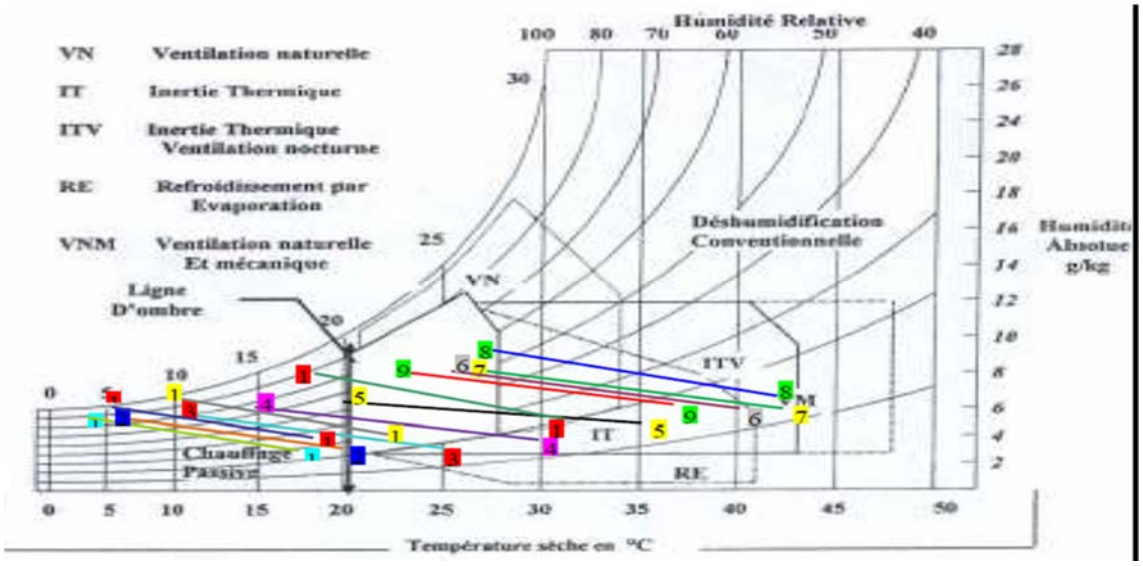


Fig. 3. GIVONI psychometric diagram with application to the city of Hassi Messaoud [21].

According to the psychrometric diagram of the city of Bechar (Figure 4). The thermal mass and natural ventilation can ensure an acceptable level of comfort during a good part of the months of May and September.

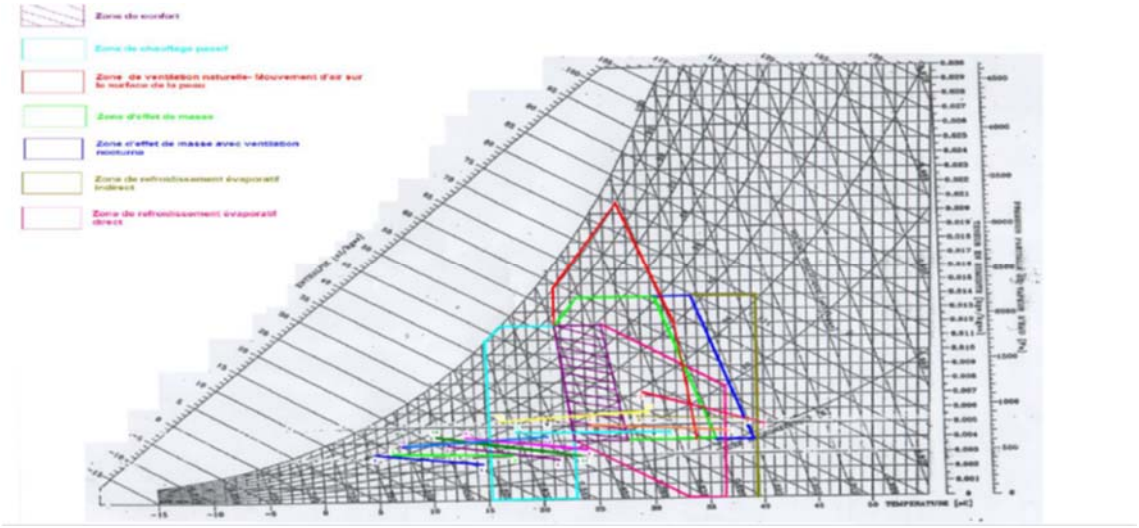

Fig. 4. The GIVONI psychometric diagram with application to the city of Bechar.

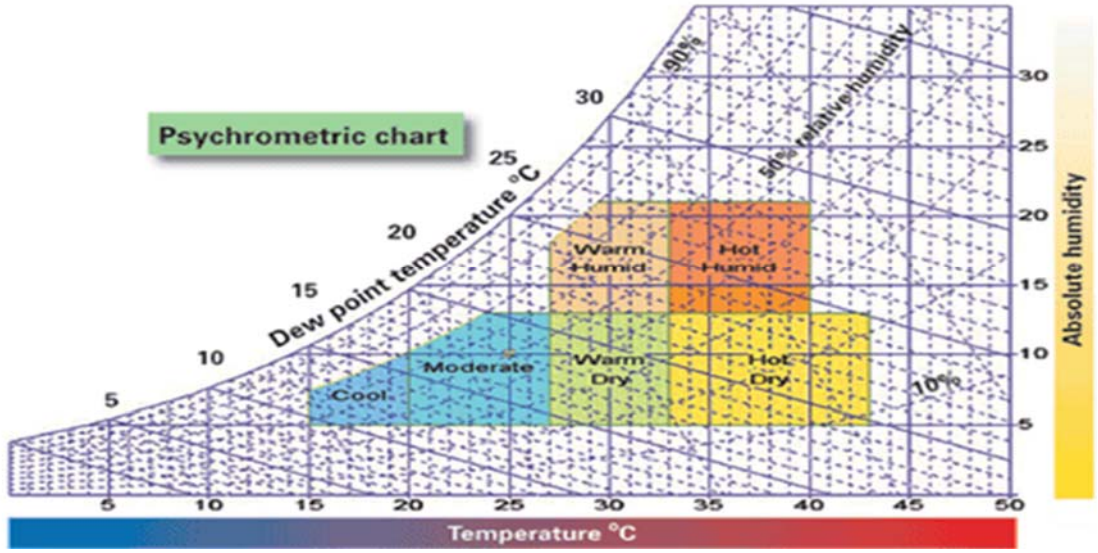


Fig.5. Szokoly diagram for hot and dry climate and Mediterranean climate

According to Szokoly's diagram, natural ventilation is not suitable for summers in hot and dry climates (Figure 5). However, for a Mediterranean climate, night ventilation contributes well to improving comfort in summer. For this reason and for the selected cities representative of each climate zone, we wanted to test the ventilation

potential in summer for coastal cities in the north of the country, and the highlands. For the cities of the south of the country we limited our study to the midseason period.

Finally and to properly conduct our study, we selected seven cities according to the new climate zoning [1].

## 3. Description of the configurations studied

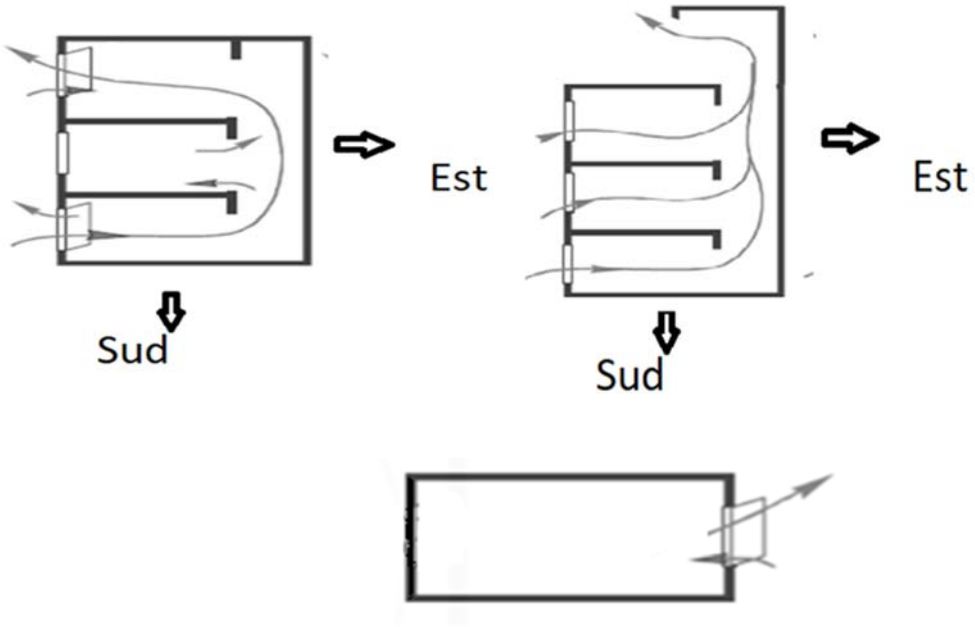


Fig.6. The three configurations to study: top right case A, top left case E, below case B

## 4. Description of the configurations studied

Our research concerns the analysis of three basic configurations of natural ventilation illustrated schematically in Figure 3.

### 4.1 Description of the reference case (mono zone)

The basic cell has an area of 20m$^2$, a height of 2.8m. It has a single dimension window (1.4X1.2) m$^2$ facing west.

### 4.2 Configurations of the analyzed cases

**Case "A":** the block consists of a ground floor (Z3) and two floors, Z2 (1st floor) and Z1 (last floor). The zones are connected to a stairwell, zone 1 and zone 3 have a single window of the same size as the base cell ($1.4x1.2$) m$^2$, facing west.

**Case "B":** the cell consists of a single zone with two windows of dimensions $(1.4X1.2)$ m$^2$ located on two opposite facades.

**Case "E":** the block consists of a ground floor ($Z3$) and two floors, $Z2$ (1st floor) and $Z1$ (last floor) each with a dimension window $(1.4X1.2)$ m$^2$ and connected by a door of $(1X2)$ m$^2$ at the stairwell of dimensions $(2.10X9.2)$ m$^2$ equipped with a terrace opening of dimension $(1.5X1)$ m$^2$ and oriented towards the west.

*Table 1*

**Composition of the cell envelope**

| Matériaux de construction | | | U[W/(m°2K)] |
|---|---|---|---|
| WALL | Constitution (from the inside to the outside) | Thickness | |
| wall OUTSIDE / INTERIOR WALL | Interior plaster | 3 cm | 0.637 |
| | Red brick | 10cm | |
| | Expanded polystyrene | 3cm | |
| | Red brick | 15cm | |
| | Exterior plaster | 3cm | |
| ROOF roof Ext | Interior plaster | 3cm | 2.352 |
| | hourdi 16 | 16cm | |
| | Concrete | 4cm | |
| | Floor tile | 3cm | |
| FLOOR BASIC | Floor tile | 2cm | 0.864 |
| | Concrete | 20cm | |
| | Expanded polystyrene | 2cm | |
| | Pierre | 40cm | |
| BETWEEN TWO FLOORS ROOF | Interior plaster | 3cm | 2.352 |
| | Hourdi 16 | 16cm | |
| | Concrete | 4cm | |
| | floor tile | 3cm | |

## 5. Internal Earnings and Occupancy Strategy

We assume that the internal inputs and the use scenarios of the buildings are similar for the different zones. The same likely scenario of occupation is applied to each zone. We then assume that each cell houses two people from 00h à 7h et de 17h à 00h. A person is supposed to be present between 12h à 17h. The level of metabolic activity is 1.5 met from 8h to 23h and 1met from 23h to 8h. Regarding the thermal resistance of clothing she is equal to 0.5 clo (summer outfit). The relative speed of air is equal to 0.1 m/s [16]

Another scenario concerning the use of artificial lighting and the use of computers and televisions has also been proposed and built-in simulations (table .2).

*Table 2*

**Devices**

| Apparatus | Time of use |
|---|---|
| TV | 7-14 and of 17-23 |
| computer | 10-12 and of 17-23 |
| The lighting | 7-8 and 18-23 |

## 6. Night ventilation method used

Natural ventilation and simple exposure type, cross, transverse and by thermal draw It is created by opening the openings in the building [22]. Two types of windows characterize these configurations. We have those who are in contact with the exterior of the building and those who directly overlook the stairwell. In order to test the effectiveness of the natural ventilation potential generated by each configuration according to the nature of the climate, five scenarios are proposed The seven cities have been chosen and represent each climatic zone of Algeria.

*Table 3*

**Door and window opening scenarios**

| Case | month | | Opening on the outside | | Sashes opening onto the stairwell | |
|---|---|---|---|---|---|---|
| | | Towns | Opened | closed | Opened | closed |
| V1 | May, September, October | Adrar, Bechar, Ilizi, Ourgla, Borj-Baji-Mokhtar- | - | 24 h | | 24h |
| | Juin, juillet, aout | Oran, Djelfa | | | | |
| V2 | May, September, October | Adrar, Bechar, Ilizi, Ourgla, Borj-Baji-Mokhtar- | 9h-19h (90%) | 19h-19h | 9h-19h (90%) | 19h- 9h |
| | Juin, juillet aout | Oran, Djelfa | | | | |
| V3 | May, september, october | Adrar, Bechar, Ilizi, Ourgla, Borj-Baji-Mokhtar- | 9h-19h (90%) | 19h- 9h | Opened if Tcage< Tint | Closed if Tcage< Tint |
| | Juin, juillet aout | Oran, Djelfa | | | | |
| V4 | May, september, october | Adrar, Bechar, Ilizi, Ourgla, Borj-Baji-Mokhtar, | Opened if Tcage< Tint | Opened if Tcage< Tint | 9h-9h (90%) | 19h- 9h |
| | Juin, juillet aout | Oran, Djelfa | | | | |

| | | | | | | |
|---|---|---|---|---|---|---|
| V5 | May, september, october | Adrar, Bechar, Ilizi, Ourgla, Borj-Baji-Mokhtar, | Opened if Text< Tint | Opened if Text< Tint | Opened if Tcage< Tint | Opened if Tcage< Tint |
| | Juin, juillet aout | Oran, Djelfa | | | | |

## 7. Numerical simulation

The thermal aeraulic modeling of each configuration is carried out by the TRNSYS software coupled with the COMIS software. The climatic data of the chosen cities comes from the METEONORM software. The soil temperature is determined by the simple type 77 describing the soil temperature. The values of the pressure coefficients (Cp) characterizing the effect of the wind on the facades and roofs of the building, are calculated on the basis of the (Cp) Generator tool [16]. The values of the discharge coefficients (Cd) which take into account the physical effects of the contraction of the flow and the frictional forces as well as the values of the flow coefficient for the cracks (Cs) and (n) exponent of the air flow were calculated with reference to the works of [ 16,23].

## 8. Results and discussion

Results are presented in terms of hours of hot and cold discomfort (HTC, HTF) obtained according to the standard EN-15257, In order to complete the thermal comfort of each configuration, to complete our analysis we used maximum and minimum temperatures (Tmax,Tmin). In order not to burden the manuscript we presented only the results that we think are the most interesting for all selected cities.

First of all, and as a first reading of our simulation results, we traced the evolution of the temperature during four days of mid-May for the cities of Oran, Djelfa and Adrar for the three zones and for the different configurations by comparing them with the reference case. The analyzes performed in Figures 7; 8; 9 lead to the following observations.

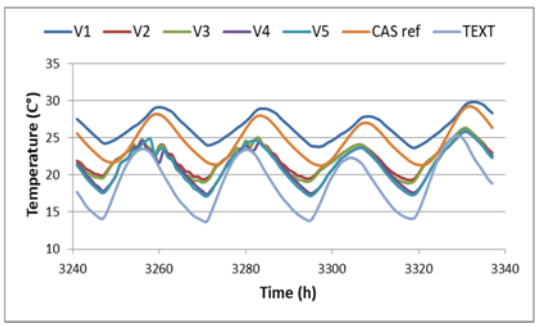


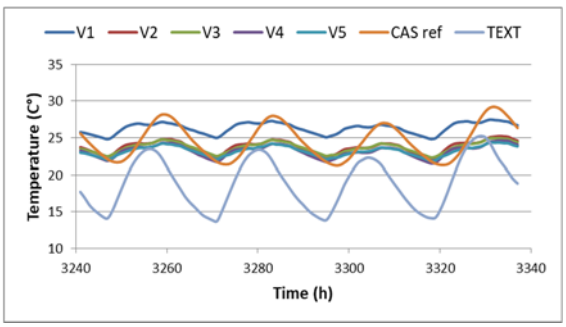

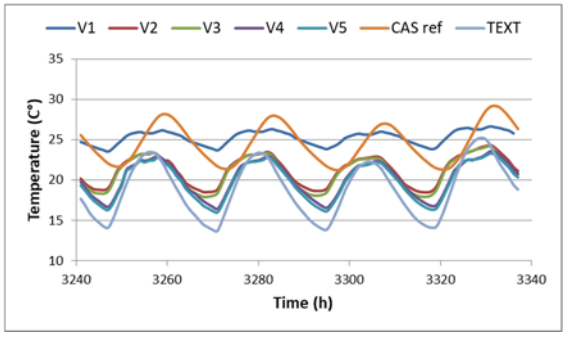


Fig.7. Case A, city of Oran at the top right (Z1), at the top left (Z2), at the bottom (Z3)

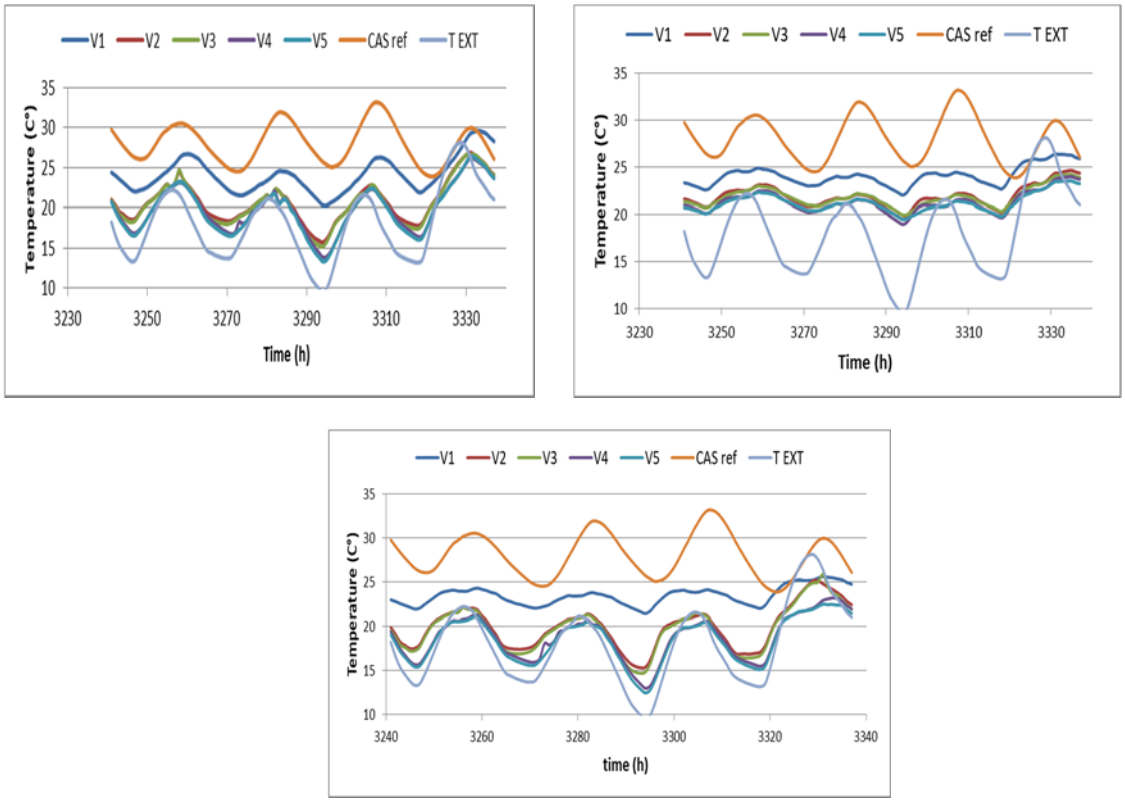


Fig.8. Case A, city of Djelfa top right (Z1) top left (Z2) bottom (Z3)

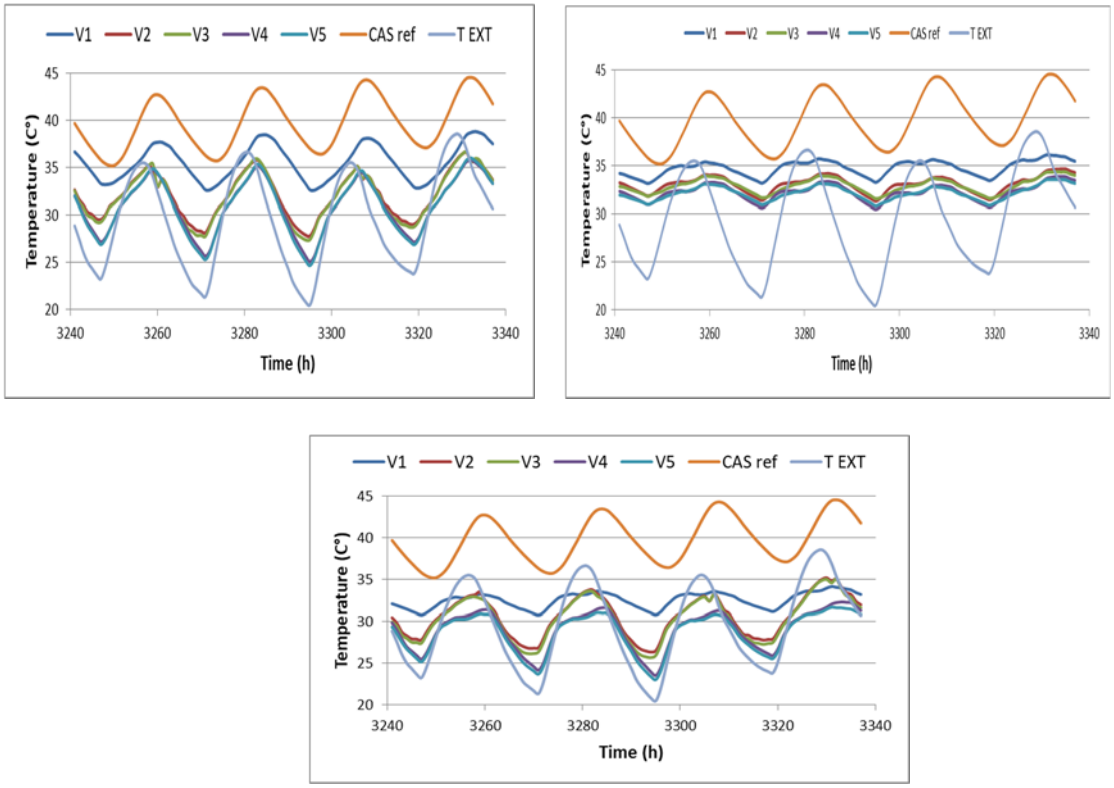


Fig.9. Case A, City of Adrar top right (Z1), top left (Z2) bottom (Z3)

The fluctuations observed in zone1 and zone3 for the cities of Oran, Djelfa, Adrar, are more pronounced than those in zone 2, mainly due to the level of air flow ( figure 10). The one from zone 3 is the highest, The one from zone3 is the highest, followed by the level of zone1. The flow in zone 2 is insignificant. As we pointed out previously, the air circulation is between zone 3 and zone 1.

The temperatures recorded on the graphical representations of Figures 7; 8; 9 are all below the temperature of the reference case. But it's zone3 that benefited the most from natural ventilation since the night temperatures recorded in zone 1 are slightly higher than those from zone 3.

Analysis of Figures 7; 8; 9 also shows us that the V4 method is better than the V3 method due to the level of air flow displayed by a higher level for windows in contact with the exterior than the openings in contact with the stairwell.

In short, the V5 method seems to us to be the most efficient the fact that all the windows opening onto the stairwell and the exterior are open by condition ventilation.

For the city of Adrar (figure 9) the temperatures are all above 30° C which represents the limit temperature for summer comfort (EN 15257). The temperature of zone2 oscillates in an interval of 2.5 ° C while those of the top floor (Z1) and the ground floor (Z3) oscillate respectively in an interval of 13° C and 8° C. This

difference in the thermal behavior of the three zones is the result of the position of each zone. Zone 1 is in direct contact with the roof which represents the part most exposed to direct and diffuse solar rays during the day [12]. The horizontal surface receives more sunlight than other surfaces, whether in summer or mid-season. However zone3 located on the ground floor benefits from the freshness of the basement. Even with windows closed, the rate of air infiltration in this area is considered relatively high.

On the other hand, natural night ventilation did not play its full role in zone 2 since the calculated difference is 9 ° C between the displayed temperature and the outside temperature during the night (especially around 4 a.m. when the outside temperature reaches its maximum for the month of May)

But an in-depth analysis of the thermal behavior of zone3 shows us that the temperatures from the variants V2 and V3 (opening onto the exterior or the stairwell are open from 7 p.m. and 9 a.m.) exceed the temperature of variant V1 (open during 24 hours), for a time that we estimated at 4 hours. . This situation leads us to think that natural ventilation cannot be considered as a technique which can provide an answer to the problem of controlling thermal comfort even during the mid-season in regions characterized by a hot and arid climate.

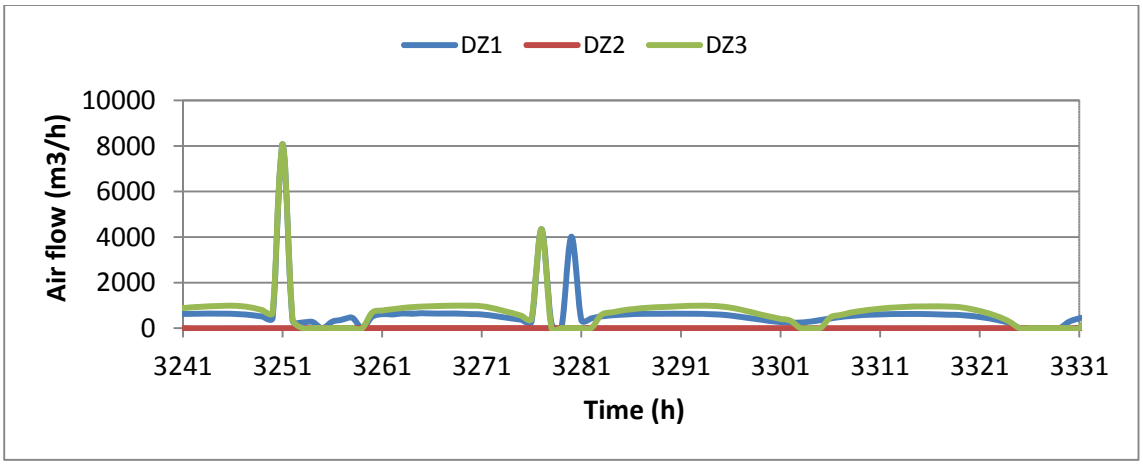


Fig.10. Variation of air flow in the three zones.

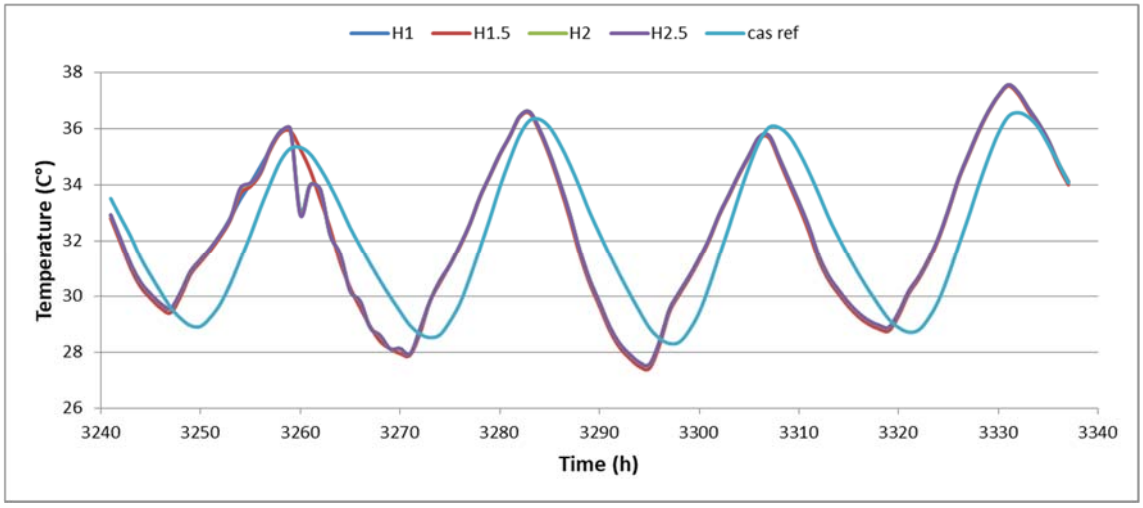


Fig.11. The influence of the variation of the height of the large high opening on the night temperature for the month of May for the city of Adrar.

Now let's see if increasing massive air flows is possible by increasing the height of the opening to be added to the building's terrace.

The graphical representation of Figure 11 shows the influence of the variation in the height of the night opening for the month of May. Note first that the graphs in Figure 11 have the same general appearance. The evolution of the temperatures shows that the representative temperatures of the heights register compared to that of the reference case an increase 1°C during the day and a decrease of 1 ° C in the evening.

It can therefore be said that the variation in height up to 6m did not register an improvement in the natural ventilation of zone 1.

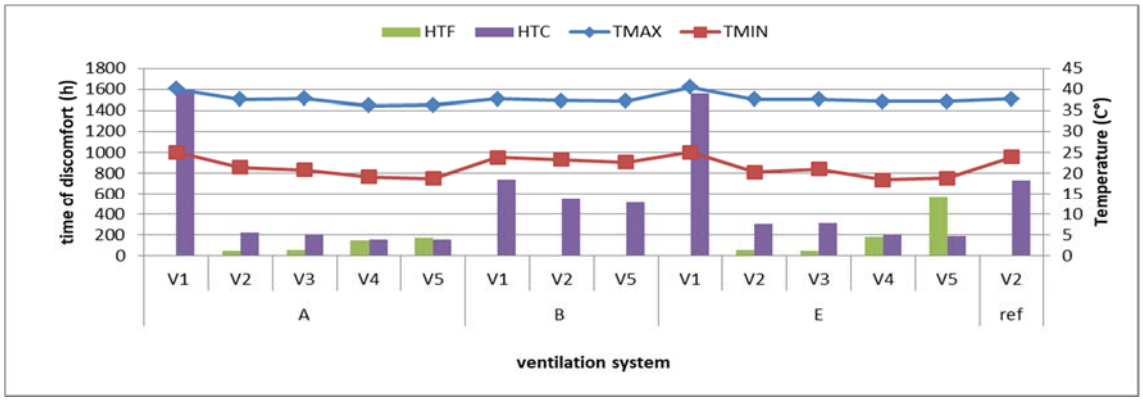


Fig.12. Variation in hours of discomfort and maximum and minimum temperatures as a function of time for the city of Oran

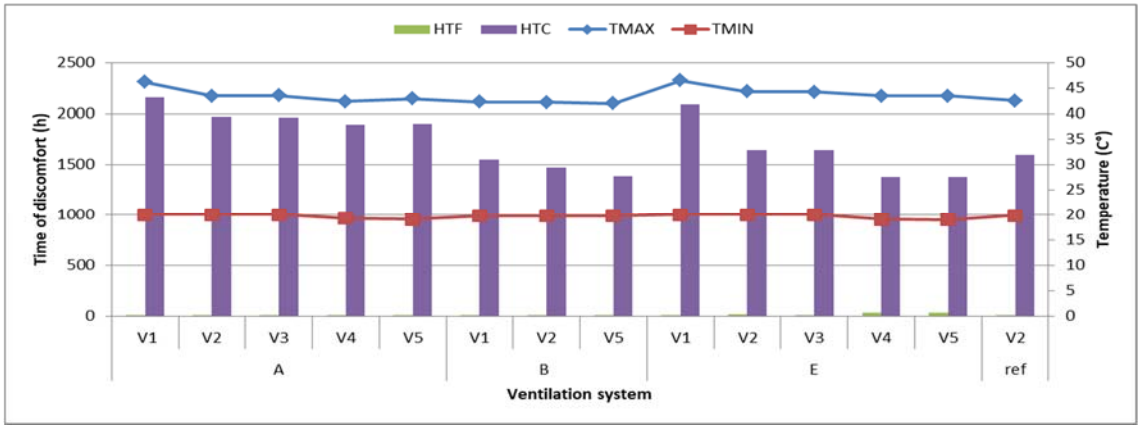


Fig.13. Variation in hours of discomfort and maximum and minimum temperatures as a function of time for the city of Adrar

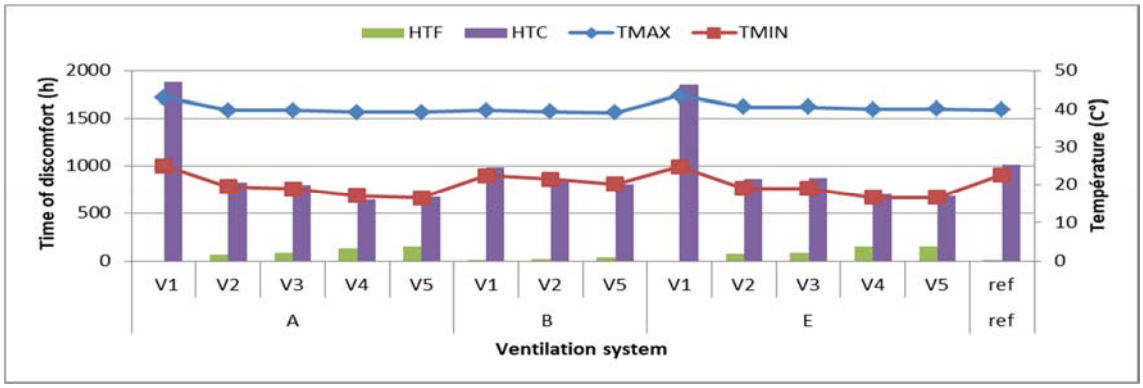


Fig.14. Variation in hours of discomfort and maximum and minimum temperatures as a function of time for the city of Djelfa

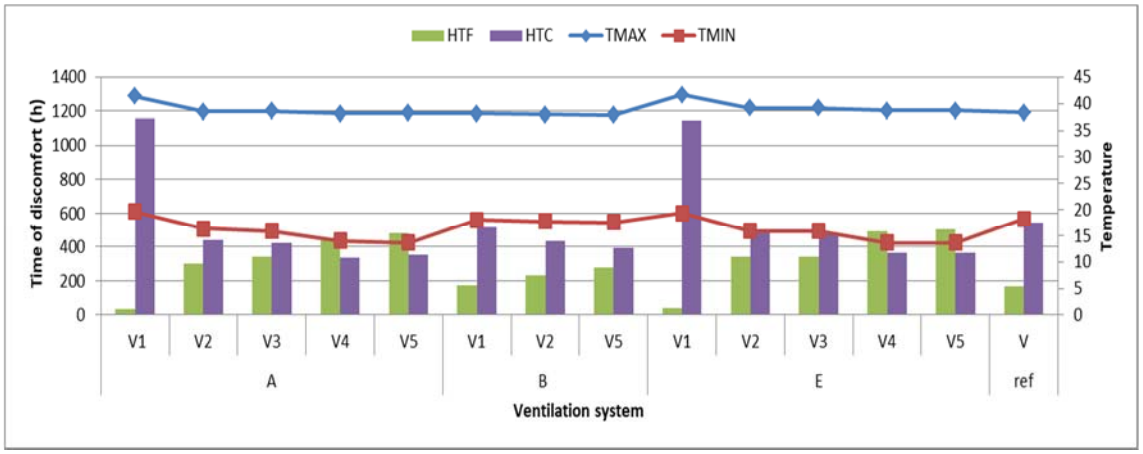


Fig.15. Variation des heures d'inconfort et des températures maximales et minimales en fonction du temps pour la ville de Bechar

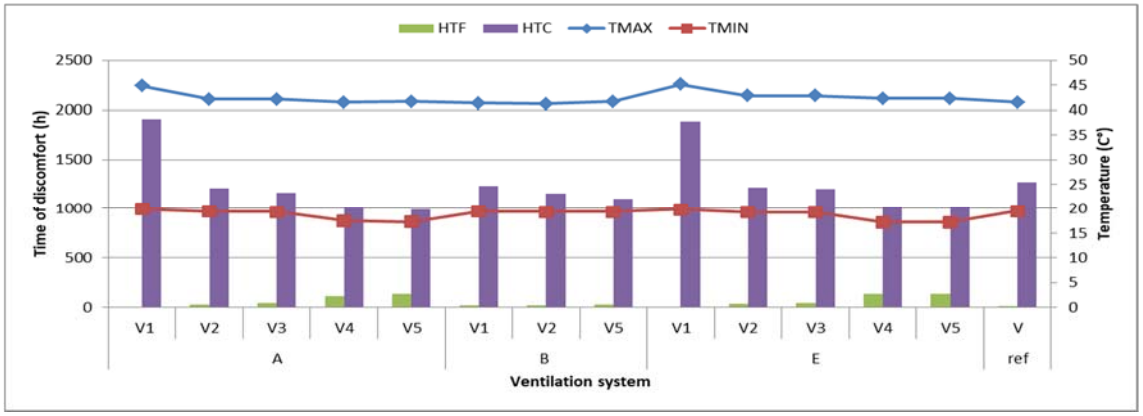


Fig.16. Variation des heures d'inconfort et des températures maximales et minimales en fonction du temps pour la ville d'Ouargla.

The analysis of the graphical representation of the hours of discomfort makes it possible to identify the most favorable case for ventilation. The analysis will relate only to the results of Z1 which represents the hottest zone such as we underlined it during the study of the results of the temperature curves by zone.

In order to complete our study it seems important to us now to analyze the results in terms of hot discomfort hours and cold discomfort hours obtained according to standard EN15257.

The results show first of all that scenario V5 represents the best performing scenario due to the level of HTF (hour of cold discomfort) and HTC (hour of hot discomfort) noted on the histograms of the figures. This observation is valid for all cities. Also our analysis will only relate to scenario V5.figure 12 shows that for the city of Oran, case B presents the level of HTF almost zero. More, we note for case E that case A presents better results. So, the level of HTC in case A and case E shows a decrease of 78.34% and 73.94% respectively compared to the level of the reference case. In addition, the Tmax (maximum temperature) corresponding to case E exceeds by 1 ° C that of case A. Case A seems to be the most favorable case, The level of Tmax is in the range between 35 ° and 40 ° for all of the cases studied. So, it seems to us that the opening method was not sufficient to decrease the temperature below 30°

The city of Adrar (figure 13) is characterized by a zero HTF level. But the level of HTC is considerable and far exceeds the level of other cities in the country. The level of HTC in case A exceeds by 19.22% that relating to the reference case. En revanche, le niveau de HTC dans le cas E a enregistré une baisse de 13,31% par rapport au niveau du cas de référence. This leads us to think that case E is the most favorable case. The fluctuation in Tmax is low and lies in the range between 43 ° C and 46 ° C, but the Tmax remains much higher than the temperature of the reference case. Tmin (minimum temperature) is between 19 ° and 20 °.

This analysis highlights the arid character of Adrar's climate even in mid-season. Despite our choice in favor of case E, analysis has shown us that the arid climate of the city of Adrar is an obstacle to the use of openings as a technique for improving the thermal efficiency of natural ventilation.

**Zone 1 Djelfa:**

Like other cities, the level of HTC is considerable and far exceeds the level of HTF which seems insignificant. The Tmin is located at 16 ° C while the Tmax displays a level above 40 ° C and considerably exceeds the level of the reference case. The appearance of the histograms shows us that the HTC and HTF of case A are at an equivalent level than those of case E. The choice in favor of case E would lead to an increase in the costs linked to taking charge of the upper opening.

**Zone 1 bechar:**

Analysis of the graphic representations of the city of Bechar shows us the high level of HTF compared to that found in other cities. As in the previous cases the level of HTC greatly exceeds the level of HTF. It then seems to us that case A is the most favorable case because it has a low level of HTC compared to that of case E.

Specify, otherwise, that natural ventilation by opening windows should be used with caution in cities with a temperate climate because and as we noted the mid-season period can present hours of hot discomfort but also hours of cold discomfort which requires careful control of the level of air flow induced by the opening of windows.

**Zone 1 Ouargla:**

The results obtained for the city of Ouargla are completely comparable to those of other cities. The level of HTC is much higher than that of HTF observed in Figure 13. The fluctuation of the maximum temperature is small the difference of 1 ° C between the Tmax of case A and of case E while the difference between Tmin of the 2 cases is located at 3 ° C. The decrease in the level of HTC in cases A and in case E compared to the level in the reference case was 21.92% and 20.03% respectively. This difference is not significant and does not allow one to choose one or the other.

## 9. Conclusion

This article presented a study aimed at testing the efficiency of natural ventilation on the thermal comfort of occupants by the application of different configurations in various climates in Algeria. Regarding the thermal behavior of the areas studied, it should be noted that whatever the ventilation scenario zone 3 benefited most from natural ventilation. On the other hand, zone 1 remains the hottest zone due to the high level of hot discomfort hours and cold discomfort hours. The study showed that it is the fifth scenario (V5) applied which gave the best results among all the opening

scenarios proposed, especially in the regions from littoral and highlands. Even with the use of the top opening (case E) we did not see any improvement in results for all selected cities. Maximum temperatures have exceeded the 30 ° C threshold and lie in an interval between [43 ° -44 °] in Adrar, [35 ° -40 °] in Oran, [40 ° -45 °] in Djelfa, and [38-44] in Bechar. Minimum temperatures have dropped to 13 °Cin Bechar, 10 ° in Djelfa, 20 ° in Adrar. As a last resort, it seems that the natural ventilation created by the effect of air remains an applicable method in the regions from littoral and highlands provided it is carefully checked. On the other hand, natural ventilation is difficult to apply in regions characterized by extreme climatic conditions even in mid-season. Overheating of the interior environment of the building can occur and direct natural ventilation becomes unnecessary under these conditions. Wait for the recommended comfort temperature levels, alternatives need to be found by coupling natural ventilation with other passive cooling systems.

## References


[1] *R. Ghedamsi, N. Settou, A. Gouareh, A. Khamouli, N. Saifi, B. Recioui, B. Dokkar*. "Modeling and forecasting energy consumption for residential buildings in Algeria using bottom-up approach." Building and Environment, vol. 121, no. 1, June. 2016, pp. 309-317.

[2] *G. Evola, V. Popov*. "Computational analysis of wind driven natural ventilation in buildings." Energy and Buildings, vol. 38, no. 5, May. 2006, pp. 491-501

[3] *M. Santamouris*. "Cooling the buildings – past, present and future." Building and Environment,vol. 128,no. 15, sept. 2016, pp. 617-638.

[4] *A. Rinaldi, M. Roccotelli, A.M. Mangini, M. Pia Fanti, F. Iannone.* "Natural ventilation for passive cooling by means of optimized control logics." In High- Performance Built Environment Conference – A Sustainable Built Environment Conference, Procedia Engineering, Ghrdaia, vol. 180, no. 2017, pp. 841-850

[5] *N. Saïfi*. "Contribution a la conception des batiments a faible consommation d'energie dans les zones arides.", PhD Thesis, Kasdi Merbah University of OUARGLA, 2015

[6] *J.L. Alvarado, W. Terrell, M.D. Johnson.* "Johnson Passive cooling systems for cement-based roofs." Energy and Buildings, vol. 180. no. 9, Sept. 2009, pp. 1869-1875.

[7] *C. Porras-Amores, F.R. Mazarrón, I. Cañas, P. Villoría Sáez*." Natural ventilation analysis in an underground construction: CFD simulation and experimental validation.", Tunnelling and Underground Space Technology, vol. 90, no. August. 2019, pp. 162-173.

[8] *W. Guo, X. Liu, X. Yuan*. "Study on Natural Ventilation Design Optimization Based on CFD Simulation for Green Buildings." 9th International Symposium on Heating, Ventilation and Air Conditioning and the 3rd International Conference on Building Energy and Environment, Chine, nol. 121, no. 2015, pp. 573-581

[9] *S. Liu, W. Pan, Q. Cao, Z. Long, Q. Chen.* "CFD simulations of natural cross ventilation through an apartment with modified hourly wind information from a meteorological station." Energy and Buildings, vol. 195, no. 15, July. 2019, pp. 16-25

[10] *S. Omrani, V. Garcia-Hansen, B. Capra, R. Drogemuller*. "Natural ventilation in multi-storey buildings: Design process and review of evaluation tools." Building and Environment, vol. 116, no. 1, May. 2017, pp. 182-194.

[11] *A. Zaki, P. Richards, R."Sharma*. "Analysis of airflow inside a two-sided wind catcher building." Wind Engineering and Industrial Aerodynamics, vol. 190, no. July. 2019, pp. 71-82

[12] M.Y. Ferroukhi. "Modélisation des transferts thermo-hydro-aérauliques dans les enveloppes de bâtiments : évaluation des désordres causés par l'humidité.", PhD Thesis, University of La

Rochelle, 2016.

[13] E. Kyritsi, A. MichaelAn. "Assessment of the impact of natural ventilation strategies and window opening patterns in office buildings in the Mediterranean basin." Building and Environment, no. 30, August. 2019, 106384

[14] *w. Feng, Q. Zhang, H. Ji, R. Wang, N. Zhou, Q. Ye, B. Hao, Y. Lid, D. Luof, S. Lauc*. "A review of net zero energy buildings in hot and humid climates."Renewable and Sustainable Energy, no. 114, October. 2019, 10930.

[15] *J.A. Castillo, G. Huelsz*. "A methodology to evaluate the indoor natural ventilation in hot climates." Building and Environment, vol. 114, no. March. 2017, pp. 366-373

[16] N. Fezzioui, "Analyse et Caractérisation du Bilan d'Energie d'un Habitat Traditionnel 'région Sud-Ouest", PhD Thesis, Tahri Mohamed University of Bechar, 2014.

[17] A. Belakehal, "Etude des aspects qualitatifs de l'éclairage naturel dans les espaces architecturaux. Cas des milieux arides à climat chaud et sec.", PhD Thesis, Mohamed Khider University of Biskra, 2006.

[18] *M. Hamdani, S.M.A. Bekkouche, T. Benouaz, R.Belarbi, M.K. Cherier*. "The Study Natural Ventilation by Using Buildings Windows: case study in a Hot Dry climate, Ghardaia, Algeria." In: Proceedings of International Conference On Materials And Energy, Tetouan, 2015, and the International Conference On Materials And Energy, La Rochelle, 2016, vol. 139, no. December. 2017, pp. 475-480

[19] *N. FEZZIOUI, B. DRAOUI, C.A Roulet*. "Etude du comportement aéraulique des maisons à ouverture zénithale." In: Proceedings of 1st International Seminar on the Apport of the Simulation in Technological Innovation, Ghardaïa, 2017.

[20] *M. M. Osman, H. Sevinc*. "Adaptation of Climate- Responsive Building Design Strategies and Resilience to Climate Change in the Hot/Arid Region of Khartoum, Sudan." Sustainable Cities and Society, vol. 47, May. 2019, 101429

[21] *A. DJOUIMAA*. "Realisation et verification de la performance thermique d'une tour a vent pour un rafraichissement passif dans les regions chaudes et arides . Cas DE HASSI MESSAOUD." PhD Thesis, Mentouri University of Constantine, 2008.

[22] *H. Sacht, L. Bragança, M. Almeida, and R. Caram*. "Study of Natural Ventilation in wind Tunnels and Influence of the Position of Ventilation Modules and Types of Grids on a Modular Façade System." In: Proceedings of SBE16 Tallinn and Helsinki Conference; Build Green and Renovate Deep, Tallinn and Helsinki, vol. 96, no. Sept. 2016, pp. 953-964.

[23] *C. FLORY-CELINI*. "Modélisation et positionnement de solutions bioclimatiques dans le bâtiment résidentiel existant.", PhD Thesis, University of Lyon 1 Claude Bernard of France, 2008.

# Durability of ultra-high performance fibered concretes made from local raw materials in two aggressive media of hydrochloric acid and barium sulphates

Durabilitatea betoanelor fibrate de înaltă performanță obținute din materii prime locale în două medii agresive de acid clorhidric și sulfați de bariu

Farida Ait Medjber [1,2], Mohammed Saidi[2]

[1]University Mouloud Mammeri
15000 Tizi-Ouzou, Algeria.
*E-mail: farida.pcmc@gmail.com*

[2] Research Unit: Materials, Processes and Environment (RU-MPE), University M'hamed Bougara 35000 Boumerdes, Algeria.

DOI: 10.37789/rjce.2021.12.1.3

***Abstract.*** *The durability of ultra high performance fiber-reinforced concrete (UHPFC) made from local raw materials has been studied in this manuscript. An experimental study was carried out on the best variants of UHPFC using finely ground dune sand as ultrafine. The UHPFCs studied were developed from Portland cement (PC), dune sand (DS), fine sand (FS), metal fibers (MF) and superplasticizer additive (SP). The results show that it is possible to manufacture a more ductile and durable fiber concrete of 41.96 and 35.28 MPa for flexural tensile and 95.5 and 85.36 MPa for compressive strength for UHPFCs made from dune sand and immersed respectively in two chemical solutions concentrated at 5M hydrochloric acid and barium sulfate for one year. The manufacture of a concrete based on local raw materials with good mechanical properties and durability can reduce the consumption of cement.*

**Key words:** Dune sand, ultra fine, ultra high performance fiber-reinforced concrete (UHPFC), durability, mechanical properties.

## 1. Introduction

The durability of concrete structures is a very important feature, as it guarantees increased safety and service life of these structures [1]. This durability also guarantees considerable savings in the long term, as such structures will require little or no repair, resulting in cost savings from repairs, which can be very high and may even exceed initial construction costs [2]. The development of such works must necessarily involve mastering and understanding the factors affecting their sustainability [3].

Free water can penetrate the network of pores and capillaries in concrete and bring with it aggressive ions that can react with the hydrates and change their structure. A durable concrete is a concrete that resists the penetration of aggressive agents and allows a significant life span for concrete structures [4].

External aggressions such as chlorides, $CO_2$ and chemical attacks can degrade the physical and mechanical properties of concrete and its durability over time. Among chemical attacks, acids that can come from both industrial areas and urban activity most severely degrade concrete [5].

## 2. Content of the paper

## 2. Materials and experimental method

### 2.1. Used materials

Cement (CP): the cement used is of the CEMI 52.5 type, with a density of 3160 kg/m3 and a Blaine surface area of 4800 cm2/g. The physical, chemical and mineralogical characteristics are given in Table 1, and are in accordance with standard NF EN 197-1 standard [6-7].

Sand of dune (SD): in this work, finely ground dune sand up to a fineness of 4000 cm2/g is used as a substitute in cement on the one hand and as fines added in the concrete formulation on the other.

Fine sand (FS): For the sand, it was opted for quarry sand from the Bouzegza region sieved on a 2 mm screen and 76% sand equivalent, and sand expansion of 23.3%.

Superplasticizer (SP): In order to reduce the E/L ratio and increase the fluidity of the concretes for ease of application while maintaining a level of performance, a Tempo 12 high water-reducing superplasticizer from sika was used in accordance with EN 934-2 [7].

Metal fibers (MF): The metal fibers are then added to provide better strength and ductile behavior in concrete.

*Table 1*

**Characteristics of cementitious materials**

| Minerals | CEM I 52.5 (PC) | Sand of dune (SD) |
|---|---|---|
| % $SiO_2$ | 20.03 | 94.40 |
| % $Al_2O_3$ | 5.07 | 2.23 |
| % $Fe_2O_3$ | 3.43 | 0.33 |
| % CaO | 62.43 | 0.45 |
| % MgO | 1.64 | 0.06 |
| % $SO_3$ | 2.57 | 0.17 |
| % $K_2O$ | 0.59 | 1.13 |
| % $Na_2O$ | 0.04 | 0.36 |
| %$P_2O_5$ | 0.15 | 0.01 |
| %$TiO_2$ | 0.21 | 0.04 |
| % P.A.F | 3.81 | 0.82 |
| % $C_3S$ | 62.89 | - |
| % $C_2S$ | 10.33 | - |
| % $C_3A$ | 7.64 | - |
| % $C_4AF$ | 10.43 | - |
| Specific mass ($g/cm^3$) | 2.93 | 2.95 |
| Specific surface ($cm^2/g$) | 4800 | 4000 |

*Table 2*

**Characteristics of the adjuvant**

| Characteristics | The adjuvant of SIKA |
|---|---|
| Aspect | Light brown liquid |
| $Na_2O$ content Eq | ≤ 1% |
| PH | 6 ± 1 |
| Density | 1.06 ± 0.01 |
| Dry extract | 30.2± 1.3 % |
| Conditioning | 230 Kg drums<br>CP of 1000 L<br>bulk |

## 2.2 Working methodology

This study was carried out in three parts. First of all, the work consists in studying the effect of the sand of finely ground dunes (5, 10, 15 and 20% by mass) by replacing cement on the rheological behavior of the cement pastes used for the different concretes studied. In this case, the amount of superplasticizer has been optimized to ensure adequate fluidity and avoid segregation. The second part was carried out on ultra high performance concretes with an optimal percentage of dune sand substituted in the cement by measuring the mechanical strength at 2, 7 and 28 days. Then, the optimization of the BFUHP with 2, 3.5 and 5% metal fibers of the two variants BUHP1 and BUHP2 by measuring the mechanical resistance also at 2, 7 and 28 days.

Afterwards, the optimization of the substitution percentage and the fiber percentage optimization, the best variant was determined with the best mechanical properties at 28 days. Finally, the third part was devoted to studying the durability of the best variant specimens in two chemical media of 5M concentration for a period of one year.

### 2.3 Test methods

Rheological tests: Using a VT550 type viscometer with coaxial cylindrical geometry, rheological tests were carried out. The measurements were carried out according to the following protocol (first of all: Pre-shear and ramp the shear rate to 350 $s^{-1}$ for 60s. Second step: maintain a constant shear rate at 350 $s^{-1}$ for 300 seconds). All of the cementitious pastes tested were prepared with a fixed dosage of superplasticizer and a ratio of W/C=0.29 kept constant [8].

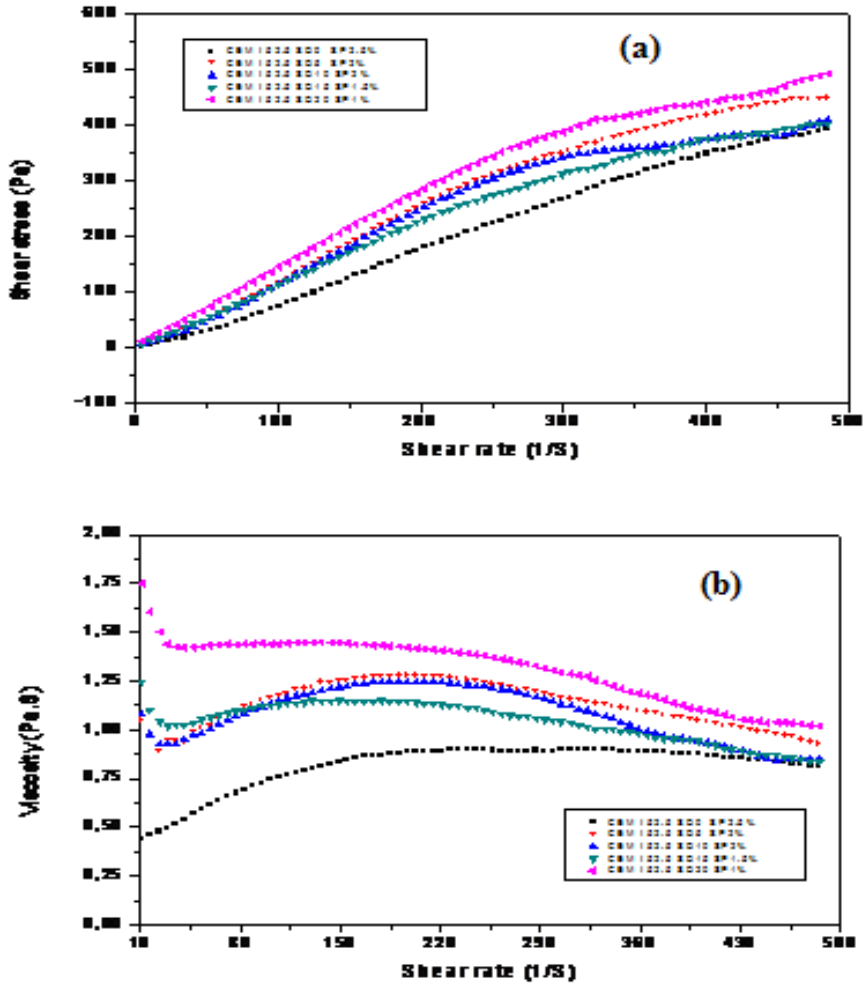


Fig. 1. Variation of shear stress (a) and plastic viscosity (b) as a function of shear rate

Mechanical tests: The specimens were made according to standard NF EN 196-1[9], cast in prismatic moulds (4x4x16 cm3) then unmoulded after 24 hours and stored in a water bath until the days of mechanical crushing. The compressive and bending strengths of the specimens were tested at 2, 7 and 28 days using a 200KN computer-controlled "IBERTEST" type apparatus. The three-point bending tests were performed on prismatic samples according to ASTM C348 [10]. The half-samples were subjected to compressive stress in accordance with ASTM C349 [11].

## 3. Results and discussion

### 3.1 Rheological study

Figures 1a and 1b show the variation in shear stress and viscosity of cement paste at different substitution rates by finely ground dune sand as a function of shear rate. It is clearly observed that the higher the doses of superplasticizer, the more fluid the cementitious pastes become [12-14]. This fluidity facilitates the formulation of ultra-high performance concretes, particularly in the presence of fibers [15].

Analysis of the experimental curves shows that the appearance of the curves remains broadly identical for all sand concentrations in the dunes. There is an increase in viscosity as the sand concentration of the dunes increases.

### 3.2 Effect of dune sand on the mechanical performance of UHPCs

Ultra high performance concretes (UHPC) with different percentages of finely ground dune sand (SDS) as a substitute in cement have been developed. Table 3 illustrates the different concrete compositions studied. Then, and in order to determine an optimal percentage of SD, the mechanical resistances were measured at 2, 7 and 28 days and the results obtained are given in Table 4.

*Table 3*

**Different compositions of ultra high performance concretes (UHPC)**

| Components | UHPC0 | UHPC1 | UHPC2 | UHPC3 | UHPC4 |
|---|---|---|---|---|---|
| PC [Kg] | 1000 | 950 | 900 | 850 | 800 |
| SD [Kg] | 148.8 | 148.8 | 148.8 | 148.8 | 148.8 |
| SDS [Kg] | 0 | 50 | 100 | 150 | 200 |
| FS [Kg] | 958 | 958 | 958 | 958 | 958 |
| SP [Kg] | 24.8 | 20.3 | 20.3 | 15 | 10 |
| Water [Kg] | 246.7 | 250.9 | 251.6 | 255.3 | 258.6 |
| W/B | 0.23 | 0.23 | 0.23 | 0.23 | 0.23 |

*Table 4*

**Mechanical Resistance of UHPC with SD Rate**

| | Flexural strength (MPa) | | | Compressive strength (MPa) | | |
|---|---|---|---|---|---|---|
| | 02D | 07D | 28D | 02D | 07D | 28D |
| UHPC0 | 8.02 | 10.14 | 11.23 | 39.07 | 54.20 | 70.66 |
| UHPC1 | 13.27 | 14.31 | 15.62 | 71.76 | 93.64 | 103 |
| UHPC2 | 12.07 | 13.5 | 14.59 | 70.21 | 90.55 | 99.6 |
| UHPC3 | 13.53 | 14.78 | 15.11 | 68.94 | 89.2 | 96.32 |
| UHPC4 | 12.93 | 14.47 | 14.9 | 68.87 | 87.73 | 96.98 |

According to Table 4, dune sand has a beneficial effect on mechanical performance and shows a significant improvement in the bending and compressive strength of the concretes studied compared to the UHPC0 control concrete. This is because the addition of finely ground dune sand affects the hydration reactions by pozzolanic reaction of well-dispersed cement grains with portlandite ($(Ca(OH)_2$), thus modifying their growth rate and morphology [16-20].

Due to their manoeuvrability, fibers are only added to the first two variants UHPC1 and UHPC2; UHPC3 and UHPC4 cannot accept the fibers they are firm.

### 3.3 Effect of dune sand on the mechanical performance of UHPFCs

In this section, and in order to assess the influence of dune sand as a mineral addition, concrete formulations were drawn from the previous section of the study. Metal fibers were selected and used at different contents in the binder mass fraction (2, 3.5 and 5%) as reinforcing fibers. Metal fibers were therefore added to ultra-high performance dune sand concrete to improve the ductility of the material, both in tension and compression [20-24]. The formulation of the UHPCs is given in Table 5.

*Table 5*

**Formulation of BFUHP Ultra High Performance Fiber Concrete in $1m^3$**

| Components | | UHPFC1 | UHPFC2 |
|---|---|---|---|
| PC [Kg] | | 950 | 900 |
| SD [Kg] | | 148.8 | 148.8 |
| SDS [Kg] | | 50 | 100 |
| FS [Kg] | | 958 | 958 |
| MF [Kg] | 2% | 20 | 20 |
| | 3.5% | 35 | 35 |
| | 5% | 50 | 50 |
| SP [Kg] | | 20.3 | 20.3 |
| Water [Kg] | | 250.9 | 251.6 |
| W/B | | 0.23 | 0.23 |

Mechanical performance was assessed by measuring compressive and bending strength at different ages (2, 7 and 28 days) and the results obtained are shown in Table 6.

*Table 6*

**Mechanical Resistance of BFUHP with Fiber Rate**

| | MF(%) | Flexural strength (MPa) | | | Compressive strength (MPa) | | |
|---|---|---|---|---|---|---|---|
| | | 02 D | 07 D | 28 D | 02 D | 07 D | 28 D |
| UPFC1 | 2 | 14.12 | 20.63 | 22.23 | 75.15 | 97.18 | 113.63 |
| | 3.5 | 13.88 | 25.66 | 30.27 | 77.23 | 105.38 | 125.15 |
| | 5 | 15.47 | 26.63 | 33.9 | 77.54 | 103.32 | 134.43 |
| UPFC2 | 2 | 14.83 | 23.16 | 30.1 | 78.2 | 95.65 | 120.55 |
| | 3.5 | 14.80 | 25.68 | 32.53 | 77.21 | 99.75 | 126.23 |
| | 5 | 16.48 | 30.2 | 34.08 | 85.25 | 102.97 | 135.33 |

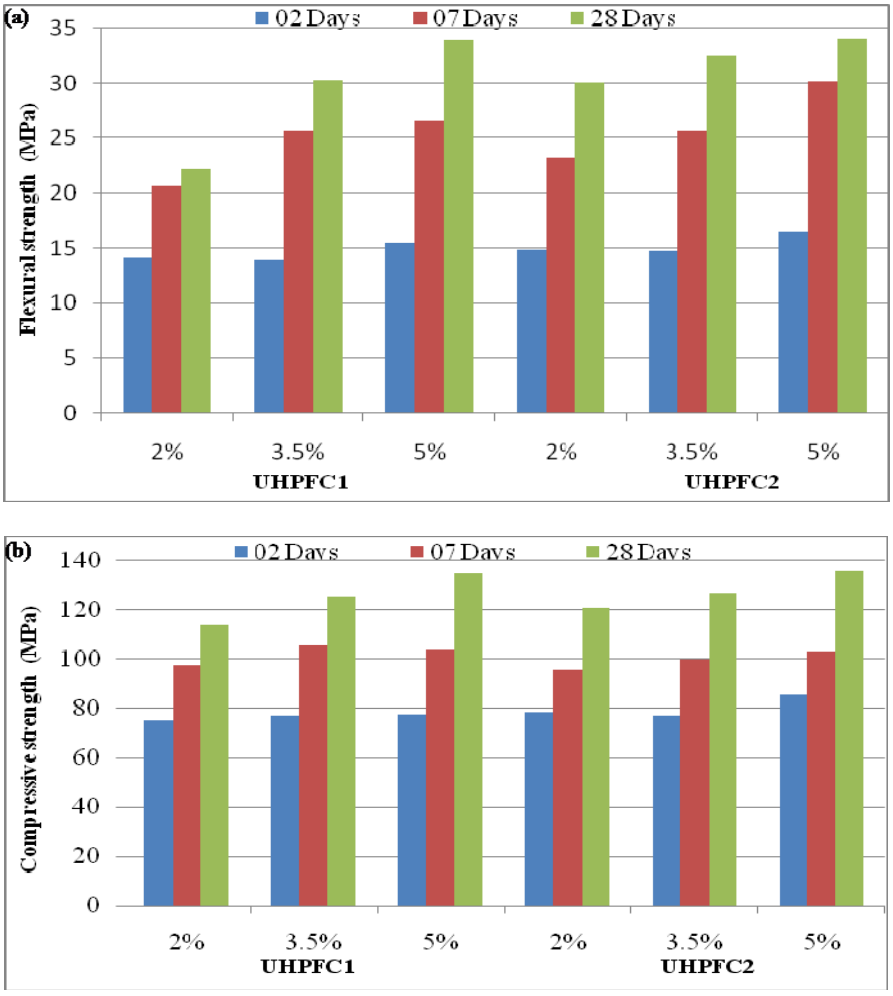


Fig. 2. Evolution of flexural (a) and compressive (b) strengths of UHPFC1 and UHPFC2 with fiber content and age

Figures 2a and 2b show the evolution of mechanical strength with age and fiber content. Resistance increases from 02 to 07 up to 28 days for each of the two variants BFUHP1 and BFUHP2, and the latter has higher values than UHPFC1 at 28 days for a percentage of 5% fiber. So the best variant is the one that substitutes 10% of the cement for the sand of the finely ground dunes with a 5% fiber content called BFUHP2 with 5% fibers.

### 3.4. Durability of UHPFC specimens

All specimens were made according to the same procedure followed in the previous section and were stored in a water bath at 20°C±2°C. After maturation, the specimens were removed from the water bath, air-dried and steamed at 105°C for 24 hours to constant masses. Two 5M solutions of hydrochloric acid (HCl) and barium sulphates (BaSO4) were prepared at PHs of 01 and 05 respectively. Then three specimens were immersed in each solution, and three others were left out in the open as a control. The chemical attack was followed in both media for one year and the solutions were repeated at the same PH after six months.

#### 3.4.1. The loss of mass

The chemical resistance was evaluated according to ASTM C 267-96 [25] by measuring the mass loss of the specimen calculated by the following formula:

$$Mass\ variation\ (\%) = \frac{M_1 - M_2}{M_1} \times 100 \qquad (1)$$

With $M_1$, $M_2$ the masses of the specimens before and after immersion, respectively. This operation was performed after 6 and 12 months of immersion.

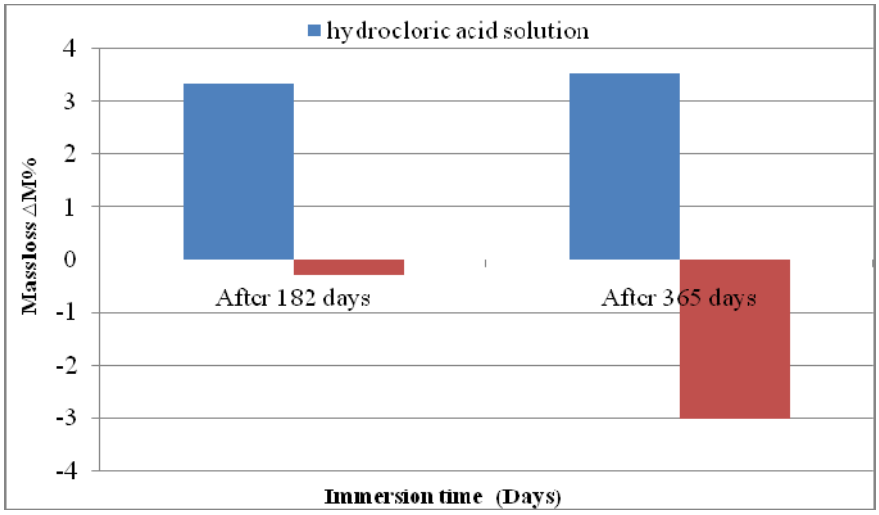


Fig.3.The loss of mass of the UHPFC as a function of the age of immersion in HCl and $BaSO_4$

UHPFCs show mass losses of 3.52% in hydrochloric acid solution and mass gains of 3.029% in the brium sulphates respectively after one year of chemical treatment:

- The loss of mass is due to the fact that the cement, after hydration, releases a considerable part of free calcium hydroxide ($Ca(OH)_2$) which can be leached out when it is subjected to attack by hydrochloric acid (HCl) by giving calcium hydroxide, according to the following chemical reaction[26]:

$$Ca(OH)_2 + 2HCl \rightarrow CaCl_2 + 2H_2O \qquad (2)$$

Hydrochloric acid, a strong acid which, by reaction with cement lime, gives rise to calcium chloride, a highly soluble salt that is very aggressive towards Portland cements [27, 28].

- The weight gain observed for BFUP immersed in the barium sulphates solution is surely due to the substitution of $Ca^{2+}$ ions by $Ba^{2+}$ [29] by giving gypsum, according to the following reaction:

$$Ca(OH)_2 + BaSO_4 \rightarrow CaSO_4 + Ba(OH)_2 \qquad (3)$$

### 3.4.2. The density

The evolution of the density of UHPFC with immersion time is shown in Figure 3, which shows a decrease in acid and an increase in sulphates.

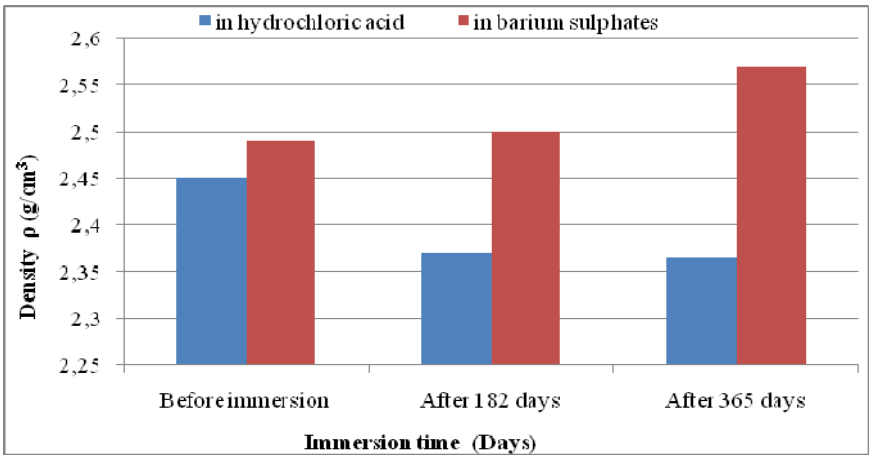


Fig. 4. The density of BFUHPs as a function of the age of immersion in HCl and $BaSO_4$

### 3.4.3. The mechanical performance of BFUPs

In order to evaluate the mechanical performance of the UHPCs left in the air as well as those immersed in the two aggressive solutions for one year, mechanical crushing was performed to measure the mechanical resistance.

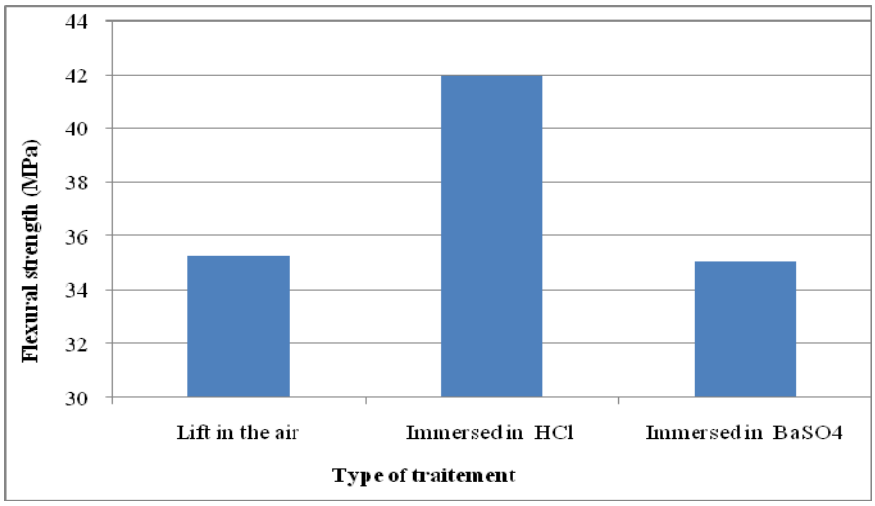


Fig.5. Evolution of flexural strengths with the type of treatment

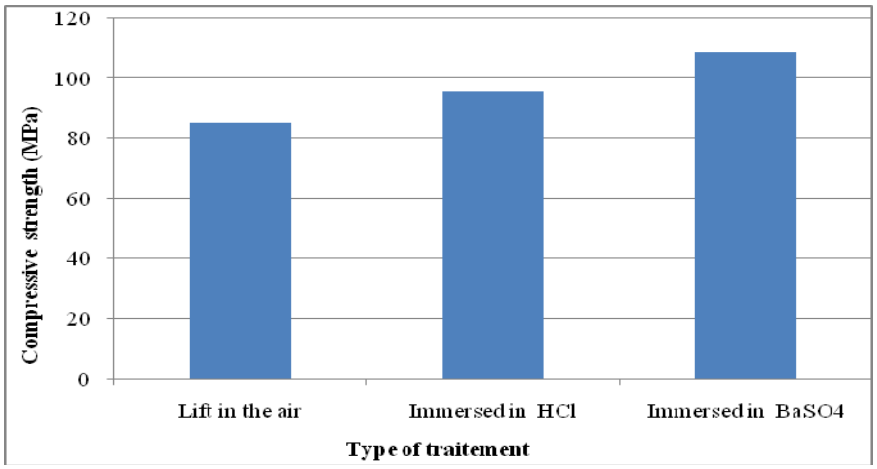


Fig.6. Evolution of compressive strengths with the type of treatment

From the results of the mechanical crashes we can see that:

- The bending tensile strength of UHPFCs immersed in five-fold molar hydrochloric acid solution is better than that of UHPFCs left in the air or immersed in barium sulfate solution for a period of one year.

- In compression, UHPFCs immersed in HCl are more resistant than those immersed in BaSO4 and less resistant when compared to those left in the air.

The results of the macroscopic study, including mass loss, density and mechanical crushing, show that the UHPFC submerged in the two aggressive five-fold molar solutions resist chemical aggression compared to those left in the air for one year.

The introduction of dune sands in the manufacture of high-performance, chemically resistant fibrated concrete is doubly beneficial in terms of strength and economy.

The presentation will be clear and concise, and the symbols used will be defined within a list of symbols (if any). The International System (SI) of units of measurement will be used. For editing use the styles defined in this document, to keep the required format of the text. Predefined styles names start with "RRIC_".

## 4. Conclusions

The use of dune sand in the production of high-performance and resistant fiber-reinforced concrete for aggressive environments is beneficial.

In order to better understand the behavior of our UHPFCs regarding the chemical reactions responsible for slowing down degradation in their cementitious matrices in response to chemical attacks, microscopic analysis by X-ray diffraction (XRD) and scanning electron microscopy (SEM)on powders from UHPFC samples is necessary and will be the subject of the next study.

## References

[1] J .Baron, J.P .Ollivier, „ La Durabilité des Bétons”, in Presses de l’ENPC, Paris, 1992.
[2] AM. Neville, „Propriétés des bétons”, Traduit par le CRIB, Edition Eyrolles, Paris, 2000.
[3] G .Arliguie, H .Horain, „Grandeurs Du Béton : Grandeurs associées à la durabilité des bétons”, in Presse de l’école nationale des ponts et chaussées, France, 2007.
[4] L .Laoufi, Y.Senhadji, A .Benazzouk, T .Lang, M .Mouli, I .Laoufi, A.S .Benosman, „ Assessment of pozzolanic mortars sustainability exposed to chemical attack”, in J. Mater. Environ. Sci, vol. 7, no. 5, 2016, pp.1835-1845.
[5] S .Lasfar, I .Mouallif, A .Latrach, M .Chergui, A .Choukir, A .Diab, „Resistance of two different types of concrete pipes used in sewer systems under sulfuric acid and sodium sulfate”, in J. Mater. Environ. Sci, vol. 6, no. 10, 2015, pp. 3002-3014.
[6] AFNOR, NF IN 197-1, „Composition, spécifications et critères de conformité”. Ciment -Partie 1, Février 2001.
[7] AFNOR, NF EN 934-2/A2, „adjuvants pour béton- Définitions, exigences, conformité, marquage et étiquetage”. Adjuvants pour béton, mortier et coulis- Partie 2, Avril 2006.
[8] F .Ait Medjber, M .Saidi, B .Safi, M .Samar, „Strength improvement of a High Performance Fiber Reinforced Concrete (HPFRC) containing local raw materials”, in International Journal of Physical Sciences, vol. 9, no. 18, 2014, pp.402-412.

[9] NF EN 196-1. P15-471-1, „Méthodes d'essais des ciments"- Partie 1: détermination des résistances", Septembre 2016.
[10] ASTM C348 – 08, Standard Test Method for Flexural Strength of Hydraulic-Cement Mortars, which appears in the Annual Book of ASTM Standards Vol. 4, no. 1.
[11] ASTM C349 – 08, „Standard Test Method for Compressive Strength of Hydraulic-Cement Mortars (Using Portions of Prisms Broken in Flexure), which appears in the Annual Book of ASTM Standards Vol. 4, no.1.
[12] B .Safi, A .Benmounah, M .Saidi, „Rheology and zeta potential of cement pastes containing calcined silt and ground granulated blast-furnace slag", in Materiales de Construcción, vol. 61, no. 303, 2011, pp. 353-370.
[13] L .Struble, G.K .Sun, „Viscosity of Portland cement Paste ace has Function off Concentration. Advanced Cement Based Materials", vol. 2, no. 2, 1995, pp. 62-69.
[14] C.F .Ferraris, „Measurement of the rheological properties of performance high concrete; State of the art carry forward", in Newspaper of Research, the National Institute of Standards and Technology, vol.104, no. 5, 1999, pp.461–478.
[15] F .Ait Medjber, M .Saidi, H .Mechakra, B .Safi, „Assessing the effectiveness of dune sand as a mineral addition to produce ultra-high performance fiber reinforced concrete", in Romanian Journal of Civil Engineering, vol. 10, no. 1, 2019, pp. 34-50.
[16] M .Zeghad, J .Mitterpach, B .Safi, B .Amrane, M .Saidi, „Reuse of refractory brick wastes (RBW) as a Supplementary cementitious material in a concrete". In Periodica Polytechnica Civil Engineering, vol. 61, 2017, pp. 81–87.
[17] R .Yu, P .Tang, P .Spiesz, H.J.H .Brouwers, „A study of multiple effects of nano-silica and hybrid fibers on the properties of Ultra-High Performance Fiber Reinforced Concrete (UHPFRC) incorporating waste bottom ash (WBA)", in Construction and Building Materials 60, 2014, pp. 98–110
[18] H.S ,Arel, „Effects of curing type, silica fume fineness, and fiber length on the mechanical properties and impact resistance of UHPFRC", in Results in Physics, vol.6, 2016, pp.664–674.
[19] N.H .Yi, J.H.J .Kim, T.S .Han, Y.G .Cho, J.H .Lee, „Blast-resistant characteristics of ultra high strength concrete and reactive powder concrete", in Constr Build Mater, vol. 28, 2012, pp. 694–707.
[20] P .Richard, „Reactive Powder Concrete: A New-Ultra High Strength Cementitious Material", in Proceedings of the Fourth International Symposium on the Utilization of High-Strength/High-Performance Concrete, 29–31 May 1996, Paris, France, Ed. F. de Larrard, R. Lacroix, pp. 1343–1349.
[21] S .Kazemi, A .Lubell, „ Influence of Specimen Size and Fiber Content on Mechanical Properties of Ultra-High-Performance Fiber-Reinforced Concrete", in ACI Materials Journal, vol.109, no. 6, November–December 2012, pp. 675–684.
[22] M. Schmidt, „Sustainable Building With Ultra-High-Performance Concrete (UHPC) Coordinated Research Program in Germany", Proceedings of Hipermat 3rd International Symposium on UHPC and Nanotechnology for High Performance Construction Materials, Ed., Schmidt, M., Fehling, E., Glotzbach, C., Fröhlich, S., and Piotrowski, S., Kassel University Press, Kassel, Germany, 2012, pp. 17–25.
[23] S .Abbas, A .M .Soliman, M. L .Nehdi, „ Exploring mechanical and durability properties of ultra-high performance concrete incorporating various steel fiber lengths and dosages", in Construction and Building Materials vol.75, 2015, pp.429–441.
[24] D. J .Kim, S. H .Park, G .S .Ryu, K. T .Koh, „Comparative flexural behavior of Hybrid Ultra High Performance Fiber Reinforced Concrete with different macro fibers", in Construction and Building Materials vol. 25, 2011, pp.4144–4155.
[25] ASTM C 267-96, "standard test methods for chemical resistance of mortars, grouts, and monolithic surfacing and polymer concretes", Annual Book of ASTM Standards, American Society for Testing and Structures, June 1996.

[26] L .Laoufi,Y.Senhadji, A .Benazzouk, T .Langlet, M .Mouli, I .Laoufi, A.S .Benosman, „Assessment of pozzolanic mortars sustainability exposed to chemical attack", in J. Mater. Environ. Sci. vol.7 no.5, 2016, pp.1835-1845.

[27] V .Zivica, A .Bajza, „ Acidic attack of cement based materials- a review. Part1: Principle of acidic attack", Construction and Building Materials, vol.15, 2001, pp. 331-340.

[28] V .Zivica, A .Bajza, „ Acidic attack of cement based materials- a review. Part2: Facto„rs of rate of acidic attack and protective measures", in Construction and Building Materials, vol. 16, 2002, pp. 215-222.

[29] Nicolas Bur, „ Etude des caractéristiques physico-chimiques de nouveaux bétons éco-respectueux pour leur résistance à l'environnement dans le cadre du développement durable", PhD Thesis, University of Strasbourg, INSA of Strasbourg, 2012.

# About the production and interconnection of electricity obtained from geothermal energy

Carmen Mârza [1], Georgiana Corsiuc [1]

[1] Faculty of Building Services Engineering, Technical University of Cluj-Napoca, Romania
21 Decembrie 1989 Street, no. 128-130, Cluj-Napoca, Romania
*E-mail: Carmen.Marza@insta.utcluj.ro, Georgiana.Corsiuc@gmail.com*

DOI: 10.37789/rjce.2021.12.1.4

**Abstract.** *In the context of sustainable development, the use of renewable energy sources and the decrease of greenhouse gas emissions have become global priorities. Geothermal energy represents an important potential for many countries, including our country. If the exploitation of thermal energy has a relatively widespread, the production of electricity is less developed, even if there are countries that cover a significant part of the electricity demand from this resource. In this paper, the authors aim to present the main technical solutions that produce electricity from geothermal sources, but also present some topological models for integrating the obtained electricity in the public network.*

**Key words:** geothermal energy, electricity, renewable energy sources, interconnectation of electricity

## 1. Introduction

Geothermal energy is the energy obtained from the heat inside the Earth. It can be classified, in terms of thermal potential, in:
- geothermal energy of high thermal potential;
- geothermal energy of low thermal potential.

Geothermal energy with high thermal potential is characterized by high temperatures (> 150$^{o}$C) and can be used for both electricity generation and heat production. Geothermal energy with low thermal potential (temperatures <150$^{o}$C) can be used mainly for the production of thermal energy, while for the generation of electricity requires binary technologies [1].

The category of high thermal potential geothermal energy resources includes: volcanoes, hot springs and geysers, the most important resources being found along the "Pacific Circle of Fire".

The use of geothermal energy for the production of thermal energy had applications in our country, especially in the last decades of the 20$^{th}$ century, after the fossil fuel crisis of the '70s, when the importance of using renewable energy resources was highlighted. Thus, research in this field was encouraged, having as result the

construction of installations that exploit the geothermal potential of Romania. This should not be neglected, being distributed in the Western Region, in the Getic Depression (Cozia –Căciulata) and the Moesian Platform (Bucharest area) [1].

Currently, the exploitation of low-potential geothermal energy has an important development due to special equipment, namely heat pumps that, as it is known, extract heat from soil, water or air.

In this paper, the authors aim to bring attention to aspects related to electricity production, which in our country did not have direct applications until the time of involvement in the large-scale European project GeoSee [2], in which several countries in Southeast Europe came together to study and develop hybrid systems for producing electricity using geothermal energy in combination with another renewable energy source. At the Oradea power plant, the choice of solar energy produced with photovoltaic panels was chosen as a complementary source.

## 2. Types of geothermal power plants for electricity production

The statistics published in 2016 shows that geothermal heating energy is exploited in 70 countries, while electricity is produced in 24 countries. Table 1 presents the main countries producing electricity based on geothermal energy. Recently, major power plants have been built in China and Russia.

*Table 1*

**Geothermal power plants installed capacity**

| Country | Capacity (MWe) | Country | Capacity (MWe) |
|---|---|---|---|
| Costa Rica | 142.5 | Japan | 546.9 |
| El Salvador | 161 | Mexico | 755 |
| Iceland | 170 | New Zealand | 437 |
| Indonesia | 589.5 | Philippines | 1909 |
| Italy | 785 | United States of America | 2228 |

There are currently three main types of geothermal power plants in the world that are used to transform the power of geothermal water into electricity, which depend on the state of the fluid used (vapor or liquid), or its temperature [3], [4]:

- **Geothermal power plants based on dry steam**; these were the first types of power plants built (Larderello, Italy, in 1904) and use steam at high temperature (> 235ºC) and only a small amount of water from the geothermal tank; the steam is brought from the tank through a pipe directly into the turbine, to drive a generator that produces electricity;
- **Wet saturated steam geothermal power plants** (also known as flash power plants); is the usual option for plants with 5 MW up to 100 MW installed capacity; these plants use hot water (> 182ºC) from the geothermal tank; the water is pumped into the expander at the pressure provided by the underground tank where a sudden

drop in pressure takes place, which causes some of the water to evaporate, the steam formed driving the turbine.

- **Geothermal power plants with binary cycle**; in binary systems, hot geothermal fluids are conveyed through one of the parts of a heat exchanger to heat a working fluid; the working fluid, with a low boiling point, vaporizes and passes through a turbine to generate electricity.

The usual installed capacity in this category is in the range 500 kWe - 10 MWe.

Since most geothermal reserves are characterized by relatively low temperatures, below the level of 180°C, the following is the diagram of a binary cycle geothermal power plant, which is the optimal solution for the conversion of geothermal energy into electricity, at these temperature values (see figure 1).

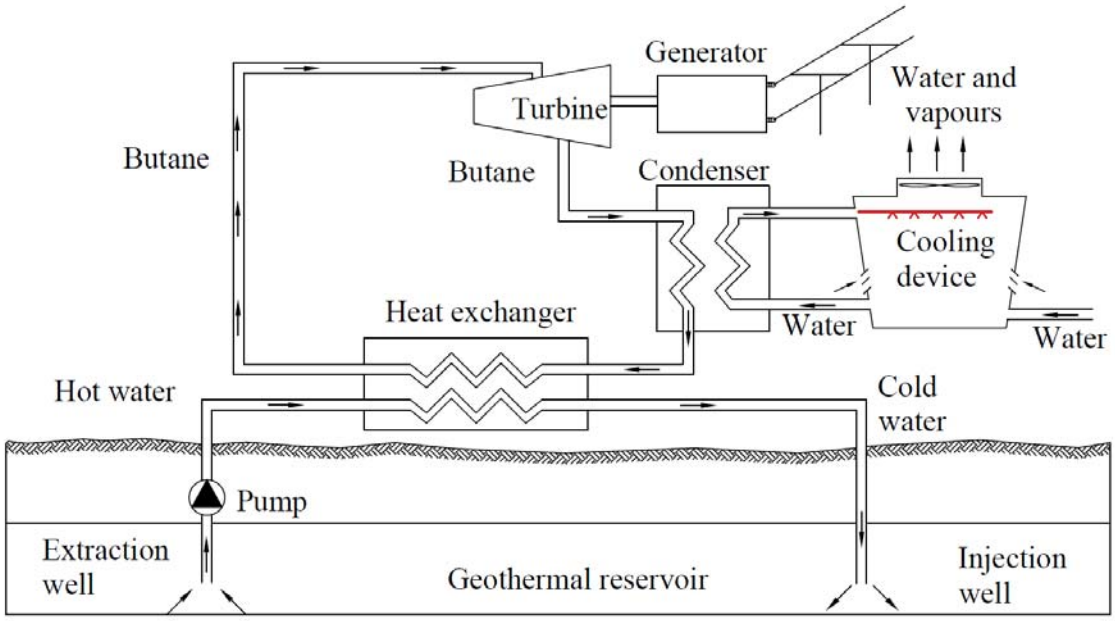


Fig. 1. Binary cycle geothermal power plant.

These types of plants are based on the thermodynamic Organic Rankine Cycle, abbreviated in the technical literature as ORC.

Water from the geothermal source transfers heat through a heat exchanger to a fluid (such as pentane, isopentane, butane) that evolves in the engine cycle of the plant. This fluid is characterized by a significantly lower boiling temperature than water. In this way a relatively low geothermal thermal potential can be used. In addition, due to the two circuits, impure geothermal water can also be used, especially if certain pressure conditions are maintained in the installation (which does not allow boiling), so that it is not possible to release harmful gases into the atmosphere. On the other hand, this is also a disadvantage due to the fact that it requires additional energy consumption [3].

The working agents in the installations, that operate using the Rankine cycle, present different thermodynamic properties, which influence both the working

conditions, such as pressures and temperatures, as well as the energetic performances, quantified by means of the efficiencies.

Thus, one can define [5] the thermodynamic efficiency $\eta_m$:

$$\eta_m = \frac{L_u}{Q_a} \qquad (1)$$

where, $L_u$ = useful mechanical work,
$Q_a$ = consumed heat,

respectively, the electrical or global efficiency $\eta_e$:

$$\eta_e = \frac{E_e}{Q_a} \qquad (2)$$

where, $E_e$ = electricity produced,
$Q_a$= consumed heat.

Another example of a plant is one that uses the Kalina cycle instead of the Rankine cycle in which an aqueous ammonia-based solution is used as the working agent. Due to the fact that the working fluid is a mixture, the intake and release of heat take place at different temperatures [3], which has the effect of increasing the efficiency of the Kalina cycle by 10-30%.

- **The combined cycle** which consists of a combination between those with steam cycle and those with binary cycle, which allows to achieve a high efficiency of the plant.

In the European project developed in Oradea, after an analysis of specialists, which took into account the temperature, pressure and flow of geothermal water, it was found that the most efficient solution is, in terms of efficiency, the one based on the Kalina cycle and was proposed the scheme of the geothermal power plant presented in figure 2 [2].

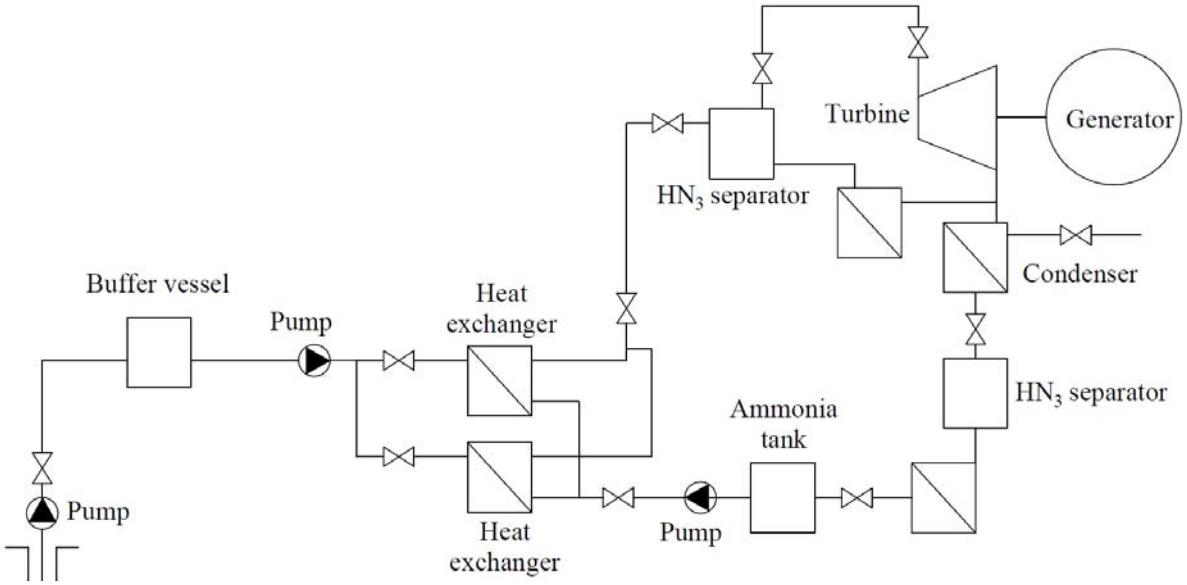


Fig. 2. Diagram of the proposed power plant.

## 3. Interconnection of electricity obtained from renewable resources

In the production of electricity from renewable sources, given their variable nature, an important role is played by the interconnection or integration into the public grid of electricity. Without a prior study by specialists in the field of electricity, the connection of renewable sources to the grid can cause significant disturbances that affect the quality of electricity in the system. It can also be affected by the operation of frequency converters at the interface between the renewable energy source and the public electricity grid, in the absence of an efficient system for limiting the distortion of the electric current curve [6].

The topological models are chosen according to the renewable source used and the type of current obtained (continuous or alternating). One of the methods that allows increasing the efficiency of generation but also the separation of consumption production, is the storage of electricity, which facilitates the transition from the microgrid that generated energy from RES to the public grid.

Among the methods of interconnection of renewable energy sources that produce direct current, we mention the following topologies: the use of buck (down), boost (fly) or flyback converters, controlled by PWM (pulse-width modulation) followed by an inverter [7], [6].

Figure 3 shows the block diagram of the conversion system in which the connection of the renewable energy source to the grid is made by means of a quasi-resonant buck type converter (descending) with zero current switching followed by an inverter. This reduces the switching losses for the main circuit switch and improves system efficiency. The buck converter switch is PFM controlled. If the quasi-resonant topology is used, the current and the voltage take higher values than in the case of non-resonant topologies, but due to the current technologies for the realization of electronic devices, the voltage drops on the conducting devices are reduced [2].

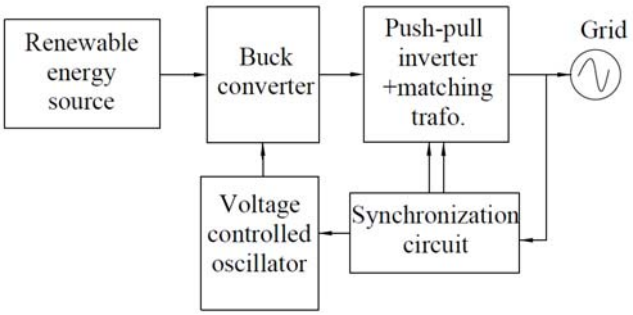


Fig. 3. Block diagram of the conversion system.

In the case of devices interconnected to an AC voltage system, the relationship between the variation of the active power produced and the frequency must be implemented by controlling the interface converters of renewable sources, as well as by a voltage control system.

Figure 4 shows the microgrid through which the energy obtained from a renewable source through which an alternating current was obtained is interconnected, but which is provided with the possibility of storage in batteries [7].

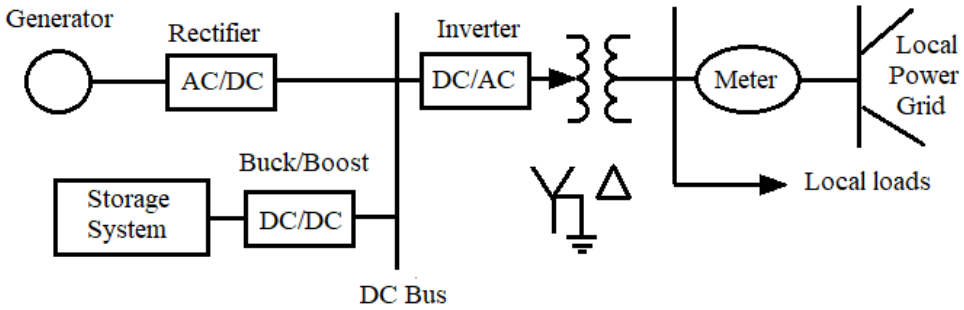


Fig. 4. The interconnection of alternative current to the network.

If it is desired to interconnect several sources that produce electricity to a network (Smart) it is necessary to provide a digital signal processor, which controls the amount of energy and the frequency of the network.

## 4. Conclusions

As the exploitation of geothermal potential for electricity production is expanding, finding efficient conversion technologies becomes imperative. National research becomes very important, given that the actual sources vary from one country to another, even from one area to another (temperature, flow, constancy, etc.). Of course, there are global solutions, but they must be adapted to particular conditions.

As a general feature, it is mentioned that geothermal power plants must be located and operated in the vicinity of the source.

Prior to making a major investment, a feasibility study is required, which involves both a technical and an economic analysis. The latter is based on, inter alia, the annual operating interval, the period for which the possibility of operation is estimated, the cost, the feasibility and the maintenance costs of the equipment are estimated and obviously the real price at which the Kilowatt of electricity will be obtained.

## References

[1] C. Mârza, A. Hoţupan, R. Moldovan, G. Corsiuc, Surse neconvenționale de energie, UT Press, Cluj-Napoca, 2013.
[2] ***Raport Proiect Geo SEE, Oradea 2016, Accesat in 02.05.2020 http://remsis.utcluj.ro/wp-content/uploads/2016/11/Raport-2016-Oradea.pdf.
[3] G. Boyle, Renewable Energy, Renewable Energy – power for sustainable future, Oxford University Press, 2012.
[4] ***https://energyeducation.ca/encyclopedia/Geothermal_power_plants
[5] M. Angelino, M. Gaia, E. Macchi, A review of italian activity in the field of Organic Rankine cycles, Preoceedings of the International VDI- Seminar, Zurich, September, 1984.
[6] ***Raport Holistica impactului surselor regenerabile de energie asupra mediului şi climei 2018, Accesat in 05.05 2020 https://cmu-edu.eu/horesec/wp-content/uploads/sites/17/2019/11/Raportare-stiintifica
[7] A. Keyhani, Design of Smart power grid Renewable energy Systems, Wiley Publications, New Jersey, 2011.

# Modelarea și acționarea electrică a unei mașini de gravat/tăiat cu laser

## Modeling and electric drive of a laser engraving / cutting machine

Cristina Gabriela Sărăcin[1], Mihai Sorin Dincă[1]

[1]Universitatea Polithnica din București, România
Splaiul Independenței Nr.313
*E-mail: cristina.saracin@upb.ro, mihai.dinca98@gmail.com*

DOI: 10.37789/rjce.2021.12.1.5

**Rezumat.–** *Această lucrare prezintă o soluție viabilă de realizare practică a unui mașini de tăiere și gravare cu laser ce poate fi acționată manual sau în regim automat. Aparatul propus este portabil și este ideal pentru gravura simplă și rapidă a diferitelor tipuri de materiale. Aparatul poate grava lemn, carton, plastic, piele, plastic dar, nu poate grava sticlă, ceramică, metal, piatră, marmură. Este un dispozitiv de mici dimensiuni, ce încape pe orice fel de birou și poate fi transportat cu ușurință. Transmiterea informațiilor din procesul de gravare se poate face printr-un program de calculator sau gravarea se poate face manual cu ajutorul unui joystick. În aceste condiții, devine posibilă comanda manuală cât și automată a dispozitivului de tăiere sau gravare cu laser. Având în vedere acest aspect, lucrarea pune accentul atât pe managementul comandării automate a dispozitivului de gravare cât și pe realizarea unei comenzi electronice manuale cu ajutorul unui joystick. Puterea de 1000mW a laserului este suficientă pentru proiecte cum ar fi personalizarea de huse pentru telefon, personalizarea unor obiecte de mici dimensiuni, realizarea de invitații sau cărți poștale decupate, semnarea unor obiecte de design. Aparatul nu poate înlocui un aparat de gravură profesional, de putere mult mai mare, capabil să taie sau să graveze orice fel de material.*

**Cuvinte cheie: gravare cu laser, joystick**

**Abstract.**– *This paper presents a viable solution for the practical realization of a laser cutting and engraving device that can be operated manually or automatically. The proposed device is portable and is ideal for simple and fast engraving of different types of materials. The device can engrave wood, cardboard, plastic, leather, plastic, but it cannot engrave glass, ceramics, metal, stone, marble. It is a small device that fits on any desk and can be easily transported. The transmission of the information from the engraving process can be done through a computer program or the engraving can be done manually with the help of a joystick. Under these conditions, it becomes possible to manually and automatically control the laser cutting or engraving device. Given this aspect, the paper focuses on both the management of the automatic control of the engraving device and the realization of a manual electronic control with a joystick. The 1000mW power of the laser is sufficient for projects such as customizing phone cases, personalizing small objects, making cut invitations or postcards, signing design objects. The machine cannot replace a professional engraving machine with much higher power, capable of cutting or engraving any kind of material.*

**Key words: laser engraving, joystick**

## 1. Introducere

Cea mai importantă funcție a unei mașini cu comandă și control numeric (CNC) este controlul precis și riguros al mișcării. Toate echipamentele CNC au două sau trei direcții de mișcare, numite axe. Aceste axe pot fi mișcate și poziționate precis, de-a lungul intervalului de deplasare. Cele mai cunoscute tipuri de axe sunt cele liniare și de rotație (mișcare curbilinie). Tipul de mișcare (rapid, liniar, circular), axele care se mișcă, distanțele de mișcare și vitezele de mișcare (de prelucrare) sunt programabile.

Avantajele utilizării mașinilor CNC constau în: flexibilitate, repetabilitate, reducerea costurilor pentru scule speciale și a timpilor de pregătire a mașinii, reducerea timpului de calificare pentru operatori, reducerea necesarului de forță de muncă, creșterea calității produselor, creșterea productivității, creșterea siguranței în exploatare.

Totodată gravura laser își dovedește utilitatea într-o mulțime de domenii, precum: evenimente speciale, marketing și domenii industriale.

Plecând de la cele prezentate anterior am încercat să modelăm și să acționăm electric o mașină de tăiat/gravat cu laser de mici dimensiuni.

## 2. Structura sistemului de acționare a mașinii de gravat

Structura metalică care stă la baza realizării dispozitivului, a fost realizată din țeavă pătrată 30x30x2mm. Acest sistem de acționare are rolul de a grava/tăia în diferite forme/modele. În figura 1 se pot observa elementele componente ale sistemului de acționare.

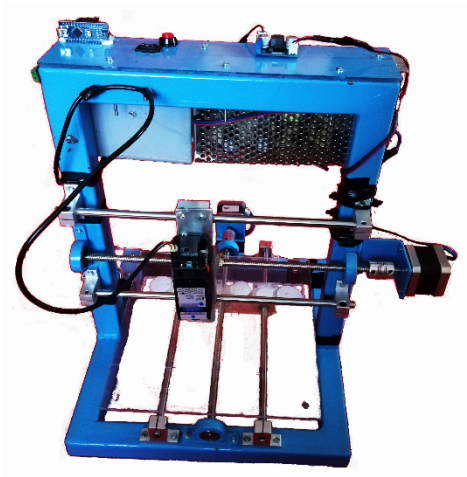

Fig. 1. Structura sistemului de acționare al mașinii de tăiat/gravat cu laser

Pentru realizarea acestuia au fost necesare următoarele elemente:

- cadru metalic;
- bare de ghidaj pentru a asigura deplasarea liniară pe axe;
- bare filetate pentru a realiza efectiv deplasarea pe barele de ghidaj;
- motoare pas cu pas;
- rulmenți liniari;

- Joystick;
- unități de comandă și control;
- sursă 12V;
- modul coborător de tensiune;
- laser pentru gravat.

Sistemul este compus din două părți principale, una orizontală și una verticală. Fiecare parte are la bază trei bare metalice din oțel dispuse paralel, bara din mijloc fiind filetată, aceasta având rolul de acționare a celor două părți mobile, suprafața suport și laserul, antrenate de două motoare pas cu pas.

Barele de ghidaj sunt prinse de cadru metalic prin intermediul unor suporți, iar tija filetată cu ajutorul unor bucși cu rulment. Legatura între bara filetată și motor este realizată printr-un cuplaj flexibil cu diametru interior de 8mm în partea tijei și 5mm în partea motorului.

Translația pe axe se face prin rotirea tijei filetate și alunecarea suportului pentru laser pe barele de ghidaj.

Alunecarea are loc prin intermediul rulmenților liniari SC8UU aflați pe cele două bare de ghidaj.

## 3. Software BenBOX și ABViewer

Software-urile necesare operațiilor de tăiere/gravură sunt: BenBOX și ABViewer 14.

*BenBox* este un software dedicat aplicațiilor de tip CNC, cu o interfață ușor de intuit, care permite comandarea procesului de gravare prin introducerea unui desen, unui text, dar și prin scrierea comezilor în limbajul G-Code (limbaj comun mașinilor de tip CNC). Un exemplu de gravare a unui text utilizând programul BenBox este prezentat în figura 2.


Fig. 2. Exemplu de gravare cu textul “Licență”

Două dintre metodele de gravat utilizate sunt: Outline (urmărește conturul exterior al literelor) și Scan by Z-Shapes (gravarea completă a textului).

Exemplificăm în figura 3 realizarea acestei gravări pe carton în cele două moduri.


Gravare Outline


Gravare Scan by Z-Shapes

Fig. 3. Rezultatul gravării

*ABViewer 14* este un software ce permite desenarea și importarea de fișiere tip CAD și exportarea acestora în fișiere de tip G-Code.

Etapa 1 constă în realizarea unui desen și transformarea acestuia în linii de cod. Acest lucru este realizat în secțiunea Imprimare > CAD to G-Code.

Fișierul obținut prin conversie este prezentat în figura 3.

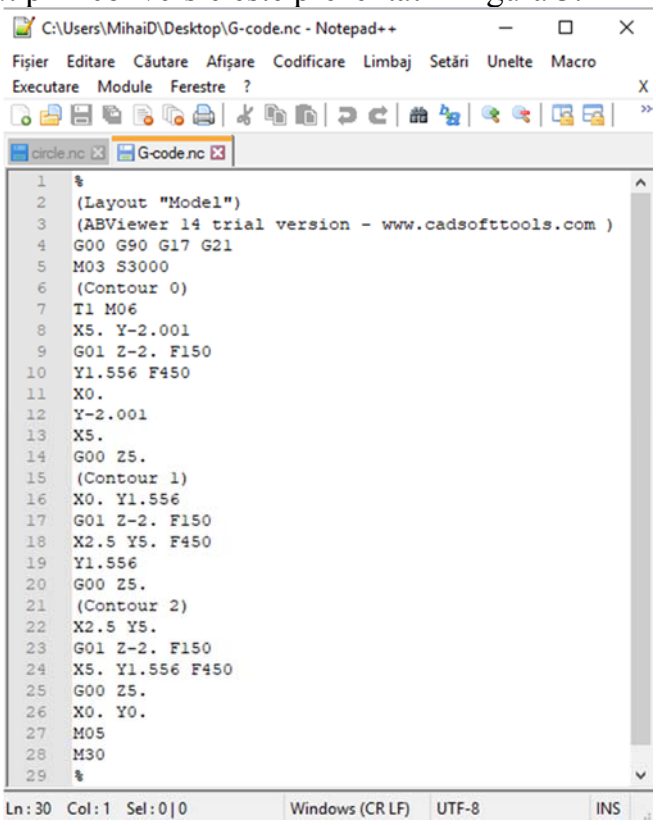


Fig. 3. Linii de cod in limbajul G-code.

Etapa a doua constă în trecerea codului din figura 3 în secțiunea dedicată ecranului GCode a software-ului Benbox și rularea instrucțiunilor generate (figura 4).

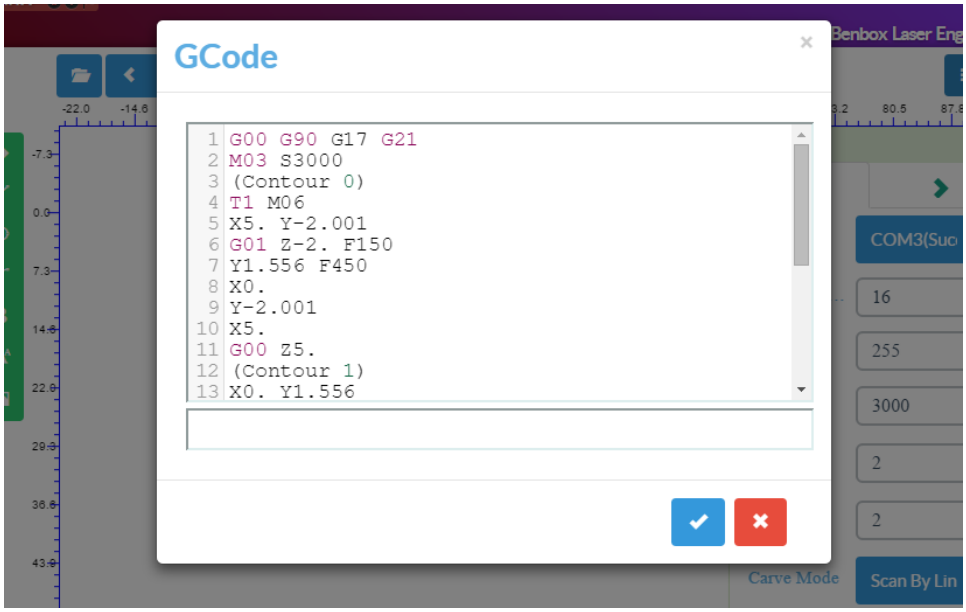


Fig. 4. Rularea programului generat în Benbox

Etapa a treia constă în obținerea imaginii pe materialul dorit.

## 3. Utilizarea software-ului Arduino IDE

Utilizarea plăcilor de dezvoltare Arduino a condus la alegerea software-ului Arduino IDE. Acest soft a fost utilizat pentru scrierea programului de regim manual care presupune controlul deplasării pe cele două axe prin intermediul unui Joystick.

O secvență din acest program este prezentată în figura 5.

```
#define EN        8
#define x_pin     A0
#define y_pin     A1
#define LASER     4
#define SW        A2
//Direction pin
#define X_DIR     5
#define Y_DIR     6

//Step pin
#define X_STP     2
#define Y_STP     3
int valx=0;
int valy=0;
int valsw=0;
void setup(){
```

```
pinMode(X_DIR, OUTPUT); pinMode(X_STP, OUTPUT);

pinMode(Y_DIR, OUTPUT); pinMode(Y_STP, OUTPUT);

pinMode(EN, OUTPUT);
pinMode(x_pin, INPUT);
pinMode(y_pin, INPUT);
pinMode(LASER, OUTPUT);
pinMode(SW,INPUT);
digitalWrite(LASER, LOW);
digitalWrite(EN, LOW);
digitalWrite(X_STP, LOW);
digitalWrite(X_DIR, LOW);
digitalWrite(Y_STP, LOW);
digitalWrite(Y_DIR, LOW);
```

Fig. 4. Programul necesar regimului manual al Joystick-ului

În prima parte a programului s-au declarat pinii necesari intrărilor respectiv ieşirilor. Apoi în partea a doua, am setat patru intervale de valori, pentru cele patru sensuri de mişcare şi un interval pentru butonul joystick-ului ce întrerupe raza laser.

Diagrama procesului de gravare este prezentată în figura 6.

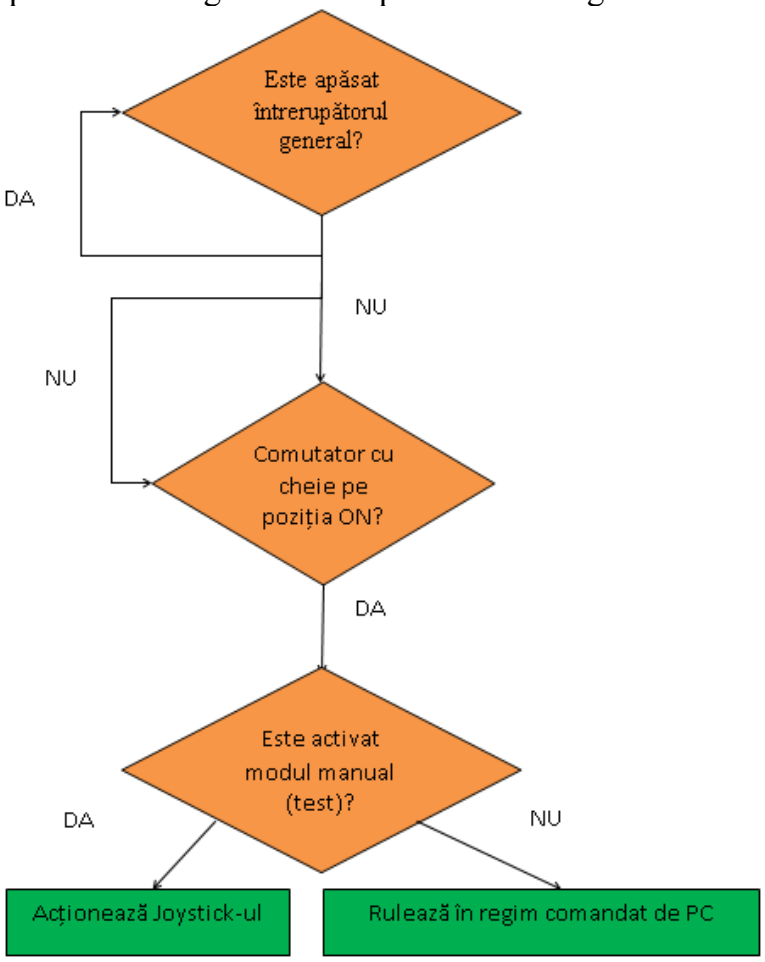


Fig. 5. Diagrama procesului manual/automat de gravare

## 4. Modul de funcţionare al maşinii de gravat

Se realizează alimentarea la 230V CA si prin intermediul sursei de 12V se face alimentarea shield-ului CNC, modulului StepDown şi a laserului.

Pentru utilizarea maşinii de gravat în mod automat se conectează placuţa Arduino Uno la PC, se deschide programul Benbox, se setează parametrii de gravare/taiere, se încarcă imaginea de prelucrat, se poziţionează laserul în punctul zero (punct de plecare) şi se iniţiază procesul.

Utilizarea maşinii în modul manual, presupune întreruperea conexiunii cu calculatorul şi apăsarea butonului de regim manual. În acest mod comenziile de mişcare şi pornire/oprire a laserului sunt date de la Joystick.

Programul de regim manual este încarcat pe plăcuța Arduino NANO. Aceasta primește diferite valori de tensiune de la Joystick, și trimite mai departe comanda către Shield-ul CNC.

Întrucât Arduino NANO are un număr redus de pini, pentru punerea în funcțiune a Shield-ului se impune și alimentarea Arduino UNO în paralel. Alimentarea se face prin modulul coborâtor, care transformă tensiunea de 12V de la intrare, în tensiune de 5V la ieșire. Această alimentare se face cât timp mașina este în regim manual; pentru regimul automat această alimentare are loc prin USB.

Pe partea de comandă între Arduino NANO și Shield s-au folosit diode pentru a evita alimentare plăcuței Arduino atunci când comenzile sunt date de la calculator.

În cazul unor defecțiuni sau erori de comandă, alimentarea cu energie electrică poate fi întreruptă prin apăsarea butonului roșu poziționat la vedere.

În urma testelor realizate s-au efectuat următoarele operații și reglaje:

- barele de ghidaj și tija filetată să fie paralele, cu o abatere de maxim 1mm;
- valoarea tensiunii de ieșire a modulului coborâtor să fie 5V;
- calibrare motoare pas cu pas.

În continuare s-au calibrat driverele A4988 ale motoarelor pas cu pas conform specificațiilor tehnice. Valoarea tensiunii a fost calculată conform relației:

$$Vref=Imax*(8*Rs)*0.7$$

unde: $Imax=1.7A$, $Rs=R100=0.1\Omega$ (driver A4988)

Rezultă: $Vref=1.7*(8*0.1)*0.7=0.952V$

În funcție de materialul folosit și de distanța dintre acesta și laser se reglează viteza de translație și focalizarea laserului. În modul automat acest lucru se face prin setarea unei valori mai mici în secțiunea Speed. În modul manual viteza motoarelor se micșorează prin mărirea delay-ului dintre liniile de cod. De la 5 microsecunde la 10, 20, 30 de microsecunde.

Focalizarea laserului se realizează prin ajustarea distanței dintre cele două lentile.

## 5. Concluzii

În această lucrare este descrisă structura sistemului de acționare al unei mașinii de gravat/tăiat cu laser și programele necesare realizării fișierelor G-Code. Totodată este prezentat programul de comandă realizat pentru placa Arduino, program necesar acționării electrice a motoarelor mașinii de gravat/tăiat cu laser.

Rezultatele acestei lucrări constituie baza construcției unei mașini de gravat și evidențiază procesul de transformare a unui dispozitiv din stadiul de proiectare în stadiul de realizare practică.

Totodată, principalul aspect prin care dispozitivul realizat se diferențiază de alte variante de astfel de echipamente, îl reprezintă implementarea regimului manual. Acest lucru a fost realizat prin acționarea a două plăci Arduino în paralel comandate printr-un Joystick.

Îmbunătățirile care pot fi aduse acestui dispozitiv sunt următoarele: laser mai puternic capabil să taie sau să graveze orice tip de material, alimentare pe baterie,

modificarea sistemului electronic pentru transmisie prin Bluetooth sau pentru implementarea celei de-a treia axe. În acest mod, maşina de gravat/tăiat poate fi transformată într-un dispozitiv de gravare 3D care poate funcţiona pe baterii şi poate primi prin bluetooth coordonatele de gravare de la un laptop.

## Referinţe

[1] C. G. Sărăcin, M. Sărăcin, V.V. Golea, „Sisteme de telemăsurare”, Editura Matrix ROM, 2004.
[2] C. G. Sărăcin, „Instalaţii electrice”, Editura Matrix ROM, 2009.
[3] https://www.ulsinc.com/learn/history-of-lasers
[4] https://www.slideshare.net/amtecincproduct/laser-engraving-machine-85906538
[5] https://www.laserinventor.com/bio.html
[6] https://ethw.org/Theodore_H._Maiman?gclid=CjwKCAjw88v3BRBFEiwApwLevaSdlBrUxkjmvj3nXYjax4r5EPaR-VqYUhACXJwdrtJnymtvLKROiRoC6VYQAvD_BwE
[7] https://ethw.org/Oral-History:Kumar_Patel

[8] https://techchannel.att.com/play-video.cfm/2012/5/25/AT&T-Archives-Invention-of-Laser
[9] https://endurancelasers.com/how-to-run-benbox-mdraw-and-cncc-laseraxe/
[10] https://www.pololu.com/file/download/A4988.pdf?file_id=0J450
[11] http://www.zyltech.com/arduino-cnc-shield-instructions/
[12] https://www.thefabricator.com/thefabricator/article/plasmacutting/the-life-and-times-of-plasma-cutting
[13] http://ro.jiahecncrouter.com/info/classification-of-cnc-engraving-machine-20393091.html
[14] https://www.woodworkweb.com/woodwork-topics/wood-turning-and-carving/580-how-to-use-benbox-software.html
[15] https://diymachining.com/g-code-example/
[16] https://www.epiloglaser.ro/laser-engraving/

# Contribution of compressed stabilized earth bricks (CSEB) to the control of indoor air quality in buildings: case study of Algeria

Fezzioui Naïma [1], Miloudi Yassine [1], Roulet Claude-Alain [2]

[1] Laboratory of Mechanical and structures L.M.S., Tahri Mohamed University Institute. BT214, Bechar, Algeria
*E-mail: naifez@gmail.com, miloudi.yacine@hotmail.fr*

[2] École Polytechnique Fédérale de Lausanne
CH-1015 EPFL; City: Lausanne; Country: Switzerland
*E-mail: claude.roulet@epfl.ch*

DOI: 10.37789/rjce.2021.12.1.6

**Abstract.** *The aim of this work is to examine the thermohydric behavior of a building made of compressed stabilized earth bricks (CSEB), by testing its effectiveness in stabilizing the quality of indoor air, compared to four conventional materials. The study is carried out using TRNSYS-COMIS software with its Buffer Storage Humidity Model for three types of climates: desert, Mediterranean, and dry and cold semi-arid climate. The results highlight the contribution of the CSEB material in regulating the indoor relative humidity of buildings, also in limiting the effects of condensation thanks to its adsorption effect.*

**Keywords:** Indoor air quality, condensation, compressed stabilized earth bricks, simulation, hygrothermal behavior.

## 1. Introduction

The transport of heat and moisture in building materials has a direct impact on air quality, mold development, temperature fluctuation and thermal comfort, and therefore on the reduction of energy consumption, in addition to their direct impact on the sustainability of the building [1-3]. The indoor air quality of buildings has itself a direct impact on the health of occupants and their thermal comfort; it is managed by certain parameters linked to habitable environments[4]. Humidity is an intrinsic parameter in buildings, and its excess can increase the prevalence of certain pathologies, and cause moisture condensation, mold growth, insulation failure and degradation of materials, etc [5]. Too dry air favors the irritation of mucous membranes. In addition, experimental studies on airborne-transmitted infectious bacteria and viruses [34] have shown that the survival or infectivity of these organisms is minimized by exposure to relative humidity between 40 and 70%.

Earth blocks and other naturally based hygroscopic materials have become a promising new way of achieving a sustainable and ecological building. Globally, about a third of the human population resides in earth shelters. In developing countries, this number is estimated at 50% [6]. According to several studies, the earth material has a good ability to regulate and stabilize internal humidity [7, 8] and thus contributes to the creation of a healthy and comfortable atmosphere in buildings. Some research has shown that unfired earth stabilizes the relative humidity of a house at 60% around the year [9], and that the absorption capacity of earth blocks can reach 10 times that of ordinary brick [10].

The disadvantage of the earth material dwells in its sensitivity to climate change which makes it relatively fragile. Compressed stabilized earth brick (CSEB) presents itself as one of the types of stabilized earth materials which aim to improve the mechanical performance of earth [11]. Several studies which have shown its resistance to compression, which can reach that of ordinary brick [12], and its good contribution to the regulation of internal humidity in buildings by comparing it to brick and to other common building materials [13]. Several studies have examined the hygroscopic behavior of earth brick: whether it is compressed and or stabilized by examining the effect of stabilizers which may constitute it and the influence of their percentage [14-16] or the effect of compaction [16]; but the majority of this research was carried out on the scale of the material or on the level of the wall [17, 18]. Indeed the type of stabilizer and its concentration modifies the microstructure of the material and thus causes a big change in its hygrothermal behavior [15]. Stabilization decreases the hygroscopic capacity of the earth [16, 17]. Some have experimentally examined the temperature and relative humidity in earthen material buildings [19-21]; but few studies have evaluated the quality of indoor air by measuring condensation and relative humidity in buildings made of CSEB.

The hygroscopic behavior of a material differs according to the nature of the climate, and according to the domestic activities and the behavior of the occupants [22]. The studies examining the effect on indoor air quality were mostly performed for humid climates. Very few have studied hygroscopic behavior in a hot and dry climate, and from our observations, even in a dry climate, a building can have risks of condensation in the absence of adequate ventilation, especially in winter and mid-season. Zhang et al [5] examined the behavior of a building in earth brick in the desert climate of the Turpan Prefecture in Northwest of China, assessing its relative humidity and indoor temperature. Therefore, the objective of this work is to examine the contribution of CSEB in the regulation of indoor relative humidity, and the generation of condensation, following the domestic activities, and depending on the contributions of the water vapor generated during the use of the building, by comparing it to other materials commonly used in construction, and this for three Mediterranean sub climates: mild Mediterranean climate, temperate climate, dry and cold semi-arid climate, desert climate and very desert hot climate.

## 2. Earth construction and climate

The effectiveness of earth material strongly depends on the climate, and in particular on the rain which is the first responsible for the degradation of earth building, especially if it is not stabilized [23]. During its history, Algeria has used raw earth for buildings since ancient times. The country experiences precipitation rates that encourage earth construction; it rains in the south a few days a year and in the north between 70 and 100 days a year [24].

Algeria presents a variety of climates which goes from the Mediterranean climate (Köppen classification Csa) to Tell and more exactly in the north of the country, to the desert climate (Köppen classification BWh) in the south, crossing the highlands with a semi-arid climate (Köppen classification BSk), and other inland cities whose climate varies from warm temperate climate, steppe climate, to a semi-arid Mediterranean climate. The desert climate itself is classified according to its aridity: Desert climate in the pre-Saharan zone, typically Saharan hot desert climate and Hyper-arid climate.

Ghedamsi et al [25] produced a map of climatic zones in Algeria based on the heating and cooling energy costs. Following this map, we selected five cities to test our hygroscopic behavior of the CSEB matrix: Oran (mild Mediterranean climate), Constantine (a temperate climate), Elbayadh (dry and cold semi-arid climate of the highlands), Bechar (desert climate), Naama (steppe climate) and Adrar (very hot desert climate).

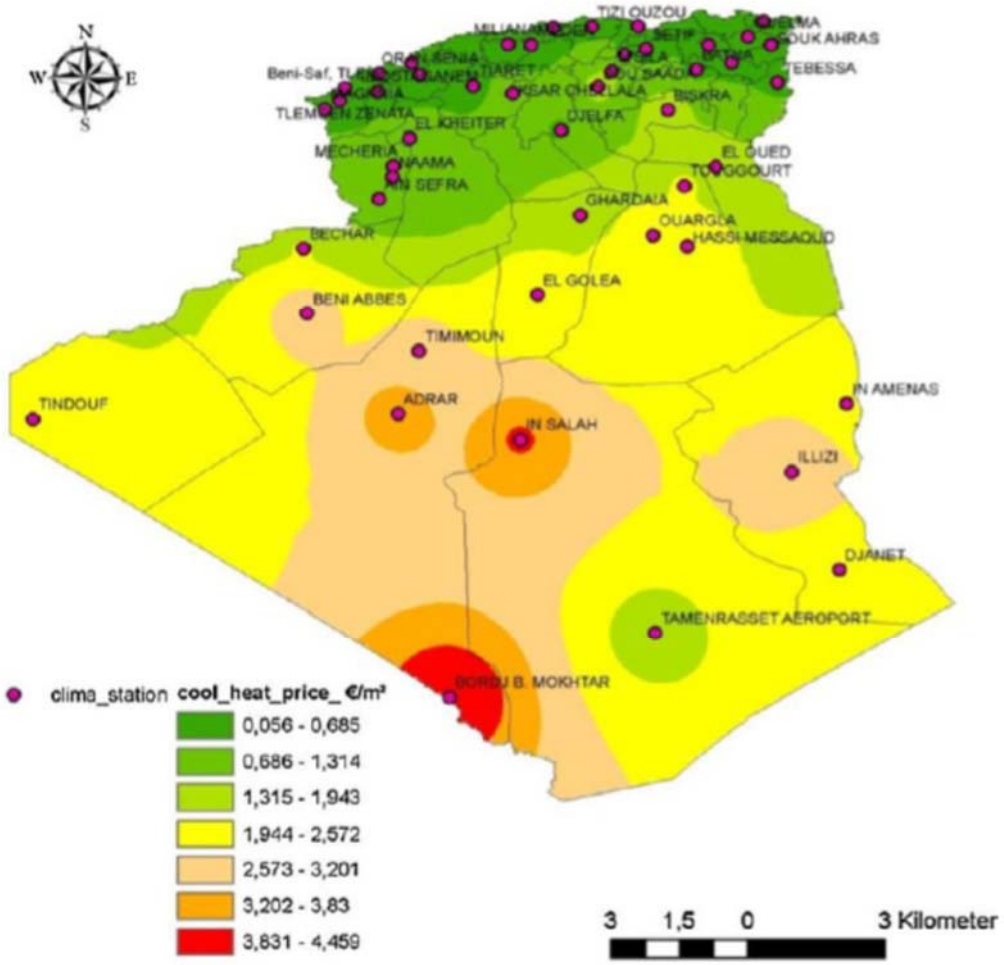


Fig. 1. Climatic zones in Algeria according to energy consumption costs [25]

## 3. Building Characteristics

The compressed stabilized earth bricks (CSEB) used in this work was thermally and hygroscopically characterized in the work of Miloudi et al [26] and mechanically in the work of Mahdad et al [27]. Table 1 describes the characteristics of this CSEB material. Our simulations are carried out on a two-storey building whose standard plan of one of these apartments is given in Figure 2. The different layers of the building envelope are defined from the outside to the inside of the area in the table 2.

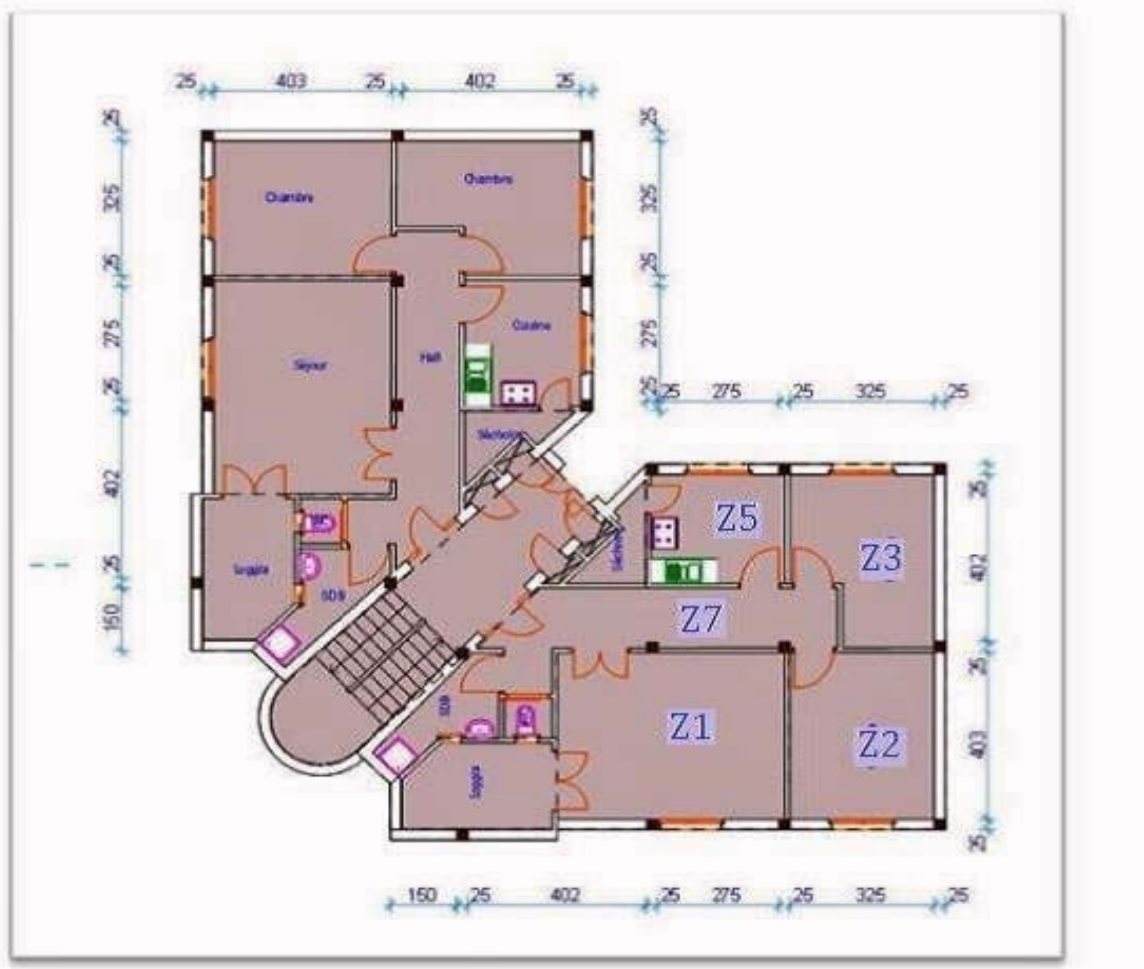


Fig.2. Standard floor plan of studied building

*Table1*

**CSEB properties [26] [27]**

| Property | |
|---|---|
| Thermal conductivity [W/m°K] | 0.75 |
| Specific density [kg/m$^3$] | 2125 |
| Bulk density [kg/m$^3$] | 2100 |
| Specific heat [J/kg.K] | 1054 |
| Vapor permeability in air "$\delta p$" [kg/m².s.Pa] | 1,175. $10^{-11}$ |
| Water vapor permeability "W" [kg/m².s.Pa] | 5,9. $10^{-10}$ |
| Water vapour diffusion resistance factor "$\mu$" [-] | 17,03 |
| Total porosity [%] | 23% |
| Open porosity [%] | 19% |
| Closed porosity [%] | 4% |
| Resistance in compression (MPa) | 7,1 |

*Table 2*

Composition of the building components

| Designation | Material and thickness | U [W/ (m².K)] |
|---|---|---|
| External wall | CSEB 14 cm | 2.804 |
| Inner Walls | CSEB 12 cm | 3.030 |
| Low floor on ground | Tiling 2cm<br>Cement mortar 2 cm<br>Sand 1cm<br>Reinforced concrete 4cm<br>Stones 20cm | 2.494 |
| Middel floors | Tiling 2cm<br>Cement mortar 2 cm<br>Sand1 cm<br>Reinforced concrete 4 cm<br>Slab 16 cm<br>Internal finishing 2 cm | 1.846 |
| Roof | Cement mortar 2 cm<br>Slab 16 cm<br>Reinforced concrete 4cm<br>Watertight layer1 cm | 2.102 |

The ground floor is in direct contact with the ground while the ceiling of the top floor is in contact with the outside atmosphere. The windows have a **PV**C frame with single glazing, their heat transfer coefficient U and solar factor are 5.75W / m²K and 75% respectively. The occupancy characteristics are assumed to be the same for each apartment, and they are managed by the building use scenarios as shown in the histograms 3-4, and in Table 3.

Table 3

**Use schedule and Powers released by household appliances**

| Apparatus | Zone | Use schedule | | Power w |
|---|---|---|---|---|
| Refrigerator | Z5<br>(Cuisine) | 24/24 | | 100 |
| Television | Z1, Z4, Z3 | In Winter:<br>Z1 :Occupied<br>Z3 :18h to23h<br>Z4 :21h to23h | In Summer:<br>Z1 : occupied<br>Z3 :9h to 12h&<br>18h to 24h<br>Z4 :14h to 17h &<br>21h to 23h | 150 |
| Computer | Z2, Z3 | Z2 : 13h<br>to14h & 18h<br>to23h<br>Z3 :17h to 23h | Z2 : 10h to12h &<br>14h to 17h & 21h<br>to 24h | 100 |

| | | | | |
|---|---|---|---|---|
| | | | Z3 : 9h to12h & 18h to 24 | |
| Cooker | Z5 (Kitchen) | Occupied | | 550 |

We have assumed a mechanical exhaust ventilation for stale air at 15m³ /h for the bathroom and the toilets, these values are recommended by the document [28]. However, for the kitchen and the other rooms of the apartment, we assumed scenarios of door and window openings as indicated in the table 4. The aeraulic modeling of the building is carried out with TRNSYS / COMIS coupling through TYPE 157 which exchanges information between the two programs at each time step, in order to calculate the air flow exchanged between the zones and between zones and outside, from weather data transmitted to COMIS through TRNSYS.
The boundary conditions of the apartments on the ground floor and upstairs are identical.

Table 4

**Scenarios openings of doors and windows**

| Period | Windows | | Doors | |
|---|---|---|---|---|
| | Closed | Opened | Closed | Opened |
| Summer | 10h – 18 h | 18h – 7h | - | 24h: de 7h to 18h at 100% and from 18h to 7h at 10% |
| Winter | 10h to 09h | 09h – 10h at 50% | 18h – 10h | 10h – 18h |

The TRNSYS Buffer Storage Humidity Model [29] was used to calculate the moisture adsorption-desorption of building materials.

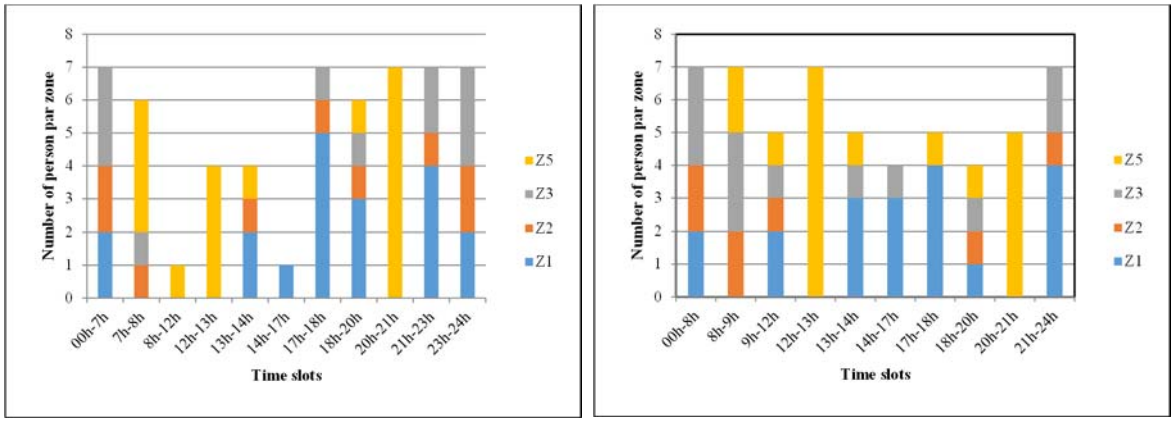


Fig. 3. Occupancy scenarios of the different zones in winter for the apartment (left during the week, right for the weekend)

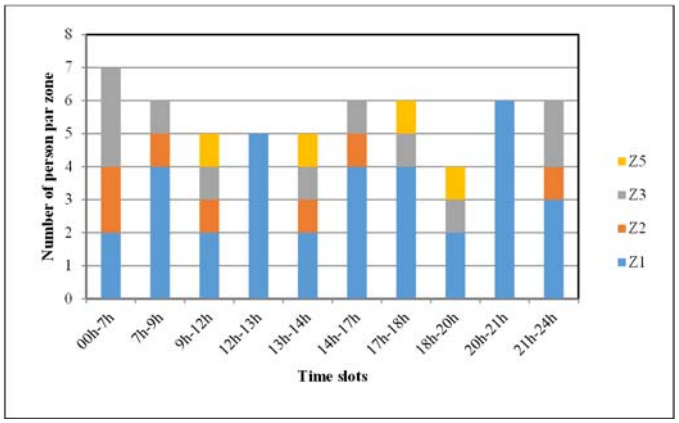


Fig. 4. Occupation scenarios of the different zones in summer for the apartment

Tables 4 and 5 give the values of the parameters of the Buffer Storage Humidity Model for CSEB materials and aerated concrete.

Table 5

**Parameters of the buffer storage humidity model for a standard apartment in the building studied / CSEB case**

| zone | Surface Buffer Storage | | | Deep Buffer Storage | | |
|---|---|---|---|---|---|---|
| | $\kappa_{surf}$ | $M_{surf}$ | $\beta_{surf}$ | $\kappa_{deep}$ | $M_{deep}$ | $\beta_{deep}$ |
| Z1 | 0.005 | 684 | 163 | 1 | 19 | 54. |
| Z2 | 0.005 | 500 | 119 | 1 | 14 | 40 |
| Z3 | 0.005 | 625 | 149 | 1 | 15 | 50 |
| Z5 | 0.005 | 420 | 100 | 1 | 9 | 33 |
| Hall | 0.005 | 400 | 95 | 1 | 143 | 31 |

Table 6

**Parameters of the buffer storage humidity model for a standard apartment in the building studied / case Aerated concrete**

| zone | Surface Buffer Storage | | | Deep Buffer Storage | | |
|---|---|---|---|---|---|---|
| | $\kappa_{surf}$ | $M_{surf}$ | $\beta_{surf}$ | $\kappa_{deep}$ | $M_{deep}$ | $\beta_{deep}$ |
| Z1 | 0.04 | 717.02 | 162.96 | 1 | 44.23 | 54.32 |
| Z2 | 0.04 | 522.72 | 118.8 | 1 | 32.1 | 39.6 |
| Z3 | 0.04 | 654.72 | 148.8 | 1 | 37.71 | 49.6 |
| Z5 | 0.04 | 138.24 | 99.8 | 1 | 24.89 | 33.23 |
| Hall | 0.04 | 415.53 | 94.44 | 1 | 22.23 | 31.49 |

Table 7 describes the configurations used in this study. The composition of the floors is the same as that of the reference case (Table 3).

Table 7

**Composition of the walls of each configuration**

| Configuration | External walls | | Internal walls | |
|---|---|---|---|---|
| Plaster | Plaster 8 cm, aerated concrete 25 cm, Cement mortar 2cm | 2.07 W/m²k | Plâtre 2 cm, aerated concrete 10 cm, Cement mortar 2cm | 3.29 W/m²k |
| Aerated concrete | Aerated concrete 14 cm | 3.70 W/m²k | Aerated concrete 12 cm | 3.91 W/m²k |
| Brick | Cement mortar 2 cm, red brick 25 cm, Cement mortar 2cm | 2.57 W/m²k | Cement mortar 2 cm, red brick 10 cm, Cement mortar 2cm | 3.65 W/m²k |
| Concrete blocks | Cement mortar 2 cm, aerated concrete 25 cm, Cement mortar 2cm | 2.57 | Cement mortar 2 cm, aerated concrete 10 cm, Cement mortar 2cm | 3.73 W/m²k |

## 4. Results and discussion

Our analysis of the results is based on indoor air relative humidity as well as surface condensation as indicators of air quality. Condensation occurs when the water vapor pressure at a certain point reaches the corresponding saturation vapor pressure for the temperature at that point. It can be apparent (surface condensation) or hidden (internal condensation). Surface condensation can occur in the summer when a window is poorly sealed, allowing outside hot, humid air to enter the cool room, or in winter, when the thermal insulation of the building envelope, including its exterior walls, roof and windows, is insufficient, lowering the surface temperature inside the building [30].

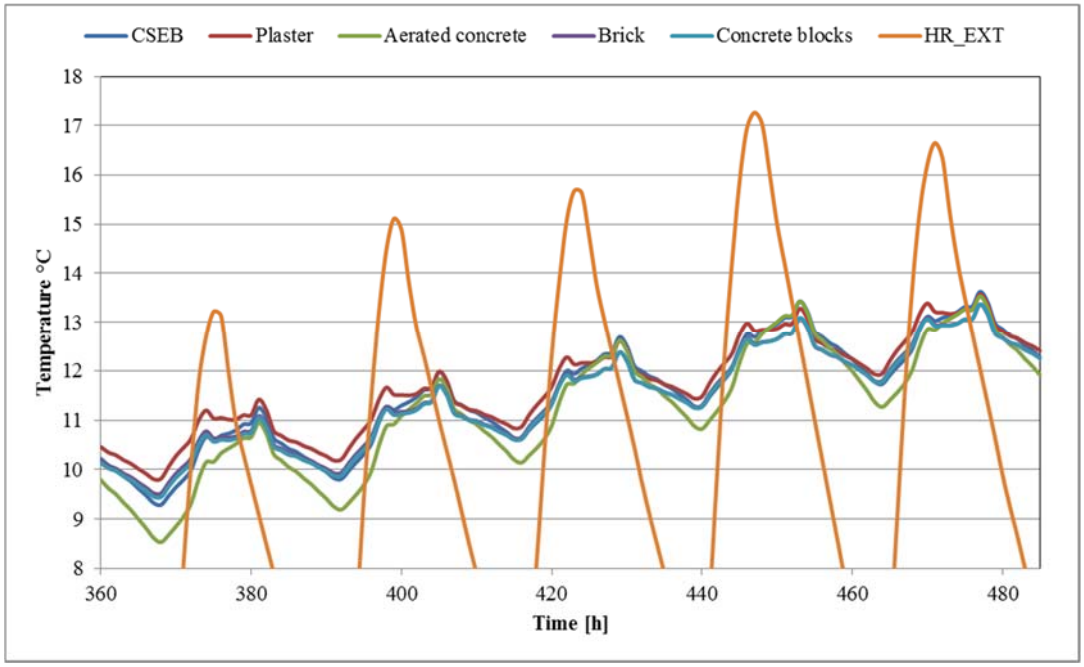


Fig.5. Temperature of zone Z1 of the apartment on the ground floor for the different materials tested during 5 days in January

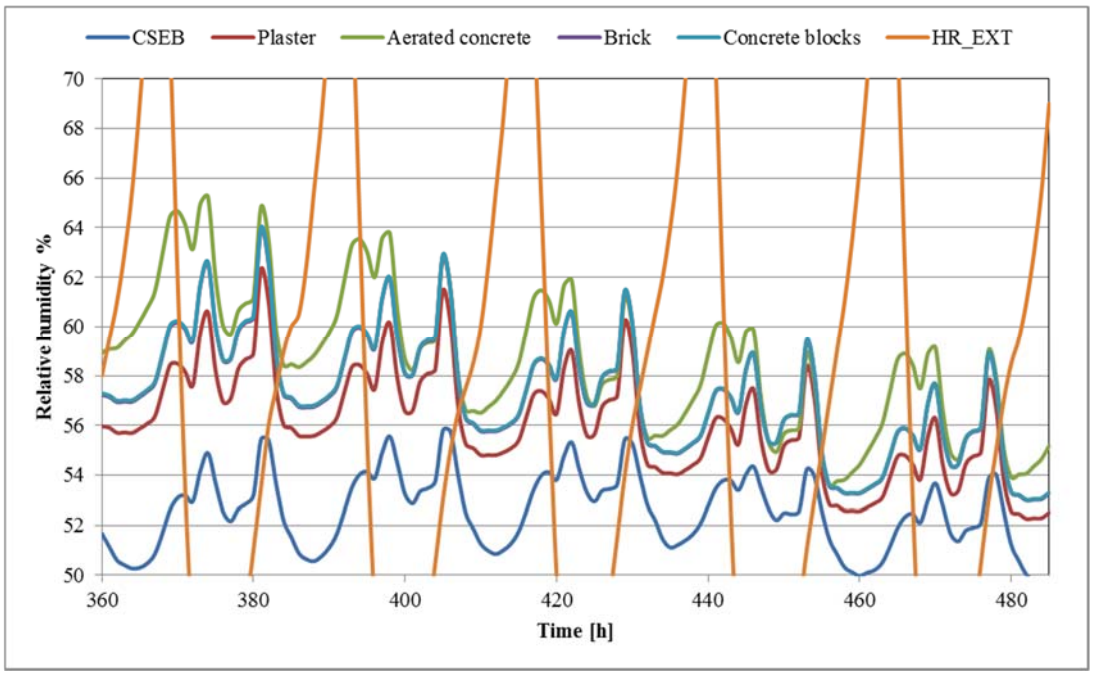


Fig. 6. Indoor relative humidity in zone Z1 of the ground floor apartment for the different materials tested during 5 days in January

Figures 5-8 compare the temperature and relative humidity in zone Z1 (living room) on the ground floor for the different materials tested, for five days in mid-July and five days in mid-January for the city of Bechar.

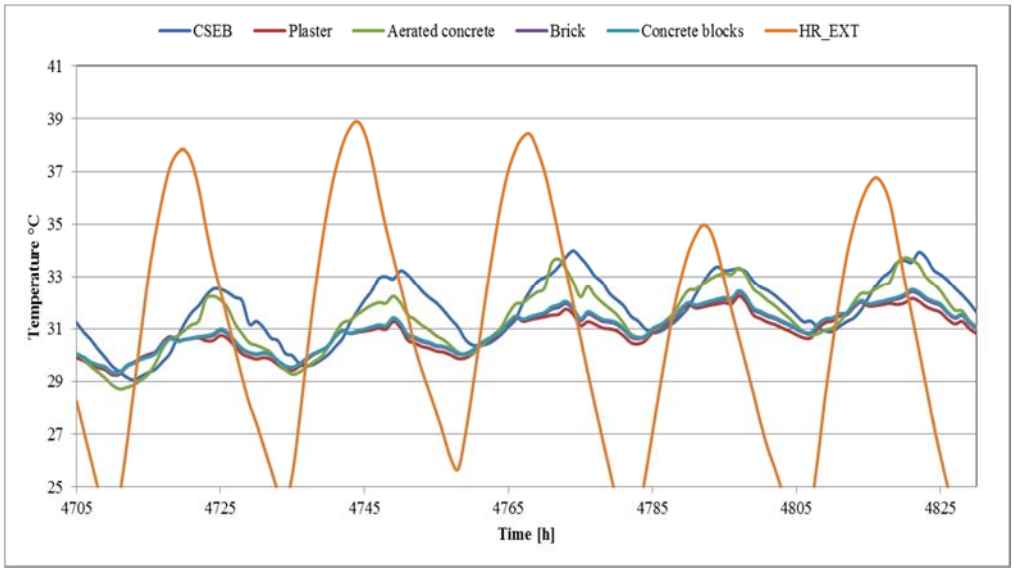


Fig.7. Interior temperature of zone Z1 of the ground floor apartment for the different materials tested during 5 days in July

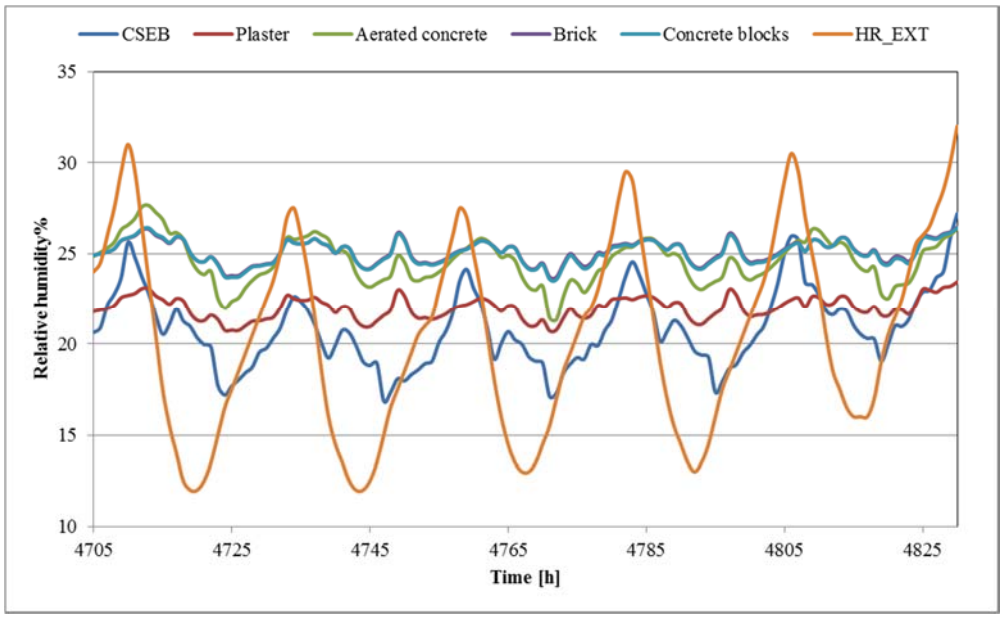


Fig.8. Indoor relative humidity in zone Z1 of the ground floor apartment for the different materials tested during 5 days in July

The effect of the humidity regulation by the CSEB material is well observed in the two figures. In fact, its curve is below all the others and varies with less amplitude in summer. This is due to its higher moisture sorption power [26].

The five configurations examined stabilize the temperature of the room and keep it lower than that of the outside during the hottest hours of the day. In the evenings, this temperature drops with a difference of 4°C compared to that during the day, without reaching the outside temperature which becomes lower in the evenings, which shows the insufficiency of the natural ventilation proposed. Differences of more than 6°C were observed between the night temperature of the room and that of the outside. The temperature with CSEB is higher than with the other materials tested. In addition, the relative humidity associated with CSEB in summer is the lowest, and varies with greater amplitude compared to other configurations. The behavior of the plaster wall is fairly close to that of brick and concrete block but with lower values. The humidity with aerated concrete evolves with a lower amplitude than that with CSEB, it sometimes reaches values higher than that of brick and concrete block but always remains higher than that with CSEB and plaster.

The annual total amount of condensing hours is shown in Figure 5.20 for the six climate zones and for both CSEB and aerated concrete.

Condensation occurs in winter, especially in December and between 5 a.m. and 7 a.m. It also occurs in the intermediate period for the cities of Oran, Constantine and Elbayadh. The risk is higher for the top floor because its roof is exposed to low temperature of outdoor air. The risk of condensation in Constantine is greatest, due to the relatively high humidity combined with very low temperatures in winter. Comes after that of the city of Oran which is less important even if the city presents a fairly humid climate in winter, but with milder temperatures. On the other hand, the probability of having this phenomenon in Adrar is almost zero, only 3 hours of condensation was observed for this city, in the kitchen on the first floor.

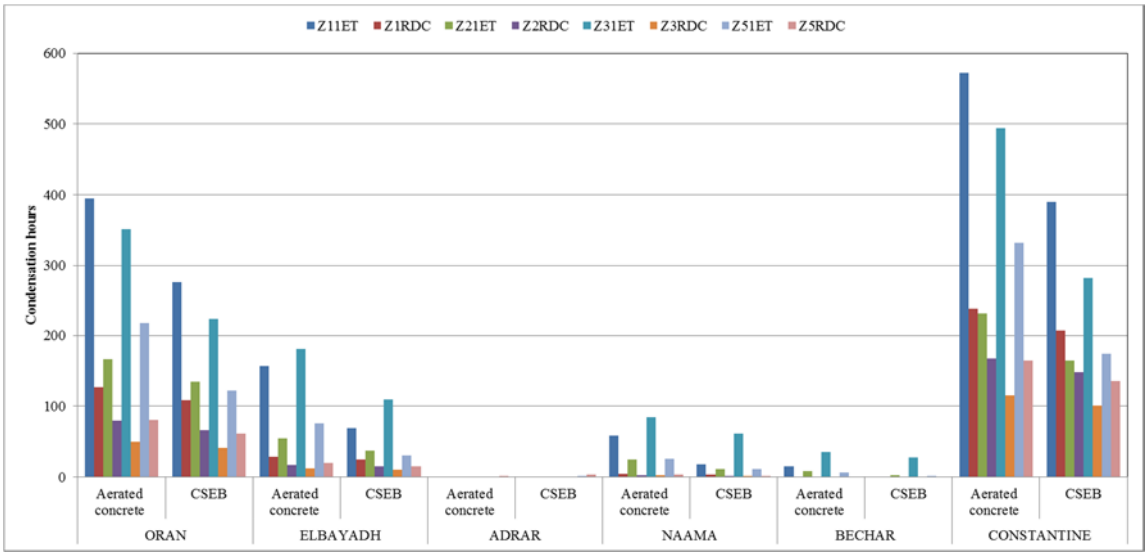


Fig.9. The total number of hours of condensation for CSEB and Aerated concrete in the different climatic zones

The top floor roof sees more hours of condensation compared to the other walls as shown in Figure 10, which gives an example of these percentages for the CSEB in Constantine. The western surface, even protected, sees more hours of condensation than the northern and southern surfaces (which is also protected). The main reason for this is that, as condensation usually occurs early in the morning [30], direct solar radiation first strikes surfaces facing north, below the horizon, after that towards the south and this reduces the number of hours of condensation with respect to surfaces facing west. The protected southern surface presents a greater risk of condensation than that of the unprotected eastern surface; and we can explain it by the solar radiation which can reach the east surface in the first place.

The CSEB presents satisfactory results in comparison with aerated concrete, especially for rooms on the top floor. For all the cities examined, it is the kitchen that is most sensitive to the integration of this material, except in Naama and Bechar where Z1 on the first floor was the most influenced. This can be explained by the less humid climate of these latter cities, where the humidity supply in the building is mainly based on the internal water supply (occupants and activity).

The impact of CSEB is significant in Constantine where differences of more than 200 hours have been determined between the two materials for zone Z3.

In Oran, the CSEB reduces the condensing hours by a percentage ranging from 15 to 24% for rooms on the ground floor and from 19 to 44% for rooms on the first floor. Nevertheless, for the city of Elbayadh, the reduction of these condensation hours varies between 32% to 60% in the 1st floor apartment, while its contribution for the areas of the ground floor is relatively poor with reduction percentages ranging from 6% to 22%. Unlike the cities of Constantine and Oran where the Z3 zone has seen a good reduction, in Elbayadh it is the Z1 which has the hours of condensation better reduced with a percentage of 56%.

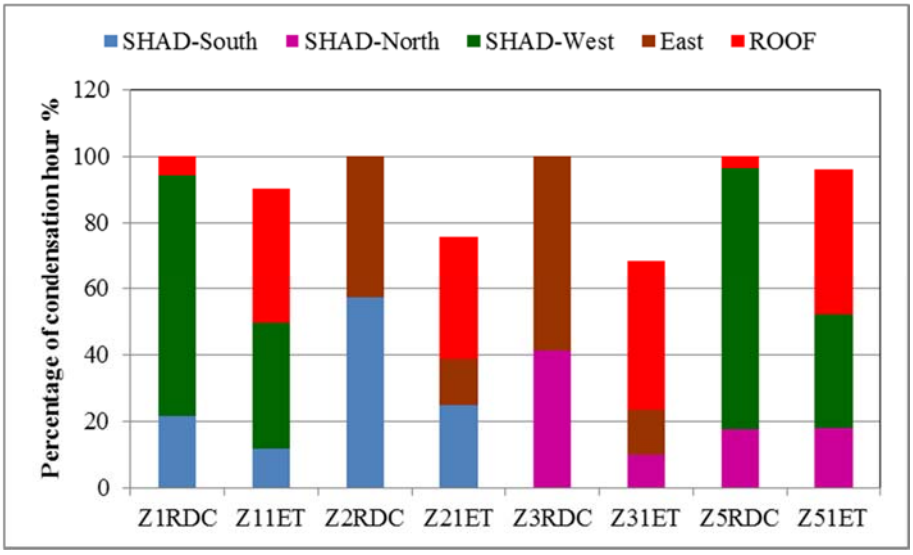


Fig.10. Percentage of occurrence of condensation on each orientation, for the BTCS, City of Constantine

Condensation on the interior surfaces of the enclosure occurs at 100% relative humidity which remains on these surfaces for periods of a few hours [31]. So for more information on the hydric behavior of the studied building, we show a distribution of the frequencies of occurrence of the indoor air relative humidity for the CSEB material and the aerated concrete (Concrete) for representative cities. The results obtained are shown in figure 11.

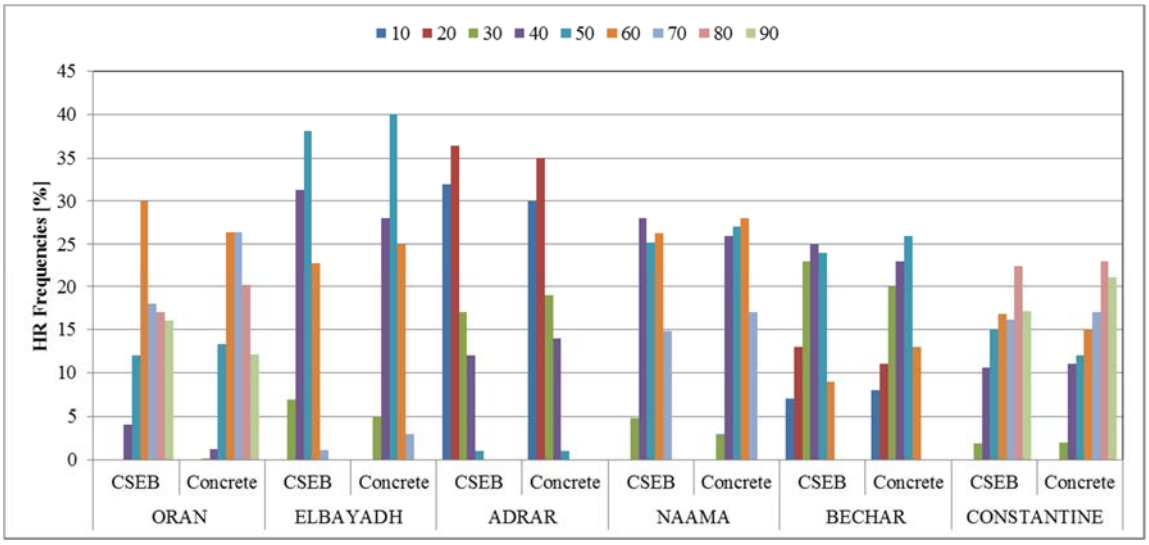


Fig.11. Occurrence frequencies of the relative humidity for CSEB and aerated concrete for six Algerian climatic zones

The difference between these frequencies is clearly visible. The CSEB generated lower relative humidity than those obtained for a aerated concrete. Cities with a dry climate are the least affected by the change in materials; however, for north cities the occurrence of high humidity is higher for aerated concrete than for CSEB. For Adrar the relative humidity does not exceed 40% in winter, however, and for more than 32% of the year it does not exceed 10%. These results illustrate the non-production of condensation in these homes because of the high aridity of its climate, in winter and in summer. For oran, the time of occurrence of RH 60% and 70% increases by 9% in comparison with the CSEB. For the city of Constantine, the time to produce 90% humidity increased with a difference of 4% for Concrete. Indeed, for the city of Béchar, a decrease in the times of humidity occurrence of 20, 30 and 40% was observed; on the other hand, a relatively slight increase in the times of occurrence of the humid 60% and 50% is illustrated.

The time during which the relative humidity exceeds 80% is estimated at 21% in Constantine and 13% in Oran, for aerated concrete against 17% and 16% for CSEB for the two cities respectively. Molds can develop if the local relative humidity is larger than 80% for a sufficient period of time (more than a week) [32].

These results show the aridity of the Saharan climate, in fact, the relative humidity is outside the optimal range, which is defined in [28] [33] and [34] to be

between 40% to 60%, is more than 46% of time (estimated over one year) at Bechar and 86% at Adrar. Concerning Oran and Constantine cities, the indoor relative humidity is within this optimal interval 52% of the time in Oran and 42% in Constantine which shows that for the majority of the year, the buildings in these northern cities do not respect indoor air quality criteria. This is due to the amount of water vapor produced associated with the poor insulation of the walls, in addition to the low rate of air renewal by natural ventilation which must be regulated so as to better evacuate the stale air without lowering the internal temperature. At the contrary, the relative humidity is within the optimal range 93% over a year in Elbayadh and 78% in Namma.

## 6. Conclusions

The aim of this work is to examine the thermo-aero-hydric behavior of buildings in CSEB and therefore assess its contribution in the regulation of humidity and the reduction of the occurrence of condensation, by simulations using the TRNSYS software coupled with COMIS . Six Algerian cities representative of the six sub-climates were selected. The results highlight the contribution of the CSEB material in stabilising the indoor relative humidity of buildings, also in limiting the effects of condensation thanks to its adsorption effect.

The construction with the earth brick was very successful in hot and dry climate thanks to its creation of a thermally comfortable microclimate. However, the thickness of the brick CSEB chosen for these simulations (12 to 14 cm), reduces the comfort when compared to other building materials with larger thicknesses.

The phenomenon of condensation occurs in winter, caused in particular by internal water vapour production or insufficient ventilation for hot and dry climates like that of the city of Bchar. Its occurrence was for rooms on the top floors in contact with the exterior and which are close to humidity sources. However, the high aridity of the hyper-desert climate prevents the occurrence of condensation, even with poor ventilation.

The contribution of CSEB in reducing condensing hours also varies from one climate to another. For coastal cities with a humid and mild climate, the CSEB reduces these hours from 24% to 44%. However, for the cities of the high plateaus with a very cold and arid climate, the percentage was higher is around 32% to 60%. This can be justified by the very cold winters in these regions combined with internal water supplies and the absence of natural ventilation. The study also showed the importance attached to the combination of natural ventilation with hygroscopic material in improving the indoor air quality articularly as a result of domestic activities that generate more water vapour and humidity, which can harm not only the health of the occupants but also the durability of the building.

## References


[1] Li, Y., P. Fazio, and J. Rao, Numerical investigation of the influence of room factors on HAM transport in a full-scale experimental room. Building and Environment, 2012. **50**: p. 114-124.

[2] Kong, F. and H. Wang, Heat and mass coupled transfer combined with freezing process in building materials: Modeling and experimental verification. Energy and Buildings, 2011. **43**(10): p. 2850-2859.

[3] Moon, H.J., S.H. Ryu, and J.T. Kim, The effect of moisture transportation on energy efficiency and IAQ in residential buildings. Energy and Buildings, 2014. **75**: p. 439-446.

[4] Martínez-Ibernón, A., et al., Temperature and humidity transient simulation and validation in a measured house without a HVAC system. Energy and Buildings, 2016. **131**: p. 54-62.

[5] Zhang, L., G. Sang, and W. Han, Effect of hygrothermal behaviour of earth brick on indoor environment in a desert climate. Sustainable Cities and Society, 2020: p. 102070.

[6] Donkor, P. and E. Obonyo, Earthen construction materials: Assessing the feasibility of improving strength and deformability of compressed earth blocks using polypropylene fibers. Materials & Design, 2015. **83**: p. 813-819.

[7] Cagnon, H., et al., Hygrothermal properties of earth bricks. Energy and Buildings, 2014. **80**: p. 208-217.

[8] McGregor, F., et al., Conditions affecting the moisture buffering measurement performed on compressed earth blocks. Building and Environment, 2014. **75**: p. 11-18.

[9] El Fgaier, F., et al., Effect of sorption capacity on thermo-mechanical properties of unfired clay bricks. Journal of Building Engineering, 2016. **6**: p. 86-92.

[10] Pacheco-Torgal, F. and S. Jalali, Earth construction: Lessons from the past for future eco-efficient construction. Construction and Building Materials, 2012. **29**: p. 512-519.

[11] Toure, P.M., et al., Mechanical and thermal characterization of stabilized earth bricks. Energy Procedia, 2017. **139**: p. 676-681.

[12] Kolawole, J.T., O.B. Olalusi, and A.J. Orimogunje, Adhesive bond potential of compressed stabilised earth brick. Structures, 2020. **23**: p. 812-820.

[13] Liuzzi, S., et al., Hygrothermal behaviour and relative humidity buffering of unfired and hydrated lime-stabilised clay composites in a Mediterranean climate. Building and Environment, 2013. **61**: p. 82-92.

[14] Allinson, D. and M. Hall, Hygrothermal analysis of a stabilised rammed earth test building in the UK. Energy and Buildings, 2010. **42**(6): p. 845-852.

[15] McGregor, F., et al., A review on the buffering capacity of earth building materials. Construction Materials, 2016.

[16] Saidi, M., et al., Stabilization effects on the thermal conductivity and sorption behavior of earth bricks. Construction and Building Materials, 2018. **167**: p. 566-577.

[17] Arrigoni, A., et al., Reduction of rammed earth's hygroscopic performance under stabilisation: an experimental investigation. Building and Environment, 2017. **115**: p. 358-367.

[18] Fouchal, F., et al., Experimental evaluation of hydric performances of masonry walls made of earth bricks, geopolymer and wooden frame. Building and Environment, 2015. **87**: p. 234-243.

[19] Nematchoua, M.K. and J.A. Orosa, Building construction materials effect in tropical wet and cold climates: A case study of office buildings in Cameroon. Case Studies in Thermal Engineering, 2016. **7**: p. 55-65.

[20] Nematchoua, M.K., P. Ricciardi, and C. Buratti, Statistical analysis of indoor parameters an subjective responses of building occupants in a hot region of Indian ocean; a case of Madagascar island. Applied Energy, 2017. **208**: p. 1562-1575.

[21] Nematchoua, M.K., et al., Effect of wall construction materials over indoor air quality in humid and hot climate. Journal of Building Engineering, 2015. **3**: p. 16-23.

[22] Bui, R., M. Labat, and S. Lorente, Impact of the occupancy scenario on the hygrothermal performance of a room. Building and Environment, 2019. **160**: p. 106178.

[23] Luo, Y., et al., Wind-rain erosion of Fujian Tulou Hakka Earth Buildings. Sustainable Cities and Society, 2019. **50**: p. 101666.
[24] Touazi, M. and J.P. Laborde, Modélisation pluie-débit à l'échelle annuelle en Algérie du nord. Revue des sciences de l'eau / Journal of Water Science, 2004. **17**(4): p. 503–516.
[25] Ghedamsi, R., et al., Modeling and forecasting energy consumption for residential buildings in Algeria using bottom-up approach. Energy and Buildings, 2016. **121**: p. 309-317.
[26] Miloudi, Y., et al., Temperature effects on sorption behaviour of compressed and cement-stabilised earth blocks. Magazine of Concrete Research. **0**(0): p. 1-11.
[27] Mahdad, M. and A. Benidir, Hydro-mechanical properties and durability of earth blocks: influence of different stabilisers and compaction levels. Sustainable Building Research Center (ERC) Innovative Durable Building and Infrastructure Research Center
2018. **9**(2): p. 44-60.
[28] DTR C3-2. Reglement thermique des batiments d'habitation; regle de calcul des peperdition calorifique FACICULE1, 1998, National Center for Integrated Building Studies and Research (CNERIB): ALGERIA
[29] Yoshino, H., T. Mitamura, and K. Hasegawa, Moisture buffering and effect of ventilation rate and volume rate of hygrothermal materials in a single room under steady state exterior conditions. Building and Environment, 2009. **44**(7): p. 1418-1425.
[30] You, S., et al., Study on moisture condensation on the interior surface of buildings in high humidity climate. Building and Environment, 2017. **125**: p. 39-48.
[31] Ferroukhi, M.Y., Modeling of thermo-hygro-aeraulic transfers in buildings envelopes : assessment of disorders caused by humidity, 2015, Université de La Rochelle.
[32] Roulet, C.-A., Santé et qualité de l'environnement intérieur dans les bâtiments. 2and edition ed2010.
[33] DTR C3-4 CLIMATISATION, Régles de calcul des apports calorifiques des bâtiments 1998, National Center for Integrated Building Studies and Research (CNERIB).

# Valorization of local kaolin in sustainable concrete and on the environment through their exploitation deposit

Tayeb Rikioui[1], Soltane Lebaili[1], Ahmed Tafraoui[2], Mekkaoui Abderahmane[2]

[1] University of Sciences and Technology Houari Boumediene, PO Box 32 El-Alia 11 116 Bab Elzouar, Algiers, Algeria.
*E-mail: tayebrikioui@gmail.com , slebaili@yahoo.fr*

[2] University Tahri Mohamed, PO Box 417, Bechar, Algeria.
*E-mail: ahmedtafraoui@yahoo.fr , mekkaouidh15@gmail.com*

DOI: 10.37789/rjce.2021.12.1.7

**Abstract.** *The exploitation of clays in the cement sector creates a great influence on the geological monuments as well as on the general geological environment. In this context, this article aims to valorize kaolin from southwestern Algeria in sustainable concrete and to exploit their deposit site as a landfill.*
*In order to obtain metakaolin, this kaolin is subjected to a thermal transformation controlled by an apparatus designed to test the ecological efficiency of this material. Subsequently, a mass substitution of 10% of cement with metakaolin in concrete was made for the study the performance of this new concrete.*

**Key words:** Kaolin; Metakaolin; Environment, $CO_2$ gas; landfill site; Durability

## 1. Introduction

Cement is a basic component of concrete and mortar used for building and civil engineering construction sectors. Therefore concrete (i.e. cement) is one of the World's most significant manufactured materials. Since it is an essential element in construction materials, understanding the environmental implications of cement manufacturing are becoming increasingly important.
The cement industry is one of the largest carbon emitting industrial sectors in the world [1]. This emissions reached in 2016 of 1.46±0.19 $GtCO_2$ [2]. Fuel combustion emissions of $CO_2$ are of approximately in total, 8% of global $CO_2$ emissions [3][4][2]. Approximately 50% emissions of $CO_2$ are directly emitted from the calcination process (decarbonation of limestone), 40% from fuel combustion in a rotary kiln, and 10% are indirect emissions accounted for quarrying and transportation of products [5][6]. For the production of cement $SO_3$ and NOx are released in addition to $CO_2$, which is source of the greenhouse effect and acid rain [7][8].
The cement industry has made significant progress in reducing $CO_2$ emissions by using of supplementary cementitious materials (SCM) in structural concrete [9][10][11][12].

Low-temperature calcined kaolins, or metakaolins, have very high pozzolanic characteristics, making them excellent supplementary cementitious materials (SCM) for cement-based mortars and concretes [13][14].

The Metakaolin ($Al_2O_3 \cdot 2SiO_2 \cdot 2H_2O$) is prepared by dehydroxilation of kaolin clay in the temperature range of 450–850 °C [15], [9].

The environment is dynamic. It undergoes modifications through several processes, including the exploitation of natural mineral deposits in construction [16].

Exploitation of mineral resources has assumed prime importance in several developing countries including Algeria.

Indeed, the extractive industry, through the application of different techniques and technologies, has always been a source of damage to the environment. Such exploitation has a massive and largely negative impact on the reliefs [17].

Also, the development of technology and population growth leads to significant generation of solid waste [18] and the continual increase in the amount of household waste and toxic industrial waste. A modern landfill is an engineered method for depositing waste in specially constructed and protected cells on the land surface or in excavations in the land surface. But the characters of the proper choice of landfill site are very difficult. These criteria encompass environmental conditions, accessibility, geological and hydro-geological conditions, ecological and societal effects.

This article articulates on two research shutters that are:

The first shutter is the study of the ecological efficiency of local metakaolin, and its effect on the durability of concrete by substitution of 10% of Ordinary Portland cement (OPC).

In the second shutter, we contribute to the valorization by geotechnical characterization to exploit the site of footprint deposit of kaolin to landfill site.

Kaolinic clays are available in Algeria, including his South- Western [19], [20].

The kaolin targeted by this study is located in the South East of new constructions of Tabelbala at 314 km south of Bechar in Algeria (fig.1.A). Geologically, the deposit belongs to the Silurian floor Ougarta Mountains [21] (fig.1.B).

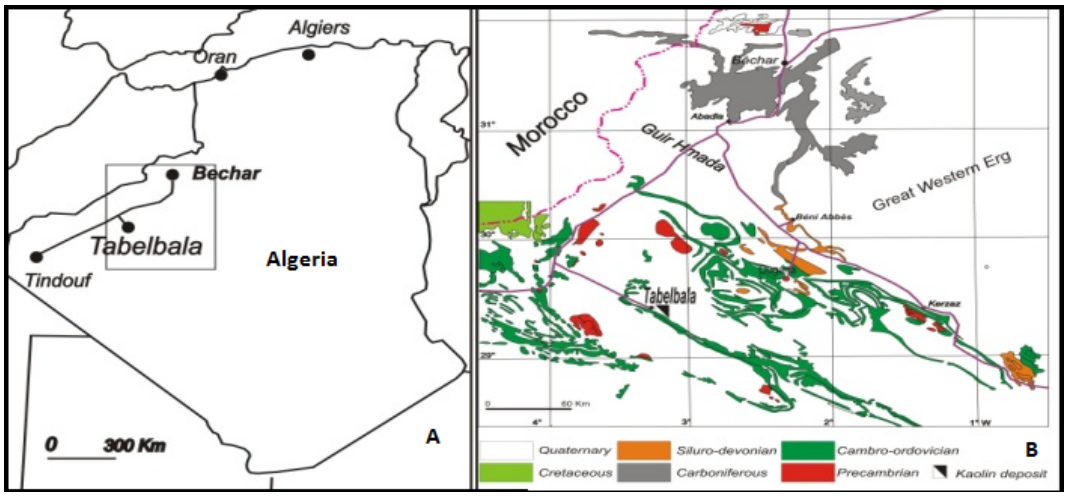


(A): localization of Tablebala city (B): Geological sketch map of the Ougarta Range [21]

Fig.1. Location and illustration of the Tabelbala kaolin deposit

For many centuries, kaolinic clays have been exploited in the Tabelbala (Algeria) as a cement or waterproof cover on the roofs. They are associated with lower Paleozoic sandstones [22].

This kaolin is in the form of lentils of 3 to 5 km in length, estimated at 500 thousand tons, and is located more precisely in the village of Mekhlouf, south of the city of Tabelbala, which constitutes a prodigious wealth [19].

Our principal objective of this research is the used the means, equipments, and materials simple locally available.

Remark: To lighten the writing of the article, metakaolin is sometimes replaced by the symbol MK.

## 2. Materials and Methods

### 2.1. Mineral addition

#### 2.1.1. Sampling

The clay mineral kaolinite is formed by the breakdown of feldspar by the action of water and carbon dioxide. Kaolin samples were taken in the open-air after stripping a thin slender layer of waste rock composed of scree.

#### 2.1.2. Geotechnical characteristics

The collected samples were subjected to laboratory tests for to define of essentials geotechnical parameters. These parameters, concerns namely grain size distribution by Hydrometer analysis, water content, Atterberg limits, solid grain density, methylene blue value, and volumetric mass wet and dry determine according to standards edited by AFNOR (French Standards Association).

Using the correlation formulas and the grading curve must , porosity, void ratio, median grain size, percentage of the clay fraction, activity value and the permeability have been determined of this type of clay.

The activity and permeability are two properties particularly important in environmental protection for the determination of water and contamination retention capability of soils.

By relationship (1), Skempton (1953) defined activity as the ratio of plasticity index to < 0.002 mm clay fraction.

$$\mathbf{S} = \frac{\boldsymbol{I_P}}{\boldsymbol{C}\ [\%]} \qquad (\mathbf{1})$$

Respectively *S*, *Ip* and *C* are activity values, plasticity index and clay fraction percentage. The coefficient of permeability is calculated from the Berg relationship by formula (2).

$$\mathbf{k} = \mathbf{8.4}\boldsymbol{x}\mathbf{10}^{\mathbf{-2}}(\boldsymbol{d})^{\mathbf{2}}\boldsymbol{\Phi}^{\mathbf{5.1}} \qquad (\mathbf{2})$$

Where: *k*, *Φ* and d are permeability (mD), Porosity and fraction median grain size (microns) respectively.

The average values of the geotechnical parameters obtained from the tests carried out on four samples of kaolin are mentioned in table 1.

Table1. Results of geotechnical parameters of kaolin samples

| Parameters | Average values |
|---|---|
| Water content (%) | 0,75 |
| Volumetric weight $\gamma$(t/m$^3$) | 1,98 |
| Dry volumetric weight $\gamma_d$ (t/m$^3$) | 1,96 |
| Clay fraction C [%] | ≈ 51 |
| Plasticity index $I_P$ | 24,6 |
| Density of the solid particles $\rho_p$ (t/m$^3$) | 2,66 |
| Porosity fraction ($\Phi$) | 0,26 |
| Void ratio | 0,35 |
| median grain size $d$ (mm) | 0,0018 |
| Skempton's Activity value S | ≈ 0,48 |
| Permeability k (mD) | ≈2,82E-4 |
| Methylene Blue Value : MBV (mg/g) | 2,17 |

The particle size distribution of this kaolin determined by Hydrometer analysis can be represented graphically in fig. 2.

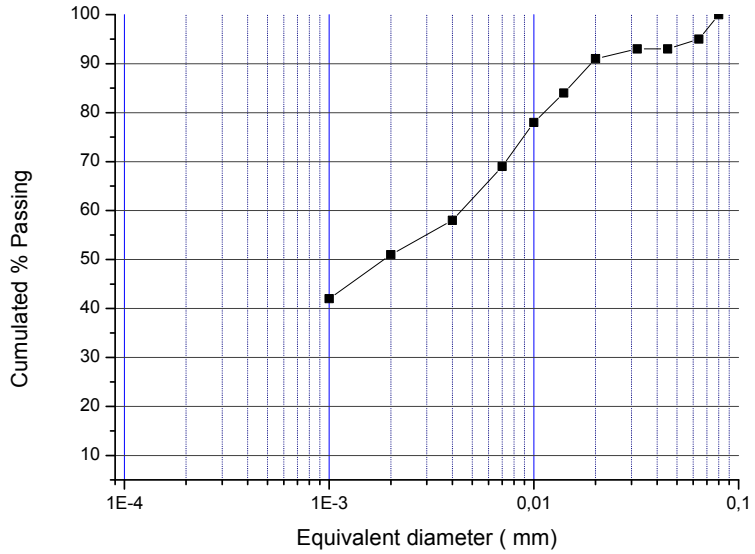


Fig.2. Particle size distribution of Kaolin

### 2.1.3. Mechanical treatment the kaolin and metakaolin samples

The mechanical treatment, comprising three successive processes of crishing: by jaws, cylinders and by discs in order to obtain fine particles having elements less than 100µm. This material is ground to a required finesse beyond of 900m$^2$/kg.

### 2.1.4. Thermal treatment of the kaolin sample (calcination)

In order to produce a metakaolin nearly complete dehydroxilization must be reached without overheating, i.e., thoroughly roasted but not burnt.

The valorization of the environmental efficiency of metakaolin requires control of the quantity of gas emitted during the calcination of kaolin. For this purpose, an apparatus composed of a sealed muffle furnace associated by its chimney with a Bernard

calcimeter by means of a flexible rubber hose (fig. 3) was created. The muffle furnace is for calcining kaolin and the calcimeter is for measuring the amount of gas emitted during calcination of kaolin. The displacement of the colored liquid in the tube graduated of calcimeter, indicates the quantity of gas emitted and is equal to the difference of the graduations before and after calcination of kaolin.

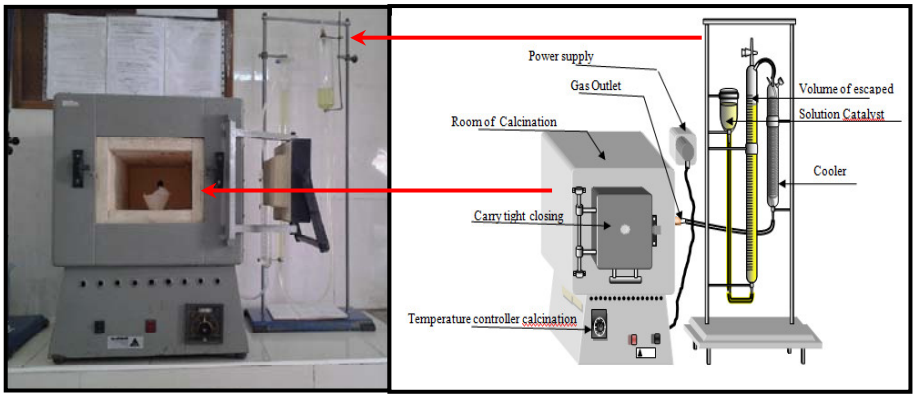


Fig.3. Gas measuring device (muffle furnace – Calcimeter)

The metakaolin studied, is obtained by calcination of the kaolin at temperatures between 450 and 760°C for about five (05) hours, according to the thermal cycle indicated in fig. 4.

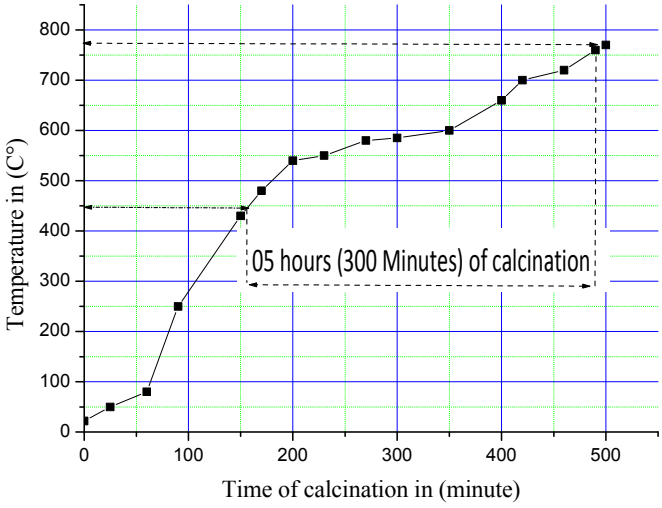


Fig.4. Cycle thermal processing of the Tabelbala kaolin

### 2.1.5. Identification chemical of metakaolin

The chemical analysis is carried out according to methods of the standard EN 196-2 [23]. The results of the chemical analysis of MK are given in Table 2.

Table2. Results of chemical composition of metakaolin sample

| Chemical Composition,% | $SiO_2$ | $Al_2O_3$ | $Fe_2O_3$ | $Na_2O$ | $K_2O$ | CaO | $SO_3$ | MgO | $TiO_2$ | Loss on ignition |
|---|---|---|---|---|---|---|---|---|---|---|
| MK | 49,38 | 36,76 | 6,68 | 0,50 | 1,89 | 0,25 | 0,88 | 0,43 | 0,79 | 2,73 |

The chemical test results of the MK specimen were compared with the ASTM C618 [24] requirements, as shown in Table 3.

Table3. Result of comparison between pozzolan chemical properties and ASTM requirements

| Test | MK | ASTM C618[24] | | | |
|---|---|---|---|---|---|
| | | Natural pozzolan N Class | Fly ash | | Silica fume |
| | | | F Class | C Class | |
| Sum of Iron Oxide ($Fe_2O_3$), Aluminum Oxide ($Al_2O_3$), and Silicon Dioxide ($SiO_2$),% | 92,82 | ≥ 70 | ≥70 | ≥ 50 | - |
| Sulfur Trioxide ($SO_3$),% | 0,88 | ≤4 | ≤5 | ≤5 | - |
| moisture content | small | ≤3 | ≤3 | ≤3 | - |
| Loss on ignition (%) | 2,73 | ≤10 | ≤6 | ≤6 | ≤6 |
| Silicon Dioxide ($SiO_2$),% | 49.38 | - | - | - | ≥ 85 |

### 2.1.6. Mineralogical Identification of metakaolin

Mineralogical analysis of this metakaolin was carried out by X-ray diffraction using standard equipment INEL CPS 120 and with the use of software X PERT DATED COLLECTOR whose results are shown in Table 4.

Table4. Mineralogical content of metakolin

| Elements | Quartz | Kaolinite | Muscovite | Ferruginous minerals | Albite |
|---|---|---|---|---|---|
| Percent by Weight | 50,00 | 19,00 | 19,50 | 6,50 | 5,00 |

### 2.1.7. Morphology of metakaolin

The morphology of MK is obtained by (SEM-SE) scanning electron microscope using secondary electrons (fig. 5).

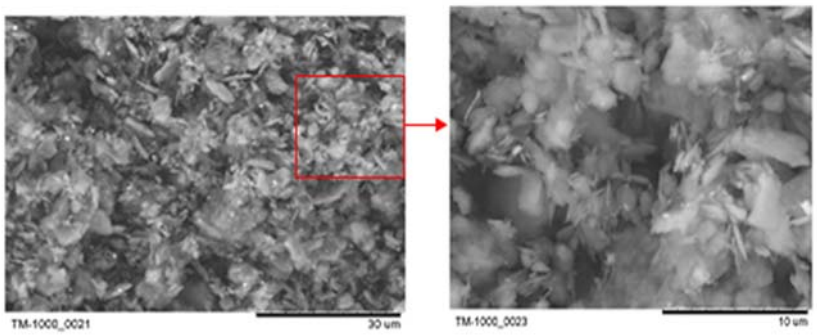


Fig.5. SEM-SE Morphology of MK: A low magnification and higher magnification.

### 2.1.8. Physical identification

Physical identification includes: pozzolan activity index (AI) realized according to the modality of the ASTM C311 standard [25] , the density was measured by hydrostatic

weighing after saturation of the sample under vacuum and specific surface measurement. The results found are shown in Table 5.
For assessed the pozzolan activity index, The materials used are the standard sand CEN conform EN 196-1 [26], cement (CEM I 52.5 N) and drinking water.
The specific surfaces (S) of metakaolin powder and cement are determined by the BET (model Brunauer, Emmett and Teller BET) method and Blaine method respectively.

Table5. Results of the principal physical identification of cement and metakaolin

| | Density (g/cm$^3$) | S (m$^2$/g) | Activity index (AI) | | |
|---|---|---|---|---|---|
| | | | 07 days | 28 days | 90 days |
| Cement | 3.14 | 0.3818 | 1.00 | 1.00 | 1.00 |
| Metakaolin | 2.7 | 16 | 0.79 | 1.00 | 1.09 |

### 2.2. Concrete mix design

For economic reasons, all components (aggregates, kaolin, cement, and water, additive) of concretes are local materials. The metakaolin obtained from local kaolin is used to replace part of the CEM I 42.5 cement

### 2.3. Concretes formulations

Two concrete compositions were made, one without MK (C1), the other MK replace 10% of the weight of cement (C2), and with superplasticizer.
For a performance comparison between C1 and C2 concretes, we selected a constant slump of Abrams cone equal to 9cm. Metakaolin consumes a higher quantity of superplasticizer compared to the cement, this is the reason that the rates of water/cement (W/C), the quantity of water and superplasticizer are different between the two formulations. The quantity of binder (cement and MK) and quantity inert components (sand and gravel) have remained constants.
The choice of 10% metakaolin as the level of cement substitute is based on the results of other researchers. In research of Barbhuiya and its collaborators, the 10% is the optimal rate comparatively 0%, 5%, 10% and 15% of metakaolin for the evaluation of compressive strength, absorption capacity and carbonation of concrete[27].The introduced proportions are given in table 6.

Table 6. Composition of concrete with and without metakaolin (kg/ m3)

| Designations | Cement CEM I 42,5 | Metakaolin | Aggregates | | | Superplasticizer (ADVA Flow 390) | Mixing water |
|---|---|---|---|---|---|---|---|
| | | | Sand 0/5 | Gravel 3/8 | Gravel 8/15 | | |
| C1 | 440 | 0 | 530 | 300 | 875 | C1 | 440 |
| C2 | 400 | 40 | 530 | 300 | 875 | C2 | 400 |

### 2.4. Performances tests

#### 2.4.1. **Dynamic Young's Module** [28]

The phase velocities of the longitudinal wave and the transverse waves measured by ultrasound (in the case of aggregates) are linked to the elastic modulus and to the Poisson's ratio by the relation (3).

The ultrasonic wave propagation velocity method was realized according to standard NF EN 12504-4 [29] of 70 × 70 × 280 mm$^3$ concrete specimens.

$$V_l = \sqrt{\frac{E_{dy}(1-\vartheta)}{\rho(1+\vartheta)(1-2\vartheta)}} \quad (3)$$

Where:

$\vartheta$: is the Poisson's ratio of the material,

$E_{dy}$: is the dynamic Young's modulus of the material,

$\rho$: is the density, known and measured independently

### 2.4.2. Compressive strengths

Compressive strength tests on cured cubic concrete specimen of 28 and 90 days ages were performed using a compression testing machine accordance with standard NF P 18-406.

### 2.4.3. Estimation of the Capillary Water Absorption Coefficient

According to ASTM C1585 [30], the capillary water absorption coefficient is the gradient of the straight fine obtained by plotting the cumulative mass of water absorbed per unit area against the square root of time t obtained from this first stage according to the following equation (4):

$$\mathbf{A_w} = \frac{\Delta \boldsymbol{M}}{\boldsymbol{A}\sqrt{\boldsymbol{t}}} \quad (\mathbf{4})$$

Where $A_w$ (mg/cm$^2$s$^{1/2}$) is the water absorption coefficient, $\boldsymbol{A}$ (cm$^2$) is the surface area of the cross section of the specimen and ΔM (mg) is the mass of the absorbed water as shown in Fig.6.

This coefficient is calculated at 24 hours that is to say between 24h-0h and 48h-24h on cubic specimens of section 10x10cm$^2$.

Fig.6. Water absorption test on concrete cubes

#### 2.4.4. Penetration depth of chloride ions in calorimetrically hardened concretes [31]

The test described here makes it possible to determine the depth of penetration of the chloride ions in a material, from the vaporization of a reagent, the silver nitrate $AgNO_3$, and optionally a developer, potassium dichromate $K_2CrO_4$.

The determination of the chloride penetration depth $X_d$ is also necessary for the calculation of the apparent diffusion coefficient $D_{app}$ expressed in $m^2.s^{-1}$ (Eq. (5)) from a non-stationary electric field migration test.

$$D_{app} = 1{,}189\frac{10^{-11}\left(X_d - 1{,}189.{X_d}^{0{,}589}\right)}{t} \quad (5)$$

Where $t$ is the test duration, [hours];

#### 2.4.5. Sulphate resistance

The sulphate resistances are determined from the concrete specimens after storage for 28 days (zero time), then a series of these specimens is immersed in the sodium sulphate solution $Na_2SO_4$ with 5% concentration and others are stored in the water. To evaluate the durability of the concretes with respect to sulphate attack, we determined the compressive strength as a function of the immersion time in the sulphate solution. For all tests, the samples are preserved at 20°C.

## 3. Results and Discussion

### 3.1. Thermal treatment of the kaolin

The values, measured by the displacement of the volume in the graduated burette of Bernard's calcimeter (Fig.4), are almost negligible. This testifies that this metakaolin during its production releases only water vapor explained by the following chemical reaction:

$$Al_2Si_2O_5(OH)_4 \rightarrow Al_2O_3\,2SiO_2 + 2H_2O\uparrow$$

Unlike metakaolin, the production of Ordinary Portland Cement requires a strong heat creating a harmful effect on the environment.

### 3.2. Chemical and mineralogical results

The chemical results of the metakaolin obtained are almost similar to those of the fly ash, but did not meet the requirement of 85% silicon dioxide for the silica fumes (see Table 3 below).

Also, the images obtained by SEM-SE for two levels of magnification, show that the MK consists essentially of agglomerates of particles. These latter are formed a stack of hexagonal plates. The dimensions of the platelets vary from 1 to 10 µm

### 3.3. Mechanical parameters

For a Poisson's ratio taken $\vartheta = 0.2$ the results are shown in Table 7.

Table7. Average values of mechanical parameters

| Formula | Bulk Density [kg/m³] | Compression Strength [MPa] | | | Modulus of elasticity [MPa] |
|---|---|---|---|---|---|
| | 14 Days | 14 Days | 28 Days | 90 Days | 14 Days |
| C1 | 2349 | 38 | 45 | 48 | 32637 |
| C2 | 2422 | 43 | 50 | 65 | 41840 |

These results shows that the substitution of cement with metakaolin leads to an improvement of the mechanical strengths at 14, 28 and 90 days, this increase is very remarkable and is consistent with that of the literature [32][33][34][35][36][37].

### 3.4. Capillarity test (capillary absorption)

The capillary water absorption coefficient is one of the most important features of durability the concrete because it governs the liquid moisture movement into it and expresses the rate of absorption of water due to capillary forces in this building material. The average results obtained by the capillary absorption test as well as those of absorption of the two (02) types of concretes at 20°C are given in the histogram of fig 7.

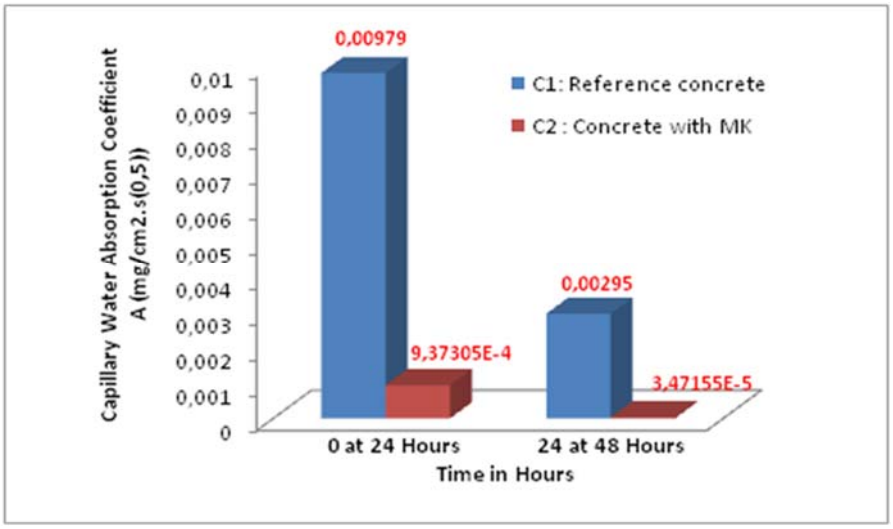


Fig.7. Evolution in 24 hours of water absorption coefficient Aw for the two samples concretes

In light of the results obtained, it is clear that the water absorption coefficient by capillarity is rapidly increased after the first 24hours. But, it is gradually decreasing for the reference concrete and stabilized for the concrete with metakaolin. These results explain that metakaolin reduced the pores of the concrete matrix and led to low capillary absorption compared to the reference concrete. This discovery was developed in the research of Wojciech Kubissa and his collaborators [38].

### 3.5. Penetration of chloride ions

The different diffusion coefficients calculated from the formula (5) are given in Table 8.

Table8. Results of the penetration of chloride ions in hardened concretes

| Formula | $X_d$ (mm) | $D_{app}$ [$m^2.s^{-1}$] |
|---|---|---|
| C1- reference concrete | 8 | $3.34.10^{-12}$ |
| C2- concrete with metakaolin | 3 | $0.48.10^{-12}$ |
| | No color | Negligible |

The diffusion of the chlorides in the control concrete and the metakaolin concrete are illustrated in fig.8A and fig.8B respectively.

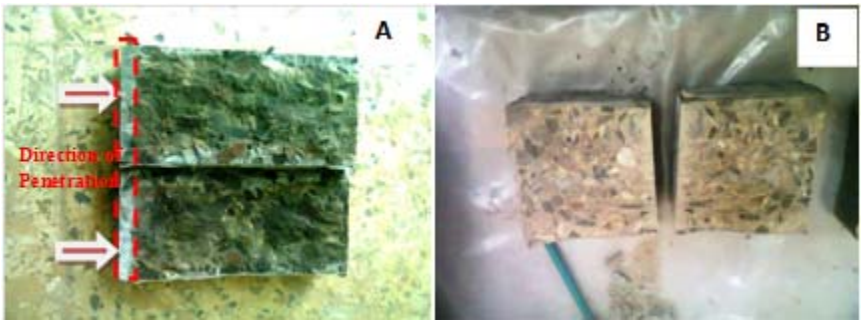


Fig.8. Diffusion of chlorides in control concrete (A) and concrete with metakaolin (B)

These experimental results reveal that the diffusion coefficient in metakaolin concrete is very low to negligible (fig. 9B) compared in the reference concrete (fig. 9A) because of its very dense porous structure. This shows that this concrete has not been degraded by penetration of chloride ions over time. The diffusion coefficient of concrete C2 is less than 2 x $10^{-12}$ $m^2$/ s attests a very good resistance to chloride penetration [38].

### 3.6. Sulphate resistance of concretes

After the specified days, the samples were immersed in 5% sodium sulphate solution ($Na_2SO_4$) for 24 months. The results of the variation in compressive strength for the two types of concrete immersed for 4 months, 8 months and 12 months in his solution prepared are shown in (fig 9).

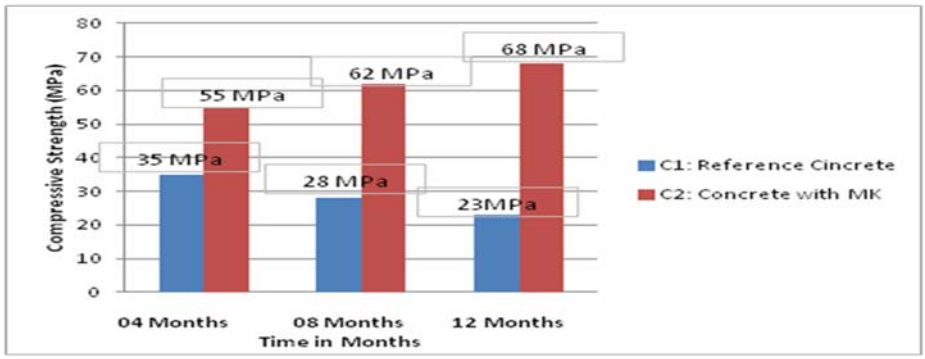


Fig.9. Variation of compressive strength of concretes immersed in sulfate solutions as a function of shelf life

Metakaolin addition proved to be beneficial in improving the resistance of concrete to sulphate attack. It can be seen that the compressive strength of the reference concrete was inversely proportional to the conservation time them in the sulfated solution and on the contrary, concrete with metakaolin have the slightly increased resistances, this is due to the dense matrix (cement / metakaolin).

The action of sulfates can also lead to a loss of resistance and a loss of mass of the concrete ordinary (reference) in surface. These effects are explained by author Saida BOUALLEG [39], by the fact that they are due to the alteration of binding properties of certain hydrates.

### 3.7. Landfill Site

The impermeability of the geological formation is highly recommended for the choice of the sites of the landfills and this to prevent any possible infiltration of pollutants which may jeopardize the water resources and especially groundwater as it is difficult to know the formations of polluting flows generated by the anaerobic decomposition of waste.

Knowledge of the principal clay mineral (e.g. montmorillonite, illite, and kaolinite) property is particularly important in environmental protection for the determination of water and contamination retention capability. Skempton's Activity value (S) [40], is especially useful for evaluating this behavior. Skempton's Activity is not a consistency parameter, but affects the values of consistency limits.

Skempton activity values found (fig.10) show that Tabelbala kaolin is inactive clay.

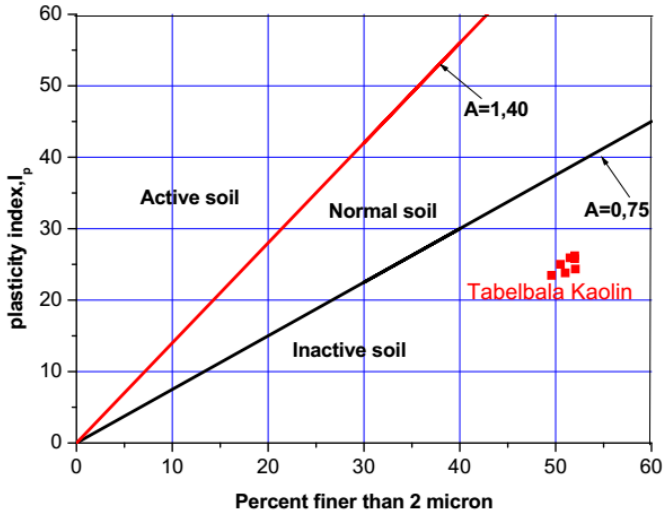


Fig.10. Classification of the Tabelbala kaolin according to activity

According to the Unified Soil Classification System (USCS) and using the Casagrandes plasticity table, this kaolin is inorganic clay of moderate plasticity.

Because of their impermeability, this kaolin plays an important role in the circulation and accumulation of various fluids (e.g. water, oil, gas); this finding is approved by its low coefficient of permeability found.

## 4. Conclusions

The compositional analyses of Tabelbala kaolin deposit have been carried out in this study. Comparisons have been made with the works of other authors and inferences also drawn to confirm the results of the analyses and economic viability of the deposit. The analysis results show that kaolin of Tabelbala could be a suitable raw material in the production of addition and / or substitution of Portland cement.

Ecologically, unlike the cement manufacturing method, the heat treatment of kaolin from the Tabelbala region confirmed that there is no release of greenhouse gas emissions during the production of metakaolin and releases only the water vapor.

Economically, the production of metakaolin requires a single deposit (kaolin) compared to cement which requires several (limestone, clay, gypsum...).

In terms of performances, the substitution of 10% of the cement by the metakaolin allows a significant improvement of the performances of the concrete (dynamic Young's modulus, Compressive strengths, capillary absorption, penetration of chloride ions and sulphat resistance).

In addition, the geological formation in place of the kaolin exploitation site is of an impermeable and inactive nature which leads us to an economic choice of this site for the realization of a landfill.

At the completion of the operation of the exploitation of material deposit, a sufficient thickness of the kaolin layer must be compacted superficially about 20 to 25 cm to ensure good sealing and good support of waste depositing.

A waterproof membrane is then placed over the exposed soil to prevent leachate from soaking into the surrounding soil and groundwater.

The kaolin is spread across the membrane to form another protective layer.

In the end, local metakaolin is both a less polluting cementitious material, high-performance in new concrete, economical, and ecologically efficient.

## References

[1] Mikulcic H, Vujanovic M, Markovska N, Filkoski R, Ban M and Duic N, $CO_2$ emission reduction in the cement industry, Chemical Engineering Transactions, 35,pp 703-708, 2013

[2] Robbie M, Andrew, Global $CO_2$ emissions from cement production, Earth Syst. Sci. Data, 10, pp 195–217,2018

[3] Olivier, J.G.J, Janssens Maenhout, G, Muntean, M. and Peters, J.A.H.W, Trends in global $CO_2$, 2015

[4] Alujas A, Rodrigo F, Rafael Q, Karen L and Fernando M, Pozzolanic Reactivity of Low Grade Kaolinitic Clays: Influence of Calcination Temperature and Impact of Calcination Products on OPC Hydration. Applied Clay Science 108, pp 94–101, May 2015

[5] Bosoaga A, Masek O and Oakey J.E, $CO_2$ Capture Technologies for Cement Industry. Energy Procedia, 2009

[6] Naqi Ali and Jeong G .Jang, Recent Progress in Green Cement Technology Utilizing Low-Carbon Emission Fuels and Raw Materials: A Review. Sustainability , 11, 537, 2019

[7] Rashad A.M and Zeedan S.R, The effect of activator concentration on the residual strength of alkali-activated fly ash pastes subjected to thermal load. Construction and Building Materials, 25(7), pp 3098–3107, 2011

[8] Valipour M, Yekkalar M, Shekarchi M and Panahi S, Environmental assessment of green concrete containing natural zeolite on the global warming index in marine environments. J. Clean. Prod. 65, pp 418–423, 2014
[9] Saida Fatma, Chemical activation of metakaolin in a cement matrix, PhD Thesis, Toulouse University, 2013
[10] Kanchan Mala, Effect of mineral admixtures on properties of concrete with ternary cement blends, PhD Thesis, university of engineering and technology A.B.Road, Raghogarh, Guna (madhya pradesh) – Indian, 2014
[11] Farzad Khamchin, Sriravindrarajah, Rasiah and Vute Sirivivatnanon, Properties of Metakaolin Concrete - A Review. Int. Conference on Sustainable Structural Concrete, 15-18 Sept, La Plata, Argentina, 2015
[12] Stephen Issac and Anju Paul, A literature review on the effect of metakaolin and fly ash on strength characteristics of concrete. IJARIIE- Vol-4 Issue-2, pp 6–11, 2018
[13] Chouafa M, Behavior of Kaolin to enrichment by flotation. Case of the Tamazert mine – Jijel, PhD Thesis, University Badji Mokhtar of Annaba (Algeria), 2016
[14]. Yanguatin H, Tobón J and Ramirez J, Pozzolanic reactivity of kaolin clays, a review. Revista Ingeniería de Construcción RIC, Vol 32 Nº2, pp 13-24, 2017
[15] F. Moodi, A.A. Ramezanianpour and A.Sh. Safavizadeh., Evaluation of the optimal process of thermal activation of kaolins, Scientia Iranica A 18 (4),pp 906–912, 2011
[16] G. C. C. Ndinwa and C. O. Ohwona, Environmental and health impact of solid mineral exploration and exploitation in south-northern Nigeria: a case study of IGARRA in EDO STATE, Review of Environment and Earth Sciences, Vol.1, No.1, pp. 24-36n 2014
[17] Boukhalfa A, Analysis of cutting parameters (mechanical slaughter). Memory of Magister, Badji Mokhtar University of Annaba, 2012
[18] Hosseini S.S, Yaghmaeian K. Yousefi, N Mahvi and A.H. Mahvi, Estimation of landfill gas generation in a municipal solid waste disposal site by LandGEM mathematical model, Global J. Environ. Sci. Manage., 4(4): pp 493-506, 2018
[19] ORGM, Book non-metallic useful substances of Algeria, Edition of the Geological Survey of Algeria. 2000
[20] Mekkaoui A, The basic magmatism of the Damrane-Kahal Tabelbala axis (Daoura, Ougarta Mountains, Southwest, Algeria): Geology, Petrology, Geochemistry and Geodynamic Context, PhD Thesis, University of Oran, 2015
[21] Leonid E Popov, Philippe Legrand, Boumedienne Bouterfa and Mansoureh, G.Pour, Ordovician cold water brachiopods from the Ougarta Mountain Range, Algerian Sahara. Bulletin of Geosciences 94(1), pp 41-70, 2019
[22]. Meroufel, B and Zenasni, M. A, Preparation, Characterization, and Heavy Metal Ion Adsorption Property of APTES-Modified Kaolin: Comparative Study with Original Clay, Handbook of Environmental Materials Management, Springer International Publishing, pp 1-25, 2018
[23] EN 196-2, Method of testing cement - Part 2: Chemical analysis of cement, September 2013
[24] ASTM Standard C618-00, Specification for Coal Fly Ash and Raw or Calcined Natural Pozzolan for Use as a Mineral Admixture in Portland Cement Concrete, ASTM International, West Conshohocken, PA, 2000.
[25] ASTM Standard C311, Standard Test Methods for Sampling and Testing Fly Ash or Natural Pozzolans for Use in Portland-Cement Concrete, Annual Book of ASTM Standards, 2007
[26] EN 196-1, Method of testing cement - Part 1: Determination of Strength, (April, 2016).
[27] Barbhuiya S and Chow, P, Microstructure, hydration and nanomechanical properties of concrete containing metakaolin, Construction and Building Materials ,Vol 95, pp 696-702, 2015
[28] Ting Yu, Modeling the propagation of ultrasonic waves in concrete for improving the diagnosis of civil engineering structures, PhD thesis, Aix-Marseille University, 2018
[29] NF EN 12504-4, Testing concrete - Part 4: determination of ultrasonic pulse velocity, May 2005.
[30] ASTM C-1585, Standard Test Method for Measurement of Rate of Absorption of Water by Hydraulic-Cement Concretes, ASTM International, West Conshohocken, Pa, USA, 2011.

[31] LCPC, Microstructural characteristic and properties related to the durability of concretes: measurement methods and laboratory testing: test methods N° 58, (February 2002)
[32] Dinakar P and Manu, S. N, Concrete mix design for high strength self-compacting concrete using metakaolin, Materials & Design, Vol.60, pp 661-668, 2014
[33] Khatib J. M, Strength characteristics of mortar containing high volume metakaolin as cement replacement, Research and Reviews in Materials Science and Chemistry, Vol. 3, pp 85-95, 2014
[34] Nadeem Abid, Shazim A, Memon and Tommy Y.Lo, The performance of Fly ash and Metakaolin concrete at elevated temperatures, Construction and Building Materials, Vol. 62,pp 67-76, 2014
[35]Rashiddadash Pantea, Ramezanianpour A.Akbar and Mahdikhani Mahdi, Experimental investigation on flexural toughness of hybrid fiber reinforced concrete (HFRC) containing metakaolin and pumice, Construction and Building Materials, Vol.51, pp 313-320, 2014
[36] Sawant R. M and Ghugal Y. M, Recent trend: Use of metakaolin as admixture: A review, American Journal of Engineering Research (AJER) Vol.4.12, pp 08-14, 2015
[37] Gill A.S and Siddique R, Strength properties and sulphate resistance of self-compacting concrete incorporating metakaolin, Journal of Solid Waste Technology & Management, Vol. 41 Issue 4, pp 206-215, 2015
[38] Wojciech, Kubissa, Roman Jaskulski and Miroslav Brodnan, Influence of SCM on the Permeability of Concrete with Recycled Aggregate, Periodica Polytechnica Civil Engineering, 60(4), pp 583–590, 2016
[39] Saida Boualleg, Aggressive environment effect on durability characteristics of concrete and cement matrices, master's degree M'Sila University, Algeria, 2004
[40] Ruy A, Sa ´ Ribeiro, Marilene G, Sa ´ Ribeiro, Gregory P, Kutyla, and Waltraud M, Kriven, Amazonian Metakaolin Reactivity for Geopolymer Synthesis, Advances in Materials Science and Engineering, 2019

# Modelarea functionarii unui sistem neconventional cu panouri solare fotovoltaice si pompa de caldura care alimenteaza cladiri cu utilitati de incalzire si preparare a apei calde de consum

## Modeling the operation of an unconventional system with photovoltaic solar panels and heat pump that supply buildings with heating and hot water utilities

Florin Iordache[1], Mugurel Talpiga[2]

[1,2]Universitatea Tehnică de Construcţii Bucureşti
Bd. Lacul Tei nr. 122 - 124, cod 020396, Sector 2, Bucureşti, România
E-mail*: fliord@yahoo.com*

DOI: 10.37789/rjce.2021.12.1.8

**Rezumat**

In lucrare se prezinta modelarea functionarii unui sistem neconventional format din panouri solare fotovoltaice care alimenteaza cu energie electrica o pmpa de caldura pentru furnizare de putere termica in instalatia de incalzire centarala a unei cladiri sau de prepararea a apei calde. Se prezinta atat relatiile corespunzatoare determinarii puterii electrice furnizate de suprafata de panouri solare fotovoltaice cat si relatiil de determinare dinamica a puterii termice livrate de pompa de caldura catre instalatiile consumatorului. In ultima parte a lucrarii se realizeaza o analiza energetica si economica privind impementarea acestori tipuri de sisteme neconventionale

***Cuvinte cheie:*** *Sistem hibrid, panou fotovoltaic, pompă de căldură.*

**Abstract**

In this paper is it presented functional modelling of an unconventional system composed by fotovoltaic panels which are producing electric energy to drive the compressor of a heat pump to produce termal power for central heating unit of a building or to be used for daily hot water. Can be seen in tha paper the corresponding equations to evaluate electrical power from sollar cells and equations to establish the dynamic termal power given by heat pump to final costumer. At the end will be realized an energetic analyze and economic aspects to conclude the implementation of such unconventional systems.

***Key words***: hibryd system, fotovoltaic cells, heat pump

## 1. Introducere

Cladirile nZEB despre care se discuta tot mai mult in ultimul timp se bazeaza in majoritatea cazurilor pe utilizarea surselor regenerabile, surse care sunt capabile sa disponibilizeze o mare cantitate de energie produsa de surse clasice bazate pe hidrocarburi. Sistemul analizat in cadrul lucrarii se bazeaza pe panouri solare fotovoltaice care produc energie electrica utilizata parial sau total de o pompa de caldura care deserveste sistemul de incalzire sau de preparare a apei calde de consum pentru o cladire. Energia termica absorbita de pompa de caldura cu compresie, este o energie preluata la vaporizatorul pompei de caldura din mediul exterior (aer, apa sau sol). In acest fel se poate spune ca energia furnizata consumatorului de pompa de caldura este in totalitate bazata pe surse regenerabile. In situatia in care puterea furnizata de sistemul sursa neconventional nu acopera necesarul de putere al consumatorului, deficitul de putere este acoperit de un sistem clasic de tip centrala termica functionand cu combustibil fosil. Avand in vedere cota importanta de energie bazata pe sursele regenerabile sistemul poate fi fezabil, insa randamentul destul de scazut la care lucreaza panourile fotovoltaice reduce din punct de vedere economic agreerea implementarii unor astfel de sisteme.

## 2. Descrierea sistemului sursa neconventional. Modelarea functionarii componentelor sistemului.

Asa cum s-a mentionat si capitolul anterior sistemul sursa are doua componente de baza si anume suprafata de panouri solare fotovoltaice care produce putere electrica si pompa de caldura de caldura care utilizeaza aceasta putere electrica alaturi de o putere termica absorbita la vaporizatorul pompei de caldura pentru furnizarea de putere termica la condensatorul pompei de caldura catre sistemul de incalzire sau de preparare a apei calde al consumatorului.

In cazul primei componente a sistemului sursa neconventional, panourile solare fotovoltaice, relatia de baza se refera la randamentul de lucru al suprafetei de captare care se stabileste ca fiind:

$$\eta_{FV} = k_{pk} \cdot \eta_t \cdot \eta_{inv} \tag{1}$$

Primul dintre cei trei termeni ai produsului din membrul drept al relatiei (1) este fie factorul de putere la varf al panoului fotovoltaic fie eficienta panoului fotovoltaic care se calculeaza simplu pe baza puterii de catalog a panoului. In continuare se stabileste densitatea de putere electrica captata pe baza randamentului de lucru al panourilor solare fotovoltaice si a intensitatii radiatiei solare globale stabilite in prealabil:

$$p_{EL} = \eta_{FV} \cdot I \tag{2}$$

Intensitatea radiatiei solare se stabileste (vezi [1]) conform relatiei,:

$$I = f_{cap} \cdot I_O \tag{3}$$

In functie de valoarea intensitatii radiatiei solare pe plan orizontal si de unghiul de inclinare si unghiul azimutal al panourilor solare fotovoltaice.

In cazul celei de a doua componente, pompa de caldura, un parametru de baza este coeficientul de performnta al acesteia care se stabileste (vezi [3]), conform relatiei:

$$COP_{CD} = \eta_{EL} \cdot f_{CD} \cdot \varepsilon_{CD}^{C} \tag{4}$$

Coeficientul de performanta al pompei de caldura, $COP_{CD}$, este variabil pe parcursul utilizarii acesteia, functie de temperatura sursei reci si temperatura mediului in care se livreaza puterea termica. Atat factorul de corectie $f_{CD}$ cat si eficienta termica Carnot, $\varepsilon_{CD}$, depind de cele 2 temperaturi mentionate conform relatiilor:

$$f_{CD} = \frac{(\alpha_1 \cdot T_{CD} + \beta_1 + 1) \cdot f + (\alpha_2 \cdot T_{CD} + \beta_2 - 1)}{f + 1} \tag{5}$$

Unde: $\alpha_1 = 0.0108$ (1/K), $\beta_1 = -4.7121$ (-), $\alpha_2 = -0.0202$ (1/K), $\beta_2 = 9.3974$ (-), iar:

$$\varepsilon_{CD}^{C} = \frac{T_{CD}}{T_{CD} - T_{VP}} = \frac{f}{f - 1} \quad unde \quad f = \frac{T_{CD}}{T_{VP}} \tag{6}$$

Temperaturile absolute la vaporizatorul si condensatorul pompei de caldura se stabilesc in functie de temperaturile mediilor din care se extrage si catre care se livreaza flux termic, conform relatiilor:

$$\begin{aligned} T_{VP} &= t_{VP} + 273{,}15 = \theta_{VP} - \Delta t_{VP} + 273{,}15 \\ T_{CD} &= t_{CD} + 273{,}15 = \theta_{CD} + \Delta t_{CD} + 273{,}15 \end{aligned} \tag{7}$$

Se poate spune ca factorul de corectie $f_{CD}$ reprezinta o prima corectie aplicata eficientei Carnot, $\varepsilon^{C}_{CD}$, in urma careia se obtine o eficienta efectiva a pompei de caldura pe care o putem nota cu $\varepsilon^{*}_{CD}$. Aceasta eficienta efectiva a pompei de caldura, $\varepsilon^{*}_{CD}$, urmeaza sa fie corectata in continuare cu randamentul isentropic, rezultand in final coeficientul de performanta al pompei de caldura, $COP_{CD}$. Astfel produsul $\eta_{EL}*f_{CD}$ reprezinta corectia ce trebuie aplicata eficientei Carnot, $\varepsilon^{C}_{CD}$, pentru determinarea coeficientului de performanta al pompei de caldura, $COP_{CD}$. Cei 2 factori de corectie metionati fiind subunitari rezulta ca intre cele 3 eficiente aferente pompei de caldura exista relatia:

$$COP_{CD} < \varepsilon_{CD}^{*} < \varepsilon_{CD}^{C} \tag{8}$$

Puterea termica furnizata de pompa de caldura se stabileste conform relatiei cunoscute:

$$\Phi_{CD} = COP_{CD} \cdot P_{EL} = \eta_{EL} \cdot f_{CD} \cdot \varepsilon_{CD}^{C} \cdot P_{EL} \tag{9}$$

Sau:

$$\Phi_{CD} = \eta_{EL} \cdot f_{CD} \cdot \varepsilon_{CD}^{C} \cdot P_{EL} = \eta_{EL} \cdot f_{CD} \cdot \varepsilon_{CD}^{C} \cdot p_{EL} \cdot S_{C} \tag{10}$$

Utilizand pentru $\boldsymbol{p_{EL}}$ relatia (2), relatia (10) devine:

$$\Phi_{CD} = \eta_{EL} \cdot f_{CD} \cdot \varepsilon_{CD}^{C} \cdot \eta_{FV} \cdot I \cdot S_C \tag{11}$$

Raportand fluxul termic furnizat de pompa de caldura conform relatiei (11) la suprafata panourilor solare fotovoltaice se obtine fluxul termic unitar afferent sistemului sursa conform:

$$\varphi_{CD} = \eta_{EL} \cdot f_{CD} \cdot \varepsilon_{CD}^{C} \cdot \eta_{FV} \cdot I \tag{12}$$

Cea de a 3-a componenta a sistemului in ansamblu este instalatia de incalzire sau de preparare a apei calde de consum. Daca ne referim la utilitatea privind incalzirea spatiilor consumatorului, atunci evaluarea puterii termice necesare medii lunare poate fi evaluata conform relatiei:

$$\Phi_{NEC\_INC} = H_{INC} \cdot \left(t_{i0} - t_e\right) \tag{13}$$

Iar daca ne referim la utilitatea privind prepararea apei calde de consum, atunci relatia va fi:

$$\Phi_{NEC\_ACC} = H_{ACC} \cdot \left(t_c - t_r\right) \tag{14}$$

Capacitatile de transfer termic aferente consumatorului pe cele doua tipuri de utilitatiti (incalzire – $H_{inc}$, preparare apa calda de consum – $H_{acc}$) au relatii specifice de calcul conform [1]. Astfel:

$$\begin{aligned} H_{INC} &= \left( \frac{S}{R_m} + 0.34 \cdot n_a \cdot V \right) \\ H_{ACC} &= 1.163 \cdot G_{ACC} \end{aligned} \tag{15}$$

Temperatura exterioara medie lunara se stabileste conform standardului de numar anual de grade zile (vezi [2]).

In cadrul analizei energetice care va fi efectuata se va considera ca se porneste cu o suprafata de panouri solare fotovoltaice si cu pompa de caldura capabile sa acopere integral necesitatile consumatorului, adica in cazul incalzirii corespunzator unei temperaturi exterioare medii lunare minime. Astfel:

$$\Phi_{NEC\max} = \phi_{CD} \cdot S_{C\max} = \eta_{EL} \cdot f_{CD} \cdot \varepsilon_{CD}^{C} \cdot \eta_{FV} \cdot I \cdot S_{C\max} \tag{16}$$

Rezulta:

$$S_{C\max} = \frac{\Phi_{NEC\max}}{\phi_{CD}} \tag{17}$$

Se poate stabili in continuare gradul de acoperire energetica lunar ca fiind:

$$G_{AE} = \Phi_{CD} / \Phi_{NEC} \tag{18}$$

In situatiile in care gradul de acoperire energetica va rezulta supraunitar se va considera ca $\Phi_{CD} = \Phi_{INC}$, ceea ce inseamna ca nu toata energia electrica produsa de suprafata de panouri solare fotovoltaice va fi utilizata de catre pompa de caldura. Mai concret, din energia electrica produsa de suprafata de captare solara va fi utilizata pentru pompa de caldura numai:

$$P_{EL} = \frac{\Phi_{CD}}{COP_{CD}} = \frac{\Phi_{NEC}}{COP_{CD}} \tag{19}$$

Restul de putere electrica calculabila cu relatia:

$$\Delta P_{EL} = \frac{\Phi_{CD} - \Phi_{NEC}}{COP_{CD}} \tag{20}$$

urmand a fi livrata in sistemul national.

Desigur ca in situatiile in care suprafata de captare solara va fi mai mica decat in varianta maxima vor fi situatii in care consumatorul va fi acoperit pe parte termica atat prin contributia pompei de caldura cat si prin contributia unei central termice clasice, functionand pe baza de combustibili fosili. De asemenea vor fi si situatii in care puterea electrica furnizata de suprafata de captare solara va fi excedentara necesitatilor pompei de caldura, iar excedentul va fi livrat in reteaua nationala.

Pe baza gradului de acoperire energetica lunar se stabileste gradul de acoperire energetica anual ca medie ponderata a gradelor de acoperire energetica lunare cu numarul de zile corespunzator lunilor.

La fel, pe baza puterilor termice medii lunare, livrate de condensatorul pompei de caldura si numarului de zile corespunzator fiecarei zile se stabileste energia anuala economisita, adica acoperita de catre sistemul sursa neconventional:

$$E_{AE} = 0{,}024 \cdot \sum N_Z \cdot \Phi_{CD} \tag{21}$$

Rezulta de aici, destul de simplu, si valoarea energiei economisite care permite estimarea unei durate de recuperare a costurilor de investitie facute in sistemul sursa neconventional, utilizand si un cost pentru kWh.

Suprafata panourilor solare fotovoltaice a fost un parametru care s-a modificat in cadrul studiului de la o valoare maxima la o valoare minima. Astfel valoarea maxima de suprafata de captare solara s-a calculat astfel incat sa se realizeze o acoperire energetica integrala pentru consumator atat pentru incalzire cat si pentru prepararea apei calde de consum. In continuare, suprafata de captare solara a fost dimunuata progresiv la 90%, 80%,…,10% din valoarea maxima, atat pe partea de incalzire cat si pe parte de apa calda de consum. Pentru fiecare varianta de suprafata de captare solara astfel stabilita, atat la incalzire cat si la apa calda s-a facut evaluarea acoperirii energetice a necesarurilor consumatorului si s-a stabilit gradul de acoperire energetica anual si economia de energie realizata anual.

Mai concret spus, suprafata panourilor solare fotovoltaice de valoare maxima a rezultat astfel incat sa fie acoperit integral necesarul consumatorului in luna cea mai rece a anului atat pentru incalzire cat si pentru apa calda de consum. Valoarea suprafetei panourilor solare fotovoltaice rezulta in functie de puterea electrica necesara pentru realizarea puterii termice la condensatorul pompei de caldura care la randaul ei tribuie sa acopere puterea necesara la consummator. De aici rezulta o corelatie directa intre valoarea suprafetei panourilor solare fotovoltaice si capacitatea pompei de caldura. Asta inseamna ca atunci cand se va considera un sistem sursa avand o suprafata a panourilor solare fotovoltaice mai scazute decat valoarea maxima stabilita si capacitatea pompei de caldura implicate va fi mai scazute. Capacitatea pompei de caldura va fi astfel incat sa poata utiliza in totalitate puterea electrica maxima furnizata de suprafata de captare solara. In ipoteza in care suprafata panourilor solare fotovoltaice are o valoare intermediara mai scazuta decat valoare maxima si capacitatea pompei de caldura va avea o valoare intermediara ceea ce conduce in analiza energetica la identificarea a 2 etape de lucru si anume: etapa compusa din lunile in care pompa de caldura are posibilitatea de a acoperi in totalitate puterea necesara a consumatorului si etapa in care pompa sde caldura ne acopera in totalitate necesarul consumatorului. In prima etapa mentionata puterea termica livrata de pompa de caldura la condensator se considera egala cu necesarul termic al consumatorului si rezulta in consecinta puterea electrica absorbita de pompa de caldura, putere care va fi mai mica decat puterea electrica produsa de catre suprafata de captare a panourilor solare fotovoltaice. Surplusul de putere electrica va fi livrat in reteaua nationala. In a doua etapa puterea termica produsa de catre pompa de caldura va fi mai scazut decat necesarul de putere termica al consumatorului si in consecinta se va face o suplimentare de putere termica cu o central termica functionand cu combustibili fosili, central care lucreaza si ea cu un ransdament de cca. 90%. In acest fel se va realiza analiza energetic ape intraga perioada de functionare a sistemului format din suprafata de captare cu panouri fotovoltaice, pompa de caldura si consummator. In cazul unei luni din prima etapa in care necesarul de putere termica al consumatorului este acoperit integral de catre puterea termica livrata de pompa de caldura, se stabileste pe baza temperaturii exterioare medii lunare, $t_e$, temperatura medie a agentului termic din instalatia de incalzire centrala, $t_M$, conform relatiei:

$$t_M = \frac{t_{M0} - t_{e0}}{t_{i0} - t_{e0}} \cdot t_{i0} - \frac{t_{M0} - t_{i0}}{t_{i0} - t_{e0}} \cdot t_e \tag{22}$$

unde:

$$t_{M0} = \frac{t_{T0} + t_{R0}}{2}; \qquad t_M = \frac{t_T + t_R}{2} \tag{23}$$

care reprezinta temperatura $\theta_{CD}$ din relatiile (7). In cazul prepararii apei calde de consum temperatura $\theta_{CD}$ este media aritmetica dintre temperatura apei cade si temperatura apei reci.

In continuare cunoscand puterea termica livrata la condensatorul pompei de caldura si coeficientul de performanta al pompei de caldura, $COP_{CD}$, se determina puterea electrica necesara utilizand relatia (9). Pe de alta parte se poate determina puterea electrica produsa de suprafata de panouri solare fotovoltaice ca produs intre puterea electrica unitara produsa in luna analizata (calculabila conform relatiei (2) si suprafata de captare stabilita. Diferenta dintre cele 2 valori de putere electrica reprezinta valoarea care se transmite in sistemul national.

In etapa a 2-a se stabileste puterea termica cedata de pompa de caldura conform relatiei (9) in care cei doi termeni ai produsului se determina asa cum a fost descris mai inainte, rezultand o valoare mai mica decat necesarul de putere termica al consumatorului care se stabileste conform relatiilor (13) sau (14). Diferenta dintre puterea termica necesara la consummator si puterea termica cedata de catre pompa de caldura va fi furnizata de catre o centrala termica cu combustibil fosil care lucreaza cu un randament de 90%.

## 3. Analiza energetica privind functionarea sistemului neconventional. Aspecte economice.

Analiza energetica s-a efectuat pentru un studiu de caz in care s-a considerat un ansamblu de cladiri colective insumand 80 de apartamente cu un numar de 2,5 persoane pe apartament. Asta a condus la capacitatile de transfer de caldura: la incalzire: Hinc = 16000 W/K, si la apa calda - Hacc = 698 W/K.

Asa cum s-a mai precizat valoarea maxima de suprafata de captare solara s-a calculat astfel incat sa se realizeze o acoperire energetica integrala pentru consumator atat pentru incalzire cat si pentru prepararea apei calde de consum. In continuare, suprafata de captare solara a fost dimunuata progresiv la 90%, 80%,…,10% din valoarea maxima, atat pe partea de incalzire cat si pe parte de apa calda de consum. Pentru fiecare varianta de suprafata de captare solara astfel stabilita, atat la incalzire cat si la apa calda s-a facut evaluarea acoperirii energetice a necesarurilor consumatorului si s-a stabilit gradul de acoperire energetica anual si economia de energie realizata anual.

S-a gasit interesanta o reprezentare grafica a gradului de acoperire enrgetica functie de cota de suprafata de captare solara din suprafata de captare solara maxima asa cum a fost definita mai inainte.

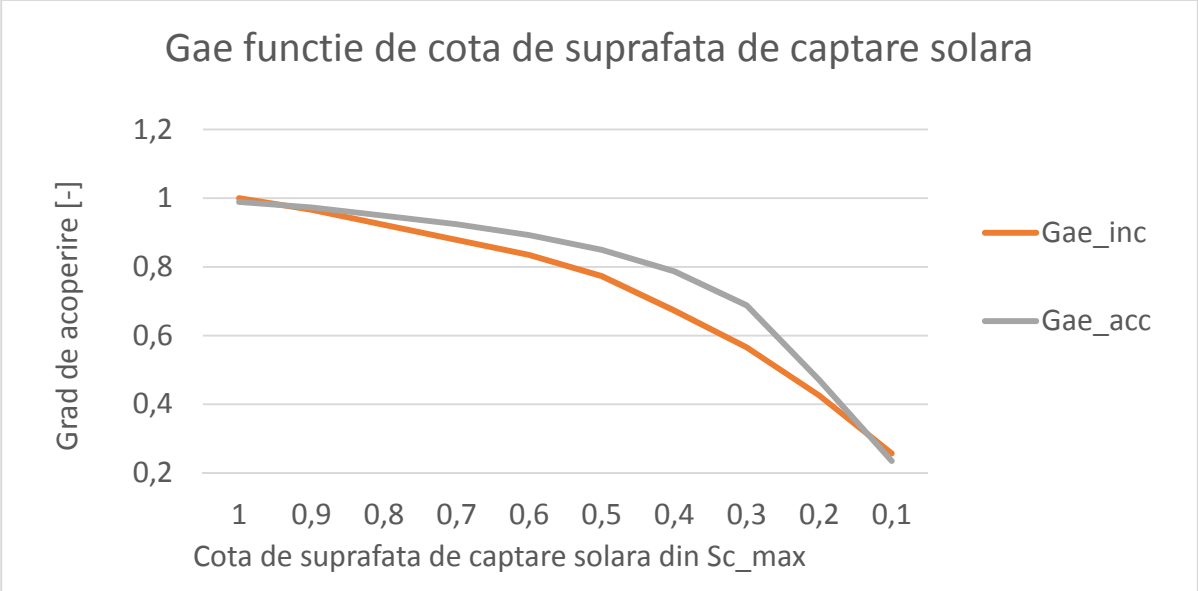


Fig.1 – Gradul de acoperire energetica functie de cota din Sc_max

Trebuie sa mentionam faptul ca in cazul utilitatii de incalzire a consumatorului analiza intreprinsa a presupus numai 6 luni in perioada sezonului rece al anului, in timp ce in cazul utilitatii de preparare a apei calde de consum analiza a presupus toate cele 12 luni ale anului.

O alta corelatie interesanta rezultata a fost intre gradul de acoprire energetica si raportul dintre capacitatea de transfer termic a consumatorului pe parte de incalzire si de apa calda de consum si suprafata de captare solara a panourilor fotovoltaice.

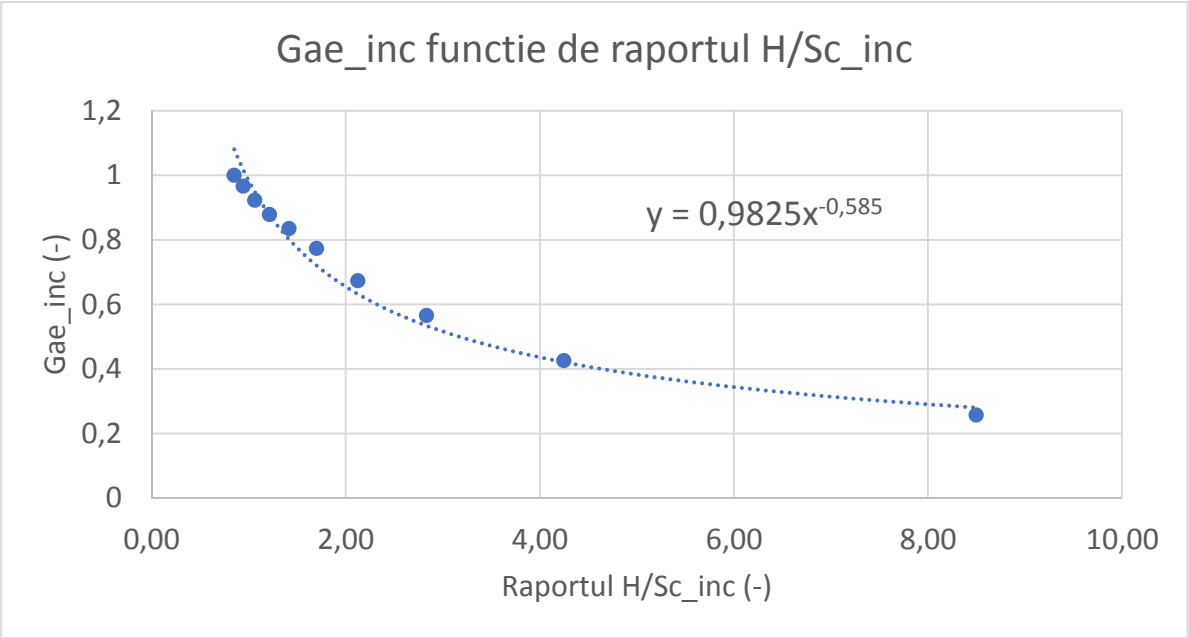


Fig. 2 – Gradul de acop. energetica, functie de raportul - H/Sc_inc

Cresterea raportului H/Sc_inc (adica capacitatea de transfer termic a consumatorului care revine la $m^2$ de suprafata de captare), inseamna de fapt scaderea suprafetei de captare solara conform procedurii prezentate pana la 10% din valoarea maxima cand inca mai poate asigura cca. 25% ca acoperire energetica. Un calcul simplu conduce la cca. 23 $m^2$ de suprafata de captare solara pe apartament in timip ce pentru o acoperire energetica de 100% suprafata de captare solara trebuie sa fie de cca. 235 $m^2$/ap, ceea ce inseamna o valoare foarte foarte mare. Trebuie insa sa nu se neglijeze faptul ca in prezentarea facuta pana in present nu s-a tinut seama de puterea electrica excedentara furnizata de suprafata de panouri solare fotovoltaice, in lunile in care necesarul de putere termica aferent consumatorului este mai redus decat cel din luna cea mai rece a anului.

In cazul utilitatii de apa calda de consum situatia se prezinta cu totul altfel dat fiind puterea necesara la consumator, care este sensibil mai scazuta. Astfel in situatia in care suprafata de captare solara scade la 10% din valoarea maxima. Cand inca se poate asigura ca acoperire energetica cca. 22% din necesarul consumatorului, rezulta cca. 1,14 $m^2$/ap., in timp ce la acoperire energetica integral rezulta cca. 13 $m^2$/ap. Nici in situatia apei calde de consum nu trebuie insa sa se neglijeze faptul ca in prezentarea facuta pana in present nu s-a tinut seama de puterea electrica excedentara furnizata de suprafata de panouri solare fotovoltaice, in lunile in care necesarul de putere termica aferent consumatorului este mai redus decat cel din luna cea mai rece a anului.

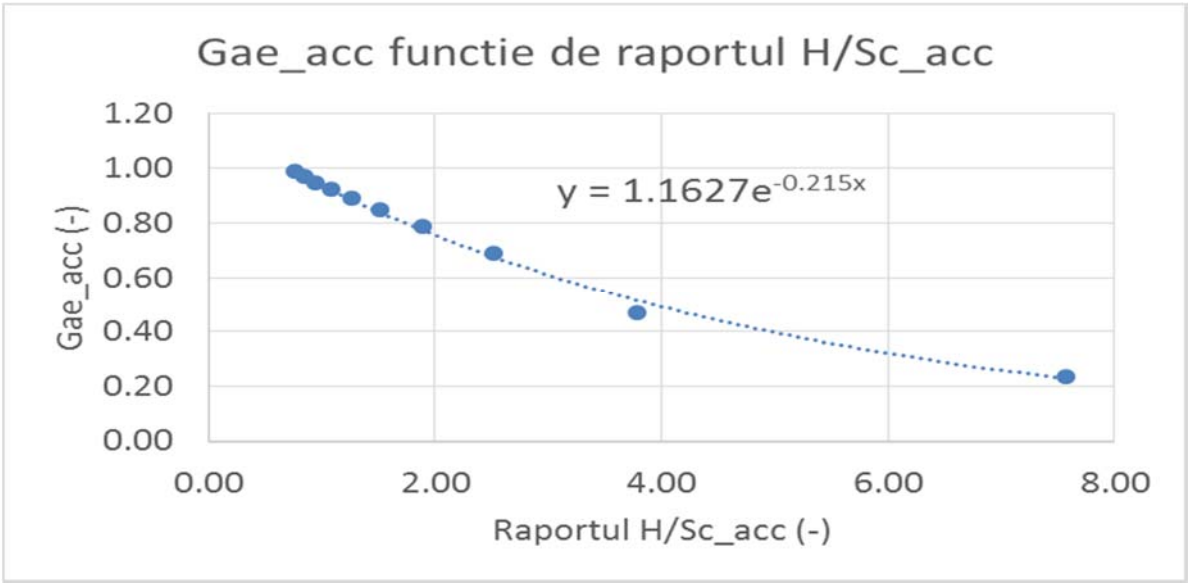


Fig. 3 - Gradul de acop. energetica, functie de raportul - H/Sc_acc

Ca in orice investitie realizarea efectiva poate deveni implementabila daca acest lucru este validat de un studiu de fezabilitate. Astfel in lucrarea de fata s-a incercat o analiza a duretei de recuperare a investitiilor facute in sistemul sursa format din suprafata de panouri solare fotovoltaice si pompa de caldura. O analiza documentara

efectuata asupra costurilor componentelor sistemului sursa neconventionala a condus la o valoare de 1000 EUR/kW instalat pentru panourile fotovoltaice si 225 EUR/kW instalat pentru pompe de caldura cu compresie mecanica. In ceea ce priveste costul specific al energiei s-a considerat 0.14 EUR/kWh. In aceste conditii au rezultat corelatii intre costurile investitiei si marimea suprafetei de panori solare instalate. Reamintim faptul ca suprafata de panouri solare fotovoltaice impune si marimea pompei de caldura, astfel incat aceasta sa fie capabila sa utilizeze intreaga putere electrica produsa de suprafata de captare solara.

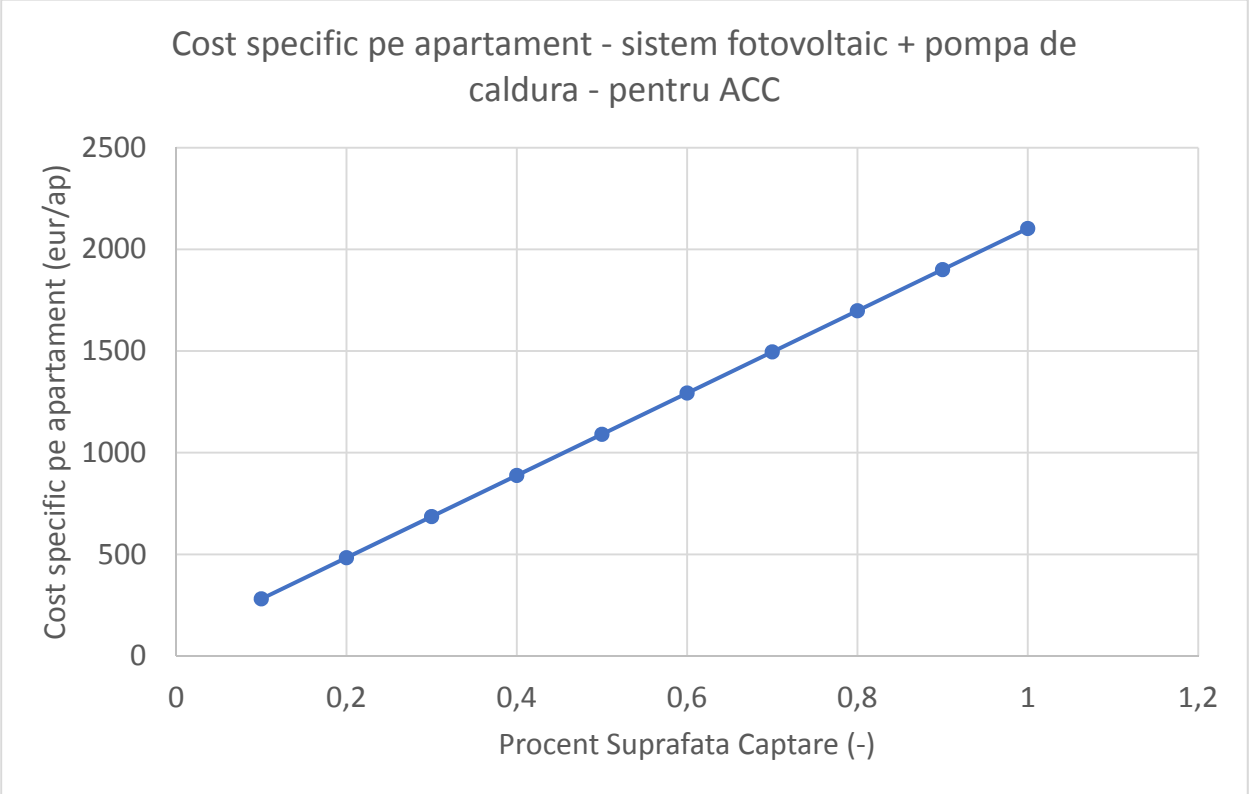


Fig. 4 – Costul specific pe apartament functie de cota de suprafata de panouri fotovoltaice implementata in cazul utilitatii de preparare a apei calde de consum

Din fig. 4 se remarca faptul ca acoperirea integrala a necesarului de putere termica pentru prepararea apei calde de consum pe baza sistemului neconventional conduce la un cost specific pe apartament de cca. 2100 EUR/ap valoarea scazand pana la cca .280 EUR/ap. in cazul in care suprafata de captare devine 10% din valoarea maxima, ceea ce insemna cca. 25% acoperire energetica. In cazul utilitatii de incalzire a spatiilor costurile de investitie specifice pe apartament sunt sensibil mai ridicate ceea ce diminueaza actualmente sansele de realizare a unor astfel de sisteme pentru incalzirea spatiilor

Problema importanta este insa durata de recuperare a investitiei pe baza diminuarii costurilor de exploatare datorita utilizarii surselor regenerabile.

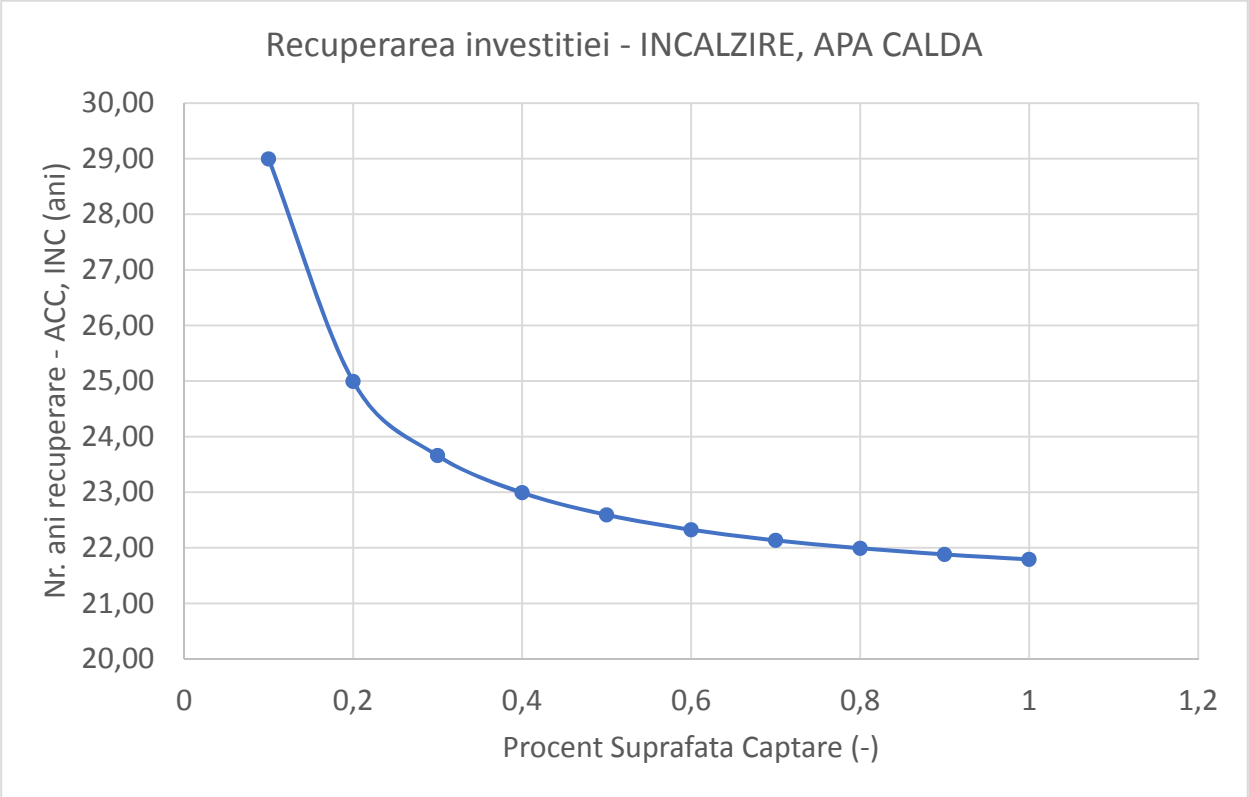


Fig. 5 – Durata de recuperarea a investitiei functie de cota de suprafata de panouri solare fotovoltaice pentru utilitati de preparare a apei calde de consum sau incalzirea spatiilor

Din fig. 5 se observa ca durata de recuperare a investitiei in astfel de sisteme se recupereaza destul de greu, durata fiind de cca 22-25 de ani atat pentru utilitatea de prepararea a apei calde de consum cat si pentru utilitatea de incalzire a spatiilor (cand insa investitiile sunt insa sensibil mai mari). Se observa ca durata de recuperare mai mare rezulta in cazul diminuarii suprafetei de panouri fotovoltaice.

Durata relativ mare de recuperare a investitiei aferente acestui tip de sistem neconventional de utilizare a surselor regenerabile face necesara subventionarea de catre stat in vederea cresterii increderii in aceste tipuri de sisteme neconventionale. Actualmente utilizarea captatoarelor solare termice pentru prepararea apei calde de consum si incalzirea spatiilor sta la baza tot a unor sisteme neconventionale insa sensibil mai rapid recuperabile ca investitie, ceea ce dupa cum este cunoscut, sa fie des intalnite in tot felul de aplicatii practice pentru alimentarea cu energie a cladirilor.

## 4. Concluzii

Conform analizei energetice, gradul de acoperire energetica pe care sistemul neconventional format din panouri solare fotovoltaice si pompa de caldura il ofera consumatorului poate fi de 100% si poate fi diminuata pana la ca 25% daca suprafata de captare solara scade la 10% din valoarea maxima corespunzatoare acoperirii integrale.

In lucrare se prezinta corelatiile intre gradul de acoperire energetica si raportul dintre capacitatea de transfer termic aferenta consumatorului pe parte de incalzire a spatiilor si pe parte de prepararea de apa calda si suprafata de captare a panourilor fotovoltaice. Se remarca faptul ca acoperirea integrala a necesarului de putere termica pentru prepararea apei calde de consum pe baza sistemului neconventional conduce la un cost specific pe apartament de cca. 2100 EUR/ap, caz in care acoperirea energetica este integrala, valoarea scazand pana la cca .280 EUR/ap. caz in care acoperirea energetica este de cca. 25%. In cazul utilitatii de incalzire a spatiilor, valorile sunt sensibil mai mari.

Recuperarea investitiei variaza intre 22 si 23 ani in majoritatea cazurilor fapt care face ca sistemul neconventional format din panouri solare fotovoltaice si pompa de caldura pentru alimentarea cu energie termica a unor consumatori de tipul cladirilor rezidentiale sau nerezidentiale sa reprezinte deocamdata solutii scumpe care pentru a fi implemetate necesita subventia din partea statului.

## Lista de Notatii

$t_{i0}$ – temperatira interioara normata, $^oC$;
$t_{e0}$ – temperatira exterioara de calcul, $^oC$;
$t_e$ – temperatura exterioara medie lunara, $^oC$;
$t_c$ – temperatura de livrare a apei calde de consum, $^oC$;
$t_r$ – temperatura apei reci de consum, $^oC$;
$t_{T0}$ – temperatura de calcul a agentului termic la intrarea in instalatia de incalzire, $^oC$;
$t_{R0}$ – temperatura de calcul a agentului termic la iesirea in instalatia de incalzire, $^oC$;
$t_{M0}$ – temperature medie de calcul a agentului termic in instalatia de incalzire, $^oC$;
$t_T$ – temperatura agentului termic la intrarea in instalatia de incalzire, $^oC$;
$t_R$ – temperatura agentului termic la iesirea in instalatia de incalzire, $^oC$;
$t_M$ – temperature medie a agentului termic in instalatia de incalzire, $^oC$;
$T_{CD}$ – temperatura absoluta de condensare a agentului termic, K;
$T_{VP}$ – temperatura absoluta de vaporizare a agentului termic, K;
$t_{CD}$ – temperatura de condensare a agentului termic, $^oC$;
$t_{VP}$ – temperatura de vaporizare a agentului termic, $^oC$;
$\theta_{CD}$ – temperatura mediului unde se livraza putere termica, $^oC$;
$\theta_{VP}$ – temperatura mediului de unde se absoarbe putere termica, $^oC$;
$\Delta t_{CD}$ – diferenta medie logaritmica de temperatura la condensator, $^oC$;
$\Delta t_{VP}$ – diferenta medie logaritmica de temperatura la vaporizator, $^oC$;
$\Phi_{NEC}$ – putere termica necesara la consumator, W;
$\Phi_{NEC\_INC}$ – putere termica necesara la consummator pentru incalzire, W;
$\Phi_{NEC\_ACC}$ – putere termica necesara la consummator pentru preparare apa calda, W;
$H_{INC}$ – capacitatea de transfer termic a consumatorului pentru incalzire, W/K;
$H_{ACC}$ – capacitatea de transfer termic a consumatorului pentru preparare apa calda de consum, W/K;

$G_{ACC}$ – debitul orar de apa calda de consum, mediu zilnic, l/h;
S – suprafata totala a anvelopei cladiri, $m^2$;
$R_m$ – rezistenta medie a anvelopei cladirii, $m^2$.K/W;
V – volumul spatiului incalzit, $m^3$;
$n_a$ – numarul orar de schimburi de aer aferent spatiului incalzit, 1/h;
I – intensitatea globala a radiatiei solare pentru locatia consumatorului si unghiul de inclinare si de azimut al panourilor solare fotovoltaice, W/$m^2$;
$I_O$ – intensitatea globala a radiatiei solare pe plan orizontal pentru locatia consumatorului al panourilor solare fotovoltaice, W/$m^2$;
$p_{EL}$ – densitatea de putere electrica absorbita de pompa de caldura, W/$m^2$;
$\phi_{CD}$ – densitatea de putere termica livrata la pompa de caldura, W/$m^2$;
$P_{EL}$ – Puterea electrica absorbita de pompa de caldura, W;
$\Phi_{CD}$ – putere termica livrata efectiv de catre pompa de caldura, W;
$\Phi_{NEC\_max}$ – putere termica necesara la consummator pentru dimensionarea sistemului sursa neconventional, W;
$E_{AE}$ – energia anuala acoperita energetic de catre sistemul sursa neconventional, kWh;
$S_C$ – suprafata panourilor solare fotovoltaice, $m^2$;
$N_Z$ – numarul de zile lunar, zile/luna;
$\eta_{EL}$ – randamentul izentropic, -;
$\eta_{FV}$ – randamentul panourilor solare fotovoltaice, -;
$k_{pk}$ – factorul de putere de varf al panourilor solare fotovoltaice, - ;
$\eta_t$ – randamentul termic al panourilor solare fotovoltaice, -;
$\eta_{inv}$ – randamentul invertorului, -;
$\varepsilon^C_{CD}$ – eficienta Carnot la condensatorul pompei de caldura, -;
$\varepsilon^*_{CD}$ – eficienta efectiva la condensatorul pompei de caldura, -;
$COP_{CD}$ – coeficientul de performanta al pompei de caldura, -;
$f_{CD}$ – factor de corectie aplicat randamentului Carnot la condensatorul pompei de caldura;
$G_{AE}$ – grad de acoperire energetica al consumatorului, -;
1.163 – caldura specifica volumica a apei, W.h/l.K;

## Bibliografie

[1] – Mc001/2019 - Metodologia de evaluare a performantelor energetice ale cladirilor;

[2] – SR 4839/2014 – Numarul anual de grade zile;

[3] - Florin Iordache, Alexandru Draghici, Mugurel Talpiga - Comportamentul termic dinamic al unei pompe de caldura functionand intre 2 rezervoare de acumulare – Revista Romana de Inginerie Civila – ed Matrixrom, Bucuresti, 2019, (in curs de aparitie);

# Influența performanțelor la foc ale plăcilor din așchii de lemn (PAL) asupra dezvoltării unui incendiu simulat la scară naturală, într-un spațiu închis

Influence of fire performance of wood chipboards on the development of a natural scale simulated fire, in a confined space

**Alexandru-Florin CHIOJDOIU[1], Ion ANGHEL[2], Valentin ENCIU[3], Ionel-Alin MOCIOI[4], Emil Florin TUDOR[5]**

DOI: 10.37789/rjce.2021.12.1.9

[1]Universitatea Politehnica București
București, sector 6, Splaiul Independenței, nr. 313
Inspectoratul pentru Situații de Urgență "Dealul Spirii" București-Ilfov București, sector 5, Calea 13 Septembrie, nr.135, România
*alex.floryn@yahoo.com*

[2]Academia de Politie "Alexandru Ioan Cuza" – Facultatea de Pompieri București, sector 2, Șoseaua Morarilor, nr.3, România
*ion_anghel2003@yahoo.com*

[3]Academia de Politie "Alexandru Ioan Cuza" – Facultatea de Pompieri
București, sector 2, Șoseaua Morarilor, nr.3, România
*val_enciu@yahoo.com*

[4]Academia de Politie "Alexandru Ioan Cuza" – Facultatea de Pompieri
București, sector 2, Șoseaua Morarilor, nr.3, România
*alin.mocioi@gmail.com*

[5]Inspectoratul pentru Situații de Urgență „Drobeta" al Județului Mehedinți
Drobeta Turnu Severin, Str. Portului Nr.2, România
*tudor_emil_florian@yahoo.com*

**Rezumat.** *În acest studiu se analizează contribuția arderii Plăcilor din Așchii de Lemn (**PAL**) la un incendiu care se manifestă într-un spațiu închis, la scară naturală. Lemnul are o importanță deosebită în dezvoltarea incendiilor la construcții, deoarece este folosit pe scară largă în structura de rezistență, pentru placare, pardoseli sau articole de mobilier. Studiul pornește de la descrierea fenomenelor fizice și chimice care au loc pe timpul procesului de ardere a lemnului și se ajunge la prezentarea performanțelor la foc în condiții de utilizare finală. De asemenea, sunt prezentate rezultatele obținute în urma testării la foc a PAL-ului pentru metodele de încercare ISO 9705 și SBI. Studiul se încheie cu simularea, la scară naturală, a contribuției plăcilor de PAL la dezvoltarea incendiilor care se manifestă în spații închise, prin utilizarea programului de simulare a incendiilor B-RISK, utilizat în cazul celor două metode de testare la foc, în baza a două scenarii de incendiu, astfel: 1. Încăperea de testare nu este prevăzută cu material de*

*finisaj interior, pereții acesteia fiind din beton cu grosimea de 100 mm, respectiv 2 mm. Încăperea de testare este prevăzută cu un lambriu din PAL de 12 mm grosime, folosit ca material de finisaj interior. Rezultă, astfel, o analiză comparativă a temperaturii stratului superior de gaze fierbinți și a plafonului, pentru valorile rezultate în urma utilizării programului B-RISK în cele două situații și metode de încercare. În urma analizei, sunt precizate câteva recomandări care pot îmbunătăți securitatea la incendiu în cazul spațiilor închise ce conțin lemn sub formă de PAL.*

**Cuvinte cheie:** piroliză, performanța la foc, PAL, simularea incendiilor

**Abstract.** *This study analyses the contribution of wood chipboards combustion to a natural scale fire that manifests in a confined space. Wood is of particular importance in the development of fire in buildings, because it is widely used in building's frame structures, for cladding, floors or furniture objects. This study starts from the description of the physical and chemical phenomena occurring during the wood combustion process and continues with the presentation of the fire performance under final use conditions. The results obtained from the fire test of the wood chipboards for ISO 9705 and SBI test methods are presented, also. The study ends with the natural-scale simulation of the wood chipboards contribution to the development of confined space fires, by using the B-RISK fire simulation program, based on the two fire test methods and the two fire scenarios. There are two fire scenarios: 1st. The test room is not cladded with interior lining material, its walls made of concrete with a thickness of 100 mm and 2nd. The test room is cladded with 12 mm thickness wood chipboards used as interior lining material. Thus, a comparative analysis of the temperature of the upper layer of hot gases and of the ceiling results from the use of the B-RISK program in the two test situations and methods is obtained. Following the analysis, some recommendations are given that can improve fire safety in the case of confined spaces containing wood in the form of chipboards.*

**Key words:** pyrolysis, fire performance, chipboard (PAL), fire simulation

## 1. Introducere

Dintre materialele de construcție naturale, cel mai utilizat este lemnul, datorită proprietăților fizico-chimice (izolator bun), rezistenței la solicitările mecanice, datorită durabilității sale, dar și a ușurinței de prelucrare, în comparație cu alte materiale. Pe de altă parte, căldura sa, textura plăcută și valoarea decorativă a designului fibrelor lemnului au făcut ca acest material să fie foarte căutat pentru lucrările de amenajare interioară a clădirilor, dar și pentru construcția mobilierului din dotarea clădirilor.

Întrucât lemnul este utilizat pe scară largă în domeniul construcțiilor, s-au fost efectuate numeroase studii în ceea ce privește structura fizico-chimică a lemnului [1], fiind incluse și cele trei principale componente ale acestuia: celuloza, hemiceluloza și lignina [2]. Lemnul folosit în industria de construcții se împarte în lemn de esență tare și lemn de esență moale. Lemnul de esență tare are densitate ridicată [3], în schimb, lemnul de esență moale, chiar dacă are o densitate mai mică, este cel mai des folosit în construcții [4]. În general, lemnul netratat, ca material de construcție, este încadrat în clasa D de performanță privind reacția la foc, atunci când densitatea acestuia este de cel puțin 400 kg/m$^3$, așa cum se poate vedea și în tabelul 2, iar produsele cu densitate

scăzută sunt încadrate în clasa E.

În cazul aplicării tratamentelor ignifuge, produsele din lemn pot atinge nivelurile de clasă C și B. Performanța privind reacția la foc a lemnului se poate modifica odată cu schimbarea utilizărilor finale, iar acestea trebuie cunoscute atunci când sunt analizate riscurile de incendiu. Adăugarea unui strat de ignifugare poate îmbunătăți proprietățile de protecție la foc ale lemnului, însă poate acționa în detrimentul proprietăților intrinseci, cum ar fi rezistența la foc sau creșterea cantității de fum eliberat. Pentru a îmbunătăți comportamentul lemnului la acțiunea focului sunt utilizate diferite produse de ignifugare. Substanțele ignifuge sunt, de obicei, aplicate pe suprafața lemnului sau sunt impregnate în structura acestuia, folosind o tehnică de vacuum-presiune. Se mai pot utiliza minerale anorganice, cum ar fi sericitul și foliile metalice în combinație cu produsele intumescente. Au fost testate formulele care conțin siliciu, azot și fosfor, iar menținerea siliciului în lemn s-a obținut grație utilizării de micro-straturi de dioxid de siliciu [5]. O nouă generație de substanțe pentru ignifugarea lemnului este reprezentată de nanoagenții de întârziere a incendiilor, cum ar fi acoperirile nanocompozite [6]. Grafitul expandabil, utilizat, de obicei, în cazul polimerilor, poate proteja, în egală măsură, și lemnul, atunci când este folosit pentru acoperirea suprafețelor acestuia. În cazul tratamentelor studiate pentru ignifugarea lemnului, modelele predictive pot fi folosite în combinație cu datele obținute în urma testelor con-calorimetrice, în scopul de a prezice comportamentul unui material în testul SBI (în engleză: Single Burning Item) [7], stabilind, astfel, încadrarea într-o anumită euroclasă de reacție la foc.

Întrucât cererea de utilizare a lemnului și a produselor pe bază de lemn pentru aplicații în domeniul construcțiilor a crescut în ultimii ani și producția de plăci din așchii de lemn a cunoscut o evoluție remarcabilă datorită diversificării sortimentelor și a unor caracteristici îmbunătățite față de lemnul masiv. Plăcile realizate din așchii de lemn, aglomerate cu rășini sintetice, se confecționează din deșeuri sau particule de lemn de foioase moi sau rășinoase, mărunțite pe cale mecanică și aglomerate cu ajutorul unor adezivi sintetici, sub influența presiunii și a temperaturii. La panourile propriu-zise alcătuite din particule de lemn sunt folosite elemente de lemn (așchii), care pot fi fine, normale (lungime maximă 20 mm) și mari (lungime minimă 32 mm). Ca liant se folosesc rășinile sintetice, conținutul fiind de aproximativ 11% din masa totală, pentru straturile exterioare și 5% pentru stratul central. Presarea se realizează perpendicular pe fețe sau paralel cu fețele plăcii (extrudate).

În general, nu trebuie folosit doar un singur instrument de testare la foc a PAL-ului pentru a evalua proprietățile de termodegradare și de inflamabilitate ale acestuia. Combustia calorimetrică la microscală nu va arăta efectul unei acoperiri de suprafață, deoarece este destinat pentru analiza arderii în vrac [8]. Con-calorimetria este incapabilă să reprezinte propagarea flăcării pe suprafața unui specimen de testare. În schimb, standul pentru testarea aprinzibilității produselor pentru construcții în contact direct cu flacăra are această capacitate de a analiza propagarea pe suprafață a flăcării [9]. Deoarece dezvoltarea incendiului este caracterizată de evoluția în timp a fluxului căldurii degajate de incendiu (în engleză Heat Release Rate, HRR) - acesta fiind un parametru esențial în modelarea incendiilor -, în cadrul acestui studiu au fost extrase

din bazele de date internaţionale curbele HRR pentru PAL. Acestea au fost realizate conform încercărilor SBI şi ISO 9705 inter-laboratoare pentru materialele uzuale în construcţii.

## 2. Piroliza şi arderea lemnului

Când lemnul este încălzit treptat, la temperaturi ridicate încep să apară schimbări în structura sa, iar cele trei componente polimerice din lemn încep să se descompună termic într-un amestec de gaze volatile, gudron şi reziduu carbonizat cu conţinut de cărbune. Mai întâi se descompune hemiceluloza (la 180-350°C), urmată de celuloză (la 275-350°C) şi lignină (la 250-500°C) [10]. Reacţiile moleculare de oxidare deshidratează celuloza şi începe repolimerizarea levoglucosanului, care duce la slăbirea structurilor aromatice, acestea devenind structuri de carbon grafitat în jurul valorii temperaturii de 500°C, proces denumit piroliză. Pe timpul pirolizei are loc transportul umidităţii, formarea unor produse precum dioxidul de carbon, acizi formici şi acizi acetici la valori de temperatură sub 200°C, formarea unor produse ce conţin gaze inflamabile, fum şi levoglucosan, la valori de temperatură între 300°C şi 500°C, respectiv limitări ale transferului termic ce vor afecta descompunerea termică a lemnului neafectat. Transportul umidităţii (w) presupune că, atunci când începe să se încălzească, înainte de startul pirolizei, apa din compoziţia lemnului începe să se evapore. Majoritatea vaporilor de apă vor părăsi volumul ocupat de lemn, însă o parte din cantitatea de vapori va migra departe de zona expusă căldurii, în interiorul lemnului, creându-se astfel trei zone: o zonă uscată, în apropierea părţii expuse sursei de căldură (w=0), o zonă deshidratată ($w< w_{FSP}$ ) şi o zonă umedă ($w>w_{FSP}$ ), aşa cum se poate vedea în figura 1 [11]. Punctul de saturaţie a fibrei (în engleză: Fiber Saturation Point, FSP) este definit ca fiind conţinutul în umiditate la care cavităţile celulare sunt golite de apa aflată în stare lichidă, în schimb pereţii celulari sunt totuşi saturaţi cu apa legată chimic.

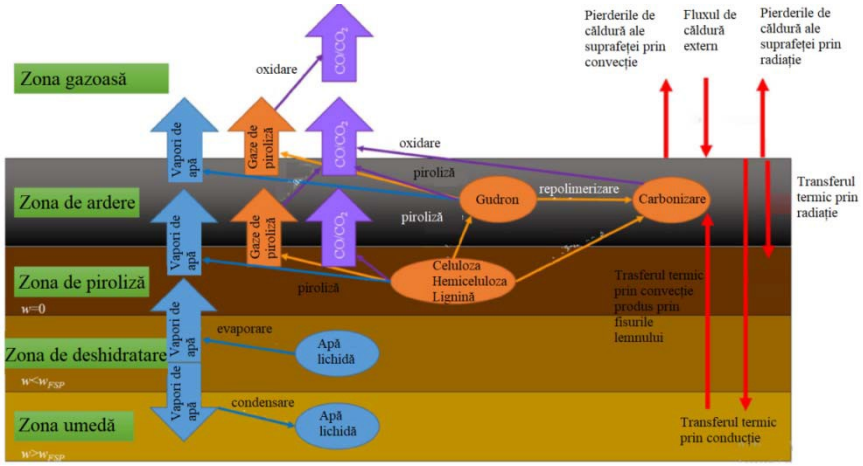


Fig. 1. Procesele fizice şi chimice care au loc în interiorul unei material lemnos care arde [11]

Piroliza lemnului a făcut obiectul unor cercetări ample în ultimii ani [12], [13],

[14], cercetări care au arătat că, în timp ce la suprafața carbonizată a lemnului se pot înregistra valori de temperatură de 800°C, piroliza principală a lemnului începe la valori de peste 225°C și se termină la valori de temperatură sub 500°C. Atunci când s-a atins concentrația adecvată a amestecului combustibil-aer, oxidarea gazelor de piroliză conduce la arderea cu flacără [15]. Oxidarea reziduului carbonizat se produce cu incandescență sau prin ardere mocnită. Dacă materialul este lăsat în faza solidă ca reziduu carbonizat, descompunerea de bază a lemnului este încetinită. Reziduul carbonizat acționează ca o creștere a rezistenței termice între lemnul de bază și frontul pirolizei. Acest lucru duce la o scădere a debitului de căldură degajată și acționează ca o barieră a transferului de masă între volatilele eliberate de combustibil și oxigenul din aer. Structura reziduului carbonizat variază în funcție de tipul de lemn, de tratamentul de ignifugare aplicat și de debitul de căldură degajată, iar stabilitatea și integritatea lemnului sunt influențate de densitate, continuitate, rezistența la oxidare, proprietățile termoizolante și permeabilitate. Producția de reziduu carbonizat depinde de debitul de căldură degajată și de lungimea de încălzire. Descompunerea ligninei are o contribuție semnificativă la formarea de reziduu carbonizat [16]. Ratele caracteristice de carbonizare a lemnului de esență moale sunt de ordinul a 0,6 $mm/min^{-1}$, în cazul utilizării metodelor de testare standard pentru determinarea clasificării rezistenței la foc a elementelor structurale și a ansamblurilor [17], [18]. Ele depind de densitatea, de grosimea stratului de reziduu carbonizat, de conținutul de umiditate, de concentrația de oxigen și de fluxul extern de căldură [19], [20]. Lemnul produce mai puțin fum când arde în comparație cu multe dintre materialele plastice. În condiții bune de ventilare, lemnul poate produce 25-100 $m^2/kg$ de fum, în timp ce materialele plastice pot elibera sute sau mii de $m^2/kg$ [21]. Formarea fumului depinde de materialul ars și de factorii ce includ alimentarea cu oxigen și tipul de ardere, cu flacără sau cu incandescență. Produsele primare ale arderii lemnului sunt monoxidul de carbon, dioxidul de carbon și apa [22], [23], însă pot fi eliberate, de asemenea, acid cianhidric și halogenurile hidrogenate dacă sunt prezente heteroelemente, cum ar fi azotul sau halogenii, care cresc producția de fum, precum și toxicitatea [24]. Prin utilizarea unor produse ignifuge inhibitoare de fum, cum ar fi boratul de zinc și molibdenul și compușii de staniu, are loc încetinirea vitezei de ardere și reducerea procentului de fum și gaze toxice [25]. Pentru analiza termică și evaluarea inflamabilității lemnului sunt utilizate tehnici precum analiza termogravimetrică [26], con-calorimetria [28] și testul SBI. Rezultatele acestor teste sunt dependente de modificările compoziției gazului, ale temperaturii, de viteza de încălzire și de dimensiunea formei eșantionului. Cel mai important parametru în baza căruia se determină comportarea la foc a unui material este fluxul căldurii degajate de acesta [29], [30], existând o serie de studii experimentale cu privire la HRR și la performanța la incendiu a unui material [32]. Rezultatele descompunerii lemnului sunt rezumate în tabelul nr. 1 [33].

**Intervalele de temperatură ale pirolizei și arderii lemnului [33]**

*Tabelul 1*

| Temperatură | Procedee de descompunere |
|---|---|
| > 100 °C | Evaporarea apei nelegate chimic |
| 160-200 °C | Cele trei componente polimerice din lemn încep să se descompună lent. Gazele formate în această etapă sunt necombustibile (elementul principal fiind $H_2O$) |
| 200-225 °C | Piroliza lemnului este încă foarte lentă, iar multe gaze produse sunt încă necombustibile |
| 225-275 °C | Se începe piroliza principală și arderea cu ajutorul unei flăcări pilot. |
| 280-500 °C | Gazele produse sunt acum volatile (CO, metan etc.) și particulele de fum sunt vizibile, iar structura fizică a lemnului se descompune. |
| >500 °C | Producția volatilă este completă, reziduul carbonizat continuă să se oxideze pentru a forma CO, $CO_2$ și $H_2O$ |

## 3. Performanța de reacție la foc a produselor pentru construcții

Pentru a asigura cerința „securitate la incendiu” este necesară limitarea inițierii și propagării focului și fumului prin reducerea contribuției la foc a materialelor de construcție, noțiunea de „combustibilitate” fiind înlocuită cu determinarea contribuției la foc/comportării la foc a produselor. Conceptul de reacție la foc este mult mai larg decât combustibilitatea, incluzând nu numai comportarea la ardere, ci și fluxul de căldură degajat, emisia de fum și gaze de ardere, radiația de căldură, propagarea flăcării. Sistemul de clasificare privind reacția la foc are la bază contribuția produsului, în utilizarea finală, la inițierea și propagarea incendiului [34]. Prin acest sistem, proiectanții și utilizatorii primesc informații complete asupra performanțelor de comportare la foc ale produsului clasificat, în condițiile de utilizare finală, precum: aprinzibilitate, propagarea flăcării, emisia de fum, emisia de gaze toxice. În tabelul 2 sunt prezentate exemple de produse de construcție utilizate în realizarea pereților și plafoanelor, pentru fiecare clasă din sistemul de Euroclase.

**Exemple de produse exprimate în Euroclase pentru pereți și tavan [27]**

*Tabelul 2*

| Euroclase | Exemple de produse |
|---|---|
| A1 | Produse din piatră naturală, beton și produse din beton, cărămizi, produse ceramice, produse din sticlă, produse din oțel, multe produse metalice. |
| A2 | Produse precum cele din clasa A1, inclusiv mici cantități de compuși organici. |
| B | Plăci din ghips-carton cu diferite (grosimi) suprafețe. ***Cel mai ridicat nivel posibil de obținut prin ignifugare pentru produse din lemn rezistente la foc.*** |
| C | Spumă fenolică, plăci din ghips-carton cu diferite suprafețe (mai puțin groase decât cele din clasa B). ***Produse din lemn rezistente la foc.*** |
| D | ***Produse din lemn cu grosimea de minim 5 mm și densitatea mai mică de 400 kg/m$^3$*** |
| E | ***Plăci din fibre cu densitate mică,*** produse de izolare pe bază de plastic |
| F | Produse netestate. |

În general, clasa de bază pentru produsele din lemn, netratat, este D (densitatea este de cel puțin 400 kg/m$^3$). Produsele cu densitate inferioară aparțin clasei E. În ceea ce privește acoperirea podelei, produsele pe bază de lemn se regăsesc, din nou, ca performanță la nivelul D, care este numit $D_{FL}$ din punct de vedere a clasificării de nivel (FL - podea). Pentru produsele pe bază de lemn, clasificarea suplimentară pentru emisia de fum este de obicei s1 sau s2 și clasificarea suplimentară pentru picături arzânde este d0. Clasificările „s" se referă la emisia de fum: clasele s1 - emisie mică de fum, s2 - emisie limitată de fum, s3 - nu se cer limitări ale emisiei de fum. Clasificările „d" se referă la prezența sau absența picăturilor/particulelor arzânde: clasele d0 - fără picături/particule arzânde, d1 - picături/particule care nu persistă peste o durată data, d2 - nu se cer limitări din punct de vedere al particulelor/picăturilor arzânde. Tratamentele ignifuge pentru lemn pot fi clasificate în trei clase generale: aplicarea ca tratament de suprafață; încorporarea integrală a agentului ignifug în produsele compozite din lemn; impregnarea prin tehnici de vacuum/presiune.

### 3.1. Metode de testare la foc a produselor pentru construcții

**Standardul ISO 9705** [35] reprezintă o metodă de testare (figura 2) care simulează un incendiu ce se manifestă într-o încăpere bine ventilată, cu dimensiunile de 3,6 m × 2,4 m × 2,4 m (lungime, lățime, înălțime), având o singură ușă deschisă. Focul pornește dintr-un colț al încăperii. Metoda folosește o sursă de aprindere specifică pentru a evalua contribuția materialelor utilizate ca finisaje pentru perete și tavan la dezvoltarea unui incendiu. Aceste materiale nu pot fi testate la scară mică.

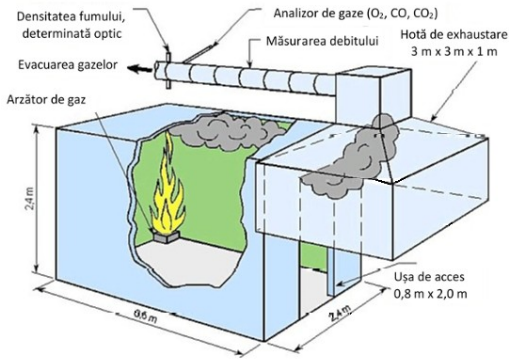


Fig. 2. Cadrul de testare al materialelor de finisaj interior în standardul ISO 9705

Metoda nu este destinată evaluării rezistenței la foc a unui produs, ci pentru a furniza date în ceea ce privește stadiile incendiului, de la aprindere până la flashover. Sursa standard de aprindere este reprezentată de o cutie cu nisip cu un arzător cu dimensiunile de 17 cm x 17 cm, de 100 kW sau de 300 kW, durata expunerii la foc fiind de 10 minute. Produsul care urmează să fie testat se montează pe trei pereți și pe plafon (nu se montează pe peretele cu ușa). Pentru această metodă de testare se iau în considerare următoarele fenomene: picurarea, apariția picăturilor care curg, căderea resturilor și delaminarea, precum și crăparea, topirea într-o anumită măsură,

expansiunea, deplasarea sau distorsiunea. În cadrul metodei de testare se măsoară timpul până la aprindere, fumul (opțional), CO, $CO_2$, $O_2$, gradul de iradiere, debitul de căldură degajată, degajarea totală de căldură, conținutul de gaze de ardere (HCl, HCN, $N_{OX}$, etc.). Nu se efectuează măsurători pentru pierderea de masă și creșterea temperaturii.

**Metoda de testare SBI** [7] este folosită pentru determinarea performanței de reacție la foc a produselor pentru construcții, cu excepția învelișului pentru pardoseală. Instalația de testare trebuie să cuprindă o incintă de încercare, aparatura de încercare (cărucior, cadru, arzătoare, hotă, colector și tubulatură), sistemul de exhaustare al fumului și echipamentul general de măsurare, așa cum este reprezentat în figura 3.

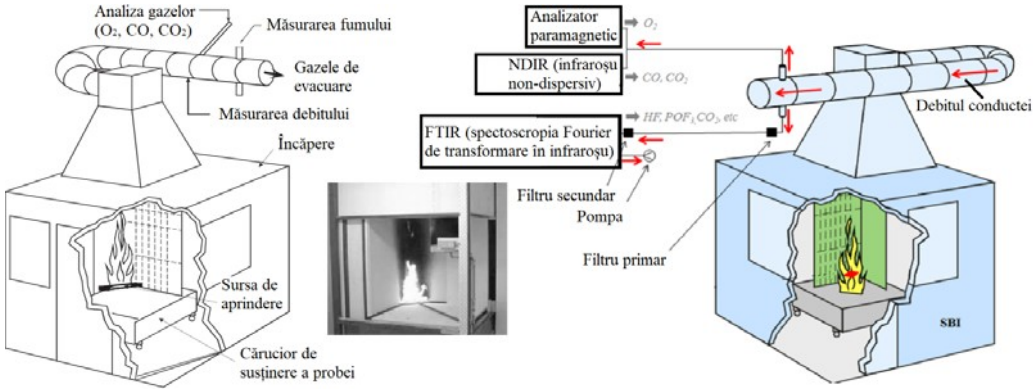


Fig. 3. SBI - Încercarea la foc a unui singur element arzând [36], [37]

Incinta de testare trebuie să aibă o înălțime la interior de 2,4 ± 0,05 m și o suprafață interioară a pardoselii de 3,05 ± 0,05 $m^2$ în ambele direcții. Pereții trebuie să fie construiți din blocuri de construcție, de exemplu beton celular, plăci de ipsos și plăci de silicat de calciu. Epruvetele sunt expuse timp de 20 minute atacului termic al unui arzător tip cutie cu nisip alimentat cu propan, arzătorul având o putere de 30,7 kW. Epruveta pentru colț este formată din două aripi, denumite aripa scurtă și aripa lungă, grosimea maximă a unei epruvete fiind de 200 mm. Proba de testare trebuie să aibă dimensiuni medii (dimensiunea maximă trebuie să fie cuprinsă între 1 și 3 m conform ISO 29903). Parametrii de clasificare determinați cu ajutorul metodei SBI sunt: FIGRA (viteza de dezvoltare a focului) [W/s], $THR_{600s}$ (căldura totală degajată) [MJ], LFS (propagarea laterală a flăcării), SMOGRA (viteza de emisie a fumului) [$m^2/s^2$], $TSP_{600s}$ (emisia totală de fum) [$m^2$]. Testul SBI simulează arderea unui obiect în colțul unei camere. Proba utilizată constă din două părți care formează un unghi de 90 de grade. Configurația testului presupune existența unei podele nu și a tavanului. Podeaua, proba și arzătorul sunt instalate pe un cărucior care poate fi scos din încăpere pentru o amplasare ușoară a probelor. Gazele de ardere sunt colectate de o hotă și transportate printr-o conductă. Conducta conține o secțiune de măsurare a fumului și a producției de fum cu ajutorul unei sonde de presiune diferențială, termocuple, o sondă de gaze și un sistem de măsurare a fumului [38]. Valorile HRR se calculează prin metoda consumului de oxigen [39].

## 3.2. Produsele din lemn clasificate fără teste suplimentare, CWFT

În sistemul european, toate produsele trebuie testate în condiții care reprezintă utilizările lor finale, produsele din lemn având deja statutul de CWFT (în engleză: Classified Without Further Testing), acest statut reprezentând clasificarea fără testarea finisajelor pereților. În tabelul 3 este prezentată o listă tip CWFT pentru produsele din panouri din lemn. Celelalte valori similare din tabel se referă și la produsele din lemn, dar și la cele laminate, lipite.

**Listă CWFT pentru produsele din panouri din lemn [27]**

*Tabelul 3*

| Produse din panouri din lemn* | Gradul de referință al produselor EN | Densitatea minimă ($kg/m^3$) | Grosimea minimă (mm) | Clasa (fără podele) | Clasa podelelor |
|---|---|---|---|---|---|
| Plăci din fibre de lemn de densitate mică (PAL) | EN 312 | 600 | 9 | D-s2, d0 | $D_{FL}$-s1 |
| Plăci din fibre de lemn, dure | EN 622-2 | 900 | 6 | D-s2, d0 | $D_{FL}$ -s1 |
| Plăci din fibre de lemn, medii | EN 622-3 | 600 | 9 | D-s2, d0 | $D_{FL}$-s1 |
| | | 400 | 9 | E | $E_{FL}$ |
| Plăci din fibre le lemn, moi | EN 622-4 | 250 | 9 | E | $E_{FL}$ |
| Plăci din fibre de lemn, de densitate medie (MDF) | EN 622-5 | 600 | 9 | D-s2, d0 | $D_{FL}$ -s1 |
| Plăci din particule de lemn și ciment | EN 634-2 | 1000 | 10 | B-s1, d0 | $B_{FL}$ -s1 |
| OSB | EN 300 | 600 | 9 | D-s2, d0 | $D_{FL}$ -s1 |
| Placaj din lemn | EN 636 | 400 | 9 | D-s2, d0 | $D_{FL}$ -s1 |
| Panouri din lemn solide | EN 13353 | 400 | 12 | D-s2, d0 | $D_{FL}$ -s1 |

* Panouri din lemn montate fără goluri de aer pe produse din clasa A1 sau A2-s1, d0, cu densitate minimă de 10 $kg/m^3$ sau cel puțin produse din clasa D-s2, d0, cu densitatea minimă de 400 $kg/m^3$.

## 3.3. Factorii care afectează performanța la foc a produselor din lemn

Atât în cazul testelor de incendiu, cât și al incendiilor reale, există doi parametri importanți care afectează performanța la foc a produselor din lemn: densitatea și grosimea. Cu cât densitatea este mai mică, cu atât este nevoie de o perioadă mai scurtă de timp pentru ca suprafața lemnoasă să ajungă la temperatura de aprindere (aproximativ 360°C pentru aprinderea pilotată a lemnului). Densitatea inferioară înseamnă difuzia mai lentă a căldurii în materialul lemnos. După apariția aprinderii, propagarea flăcării va fi mai rapidă pentru densitățile mai mici. Efectul grosimii se referă la arderea produsului din lemn. Grosimea produsului crește zona expusă și poate duce la propagarea focului prin cavități. Amplasarea produsului într-o clădire (pentru realizarea tavanului, peretelui, sau a podelei) este de o importanță deosebită. Plafoanele și părțile superioare ale pereților au o dispunere critică în caz de incendiu,

comparativ cu zonele inferioare. Grosimea este deosebit de importantă pentru arderea probelor, mai ales atunci când există un spațiu de aer în spatele produsului. În testul SBI, o creștere considerabilă a ratei de eliberare de căldură se datorează arderii pe ambele părți ale eșantionului după aprindere, ceea ce poate conduce la încadrarea într-o Euroclasă inferioară clasei D, cea pentru produsele din lemn netratate. Acest lucru este ilustrat în figura 4, care prezintă un al doilea vârf al ratei de eliberare de căldură, la aproximativ 7 minute după aprindere pentru placajul de 9 mm grosime. Pentru produsele mai subțiri, acest vârf va avea loc mai devreme și va afecta în final și valoarea parametrului FIGRA, așa cum se poate vedea în figura 4, unde HRR (în engleză: Heat Release Rate) reprezintă fluxul căldurii degajate de incendiu, iar THR (în engleză: Total Heat Release) reprezintă căldura totală degajată.

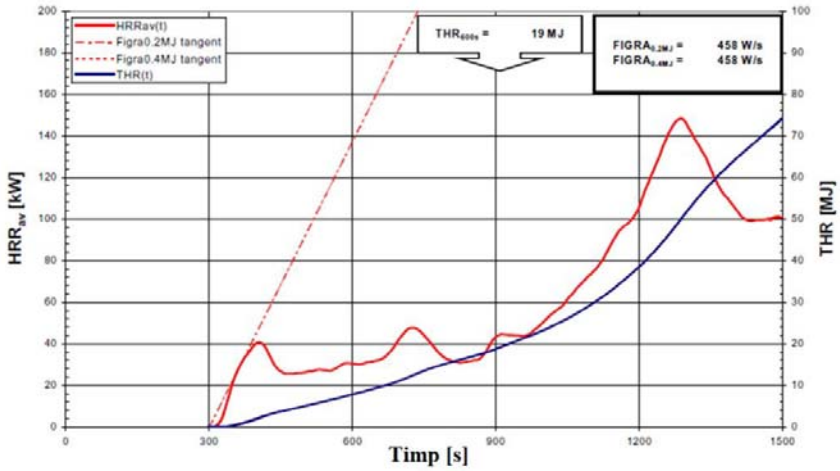


Fig. 4. Curbele HHR și THR pentru o bucată de placaj cu grosimea de 9 mm cu un spațiu de aer (neventilat) [27]

Dependența de densitate a parametrului FIGRA a fost studiată pentru produsele din lemn în timpul clasificărilor fără teste suplimentare CWFT. Valorile FIGRA scad cu creșterea densității lemnului. Limita superioară pentru Euroclasa D este de 750 W/s și astfel, conform figurii 5, produsele din lemn cu o densitate de cel puțin 350 kg/m$^3$ pot atinge nivelul clasei D (cu o grosime suficientă/fără spații de aer).

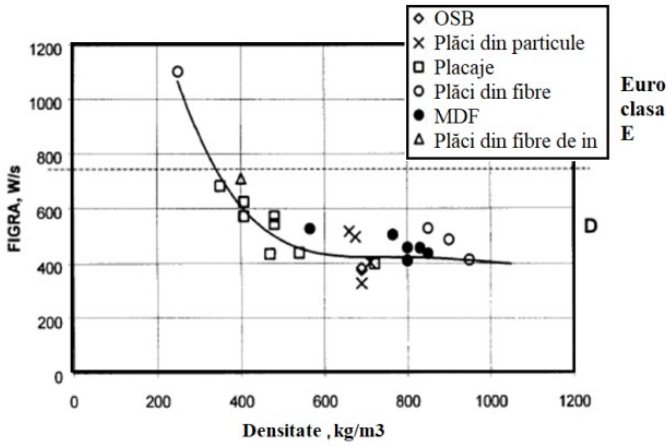


Fig. 5. Reprezentarea valorilor FIGRA ca o funcție pentru densitatea panourilor din lemn [27]

## 3.4 Rezultatele statistice ale încercărilor SBI pentru lemn

Datele măsurate în testul de colț ISO 9705 și SBI sunt prezentate în tabelul 4.

**Rezultate privind caracteristicile de reacție la foc ale lemnului [36], [37]**

*Tabelul 4*

| Cod. | Produs | FIGRA kW/s | SMOGRA $m^2/s^2$ | Timpul până la (s): | | Vârful HRR kW | Vârful SPR $m^2/s^2$ |
|---|---|---|---|---|---|---|---|
| | | | | Flashover | Vârful SPR | | |
| M05 | Cherestea de rășinoase finisată | 8,5 | 123 | 106 | 106 | >1000 | 13 |
| M12 | Cherestea de rășinoase nefinisată | 5,3 | 27 | 170 | 170 | >1000 | 4.6 |
| M15 | Acoperire termospumantă pe placă aglomerată din așchii de lemn | 1 | 36 | 700 | 700 | >1000 | 25 |
| M16 | Placă din fibre de lemn cu densitate medie placată cu melamină | 6 | 51 | 150 | 135 | >1000 | 6.9 |
| M20 | Placă aglomerată din așchii placată cu melamină | 5,5 | 53 | 165 | 165 | >1000 | 8.7 |
| M22 | Placă aglomerată din așchii | 5,8 | 81 | 155 | 155 | >1000 | 12.5 |
| M23 | Placaj (mesteacăn) | 5,6 | 51 | 160 | 160 | >1000 | 8.1 |
| M25 | Placă din fibre de lemn cu densitate medie | 4,7 | 48 | 190 | 175 | >1000 | 8.4 |
| M26 | Placă din fibre de lemn cu densitate mică | 16 | 244 | 58 | 0.55 | >1000 | 13.4 |

Termenul SPR (în engleză: Smoke Production Rate) reprezintă rata producției de fum. Euroclasa principală D a fost verificată pentru majoritatea tipurilor de panouri din lemn existente pe piața materialelor de construcții. Densitatea și grosimea panoului sunt decisive pentru valorile FIGRA, în timp ce îmbinările panourilor și alegerea substraturilor standard nu influențează clasa. Numai produsele cu densitate scăzută sunt din clasa E. Clasa de fum s2 ar trebui să fie utilizată pentru toate panourile pe bază de lemn ca garnituri de suprafață pentru a obține o clasificare robustă. Conform rezultatelor testului, multe produse ating clasa de fum s1. Clasa d0 de picături / particule aprinse a fost verificată pentru toate panourile din lemn din clasa D. Marjele de siguranță pentru aceste subclase sunt foarte ridicate, de 20-90%. Este avută în vedere o prelungire a clasificării pentru panourile din lemn pentru a putea include și alte aplicații, de exemplu prize de aer în spatele panoului.

Rezultatele obținute în urma efectuării testului la foc SBI pentru PAL sunt prezentate în Tabelul 5. În acest tabel, codul caracterizează același tip de material testat în laboratoare diferite.

*Tabelul 5*

**Rezultate ale testelor la foc după încercarea SBI inter-laboratoare pentru materialele uzuale în construcții (PAL) [7], [36], [37], [40]**

| Cod | Produs (produsele nu sunt ignifugate, cu excepția celor pentru care se specifică acest aspect) | Grosimea [mm] | Densitatea [kg/m$^3$] | Timpul pana la (s): | | | Viteza maximă de degajare a căldurii [kW] | FIGRA Viteza de dezvoltare a focului [W/s] | THR600s Căldura totală degajată [MJ] | SMOGRA Viteza de emisie a fumului [m$^2$/s$^2$] | TSP600s Emisia totală de fum [m$^2$] | $\Delta T_{max}$ | Clasa de reacție la foc |
|---|---|---|---|---|---|---|---|---|---|---|---|---|---|
| | | | | Flashover [sec] | Vârful HRR [kW] | Vârful SPR [m$^2$/s] | | | | | | | |
| M06 | PAL ignifugat | 12 | 780 | - | 723,46 | 18,16 | 423 | 0,35 | 210 | 16 | 7798 | 44.2 | ≥B |
| M20 | Placă aglomerată din așchii placată cu melamină | 12 | 680 | 165 | 1998,2 | 14,99 | - | 5,5 | - | 53 | - | 110,5 | D |
| M22 | Placă aglomerată din așchii | 12 | 700 | 155 | 2221 | 22,27 | - | 5,8 | - | 81 | - | 127,3 | D |

Diagramele comparative ale curbelor de evoluție ale HRR și SPR în cazul PAL-ului ignifugat (M06), plăcii aglomerate din așchii placată cu melamină (M20) și în cazul plăcii aglomerate din așchii (M22), prin utilizarea metodei ISO 9705, respectiv a metodei EN 13823 SBI sunt prezentate în figurile 6, 7, 8 și 9.

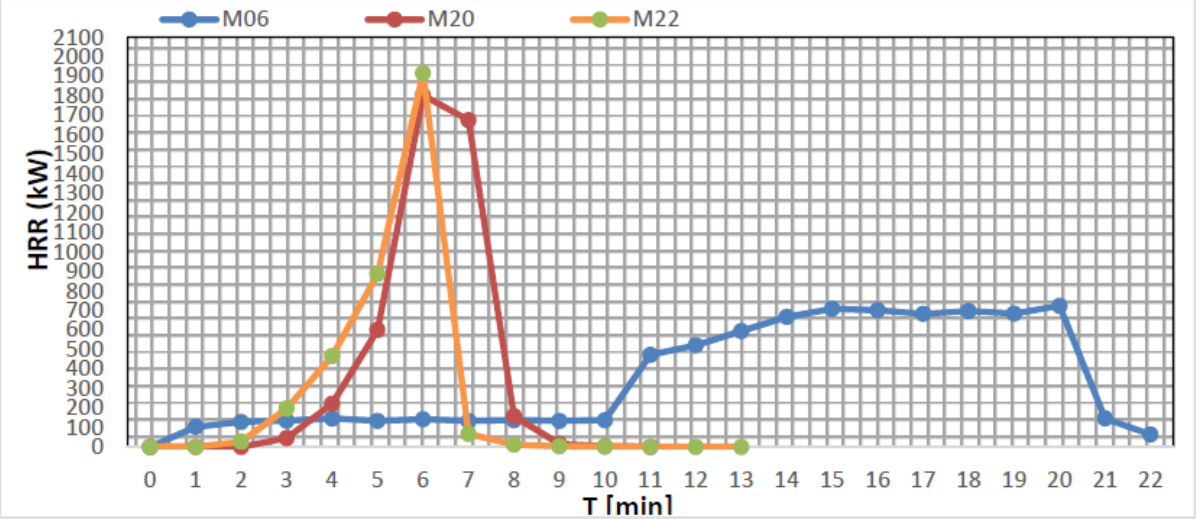


Fig. 6. Curbele de evoluție a HRR pentru M06, M20 și M22 conform metodei ISO 9705 [45]

Conform figurii 6, prin utilizarea metodei ISO 9705, valoarea HRR în cazul M22 atinge maximul de cca 1915 kW în timpul cel mai scurt - 6 minute, în cazul M20 atinge maximul de cca 1800 kW, în 6 minute, și în cazul M06 atinge maximul de cca 720 kW, în 20 de minute.

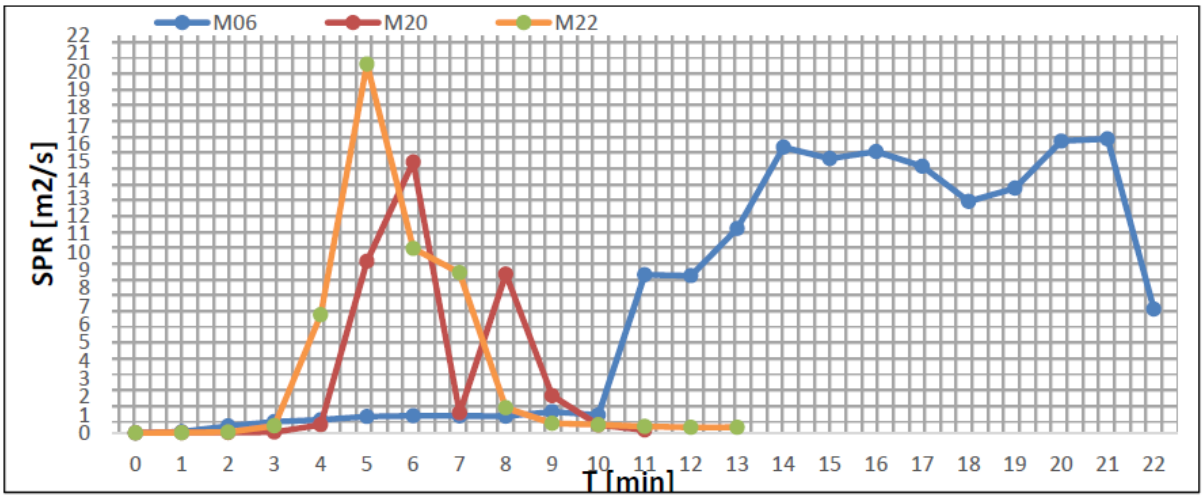


Fig. 7. Curbele de evoluție a SPR pentru M06, M20 și M22 conform metodei ISO 9705 [45]

Conform figurii 7, prin utilizarea metodei ISO 9705, valoarea SPR în cazul M22 atinge valoarea maximă de cca 20 $m^2/s$, iar timpul total de producere a fumului fiind de 13 minute, în cazul M20 atinge valoarea maximă de cca 15 $m^2/s$, iar timpul total de producere a fumului fiind de 11 minute și în cazul M06 atinge valoarea maximă de cca 16 $m^2/s$, iar timpul total de producere a fumului fiind de 22 de minute.

Analizând valorile parametrilor fluxului căldurii degajate și a ratei de producere a fumului, așa cum rezultă din figurile 6 și 7, se constată că se poate recomanda utilizarea PAL-ului ignifugat M06, deoarece în cazul manifestării unui incendiu, utilizarea acestuia ar conduce la mărirea timpului de evacuare a persoanelor surprinse prin degajarea unei cantități mai mici de fum și de căldură în fazele inițiale ale incendiului.

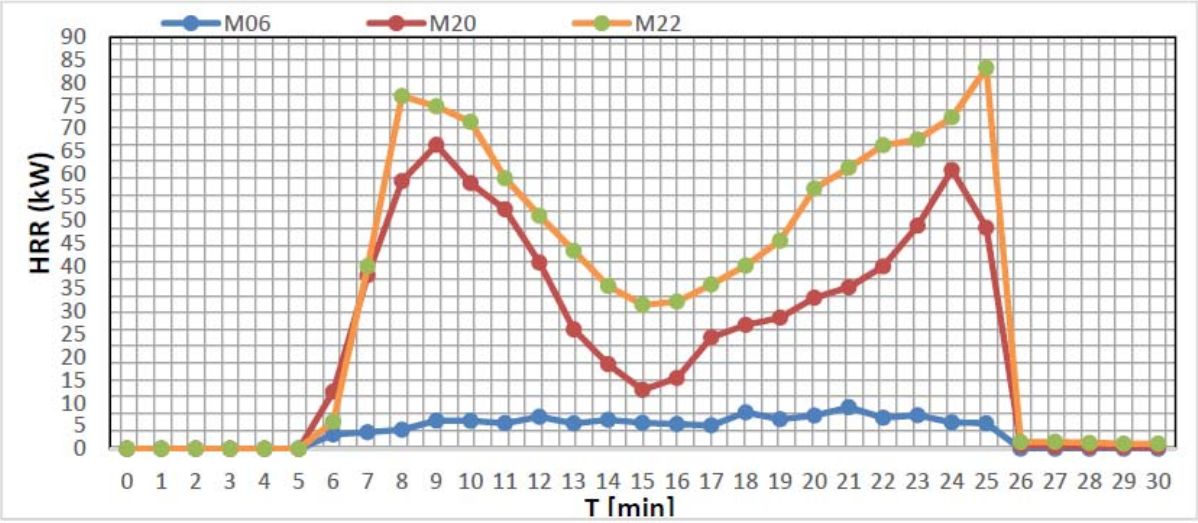


Fig. 8. Curbele de evoluție a HRR pentru M06, M20 și M22 conform metodei EN 13823 SBI [9]

Conform figurii 8, prin utilizarea metodei EN 13823 SBI, valoarea HRR în

cazul M22 atinge două valori maxime de cca 77 kW în 8 minute și 83 kW în 25 minute, în cazul M20 atinge 2 valori maxime de cca 66 kW în 9 minute și 61 kW în 24 minute și în cazul M06 atinge o valoare aproximativ constantă de cca 5 kW, din minutul 9 până în minutul 25, recomandându-se, astfel, utilizarea PAL-ului ignifugat M06 întrucât acesta a înregistrat cea mai mică valoare a fluxului căldurii degajate de incendiu.

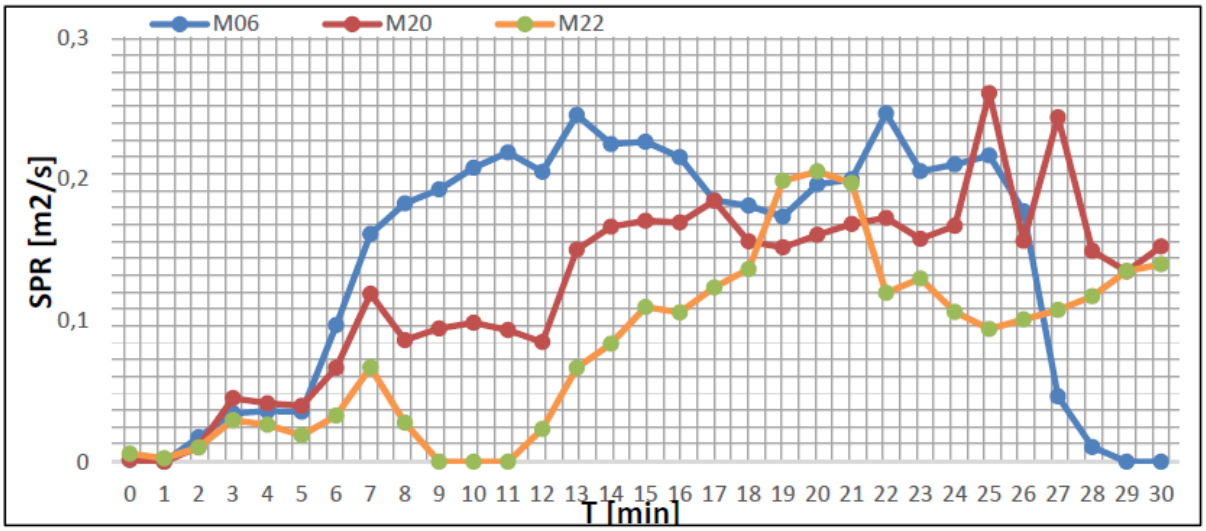


Fig. 9. Curbele de evoluție a SPR pentru M06, M20 și M22 conform metodei EN 13823 SBI [9]

Conform figurii 9, prin utilizarea metodei EN 13823 SBI, valoarea SPR în cazul M20 atinge valoarea maximă de cca 0,26 $m^2/s$, în cazul M06 atinge valoarea maximă de cca 0,24 $m^2/s$, și în cazul M22 atinge valoarea maximă de cca 0,20 $m^2/s$, observându-se că toate cele trei produse degajă fum pe întreaga durată de efectuare a testului de 30 de minute.

## 4. Simularea incendiilor utilizând programul B-RISK

B-RISK este o aplicație software de simulare a incendiilor și de descriere a ipotezelor și a fizicii care stau la baza modelului computerizat de incendiu. Programul software B-RISK este destinat pentru a evalua performanțele și pericolele asociate incendiilor care se manifestă într-o încăpere sau în mai multe încăperi, care pot fi conectate prin goluri de ventilație sau pot avea pereți comuni. Acest program cuprinde un simulator de risc de incendiu pentru generarea distribuțiilor de probabilități.

B-RISK este un model zonal de incendiu dezvoltat anterior și cunoscut sub numele de BRANZFIRE [41], [42], [43]. Modelul B-RISK poate fi utilizat, atât pentru simulări deterministe unice, pentru predicțiile privind răspândirea fumului în incinte, cât și pentru iterațiile multiple ale unui scenariu de incendiu. Scenariul este util pentru analiza sensibilității sau pentru elaborarea descriptorilor probabilistici ai riscului de incendiu în condiții definite.

În vederea observării cât mai clar a influenței materialelor de finisaj interior asupra dezvoltării incendiilor în spații închise, s-au luat în calcul două cazuri:

- în primul caz, încăperea nu a fost prevăzută cu niciun material de finisaj interior, pereții încăperii având structura de beton, cu grosimea de 100 mm.

- în al doilea caz, încăperea a fost prevăzută cu material de finisaj interior. Materialul folosit ca structură de rezistență a pereților, respectiv planșeului, în modelul din programul B-RISK, este betonul armat prefabricat, având grosimea de 100 mm. Pereții și planșeul vor fi îmbrăcați în PAL neignifugat clasa D s2, d0 reacție la foc, având grosimea de 12 mm.

În vederea efectuării simulărilor pe baza celor două scenarii de incendiu, se aleg dimensiunile încăperii de testare, a materialului de finisaj, a golurilor de ventilație, a arzătoarelor, precum și poziționarea acestora.

Pentru crearea și proiectarea modelului fizic de simulare a incendiului s-a folosit spațiul de testare la scară naturală, aflat în incinta Facultății de Pompieri, prezentat schematic în figura 10.

Simularea a fost executată cu scopul de a se analiza influența pe care o are PAL-ul (M06) - utilizat ca finisaj interior - asupra dezvoltării incendiului, comparativ cu un material inert, cum ar fi betonul. Pentru simulare s-au folosit condițiile prezentate în metodele de testare ISO 9705 și SBI, cu deschiderile prezentate în figura 10, folosindu-se următoarele arzătoare cu dimensiuni de 0,3 x 0,3 m, montate în același loc (în colțul din dreapta jos al încăperii):

- arzătorul standardului ISO 9705 a cărui putere este 100 kW pentru primele 10 minute ale testului, urmând ca puterea să crească la 300 kW în următoarele 10 minute, iar în ultimele 10 minute ale testului acesta va avea puterea de 900 kW.

- arzătorul standardului SBI, care are o putere constantă de 30 kW timp de 20 de minute.

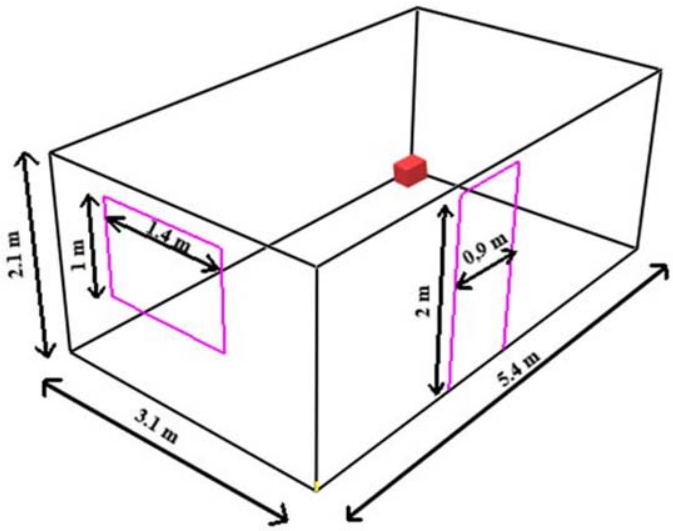


Fig. 10. Dimensiunile încăperii folosită pentru simularea metodelor de testare ISO 9705 și SBI în condiții naturale (cameră de testare cu deschideri uzuale: ușă și fereastră)

În graficele 11, 12, 13 și 14 sunt prezentate curbele valorilor de temperatură

înregistrate la partea superioară a încăperii, în cazul montării PAL-ului, comparativ cu un material inert (betonul), folosind arzătorul standardului SBI și al standardului ISO 9705.

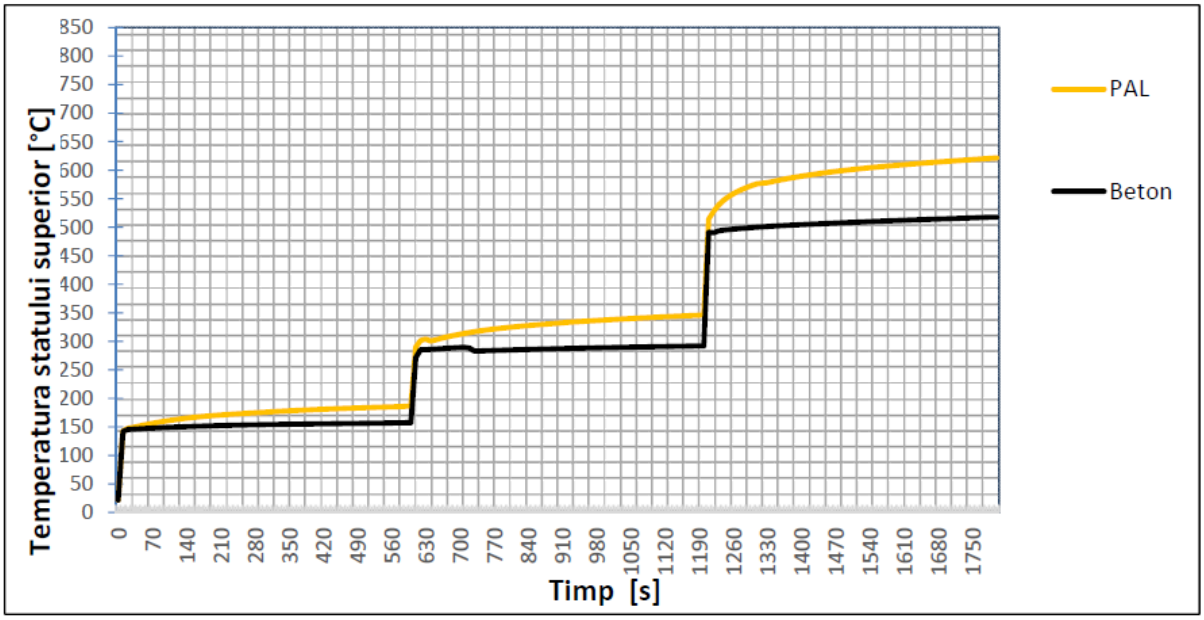


Fig. 11. Temperatura stratului superior de gaze în cazul folosirii metodei ISO 9705

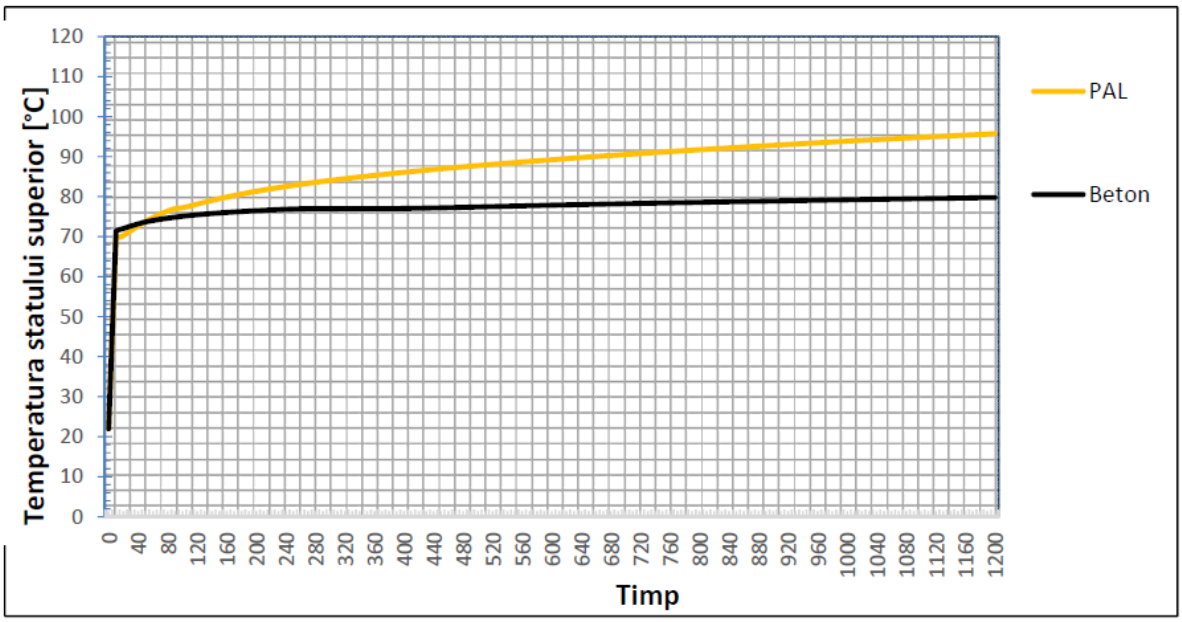


Fig. 12. Temperatura stratului superior de gaze în cazul folosirii metodei SBI

Conform figurilor 11 și 12, atât în cazul folosirii metodei ISO 9705, cât și în cazul metodei SBI, temperatura maximă a stratului superior de gaze este mai mică în cazul betonului, fiind de cca 517°C, respectiv, 79°C, comparativ cu PAL-ul, unde se

înregistrează valorile de 634°C, respectiv 95°C.

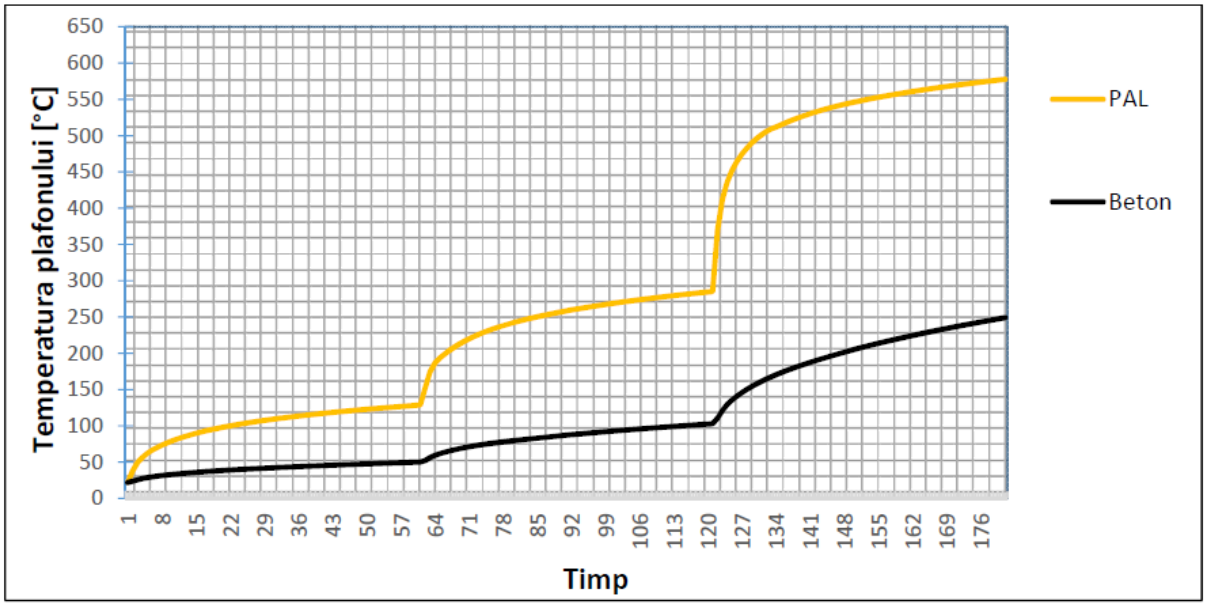


Fig. 13. Temperatura plafonului în urma folosirii metodei ISO 9705

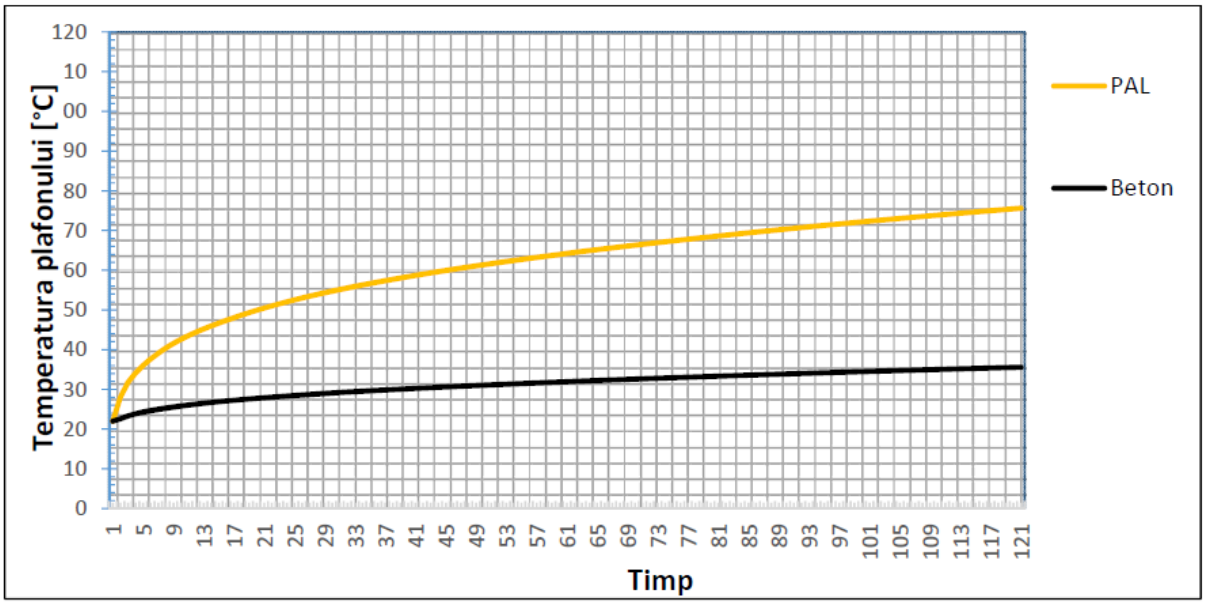


Fig. 14. Temperatura plafonului în urma folosirii metodei SBI

Temperatura plafonului este importantă, întrucât plafonul constituie o parte comună a compartimentului incendiat cu celelalte compartimente neincendiate și, astfel, din cauza temperaturii ridicate ale elementelor de construcție comune, pot apărea noi focare la etajele superioare. Această temperatură influențează și comportarea planșeului din beton armat, deoarece rezistența betonului scade începând cu temperatura de 300°C, ajungând ca la 600°C rezistența să fie cu 20-30% mai mică decât la valorile normale de temperatură. Betonul supus la temperaturi ridicate influențează acțiunea de stingere a echipelor de intervenție, atât din punct de vedere a

eficienței stingerii, ca urmare a radierii prelungite a căldurii acumulate, cât și ca urmare a reducerii capacității portante a planșeului, prin deteriorarea stratului de beton în contact cu apa rece utilizată la stingere. Trebuie menționat că aceste aspecte nu reprezintă scopul prezentului studiu, ele urmând a fi analizate, în detaliu, în alte cercetări ce vor fi investigate ulterior.

În cazul folosirii arzătorului SBI, nu se ajunge la temperaturi suficient de mari pentru a constitui noi focare în încăperile vecine, dar se pot forma noi focare în interiorul aceleiași încăperi, deoarece pot exista materiale cu temperaturi de inflamabilitate mici, cum ar fi perdelele și jaluzelele, care se află la partea superioară a încăperii.

Conform figurilor 13 și 14, atât în cazul folosirii metodei ISO 9705, cât și în cazul metodei SBI, temperatura maximă a stratului superior de gaze este mai mică în cazul betonului, fiind de cca 205°C, respectiv 35°C, comparativ cu PAL-ul, unde se înregistrează valori ale temperaturii de 460°C, respectiv 205°C.

## 5. Concluzii

Parametrii principali, care influențează caracteristicile de reacție la foc ale panourilor și placărilor de izolare din lemn, sunt: grosimea, substratul și densitatea.

În acest studiu a fost realizată simularea la scară naturală a contribuției plăcilor de PAL la dezvoltarea incendiilor care se manifestă în spații închise, prin utilizarea programului B-RISK de simulare a incendiilor. Astfel, ținând-se cont de cele două scenarii de incendiu utilizate în studiu, se pot desprinde o serie de concluzii.

Un prim aspect constatat îl reprezintă faptul că valoarea temperaturii maxime a stratului superior de gaze este mai mare în cazul utilizării metodei ISO 9705, decât în cazul metodei SBI, întrucât puterea arzătorului folosit în prima metodă de testare (100 kW, 300 kW, respectiv 900 kW) este mai mare decât cea folosită în a doua metodă (30 kW).

Reprezentarea grafică a temperaturii stratului superior de gaze fierbinți, în cazul metodei de testare ISO 9705, este influențată de HRR-ul arzătorului. Reprezentarea grafică are forma valorilor date de modificarea puterii arzătorului, observându-se (după primele 10 minute, 20 de minute, respectiv după 30 de minute de la începerea testului) o creștere semnificativă a temperaturii stratului de gaze fierbinți, odată cu mărirea puterii arzătorului. Acest lucru se datorează faptului că puterea arzătorului este destul de mare, arzătorul acționând pe toată durata testului și neexistând alte obiecte care să influențeze debitul de căldură degajată.

Se observă, de asemenea, că, atunci când încăperea nu are aplicat material pentru finisaj interior, temperatura atinsă în stratul superior de gaze este mai scăzută, fiind de cca 517ºC (ISO 9705), respectiv de cca 79°C (SBI) în ultima secundă a testului (1800). În cazul în care există material pentru finisare aplicat pe pereții interiori, și anume PAL, se atinge temperatura de 634°C (ISO 9705), respectiv de 95 °C (SBI), în secunda 1220, moment în care se și întrerupe testul, întrucât materialul combustibil este consumat în întregime.

Având în vedere performanțele la foc ale PAL-ului, în conformitate cu reglementările tehnice în vigoare [44] și în urma studiului efectuat se poate concluziona că acest material poate fi folosit ca material de finisaj cu următoarele recomandări:

- în situația în care se montează pe pereți rezistenți la foc, se vor lua măsuri de tratare cu substanțe ignifuge sau se vor prevedea instalații automate de stingere a incendiilor; de asemenea, prin montarea PAL-ului nu se vor crea goluri cu adâncimea mai mare de 20 de cm față de pereți;

- în situația în care se va monta pe pereți, va fi protejat de aparatura electrică, de corpurile de iluminat sau de alte surse de încălzire pentru a preveni aprinderea lui;

- nu se recomandă montarea acestuia în încăperi cu degajări de praf combustibil, decât dacă se permite curățirea ușoară a suprafețelor PAL-ului;

- nu se recomandă utilizarea PAL-ului pe căile de evacuare;

- nu se recomandă montarea PAL-ului ca finisaj interior în clădirile înalte și foarte înalte, în sălile aglomerate, clădiri de învățământ, deoarece se creşte densitatea de sarcină termică și se permite propagarea rapidă a incendiilor;

- nu se recomandă utilizarea PAL-ului în bucătăriile din clădirile de locuit individuale, sau în alte spații unde se utilizează focul deschis;

Aplicabilitatea rezultatelor studiului în activitatea de normare și reglementare poate consta în propunerea de utilizare a produselor din lemn tratate cu substanțe de suprimare a fumului drept finisaj în încăperile cu anumite destinații, precum sălile cu aglomerări de persoane, spațiile de birouri, sau construcțiile în care utilizatorii nu se pot evacua singuri, sau o fac într-un interval dificil de estimat, cazul spitalelor căminelor de bătrâni etc.

**Acknowledgements**

This work was supported by a grant of the Romanian Ministry of Research and Innovation, CCCDI – UEFISCDI, project number PN-III-P1-1.2-PCCDI-2017-0350 /02.03.2018 (Graphene4Life), within PNCDI III.

**Referințe**

[1] *R. M. Rowell*, The chemistry of Solid Wood. In: Advances in Chemistry Series. American Chemical Society, Washington, 1984.

[2] *R. Bergman, Z. Cai, C. G. Carll, C. A. Clausen, M. A. Dietenberger, R. H. Falk, C. R. Frihart, S. V. Glass, C. G. Hunt, R. E. Ibach, D. E. Kretschmann, D. R. Rammer, R. J. Ross*, Wood handbook- wood as an engineering material. Forest Products Laboratory, Madison, Wl, 2010.

[3] *A. C. Wiedenhoeft, R. B. Miller,* Structure and Function of Wood. In R. M. Rowell (ed) Handbook of wood chemistry and wood composites. CRC Press, Florida, p.9-32, 2005.

[4] K. A. McDonald, D. E. Kretschmann, Commercial Lumber. In: Wood Handbook – Wood as an engineering material. Forest Products Laboratory, Madison, 1999.

[5] *F. Laoutid, L. Bonnaud, M. Alexandre, J. M. Lopez-Cuesta, P. H. Dubois*, New prospects in flame retardant polymer materials: from fundamentals to nanocomposites. Materials Science and Engineering R 63: 100-125, 2009.

[6] *J. Alongi, R. A. Carletto, A. DI Blasio, F. Cuttica, F. Carosio, F. Bosco, G. Malucelli*, Intrinsic intumescent-like flame retardant properties of DNA – treated cotton fabrics. Carbohydr

Polym 96:296– 304, 2013a.

[7] SR EN 13823+A1:2014, Încercări de reacție la foc ale produselor pentru construcții. Produse pentru construcții, cu excepția îmbrăcămintei de pardoseală, expuse acțiunii termice a unui singur obiect arzând.

[8] Standard Test Method for Determining Flammability Characteristics of Plastics and Other Solid Materials Using Microscale Combustion Calorimetry, ASTM D 7309-07.

[9] SR EN ISO 11925-2 Aprinzibilitatea produselor pentru construcții la contactul direct cu flacăra.

[10] *H.S. Kim, S. Kim, H.J. Kim, H.S. Yang*, thermal properties of bio-flour-filled polyolefin composites with different compatibilizing agent type and content, ThermochimActa 451, 2006, p.181–188.

[11] *Bartlett, R. M. Hadden, L. A. Bisby*, A Review of Factors Affecting the Burning Behaviour of Wood for Application to Tall Timber Construction, School of Engineering, The University of Edinburgh, The King's Buildings, Mayfield Road, Edinburgh EH9 3DW, UK, 2018.

[12] *K.E. Bland*, Behaviour of wood exposed to fire: a review and expert judgement procedure for predicting assembly failure. Dissertation, Worcester Polytechnic Institute, 1991.

[13] *P. Reszka*, In-Depth Temperature Profiles in Pyrolyzing Wood, A thesis submitted for the degree of Doctor of Philosophy, The University of Edinburgh, 2008.

[14] *L. Yang, X. Chen, X. Zhou, W. Fan*, The pyrolysis and ignition of charring materials under an external heat flux. Combustion and Flame, v.133, 2003, p.407–413.

[15] *V. Babrauskas*, Ignition of wood: a review of the state of the art. Interflam, 2002, p.71–88.

[16] *F.L. Browne*, Theories of the combustion of wood and its control – a survey of the literature, FPL report number 2136. Forest Products Laboratory, Madison, WI, 1958.

[17] ASTM E119: Standard test methods for fire tests of building construction and materials. ASTM International, West Conshohocken, PA, 2012.

[18] ISO 834: Fire resistance tests - elements of building construction. International Organization for Standardization, Switzerland, 2012.

[19] *K.L. Friquin*, Material properties and external factors influencing the charring rate of solid wood and glue-laminated timber. Fire and Materials, v.35, 2010, p.303–327.

[20] *E. Mikkola,* Charring of wood, VTT Research Report 689, VTT Technical Research Centre of Finland. Espoo, Finland, 1990.

[21] *T. Hakkarainen, E. Mikkola, B. Ostman, L. Tsantaridis, H. Brumer, P. Piispanen*, Innovative eco- efficient high fire performance wood products for demanding applications. VTT, Finland, SP Tratek,

[22] Z. Karpovic, R. Sukys, R. Gudelis, Toxicity research of smouldering and flaming pine timber treated with fire retardant solutions. J.Civ.Eng.Manag, v.18, 2012, p.600–608. 10.3846/13923730.2012.709195.

[23] *E. Wilkins, F. Murray*, Toxicity of emissions from combustion and pyrolysis of wood. Wood Science and Technology**, v.14**, 1980, p.281–288. 10.1007/BF00383455.

[24] *S. Janssen,* Brominated flame retardants: Rising levels of concern. Healthcare without harm, Arlington VA, 2005.

[25] *J. Green,* Mechanisms flame retardancy and smoke suppression – a review. Journal of Fire Sciences, **v.14,** 1996, p.426–442.

[26] SR EN ISO 11358:2003, Materiale plastice. Termogravimetria polimerilor (TG). Principii generale.

[27] *E. Mikkola*, Review of reaction to fire performance of wood based products. In Proceedings of 8th World Conference on Timber Engineering, 2004, p.325-330.

[28] SR ISO 5660-1:2015 Încercări de reacție la foc. Căldură degajată, cantitate de fum produsă și viteza de pierdere de masă. Partea 1: Debitul de căldură degajată (metoda con-calorimetrului) și viteza de producere a fumului (măsurare dinamică).

[29] *V. Babrauskas, S. J. Grayson, H. C. Tran,* Heat release in fires: experimental data on

wood materials. Journal of Fire Protection Engineering, **v.12**, 1992, 163-189.

[30] *R. E. Lyon, R. N. Walters,* A microscale combustion calorimeter, US Department of Transport, Washington, Report Number: DOT/FAA/AR-01/117, 2002.

[32] *H. C. Tran,* Heat release in fires: experimental data on wood materials. In: V. Babrauskas, S. K. Grayson (eds) Heat Release in fires. Elsevier Applied Science, New York, 1992.

[33] *L. A. Lowden, T. R. Hull*, Flammability behaviour of wood and a review of the methods for its reduction. Fire science reviews, **v.2(1),** 2013, p.4.

[34] SR EN 13501-1 Clasificarea produselor pentru construcții în funcție de comportarea la foc. Partea 1: Clasificare în funcție de rezultatele încercărilor de reacție la foc.

[35] ISO 9705-1:2016, Reaction to fire tests - Room corner test for wall and ceiling lining products - Part 1: Test method for a small room configuration.

[36] *J. Axelsson, T. Hertzberg, B. Sundström*, Database for Design Fires – Brandforsk projekt 327-021, SP rapport 2005:02, SP Brandteknik, Borås, 2005.

[37] *B. Sundström, P. Van Hees, P. Thureson*, Results and analysis from fire tests of building products in ISO 9705, the Room/Corner Test. The SBI Research programme, 1998.

[38] *R. van Mierlo*, The Single Burning Item (SBI) test method – a decade of development and plans for the near future, Heron, **vol. 50**, nr. 4, 2005.

[39] *F. Larsson, P. Andersson, B. E. Mellander*, Lithium-Ion Battery Aspects on Fires in Electrified Vehicles on the Basis of Experimental Abuse Tests, 2016.

[40] *D. A. Smith, K. Shaw*, "Evolution of the Single Burning Item Test," Flame Retardant '98, London, UK, Interscience Communications, London, UK, February 1990.

[41] *C. Wade*, A room fire model incorporating fire growth on combustible lining materials. (Master of Science Thesis, Worcester Polytechnic Institute. Worcester, MA), 1996.

[42] *C. Wade, J. Barnett*, A room-corner model including fire growth on linings and enclosure smoke- filling. Journal of Fire Protection Engineering, 8, **vol.4**, 1997, 27-36.

[43] *C. Wade*, Branzfire technical reference guide. Branz Study Report SR92. Judgeford, New Zealand: Branz Ltd, 2000.

[44] Normativ de siguranță la foc a construcțiilor, P118-99.

# Studiu comparativ privind coroziunea în timp a electrozilor în sol, Partea 1 – Introducere

Comparative study regarding corrosion in time of the ground electrodes, Part 1 - Introduction

Ştefan PAVEL[(1)], Ioan Bogdan PASCU[(2)], Nicoleta NEMEŞ[(2)], Romeo NEGREA[(3)], Emilia DOBRIN[(4)], BURIAC Oana[(2)]

[(1)]Universitatea Politehnica Timişoara-ICER,
Timişoara, str. G.Musicescu, nr. 138, România
*e-mail:pavelstefanel@gmail.com*
[(2)]Universitatea Politehnica Timişoara-ICER*;* România
*e-mail: i.bogdan.pascu93@gmail.com; nicoleta.nemes@upt.ro; oana.grad@upt.ro*
[(3)]Universitatea Politehnica Timişoara-Departamentul de Matematică
Timişoara, P-ţa Victoriei, nr. 2, România
*e-mail: romeo.negrea@upt.ro*
[(4)]Institutul Național de Cercetare-Dezvoltare în Sudură și Încercări de Materiale Timişoara
Timişoara, B-dul Mihai Viteazul, nr. 30, România
*e-mail: emi_dobrin@yahoo.com*
DOI: 10.37789/rjce.2021.12.1.10

***Rezumat****:Obiectivul lucrării este de a prezenta, aspecte referitoare la: coroziunea metalelor acoperite şi neacoperite cu zinc în solul oraşului Timişoara (electrozi de împământare a Instalaţiei de Legare la Pamânt aferentă Instalaţiilor Electrice din Construcţii), analiza parametrilor de sol, prototipuri de electrozi, măsurători electrice, microbiologice şi analiza de prognoză-predicţie matematică, materiale şi dicţionare de termeni aferenţi. Un alt aspect prezentat în acest material este efectuarea de măsurători ale spectrului câmpului elecromagnetic oscilografiat al elementelor de metal acoperite şi neacoperite cu zinc din sol.*

***Cuvinte cheie****: coroziune, electrod de împământare, sol, legare la pământ, microbiologia solului*

***Abstract:*** *The objective of this paper is to present aspects related to: corrosion of metals covered, and not covered with zinc in the soil of Timişoara (grounding electrodes of a grounding installation related to Electrical Installations of Constructions), analysis of soil parameters, prototype electrodes, electrical, microbiological measurements and mathematical prognosis analysis-prediction, materials, and dictionaries of related terms. Another aspect presented in this material are the measurements related to the spectrum of the oscillograph electromagnetic field of the grounding electrodes, which are covered, and not covered with zinc.*

***Key words****: corrosion, ground electrode, soil, grounding, soil microbiology*

# 1. Introduction

## 1.1 Corrosion regulations

National and international regulations in the field of earthing installations of electrical installations for constructions are known, but the problem is the corrosion (and not only) represents an important aspect to be researched and permanently topical. The simpliest corrosion definition is: [1] *The reaction between a material, usually a metal*, and the environment. In the U.S. Corrosion Society. respectively NACE International Technical Committees, constituted to reduce the loss of billions of dollars due to corrosion, activates the T-10 underground corrosion control committee with subcommittee G01.10, corrosion in soils. Thus, this subcommittee has developed several standards (recommendations) including: [2] G51-18 Standard test method for measuring the soil pH for use in corrosion testing; G57-06 (2012) Standard test method for measuring the soil resistance field using the Wenner method with four electrodes; G97-18 Standard test method for the laboratory evaluation of magnesium sacrifice anode test samples for underground applications; G158-98 (2016) Standard guide for three methods for evaluating buried steel tanks; G162-18 standard practice for performing and evaluating laboratory corrosion tests in soils; G165-99 (2017) Standard practice for determining rail-to-ground resistance; G187-18 Standard test method for measuring soil resistivity using the two-electrode ground box method; G200-09 (2014) Standard test method for measuring soil oxidation reduction potential (ORP); Standard guide G218-19 for external corrosion protection of ductile iron pipes using polyethylene coating supplemented with cathodic protection, etc. The Romanian norms related to corrosion also include the following documents: [3] Norm for the protection against corrosion of buried metal constructions Indicative I 14-76 replaces I 14-65. Chapter 9 Measurements on the ground and buried metal constructions; pct.9.1. In order to ensure the corrosion danger of buried metal constructions and to establish the appropriate corrosion protection measures, the following measurements shall be performed:

- determining the aggressiveness of the soil and groundwater, on the route of the buried metal construction;
- establishing the existence in the area of dispersion currents;
- performing measurements of the potential and intensity of the protection current in the buried metal construction;
- performing measurements on electric traction installations in direct current, according to STAS 833-72 “Requirements for reducing stray currents,,.

The measurement method must be chosen in such a way that through the auxiliary works (excavations for access to constructions, installation of electrodes, etc.), the natural state of the soil is modified as less as possible. Pct. 9.10.: The beneficiaries of buried metal constructions or of electric traction installations in direct current are obliged to keep a record of the values resulting from the measurements provided in art. 9.1 and 9.2. [4]

Protection of equipment and steel pipes against corrosion / Technical standard; Cap. XI, art. 263. In order to ensure the electrical safety of the pipes and related installations and to carry out the corrosion status determinations, the steel pipes belonging to SD and, as the case may be, outdoor installations for the use of natural gas made of steel shall be provided with: a) stations for measuring specific parameters ( potential, current, resistance, etc.) which are mounted on the pipe in accordance with the technical regulations in effect; b) electrical insulating parts. Another important aspect is the corrosion rate and the corrosion of metallic elements covered and not covered with zinc under the influence of soil microorganisms.

## 2. Materials, equipment and measuring apparatus

*Table 1*

**Materials, equipment and measuring apparatus**

| **No.** | |
|---|---|
| 1 | Sample of carbon steel of predetermined size, not covered with zinc layer |
| 2 | Sample of carbon steel coverd with a layer ( default thickness *n*) of zinc |
| 3 | Sample of carbon steel coverd with a layer ( default thickness *nx2*) of zinc |
| 4 | Electric conductor MYF-0.5mm$^2$ |
| 5 | Apparatus for measuring the thickness of the coating on ferrous and non-ferrous materials |
| 6 | Measuring apparatus *FLUKE 287 True RMS Multimeter* |
| 7 | Temperature and humidity sensor for floor mounting |
| 8 | Above ground temperature and humidity sensor |
| 9 | Junction box |
| 10 | PVC tube of preset size |
| 11 | PVC Guaina copex flexible tube |
| 12 | Oscilloscope DSO-X 3054 A |
| 13 | Rectifier transformer |
| 14 | Wooden ruler |
| 15 | Wireless mode relay with remote control |
| 16 | Raspberry Pi microcontroller with HDMI port |
| 17 | Router |
| 19 | *Petri* plates |
| 20 | Microscope |

| | |
|---|---|
| 21 | Portable multichannel X-ray fluorescence analyzer - FRX, model Thermo Scientific NITON XL3t |
| 22 | Measuring apparatus *Metrel snuff ground* |
| 23 | Automatic colony counter Yul Flash & Go |
| 24 | Digital analyzer catv *Signal Analyzer Telemann 1730* |

## 3. Soil characteristics and properties

The measurements were performed in the ground, in the city of Timişoara, Timiş County, Romania, with the following coordinates:

- Latitude: 45.7241;
- Longitude: 21.2339;
- Elevation: 88.

The soil lot on which the measurements related to the study of corrosion of metals coated and not covered with zinc, respectively of earthing electrodes, comprises an area of 48 m2 and is predominantly made of dusty clay according to the geotechnical study [5]. The main characteristics and properties of the soil with the above mentioned coordinates are presented in the Table *2÷6*:

*Table 2*

**Soil characteristics, drilled depth, layer thickness**

| Characterization of the soil in the conformal layer SR EN ISO 14688-1 and SR EN ISO 14688-2 | Stratification column | Drilled depth, layer thickness | | Sample | |
|---|---|---|---|---|---|
| | | Depth [m] | Thickness [m] | No.sample | Nozzle depth [m] |
| Vegetal soil | | -0.30 | -0.30 | | |
| Dusty, brown, hard clay | | -0.70 | -0.40 | 1N | -0.50 |
| Dusty clay, sandy brown, plasticizer | | -1.40 | -0.70 | 2N | -1.20 |
| Dusty clay, sandy black, plasticizer | | -4.00 | -2.60 | 3N | -2.00 |

*Table 3*

**Characteristics of the soil column stratification, granularity**

| Characterization of the soil in the conformal layer SR EN ISO 14688-1 and SR EN ISO 14688-2 | Stratification column | Granulosity | | |
|---|---|---|---|---|
| | | Sand 0.002...2 mm % | Dust 0.005...0.005mm % | Clay 0.005mm % |
| Vegetal soil | | - | - | - |
| Dusty, brown, hard clay | | 21 | 52 | 27 |
| Dusty clay, sandy brown, plasticizer | | 25 | 46 | 29 |
| Dusty clay, sandy black, plasticizer | | 32 | 46 | 22 |

*Table 4*

**Soil characteristics, volumetric weight, pore index, porosity, natural humidity**

| Characterization of the soil in the conformal layer SR EN ISO 14688-1 şi SR EN ISO 14688-2 | Stratification column | Volumetric weight γ kN/mc | Pore indexe - | Porosity n % | Natural humidity w % |
|---|---|---|---|---|---|
| Vegetal Soil | | - | - | - | - |
| Dusty, brown, hard clay | | 17.2 | 0.86 | 46.3 | 21.9 |
| Dusty, sandy brown, plastic clay | | 17.7 | 0.84 | 45.6 | 23.8 |
| Dusty, sandy, black, plastic clay | | 18.6 | 0.86 | 46.3 | 33.1 |

*Table 5*

**Soil characteristics, lower and upper limit, index of plasticity and consistency**

| Characterization of the soil in the conformal layer SR EN ISO 14688-1 şi SR EN ISO 14688-2 | Stratification column | Upper limit of plasticity $W_L$ % | Lower limit of plasticity $W_P$ % | Indix of plasticity $I_P$ % | Indix of consistency $I_C$ |
|---|---|---|---|---|---|
| Vegetal Soil | | - | - | - | - |
| Dusty, brown, hard clay | | 42 | 23.5 | 18.5 | 1.09 |
| Dusty, sandy brown, plastic clay | | 52.9 | 23.5 | 29.4 | 0.99 |
| Dusty, sandy, black, plastic clay | | 47.4 | 29.3 | 18.1 | 0.79 |

*Table 6*

**Soil characteristics, edometric mode, friction angle, specific cohesion**

| Characterization of the soil in the conformal layer SR EN ISO 14688-1 şi SR EN ISO 14688-2 | Stratification column | Edometric mode $M_{2-3}$ kPa | int. friction angl Φ grad | Specific cohesion c kPa |
|---|---|---|---|---|
| Vegetal Soil | | - | - | - |
| Dusty, brown, hard clay | | 7937 | 21.7 | 33.9 |
| Dusty, sandy brown, plastic clay | | 7407 | 15.7 | 16.9 |
| Dusty, sandy, black, plastic clay | | 5333 | 23.3 | 8.1 |

The porosity of the soil n [%] between 45.6 ÷ 46.3 and the natural humidity w [%] between 21.9 ÷ 33.1, determine:

- Intense biological activity;
- Higher air capacity in the soil;
- The proportion between the soil pores determines and influences the relationship of the soil with water;
- Higher porosity implies higher permeability for water and air, so that air and aeration increase from clayey to sandy soil.

The IC Consistency Index of the soil from the lot on which the measurements were made, indicates a decrease (1.09 ÷ 0.75) over the area -0.70 ÷ -4m, so that the dusty clay, brown, hard, sandy brown, plastic and black sandy clay, has a structure that promotes water infiltration, retention and preservation. The IC Consistency Index justifies the forces that take place between the particles and the micro and macro aggregates in the soil implicitly the biologically intense activity. On the scale of 0.75 ÷ 1, the consistency of the clay soil is considered rigid, hard and compact and on the scale of 0.5 ÷ 0.75 the consistency of the clay soil is considered firm and stable. The specific cohesive strength of clay soil in [kPa] has a decrease from 33.9 ÷ 8.1 over the depth zone from -0.70 ÷ -4m, which justifies a higher presence of water percentage in the soil.

## 4. Photographic images with stages of prototype assembly for monitoring the corrosion of zinc coated and non-zinc coated metal elements

Table 7 presents the legend of the photo images and includes the following: the stage of drilling in the soil, the collection of soil samples and the assembly of metal samples covered and not covered with zinc in the soil for the study of corrosion.

*Table 7*

**The legend of photographic images**

| Foto nr. | Legend |
|---|---|
| 1 | Equipment for drilling in the ground |
| 2 | Drilling operation in the ground with a drill |
| 3 | Dusty, sandy, black, plastic clay |
| 4 | Dusty, sandy brown, plastic clay<br>Dusty, sandy, black, plastic clay |
| 5 | Soil test |
| 6 | Zinc coated and uncovered metal samples fitted with sensors |
| 7 | Installation of samples in the soil |
| 8 | Row of soil samples |
| 9 | Row of soil samples |

**Photographic images with stages of assembly of the metal samples (earthing electrodes) in soil and collection of soil samples for analysis**

Fig. 1 Drilling equipment

Fig. 2 Drilling operation in the ground

Fig. 3 Dusty, sandy, black, plastic clay

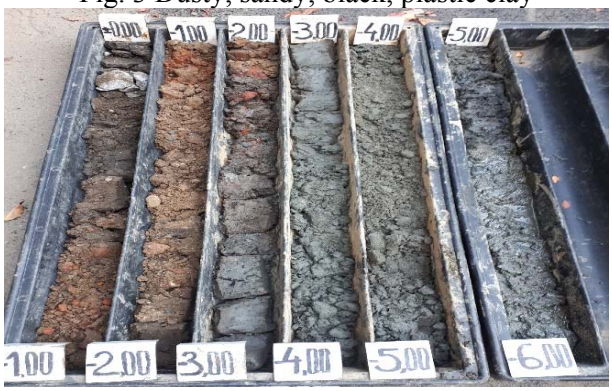


Fig. 4 Collected soil samples

Fig. 5 Non-galvanized and galvanized metal samples with senzors

Fig. 6 Installation of the samples in the soil

Fig. 7 The row of samples

Fig. 8 The row of samples

## 5. The metal analysis from soil

A pedological drill was used to take soil samples.
The analysis of the metals was performed with the portable multichannel X-ray fluorescence analyzer - FRX, Thermo Scientific NITON XL3t model.
The evaluation and interpretation of the obtained results was performed by reference to the reference values established for the soils of sensitive use, respectively Order 756/1997 for the approval of the Regulation on the assessment of environmental pollution with subsequent amendments and completions.

*Table 9*

**Results of soil metal analysis**

| **Determined chemical element** | **Sampling depth h= -1.5 m** | **Sampling depth h= -2.3 m** | **Alert limit cf Ord. 756 / 1997 actualized** |
|---|---|---|---|
| Ca | 17 ± 1 mg/kg s.u. | 9 ± 1 mg/kg s.u. | - |
| K | 9 ± 1 mg/kg s.u. | 9 ± 1 mg/kg s.u. | - |

| | | | |
|---|---|---|---|
| Zn | 287 ± 10 mg/kg s.u. | 103 ± 10 mg/kg s.u. | 300 mg/kg s.u. |
| Cu | 48 ± 10 mg/kg s.u. | 39 ± 10 mg/kg s.u. | 100 mg/kg s.u. |
| Fe | 35 ± 1 mg/kg s.u. | 32 ± 1 mg/kg s.u. | - |
| Mn | 860 ± 50 mg/kg s.u. | 560 ± 50 mg/kg s.u. | 1500 mg/kg s.u. |
| Zr | 178 ± 5 mg/kg s.u. | 224 ± 5 mg/kg s.u. | - |
| Sr | 100 ± 3 mg/kg s.u. | 96 ± 3 mg/kg s.u. | |
| Pb | 48 ± 5 mg/kg s.u. | 13 ± 4 mg/kg s.u. | 50 mg/kg s.u. |
| As | 4.4 ± 4 mg/kg s.u. | 5 ± 3 mg/kg s.u. | 15 mg/kg s.u. |
| Cr total | < 100 mg/kg s.u. | < 100 mg/kg s.u. | 100 mg/kg s.u. |
| Ni | < 20 mg/kg s.u. | < 20 mg/kg s.u. | 75 mg/kg s.u. |

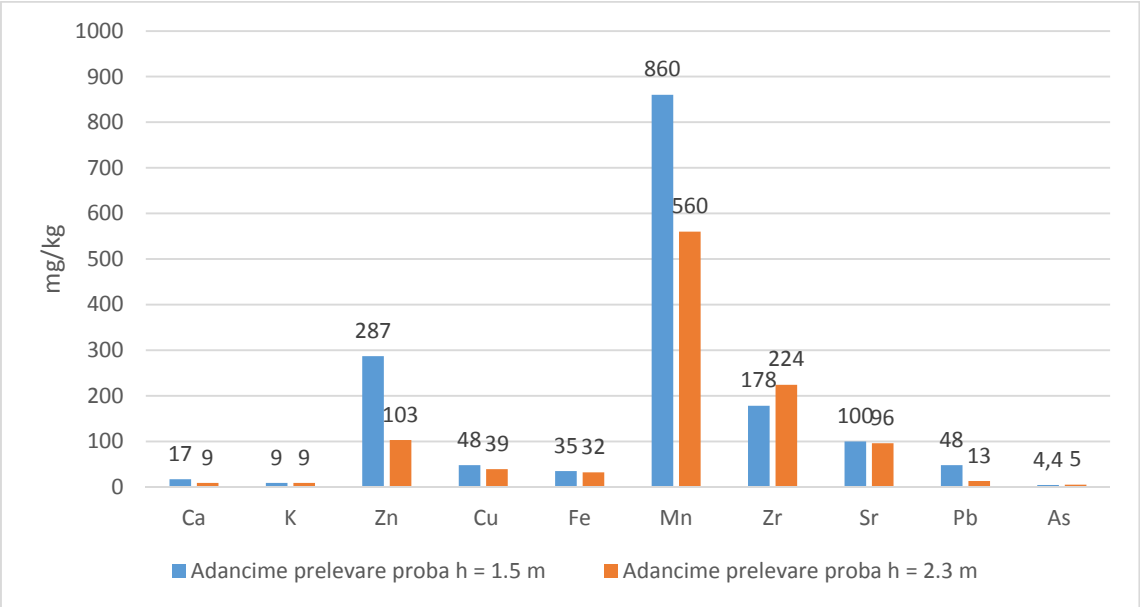


Fig. 9 The metals determined from the soil samples at 1.5 m and 2.3 m

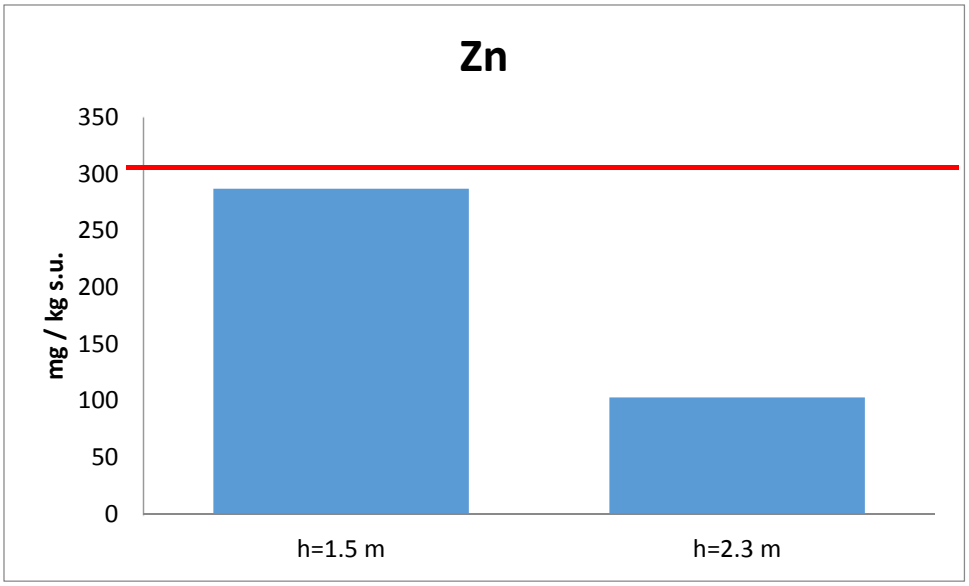


Fig. 10 Graphical representation of zinc in the soil samples

The analyzed element Zn, whose alert threshold, according to O 756/1997 is 300 mg / kg s.u, the value determined at a depth of 1.5 m is very close to this threshold value. This is justified by the fact that the soil is mixed with filler.

## References

[1] https://www.asminternational.org/;
[2] https://www.astm.org/COMMIT/SUBCOMMIT/G0110.htm;
[3]https://www.academia.edu/9159953/NORMATIV_PENTRU_PROTEC%C5%A2IA_CONTRA_COROZIUNII_A_CONSTRUC%C5%A2IILOR_METALICE_%C3%8ENGROPATE_Indicativ_I_14-76_%C3%8Enlocuie%C5%9Fte_I_14-65;
[4]https://lege5.ro/Gratuit/gi4dgnbvgazq/protectia-echipamentelor-si-a-conductelor-din-otel-impotriva-coroziunii-norma-tehnica?dp=gi3damjwgqzdimi
[5] Analiza de sol conform fişei de foraj nr. 1 din 25.06.2018 eliberată de *S.C. CARA SRL, str.Filaret Barbu, nr. 2, codul poştal 300193, Timişoara]*

# Study of the durability against carbonation of the concrete formulated with the partial replacement of cement with marble powder

Ahmed MERAH [1]
[1] University AmmarTelidji of Laghouat , Faculty of Civil Engineering and Architecture, Research Laboratory of Civil Engineering (LRGC), Laghouat, Algeria.

*E-mail: a.merrah@lagh-univ.dz*

DOI: 10.37789/rjce.2021.12.1.11

**Abstract.** *The first aim of this study is the use of marble waste powder as a partial replacement with cement (CEMI 42.5) in concrete in order to reduce greenhouse gas emissions results in the cement production and consequently on the manufacturing concrete with less environmental impact.*
*Moreover, the carbonation phenomenon influences significantly the durability of reinforced concrete structures, in this context, the second aim of this work is the study of the effect of the accelerated carbonation on the durability of concretes formulated with the cement containing the marble waste (MDP) with different percentages. For this purpose, four concrete mixtures containing 0%, 10%, 15%, and 30% MDP as cement replacement by weight basis have been prepared. These mixtures of concretes were submitted to accelerated carbonation to study their durability against this phenomenon.*
*The series of tests are conducted to study the effect of 10%, 20% and 30% replacement of cement with marble powder on carbonation depth and compressive strength and compare it with the conventional concrete.*
*The result of this present investigation indicates that the carbonation depth increases with the increase of the rate of the replacement of cement with waste marble powder (10 % to 30%) and the compressive strength decreases slightly with the increase of replacement. the compressive strength remains within the acceptable range of M25 concrete.*

***Key words:*** *waste marble powder, concrete durability, carbonation depth, compressive strength, environment.*

## 1. Introduction

The consumption of fossil fuels releases trace gases in the atmosphere that affect the climate, such as methane, Sulphur dioxide, nitrogen and carbon dioxide. The latter being responsible for half of the greenhouse effect (Retallack and Conde 2020)[1]. (Betts et al 2016)[2] shown that the global carbon dioxide ($CO_2$) content of the atmosphere reaches the symbolic and significant threshold of 400 parts per million (ppm) for the first time in 2015 and set new records in 2016.
Concrete is the most widely used composite material in the world, given its high strength and stability. this material is mainly composed of cement, aggregates, water and possibly additives, all the components of this material are available in nature with the exception of the cement which requires fossil energy for production which is the main source of pollution air.

(Diet and Schmitt 1996)[3] show that the cement industry generates enormous quantities of carbon dioxide and thus participates in increasing the concentration of $CO_2$ in the air. this concentration can reach 1% and to produce a ton of cement, the cement industry releases a ton of $CO_2$.

Furthermore, marble quarries generate marble powder waste that is harmful to the environment. In this context, two objectives are to be expected, the first consists in limiting the $CO_2$ on emissions due to the manufacture of cement, the second consists in minimizing the effects on the environment by the use of marble powder as a partial replacement for the cement, in this axe of research several researchers have carried out several studies on the effect of this partial replacement of cement with marble powder, among these researchers, (Sadek et al 2016)[4] conducted a study on the possibility of using marble powder in self-placing concrete as a partial replacement for cement, the results of this study showed that the optimal percentage of replacement is around 50% which leads to an increase in compressive strength . (Soliman 2013[5]; Aliabdo et al 2014[6]) studies the effect of the use of marble powder as a partial replacement of cement on the concrete properties, the results obtained shown that the use of marble powder improves workability, compressive and tensile strength. (Kumar and Kumar 2015[7], Vaidevi 2013[8]; Rodrigues et al 2015[9]; Ergün 2011[10]) studied the effect of different percentage of substitution of cement by marble powder on compressive strength, the results of this research shown that the optimal rate of replacement of cement by powder marble is up to 10%. In the same way, (Singh et al 2017;2019) [11-12]concluded that an optimum of 15% replacement leads to an improvement in strength and durability of concrete.

In the same way other researchers continued to explore this field, ( Singh et al 2019)[13], concluded that the marble powder incorporated in concrete shows increase in mechanical proper-ties at 15% replacement by weight of cement for lower w/b ratios 0.35 and 0.40, and for w/b ratio 0.45 the strength increases only up to 10% replacement. In their study, (Ulubeyli et al 2016[14]) found out that the use of waste marble in the conventional or self-compacting concrete can improve durability properties of the concrete.

In their study (Vardhan et al 2019) [15] show that waste marble can be used into concrete to improve its strength and permeation properties, with the maximum improvement obtained at 40% replacement level. (Ashish 2018) [16] concluded in their study that the maximum percentage of partial replacement of marble powder in cement don’t exceed 20%.

The studies cited in this work in the field of partial replacement of cement with marble dust conclude that the replacement of the cement must not exceed 20% of marble dust in order to have acceptable compressive strength of the concrete. High levels of marble dust increase the capillarity of concrete.

On the other hand, many environmental phenomena influence the durability of reinforced concrete structures. Among these phenomena, we can cite the concrete carbonation which is one of the main factors of degradation of unprotected reinforced concrete structures, and those exposed to high concentrations of carbon dioxide (such as road tunnels). This causes corrosion of the reinforcements, causing the concrete to

lose its alkalinity and consequently causes the reduction of the service life of reinforced concrete structures. carbon dioxide gas penetrates through the open porosity of concrete to react with interstitial water to give carbonic acid, this in turn reacts with portlandite $Ca(OH)_2$ (product responsible for the durability of the steels against corrosion while keeping an environment with a basic pH of the order of 13), this reaction produces calcium carbonate $CaCO_3$ which consumes the reserve of portlandite and putting steels without protection. Then, lead to disorders in the construction by swelling and cracking.
Several researchers have studied the effect of carbonation, on the durability of concretes formulated with substitution of cements with marble powder, in their study (Ashish 2019[17]; Gameiro 2014[18]) shows that the depth of carbonation increases with the increase of the replacement.
(Singh et al 2017[19]) shows that with 15% of partial replacement of the marble powder, the re-sistance for carbonation was improved. According to the experimental study, (Ashish 2018[20]; Rana et al 2015[21]) also show that the depth of carbonations increased in case of use of powder marble.
In their review study, (Kumar and Thakur 2018[22]) show that the concrete carbonation depth depends on its porosity. Carbonation values also decrease with inclusion of marble powder and reported a similar trend to carbonation depth and water absorption by immersion for the chloride mitigation coefficient.
This paper presents a contribution in this area. this contribution consists on studying the durability of concrete formulated with a partial replacement of cement with marble powder who is the first objective, the second consist to study the effect of using marble powder as partially replace of cement on the durability of concrete against the phenomenon of concrete carbonation.
The result of this investigation indicates that the carbonation depth decreases with the increase of the replacement of cement with waste marble powder (10 % to 30%) and the compressive strength decreases slightly with the increase of replacement. the compressive strength remains within the acceptable range of M25 concrete.

## 2.2. Powder Marble

The used marble powder was a waste resulting from the cutting, shaping and lustration of marble stones. This powder was supplied by the company MCA (Marble Tile and Agglo-marble installed in locality of Bordj Bou Arrérdj in Algeria). The physic and the chemical properties of the marble powder are given in Table 4.

Table 4:

Chemical properties of the marble powder [23]

| Content (%) | Marble powder |
|---|---|
| CaO | 55.6 |
| $SiO_2$ | 0.6 |
| $AL_2O_3$ | 0.4 |

| | |
|---|---|
| $Fe_2O_3$ | 0.2 |
| MgO | 0.1 |
| $NaCO_3$ | 90 |
| CL | 0.1 |
| LOI | 43 |
| Density | 2.7 |
| Blaine Specific Surface ($cm^2/g$) | 2126 |

The used sand is alluvial (0-5 mm) which produced by Oued M'zi quarry of Laghouat, Algeria , two classes of limestone aggregates (3-8 mm and 8-15 mm) were used in the concrete formulation which produced by the quarry (Laghouat).
The table 5 gives the physical proprieties of the used aggregates

Table 5:

Physical proprieties of the used aggregates

| Physical proprieties of the used aggregates | Standard | Aggregates | | |
|---|---|---|---|---|
| | | Sand | Gravel | |
| | | 0/5 | 3/8 | 8/15 |
| Apparent Density ($g/cm^3$) | NF P 18-554 | 1.564 | 1.319 | 1.255 |
| Absolute density ($g/cm^3$) | | 2.6 | 2.65 | 2.65 |
| Absorption Coefficient (%) | | 1 | 1.5 | 1.5 |

The used sand has a particle size of 0–5 mm, apparent density of 1.56 $g/cm^3$ and absolute density of 2.61 $g/cm^3$. Two sizes of aggregates (3–8 mm), (8–15 mm) are used to formulate the concretes, these aggregates are characterized by a calcareous rock with a high calcium carbonate content (_98% $CaCO_3$), their apparent densities are 1.32 $g/cm^3$ and 1.26 g/ $cm^3$ respectively. Their absolute density is 2.6 $g/cm^3$. The used water is tap water. It meets all the requirements of NFP 18-303 and EN 1008, taking into account the concentrations of suspended solids and dissolved salts.

## 3. Methods

### 3.1. Concretes Formulations

The used concrete formulation method in the present study is DREUX GORISSE method.
The results of the concrete formulation were gives in Table 6:

Table 6:

Results of control concrete Formulation

| S/G | W/C | Sand ($kg/m^3$) | Gravel 3/8 (kg) | Gravel 8/15 (kg) | Cement (CEM I) (kg) | Water (L) | Slump test (cm) |
|---|---|---|---|---|---|---|---|
| 0.60 | 0.57 | 683.7 | 146.7 | 990.25 | 374.4 | 216.42 | 8 |

Legend:
S: Sand
G: Gravels
W: Water
C: Cement

Table 6: shows the results of the control concrete formulation. According to the synthesis of this results, the concrete formulation has the density, who is a normal concrete according the standard NF EN 12350-6 (Normal concrete with a density between 2000 and 2600 $kg/m^3$).
From this control concrete formulation, three other concrete mixes were formulated by substituting different percentages (10%, 20% and 30%) of cement replace by weight with marble powder according to Table 7

Table 7:

Weights of Marble powder for different concrete formulations.

| Concretes formulations | Cement (Kg) | Marble powder (Kg) |
|---|---|---|
| B1 (0% replacement) | 374.4 | 0 |
| B2 (10% replacement) | 336.96 | 37.44 |
| B3 (20% replacement) | 299.52 | 74.88 |
| B4 (30% replacement) | 262.08 | 112.32 |

## 3.2. Confection and preservation of samples.

Before mixing the concretes, the aggregates, previously washed and dried in an oven at 10 ± 5 ° C for one day (24 h), then cooled in ambient air, then they are introduced, according to mass proportions already known. in parallel with the preparation of the concrete, the moulds (7x7x7 cm3) are prepared for the determination of the compressive strength and for the accelerated carbonation tests. All the samples are kept in the moulds for 24 hours in plastic film, after demoulding, they are immersed in

water at T = 20 ± 0.5 ° C according to standard NA 426 for 28 days and according to the recommendation of the AFPC AFREM[23](P.Rougeau,1997), until the deadlines for the start of tests (Figure 1)

Fig. 1. Samples conservation.

After 28 days of cure, the cubic samples (7x7x7 $cm^3$) of prepared concrete will be subjected to two test campaigns, compression test and accelerated carbonation test.

### 3.3. Compressive strength test.

In order to determinate the compressive strength of the four concrete formulations (B1, B2, B3 and B4) cubic samples (7x7x7 $cm^3$) were used. The compressive strength for cubic samples of carbonated and control concrete samples were determinate at age 7,14 and 28 days.

The compression resistance test was carried out on 7 × 7 × 7 $cm^3$ cubic samples according to NF P18-406. The hydraulic press used has a loading speed of 0.5 MPa / Sec with a capacity of 3000KN. the rupture stress is given directly by the testing machine with an accuracy of 0.5 MPa (Figure 2.).

Fig.2. Machine for compressive strength test.

### 3.4. Accelerated carbonation test

The concrete carbonation is a very slow phenomenon in the atmosphere, the concentration of carbon dioxide is not very important (of the order of 0.3%) in the air, the effect of this phenomenon is manifested only after several years of exposure of

reinforced concrete structures to this phenomenon, therefore, it is necessary to find a way to accelerate the carbonation of the cementitious material ensuring results representative of this natural phenomenon. This test is called "accelerated carbonation test".

### 3.4.1. Accelerated carbonation test procedure according to the AFPC-AFREM test protocol.

The test consists in following the evolution of the thickness of the carbonated concrete preserved in an atmosphere rich in carbon dioxide ($CO_2$).

**A.1. Equipment.**

✓ Ventilated oven: controlled at 40 ± 2°C, located in a room with a temperature of 20 ± 2°C

✓ Accelerated carbonation chamber: the accelerated carbonation test consists in obtaining a gas mixture (50% $CO_2$ + 50% air) in the carbonation chamber (Figure. 3) with controlling the relative humidity which must be between 40 and 80%. To monitor the relative humidity, a hygrometer was used. The carbonation test is executed using a carbon dioxide ($CO_2$) incubator according to the AFPC-AFREM test protocol [23](1997) (P. Rougeau,1997).

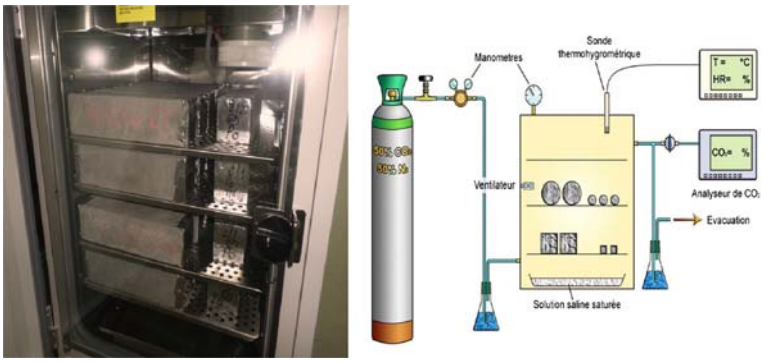

Fig.3. Accelerated carbonation chamber

To start the accelerated carbonation test, the samples must be preconditioned in two phases:

- In the first phase, the specimens undergo a cure in a humid environment (relative humidity greater than 95% or emerged into water) for 28 days (P. Rougeau, 1997) then weighed, according to the recommended procedure for determining the bulk density and the water content.

In the second phase, they are placed in an oven at 40 ± 2° C, for two days, then weighed for second time [23] (P. Rougeau,1997). The two faces of each sample must be covered with adhesive aluminium wrapper to guide the diffusion of CO2, then the samples are subjected to accelerated carbonation in the carbonation chamber for 28 days and placed distant of 2 cm one from the other (figure 4 and figure 5) [23] (P.Rougeau, 1997), while other control samples are stored in the laboratory to measure the compressive strength.

Fig. 4.: Preparation of Samples for accelerated carbonation test.

Fig.5. Samples into the chamber of carbonation

At the age 7, 14 and 28 days, concrete samples are weighed and removed from the carbonation chamber to measure the evolution of accelerated carbonation according to the experimental procedures of the AFPC AFREM 1997 recommendations (P. Rougeau, 1997). To measure the concrete carbonated depth, the samples are sliced in two parts and the reading is made immediately using the colour indicator recommended by the procedure of standard NF P18-458. It colours the uncarbonated concrete in pink while the carbonated concrete does not change. The colour indicator used to reveal the carbonated concrete is a phenolphthalein solution (Figure. 6). The number of samples required for carbonation test is four: three for measuring the concrete carbonation depth, the fourth is used to follow the evolution of the sample mass during the test. Two additional test specimens may be used to monitor the evolution of concrete subjected to natural carbonation. These samples can be stored in an ambient atmosphere at a temperature of 20 ± 2 _C and a relative humidity of 65 ± 5%. Other cubic samples were prepared for the different concrete formulations according to the recommendations of the French Association of Competitiveness Clusters (AFPC AFREM 1997) [23] (P. Rougeau,1997).

Fig.6. Determination of Carbonation depth with phenolphthalein pulverisation

## 4. Results and Discussions

### 4.1. Densities and water content of samples

In order to conduct the accelerated carbonation test and according to AFPC AFREM 97 [23](P. Rougeau,1997) recommendations, in the first pre-conditioning phase, the bulk density and water content of the samples must be determined for the accelerated carbonation test.

The table 8 show the results of densities and water content for the four-concrete formulation

Table 8:

Densities and water content for the four concrete formulations

| Concrete formulations | Densities in Kg/m$^3$ | Water content (%) |
|---|---|---|
| B1(0% replacement) | 2537.63 | 2.37 |
| B2(10% replacement) | 2566.14 | 2.32 |
| B3(10% replacement) | 2602.85 | 2.32 |
| B4(10% replacement) | 2592.64 | 2.34 |

The table 8 show that the densities increases with the increase of substitution (cement with the powder marble) for the four concrete formulations. The water content of the all concrete formulations have the same value, from these results, then, the accelerated carbonation test can be started according to AFPC AFREM 97[23] (P. Rougeau,1997).

### 4.1. Effect of the replacement (cement by the powder marble) on the compressive strength for the four concretes formulations

At the age of 28 days, samples were tested with the compressive machine, the table 9 show the effect of the carbonation on the compressive strength of the control concrete and the other concretes with different percentages of replacements of cement with powder marble (10%, 20% et 30%)

Table 9:

Compressive strength for different concrete formulations

| Age (days) | Compressive strength (MPa) | | | |
|---|---|---|---|---|
| | Formulation B1(control) | Formulation B2 (10%replacement) | Formulation B3 (20% replacement) | Formulation B4 (30% replacement) |
| 28 | 59.2 | 55.4 | 52.9 | 46.4 |

from Table 9 and the figure 7, it is clearly shown that the compressive strength decreases with increasing percentage of substitution of cement with marble powder. this decrease is slightly (of the order of 11%) up to a percentage of 20% of substitution and it is important of the order of 22% for a substitution of 30%.

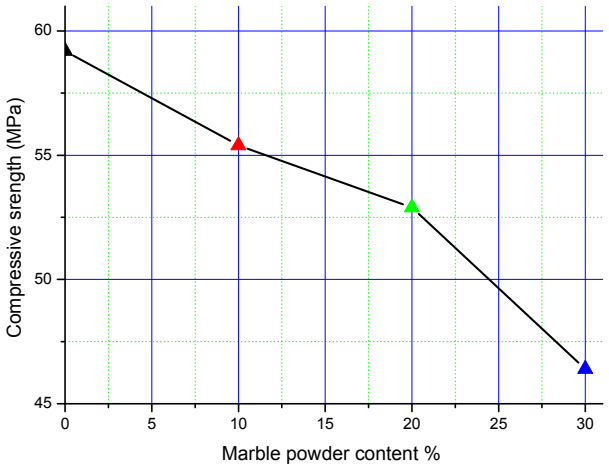


Fig.7.: Compressive strength with marble powder content

The obtained results for the compressive strength of concrete are in agreement with those obtained by [24](Tayeh 2018). The value of the compressive strength of 46 MPa corresponding to a substitution of cement with 30% of marble powder is acceptable for the realization of structural elements of reinforced concrete. this result will lower cost of making reinforced concrete structures, with condition to protecting the exposed concrete against carbonation.

**4.2 Effect of the carbonation on the gain mass for the four concrete formulations**

The table 10 show the effect of the carbonation on the gain mass for the four concrete formulations at the different ages 7,14 and 28 days,

Table 10:

Mass gain (g) for different concrete formulations.

| Age (days) | Mass gain (g) | | | |
|---|---|---|---|---|
| | Concrete B1 (control) | Concrete B2 (10% replacement) | Concrete B3 (20% replacement) | Concrete B4 (30% replacement) |
| 7 | 853.24 | 865.92 | 881.7 | 913.3 |
| 14 | 856.8 | 869.2 | 886.8 | 923.1 |
| 28 | 858.2 | 870.6 | 889.1 | 925.6 |

From this table, we draw the following curve (Figure 8)

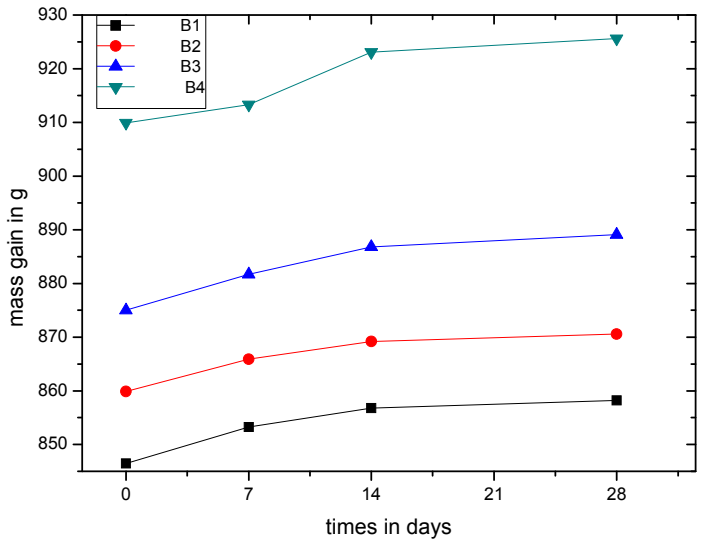


Fig.8.: Mass gain for the four concretes formulations

Figure. 8 show that the carbonation increases the mass of samples with the increase of the substitution (cement by marble powder (10%, 20%, 30%). This increase is due mainly to the concrete carbonation who makes changes in the microstructure of carbonated concrete (replacement of portlandite by calcite).

### 4.3. Effect of the accelerated carbonation on the four concretes formulations.

The carbonate depth was determined, according to the AFPC-AFREM 97 procedure [23] (P.Rougeau,1997), by a phenolphthalein method described above, applied to the face of the cubic samples ($7 \times 7 \times 7$ cm$^3$) after cutting into two parts with the 'ages 7, 14 and 28 days. Table 11: shows the evolution of the depth of carbonation at different ages for the four concrete formulations.

Table 11:
Evolution of carbonation depth at different ages for the four concrete formulations

| Age (Days) | Carbonation depth (mm) | | | |
|---|---|---|---|---|
| | Concrete B1 (Control) | B2 (10% replacement) | B3(20% replacement) | B4(30% replacement) |
| 7 | 1 | 3 | 4 | 6 |
| 14 | 2 | 5 | 7 | 8 |
| 28 | 3 | 6 | 7.5 | 9.5 |

From the table 11, we draw the following curve (figure 9).

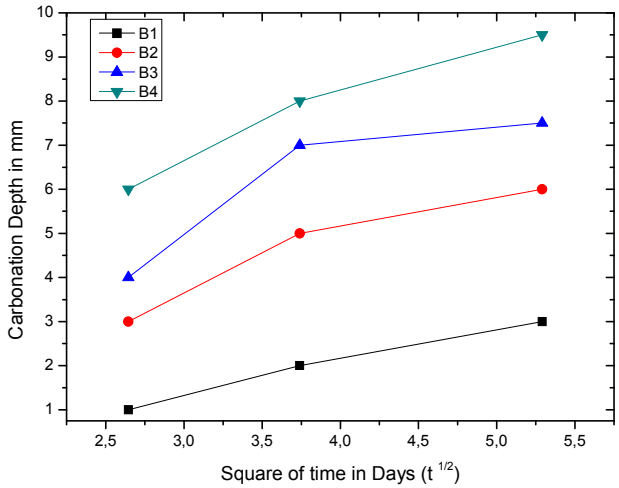


Fig.9.: Carbonation depth for the four concrete formulations

According to the curve of the evolution of the carbonation depth with the square of time for the different concretes, we note that the depth of the carbonation increases with the substitution of cement by the marble powder (10%, 20%, 30%).
In addition, it can be seen from the previous curve (Figure 9) that the evolution of the carbonation depth is relatively fast from 7 days to 14 days and stabilizes at almost constant values until the 28th days. This for all concretes (B1, B2, B3, B4). This result can be explained as follows:

- During the 7 to 14-day period, the available amount of portlandite is larger, resulting in faster carbonation with calcite formation.
- For the period between 14 and 28 days, the available amount of portlandite becomes low as it is consumed during the first period. this will reduce the carbonation rate.

This reduction is caused by clogging of pores caused by the formation of calcite which has a molar volume greater than the molar volume of portlandite.
On the other hand, it can be concluded that the depth of carbonation increases with the increase of the percentage of replacement of powder marble.

### 4.4. Correlation between the mass gain and the carbonation depth

The figure 10 show the mass gain with carbonation depth

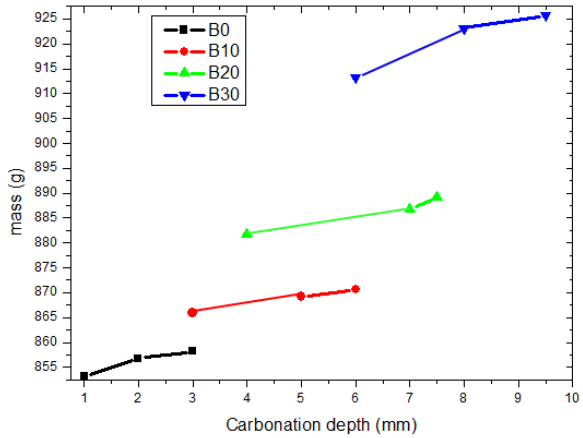


Fig 10. Mass gain with the carbonation depth

From the figure 10, it can be seen that the mass of the carbonated samples increases with the increase of the carbonation depth, which shows an important relation between the gain of the mass and the carbonation depth, which leaves to think that there is a relation which links the gain of mass to the depth of carbonation, that is to say that one can estimate the depth of carbonation from a simple weighing, thus avoiding the use of solution of phenol.

## 5. Conclusions

From this study, the following conclusions can be written

- The depth of carbonation increases with the time of exposure in the enclosure of accelerated carbonation.
- The increase in the substitution of cement by powdered marble increases the depth of carbonation. this is due to the replacement of cement by the marble powder which makes decreased, the rate of portlandite and consequently, it accelerates the consumption of this one by the reaction of carbonation.
- The increase in the mass of carbonate samples increases with the increase in the depth of carbonation, this is mainly due to the carbonation of portlandite giving rise to calcite denser than portlandite
- The compressive strength decreases with substitution of the cement by the marble powder. this decrease is slight and remains within values acceptable by Algerian standards.
- Partial replacement of cement with marble powder up to 30% can give a quality concrete (Acceptable compressive strength according to Algerian standards). moreover, this replacement contributes to reducing the harmful effects of marble waste on the environment.

- To protect this concrete and make it durable against carbonation, it must be protected by an anti-carbonation coating.
-

## 6. References

[1] Retallack, G.J., Conde, G.D., 2020. Deep time perspective on rising atmospheric CO2. Global and Planetary Change 103177.
[2] Betts, R.A., Jones, C.D., Knight, J.R., Keeling, R.F., Kennedy, J.J., 2016. El Niño and a record CO 2 rise. Nature Climate Change 6, 806.
[3] Diet, A., Schmitt, A., 1996. Electricity of France and renewable energies: this is part Solar systems (Review) 17–23.
[4] Sadek, D.M., El-Attar, M.M., Ali, H.A., 2016. Reusing of marble and granite powders in self-compacting concrete for sustainable development. Journal of Cleaner Production 121, 19–32.
[5] Soliman, N.M., 2013. Effect of using marble powder in concrete mixes on the behavior and strength of RC slabs. International Journal of Current Engineering and Technology 3, 1863–1870.
[6] Aliabdo, A.A., Elmoaty, A.E.M.A., Auda, E.M., 2014. Re-use of waste marble dust in the production of cement and concrete. Construction and building materials 50, 28–41.
[7] Kumar, R., Kumar, S.K., 2015. Partial replacement of cement with marble dust powder. International Journal of Engineering Research and Applications 5, 106–114.
[8]Vaidevi, C., 2013. Study on marble dust as partial replacement of cement in concrete. Indian journal of engineering 4, 14–16.
[9] Rodrigues, R., De Brito, J., Sardinha, M., 2015. Mechanical properties of structural concrete containing very fine aggregates from marble cutting sludge. Construction and Building Materials 77, 349–356.
[10] Ergün, A., 2011. Effects of the usage of diatomite and waste marble powder as partial replacement of cement on the mechanical properties of concrete. Construction and building materials 25, 806–812.
[11] Singh, M., Srivastava, A., Bhunia, D., 2017. An investigation on effect of partial replacement of cement by waste marble slurry. Construction and Building Materials 134, 471–488.
[12] Singh, M., Srivastava, A., Bhunia, D., 2019. Analytical and experimental investigations on using waste marble powder in concrete. Journal of Materials in Civil Engineering 31, 04019011.
[13] Singh, M., Srivastava, A., Bhunia, D., 2019. Long term strength and durability parameters of hardened concrete on partially replacing cement by dried waste marble powder slurry. Construction and Building Materials 198, 553–569.
[14] Ulubeyli, G.C., Bilir, T., Artir, R., 2016. Durability properties of concrete produced by marble waste as aggregate or mineral additives. Procedia engineering 161, 543–548.
[15] Vardhan, K., Siddique, R., Goyal, S., 2019. Strength, permeation and micro-structural characteristics of concrete incorporating waste marble. Construction and Building Materials 203, 45–55.
[16] Ashish, D.K., 2018. Feasibility of waste marble powder in concrete as partial substitution of cement and sand amalgam for sustainable growth. Journal of Building Engineering 15, 236–242.
[17] Ashish, D.K., 2019. Concrete made with waste marble powder and supplementary cementitious material for sustainable development. Journal of cleaner production 211, 716–729.
[18] Gameiro, F., De Brito, J., da Silva, D.C., 2014. Durability performance of structural concrete containing fine aggregates from waste generated by marble quarrying industry. Engineering Structures 59, 654–662.
[19] Singh, M., Choudhary, K., Srivastava, A., Sangwan, K.S., Bhunia, D., 2017. A study on environmental and economic impacts of using waste marble powder in concrete. Journal of Building Engineering 13, 87–95.
[20] Kumar, A., Thakur, A., 2018. A State of Art Review: On Usage of Waste Marble Powder In Concrete Production.

[21] Rana, A., Kalla, P., Csetenyi, L.J., 2015. Sustainable use of marble slurry in concrete. Journal of Cleaner Production 94, 304–311.
[22] P. ROUGEAU, " AFREM crossover test results, Accelerated carbonation test," CERIB, 1997.
[23]Bouziani, T., Benmounah, A., 2013. Correlation between v-funnel and mini-slump test results with viscosity. KSCE Journal of Civil Engineering 17, 173–178.
[24] Tayeh, B.A., 2018. Effects of marble, timber, and glass powder as partial replacements for cement. Journal of Civil Engineering and Construction 7, 63–71.

# Aspecte privind utilizarea dispozitivelor de amortizare cu masa acordata

Aspects regarding the use of the Tuned Mass Dampers

Zainulabdeen K. Abdulfattah Abdulfattah[1], Vlad Stefan Niculae[1], Daniel Stoica[1]

[1]Universitatea Tehnica de Constructii Bucuresti
B-dul Lacul Tei 122-124, Sector 2, Bucuresti, Romania
*E-mail: stoica@utcb.ro*

DOI: 10.37789/rjce.2021.12.1.12

**Rezumat.** *Una dintre alternativele de proiectare a clădirilor noi dar şi de intervenţii la clădirile existente este pe baza utilizării dispozitivelor de amortizare cu masa acordată. Având în vedere că acestea sunt eficiente numai la clădiri cu regim mare de înălţime, s-au realizat studii de caz pentru clădiri cu 10, 20, 30 şi 40 de niveluri, având 3 tipuri de forme diferite în plan (circulare, pătrate şi dreptunghiulare) şi două tipuri de structuri de rezistenţă (cadre din beton armat şi duale din beton armat). S-au realizat comparaţii între răspunsurile structurale obţinute pentru modele de calcul corespunzătoare clădirilor cu şi fără utilizarea dispozitivelor de amortizare cu masă acordată.*

**Cuvinte cheie:** amortizor, masă, acordată, deformaţii

**Abstract.** *One of the alternatives of designing new buildings but also for interventions to existing buildings is based on the use of the Tuned Mass Dampers (TMD). Given that they are effective only in high rise buildings, case studies have been carried out for buildings with 10, 20, 30 and 40 levels, having 3 different types of shapes in plan (circular, square and rectangular) and two types of structures (reinforced concrete frames and reinforced concrete dual systems). Comparisons were made between the structural responses obtained for the calculation models corresponding to the buildings with and without using the TMD.*

**Key words:** damper, mass, tuned, deflections

## 1. Introducere

Sistemul de amortizare cu masa acordata TMD (Tuned Mass Damper) - un sistem foarte eficient in controlul vibratiilor unei structuri - este format (la nivel teoretic) dintr-o masa, un amortizor vascos si un resort atasat unei structuri pentru reducerea vibratiilor induse de vant si de sesim. Frecventa si amortizarea acestor

sisteme sunt acordate in asa fel incat, atunci cand structura intra in rezonanta la o anumita frecventa (perioada) TMD-ul oscileaza cu aceeasi perioada, dar defazat fata de structura, astfel energia se transmitede la sistemul primar (structura) la cel secundar (TMD) si se disipa in amortizor.

## 2. Utilizarea sistemelor cu masa acordata pe plan international

Primul sistem cu masa acordata a fost propus de Fhram (1909) pentru reducerea vibratiilor produse de forte armonice monotone. El a observat ca daca un sistem secundar format dintr-o masa, un amortizor si un arc este atasat de un sistem primar, iar perioada lui este acordata cu perioada fundamentala a sistemului primar, se obtine o reducere considerabila a raspunsului dinamic.

Prima cladire echipata cu amortizor cu masa acordata este Centerpoint Tower in Sydney, Australia. Structura a fost finalizata in 1981 si masoara 309 m.

Fig. 1 Centerpoint Tower, Sydney Australia

In Canada, exista cateva cladiri echipate cu amortizori cu masa acordata printre care: CN Tower; One Wall Center.

CN Tower are 553m inaltime si a fost finalizat in 1976. La momentul finalizarii a fost cea mai inalta cladire.

Fig. 2 CN Tower, Toronto Canada

One Wall Center cunoscut si sub numele Sheraton Vancouver Wall Center Hotel are 48 etaje, si inaltimea de 158m. Pentru a contracara posibilele vibratii armonice cauzate de vantul puternic, turnul a fost echipat cu amortizor cu apa acordat. Acest sistem a fost amplasat la ultimul nivel si este format din 2 rezervoare cu capacitatea de 227 mii litri. Aceste rezervoare au fost proiectate astfel incat frecventa armonica a miscarii apei sa echilibreze miscarea armonica a turnului.

Fig. 3 One Wall Center, Vancouver, Canada

Taipei 101, cunoscut si sub numele Taipei World Finacial Center, a fost cea mai inalta constructie incepand cu 2004 pana la construirea lui Burj Khalifa. Are 101 etaje si o inaltime de 508m.

Fig. 4 Taipei 101, Taipei, Taiwan

Fig. 5 Pendulul tunului Taipei 101

Inginerii lui Taipei 101, au proiectat un pendul din otel cu greutatea de 660 tone care sa actioneze ca un amortizor cu masa acordata. Suspendat intre etajele 92 si 87, pendulul se misca decalat fata de structura, pentru a contracara efectul dat de rafalele de vant. Pendulul cu diametru de 5.5m este format din 41 placi circulare din otel, cu inaltimea de 125mm.

Alte 2 amortizoare cu masa acordata, cu greutatea de 6 tone, sunt instalate la varful spirei si ajuta la prevenirea pagubelor cauzate de incarcarile mari date de vant.

Amortizorul cu mase acordate s-a folosit si in lucrari ingineresti precum Podul Akashi Kaikyō. Cu o lungime totala de 3911m, podul are penduli proiectati sa opereze la frecventa de rezonata a podului, amortizand fortele date de incarcarile din vant si seism.

Fig. 6 Podul Akashi Kaikyō

## 3. Principii si notiuni teoretice

Principiul de reducere a vibratiilor structurale prin introducerea TMD-ului intr-o structura este de a transfera energia de vibratie catre TMD pentru a fi disipata. Astfel frecventa TMD-ului este acordata cu o anumita frecventa a structurii. Cand aceasta frecventa este atinsa, TMD-ul va rezone, defazat fata de miscarea structurii.

Comparativ cu alte metode de disipare, utilizarea TMD-ului impune folosirea unei mase si a unor deplasari mari. Prinderea si calibrarea TMD-ului este o problema foarte importanta in proiectare sistemului. In mod usual masa sistemului de amortizare se incadreaza in valori cuprinse intre 0.25..1% din masa cladiri pe modul fundamental de vibratie. In anumite cazuri, restrictia de spatiu nu permite amplasarea unui sistem traditional cu masa acordata. Aceasta limitare a dus la crearea unor sisteme alternative cum ar fi pendulul multi-stadiu, pendulul inversat, rulmenti hidrostatici. Pentru acordarea sistemelor se folosesc de obicei arcurile cu spire sau arcurile pneumatice cu rigiditate variabila.

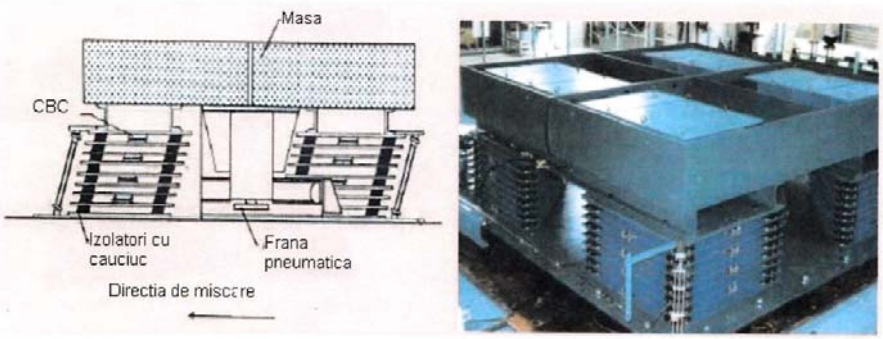


Fig. 7 Exemplu de sistem cu masa acordata

Problemele care apar cu spatiul pot fi rezolvate prin introducerea unui pendul:

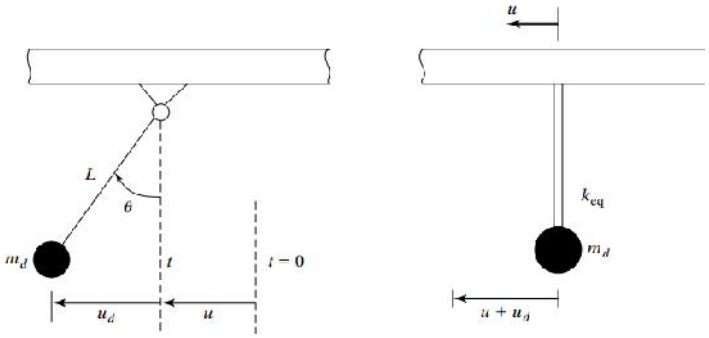


Sistem actual Sistem echivalent

Fig. 8 Schema unui pendul TMD

Ecuatia de miscare pe orizontala este: $T\sin\theta + \frac{W_d}{g}(\ddot{u} + \ddot{u}_d) = 0$

unde T este tensiunea in cablu; $u(t)$ – deplasarea structurii; $u_d(t)$ – deplasarea masei pendulului; $W_d$ – greutatea pendulului; $m_d$ – masa pendulului

$u_d = L\sin\theta \cong L\theta; \quad T \cong W_d$

Deci:

$$m_d\ddot{u}_d + \frac{W_d}{L}u_d = -m_d\ddot{u}$$

De unde se deduce ca rigiditatea echivalenta la forfecare este:

$$k_{eq} = \frac{W_d}{L}$$

Pulsatia pendulului este:

$$\omega_d^2 = \frac{k_{eq}}{m_d} = \frac{g}{L}$$

De unde rezulta perioada:

$$T_d = 2\pi\sqrt{\frac{L}{g}}$$

Singura limitare majora prin introducerea unui pendul este ca lungimea pendulului sa fie mai mare decat inaltimea unui nivel. Aceasta problema se poate rezolva utilizand schema de mai jos:

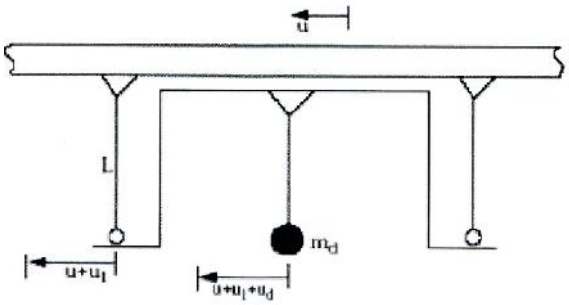


Fig. 9 Rezolvarea limitarii date de lungimea prea mare a unui pendul

Legatura interioara rigida, amplifica miscarea suportului pentru pendul rezultand urmatoarea ecuatie de echilibru:

$$m_d(\ddot{u}+\ddot{u}_1+\ddot{u}_d)+\frac{W_d}{L}u_d=0$$

Legatura rigida se misca in faza cu amortizorul si are aceeasi amplitudine a deplasarii. Considerand $u_1 = u_d$ avem:

$$m_d\ddot{u}_d+\frac{W_d}{2L}u_d=-\frac{m_d}{2}\ddot{u}$$

Rigiditatea echivalenta este $\frac{W_d}{2L}$ ceea ce arata ca lungimea efectiva este 2L. Prin urmare fiecare legatura aditionala creste lungimea efectiva cu valoarea “L”.

## 4. Calculul sistemelor de tip TMD

Analiza principiala a sistemelor TMD, implica precizarea raspunsului unui sistem cu doua grade de libertate, primul fiind gradul de libertate primar (structura), iar cel de-aldoilea fiind al TMD. Pentru aceasta se face apel la procedee matematice de calcul al raspunsului sistemului cu doua grade de libertate supus excitatiilor armonice in domeniul frecventelor. In continuare se vor ilustra aceste raspunsuri pentru diferite cazuri.

Prin urmare pentru a dimensiona un dispozitiv de tip “amortizor cu masa acordata” trebuie urmati cativa pasi de principiu:

- In prima faza se stabileste locatia (pozitia amortizorului) astfel incat aceasta sa coincide cu punctual de amplitudine maxima al formei modale ce se va controla.
- Masa sistemului primar va fi masa participanta pe modul ce se vrea controlata prin intermediul amortizorului.
- Cu cat raportul maselor, $\mu$, este mai mare cu atat raspunsul va fi mai mic (amortizorul va fi mai putin sensibil la acordare). Prin urmare se allege cel mai mare raport posibil.
- Se determina raportul optim al frecventelor (perioadelor), $f$, din care se calculeaza rigiditatea amortizorului, $k_d = m_d\omega_d^2$.
- Se determina fractiunea optima din amortizarea critica $\zeta_{d,opt}$ cu ajutorul careia se calculeaza amortizarea dispozitivului, $c_{d,opt} = 2\zeta_{d,opt}\omega_d m_d$.

Parametrul in functie de care se face optimizarea este “deplasarea“ si este folosit pentru a asigura integritatea structurii si a elementelor nestructurale. Insa, se mai poate folosi ca parametru de optimizare si “acceleratia” pentru cazul echipamentelor grele/sensibile la acceleratii mari. Pentru aplicatiile seismic de larga utilizare, Villaverde (1985) sugereaza folosirea urmatoarelor ecuatii cu parametrii optimi, cu raportul maselor bazat pe masa modala si vectorul propriu normalizat in punctual de instalare a dispozitivului:

$$f_{opt} = 1$$

$$\zeta_{d,opt} = \zeta + \mu$$

Pentru aceleasi conditii, Fadek (1997) gaseste ecuatiile:

$$f_{opt} = \frac{1}{1+\mu}\left[1 - \zeta\sqrt{\frac{\mu}{1+\mu}}\right]$$

$$\zeta_{d,opt} = \frac{\zeta}{1+\zeta} + \sqrt{\frac{\mu}{1+\mu}}$$

Observatie:

Acest tip de dispozitive, sunt eficiente in aplicatiile seismice cu amortizare scazuta $\zeta = 0.02$. Pentru structure cu amortizare $\zeta = 0.05$, nu sunt foarte eficiente deoarece raportul maselor devine prea mare. De asemenea nu sunt eficiente nici in cazul structurilor foarte rigide cu perioade de $0.1s \div 0.2s$.

| Sistem | Tipul excitatiei | Excitatie aplicata | Parametru optimizat | Raportul optim de frecvente $f_{opt}$ | Amortizarea optima $\zeta_{d,opt}$ | Raspunsul maxim optimizat al structurii $u_r$ |
|---|---|---|---|---|---|---|
| Sistem amortizat, TMD amortizat | Armonica determinista | Masei primare si bazei | Deplasarea masei primare | - | - | $\frac{(p_0 + ma_0)/k}{\sqrt{2\zeta(1-\zeta^2)}}$ |
| Sistem neamortizat, TMD neamortizat | | Masei primare | Deplasarea masei primare | - | - | - |
| Sistem neamortizat, TMD amortizat | | Masei primare | Deplasarea masei primare | $\frac{1}{1+\mu}$ | $\sqrt{\frac{3\mu}{8(1+\mu)}}$ | $\frac{p_0}{k}\sqrt{1+\frac{2}{\mu}}$ |
| Sistem neamortizat, TMD amortizat | | Masei primare | Acceleratia masei primare | $\frac{1}{1+\mu}$ | $\sqrt{\frac{3\mu}{8(1+\mu/2)}}$ | $\frac{p_0}{k}\sqrt{\frac{2}{\mu(1+\mu)}}$ |
| Sistem neamortizat, TMD amortizat | | Bazei | Deplasarea masei primare | $\frac{\sqrt{1-\mu/2}}{1+\mu}$ | $\sqrt{\frac{3\mu}{8(1+\mu)(1-\frac{\mu}{2}}}$ | $\frac{ma_0}{k}(1+\mu)\sqrt{\frac{2}{\mu}}$ |
| Sistem neamortizat, TMD amortizat | Aleatoare | Bazei | Acceleratia masei primare | $\frac{1}{1+\mu}$ | $\sqrt{\frac{3\mu}{8(1+\mu)}}$ | $\frac{ma_0}{k}\sqrt{1+\frac{2}{\mu}}$ |

| | | | | | | |
|---|---|---|---|---|---|---|
| Sistem neamortizat, TMD amortizat | | Masei primare | Deplasarea masei primare | $\frac{\sqrt{1+\mu/2}}{1+\mu}$ | $\sqrt{\frac{\mu(1+\frac{3\mu}{4})}{4(1+\mu)(1+\frac{\mu}{2}}}$ | $\frac{p_0}{k}\sqrt{\frac{(1+\frac{3\mu}{4})}{\mu(1+\mu)}}$ |
| Sistem neamortizat, TMD amortizat | Armonica determinista | Bazei | Deplasarea masei primare | $\frac{\sqrt{1-\mu/2}}{1+\mu}$ | $\sqrt{\frac{\mu(1-\frac{\mu}{4})}{4(1+\mu)(1-\frac{\mu}{2}}}$ | $\frac{p_0}{k}\sqrt{\frac{(1+\frac{3\mu}{4})}{\mu(1+\mu)}}$ |
| Sistem amortizat, TMD amortizat | | Masei primare | Deplasarea masei primare | $\frac{1}{1+\mu}-(0.2$ | $\sqrt{\frac{3\mu}{8+(1+\mu)}}+($ | |

## 5. Studii de caz I

Avand in vedere cele descrise anterior in mod teoretic, in cele ce urmeaza se considera stdii de caz, pentru structuri din beton armat cu diferite forme in plan avand un regim de inaltime pentru suprastructura de P+39E (40 niveluri). Inaltimea de nivel a fost considerat 3m. Structurile se clasifica astfel:

Functie de sistemul structural:

- sistem structural cu cadre din beton armat;
- sistem structural dual (cadre si pereti din beton armat);

Functie de forma in plan:

- Circulara;
- Patrata;
- Dreptunghiulara.

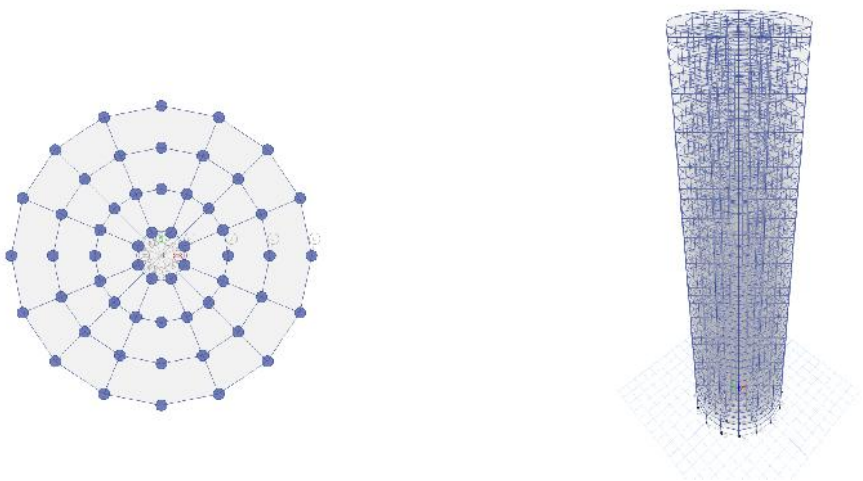

Fig. 10 Structura cu cadre din b.a. avand forma circulara - plan si elevatie

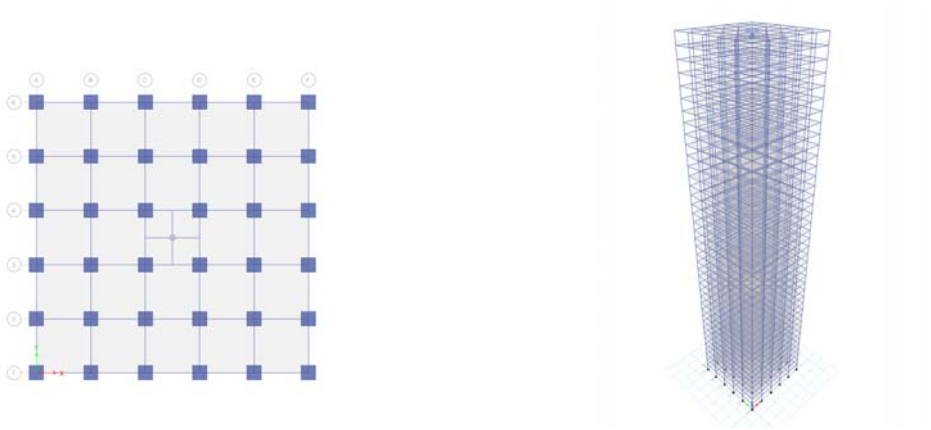

Fig. 11 Structura cu cadre din b.a. avand forma patrata - plan si elevatie

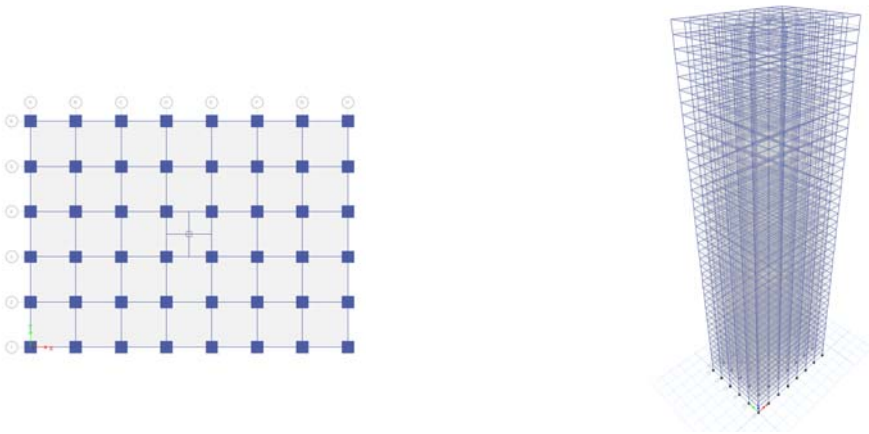

Fig. 12 Structura cu cadre din b.a. avand forma dreptunghiulara - plan si elevatie

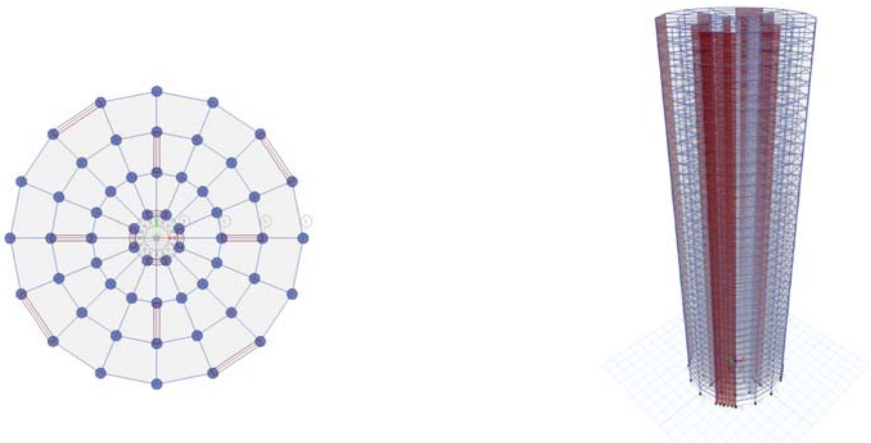

Fig. 13 Structura duala din b.a. avand forma circulara - plan si elevatie

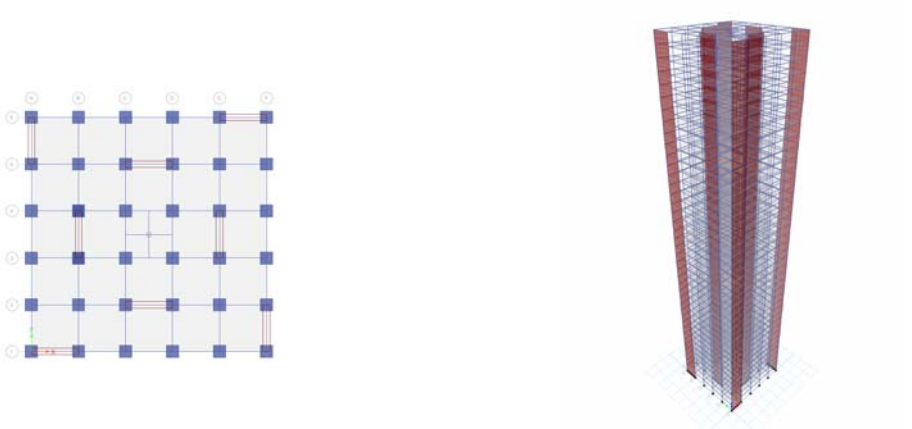

Fig. 14 Structura duala din b.a. avand forma patrata - plan si elevatie

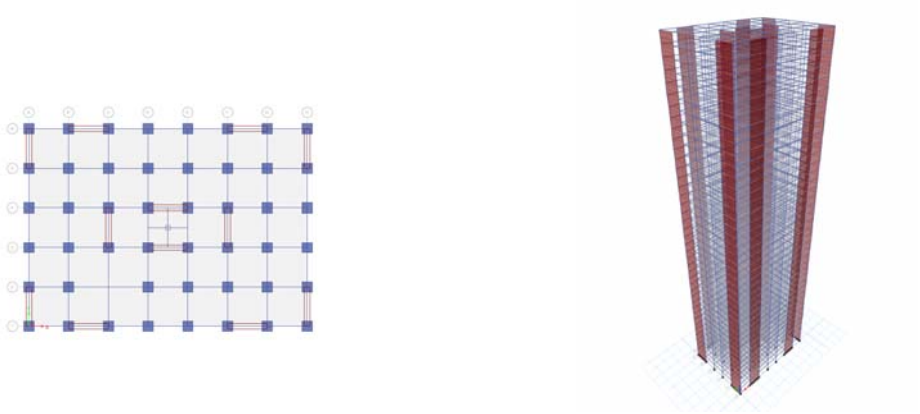

Fig. 15 Structura duala din b.a. avand forma dreptunghiulara - plan si elevatie

Pentru a minimiza numarul variabilelor si a evidentia mai bine folosirea TMD-urilor structurile au distantele intre axe 5m.

Pe langa incarcarile provenite din greutatea proprie a structurii au fost considerate si urmatoarele incarca:

Clasa betonului este C30/37 cu modulul de elasticitate E=33000 N/mm$^2$

Dimensiunile elementelor structurale considerate sunt urmatoarele:

| Tip Structura | Forma in plan | Latura Stalpilor [cm] | Grinda Longitudinala [cm] | Grinda Transversala [cm] | Grinda Radiala [cm] | Grosimi Pereti [cm] |
|---|---|---|---|---|---|---|
| Structura in cadre | Circulara | 130 | - | - | 35x80 | - |
| | Patrata | 130 | 35x80 | 35x75 | - | - |
| | Dreptunghiulara | 130 | 35x80 | 35x80 | - | - |
| Structura duala | Circulara | 130 | - | - | 35x80 | 70 |
| | Patrata | 130 | 35x80 | 35x80 | - | 70 |
| | Dreptunghiulara | 130 | 35x80 | 35x80 | - | 70 |

Pentru analiza cu spectre de raspuns s-a folosit urmatorul spectru de proiectare:

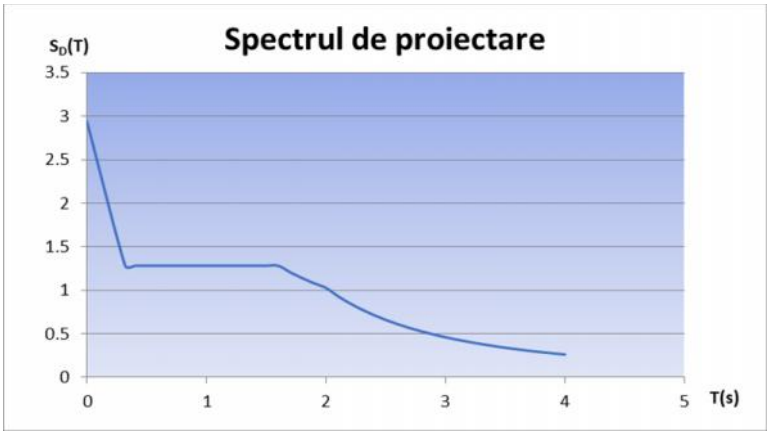


Fig. 16 Spectru de proiectare pentru $a_g$=0.30g

Pentru dimensionarea sistemelor de amortizare cu mase acordate am tinut cont de urmatorii pasi:

- In prima faza se stabileste locatia (pozitia amortizorului) astfel incat aceasta sa coincide cu punctual de amplitudine maxima al formei modale ce se va controla.
- Masa sistemului primar va fi masa participant pe modul ce se vrea controlata prin intermediul amortizorului.
- Cu cat raportul maselor, $\mu$, este mai mare cu atat raspunsul va fi mai mic (amortizorul va fi mai putin sensibil la acordare). Prin urmare se alege cel mai mare raport posibil.
- Se determina raportuloptim al frecventelor (perioadelor), $f$, din care se calculeaza rigiditatea amortizorului, $k_d = m_d \omega_d^2$.
- Se determina fractiunea optima din amortizarea critica $\zeta_{d,opt}$ cu ajutorul careia se calculeaza amortizarea dispozitivului, $c_{d,opt} = 2\zeta_{d,opt}\omega_d m_d$.

**Modelarea sistemului cu masa acordata:**

Asa cum s-a descris anterior “amortizorul cu masa acordata” trebuie pozitionat in punctual de amplitudine maxima a modului ce se vrea controlat. In cazurile studiate acest punct poate fi orice punct de pe planseul ultimului nivel.

Sistemul TMD se modeleaza cu ajutorul unui isolator de tip “pendul de frecare” (friction pendulum) iar pentru a simula miscarea fizica a TMD-ului, iar pentru partea de amortizare s-a folosit un “link” de tip “amortizor vascos” (Damper). In program se introduc 2 legaturi (link) cu aceste denumiri si cu caracteristicile determinate prin calcul.

La modelare trebuie tinut cont de modul de desenare al legaturilor (de jos in sus) pentru a putea fi definita corect miscarea de amortizare. Pentru o comportare buna, punctul aflat pe planseul de la ultimul nivel va fi situat in centrul acestuia, iar cel liber pe aceeasi verticala situat la distanta egala cu lungimea pendulului.

De asemenea trebuie tinut cont ca punctului liber trebuie sa i se atribuie mase pe directiile principale, mase determinate prin calculul TMD.

$\mu$ - Raportul maselor;

$\zeta$ – Fractiune din amortizarea critica;

$m_{mod,1}$ - masa antrenata pe modul 1 de vibratie;

$m_{mod,2}$ - masa antrenata pe modul 2 de vibratie;

$$m_d = \mu \times m_{mod,1}$$

$$f_{opt} = \frac{1}{1+\mu} - (0.241 + 1.7\mu - 2.6\mu^2)\zeta - (1.0 - 1.9\mu + \mu^2)$$

$$\zeta_{d,opt} = \sqrt{\frac{3\mu}{8+(1+\mu)}} + (0.13 + 0.12\mu + 0.4\mu^2)\zeta - (0.01 + 0.9\mu + 3\mu^2)\zeta^2$$

$$f_d = f_{mod,1} \times f_{opt}$$

$$T_d = \frac{1}{f_d}$$

$$\omega^2 = 2\pi f_d$$

$$k_d = m_d \omega_d^2$$

$$c_{d,opt} = 2\zeta_{d,opt}\omega_d m_d$$

$$L_{pendul} = \frac{T_d^2 \times g}{4\pi^2}$$

Pentru structurile analizate caracteristicile TMD-urilor sunt urmatoarele:

| Tipul structurii | Forma in plan | Lungimea pendulului [m] | Rigiditatea $k_d$ [kN/m] | Amortizarea dispozitivului $c_d$ [kN/s] | Masa pe modul 1 [kN] | Masa pe modul 2 [kN] |
|---|---|---|---|---|---|---|
| Structura in cadre | Circulara | 2.35 | 22153 | 4143 | 5275 | 5275 |
| | Patrata | 2.3 | 15451 | 2881 | 3657 | 3657 |
| | Dreptunghiulara | 2.2 | 22325 | 4030 | 5019 | 4953 |
| Structura duala | Circulara | 1.9 | 28238 | 4740 | 5418 | 5418 |
| | Patrata | 1.65 | 21450 | 3383 | 3634 | 3634 |
| | Dreptunghiulara | 1.7 | 31128 | 4934 | 5325 | 5390 |

## 6. Studii de caz II

In continuare pentru aplicarea notiunilor descrise in capitolele anterioare vom considera 1 structură în cadre din beton armat cu diferite niveluri de înălţime: P+40E, P+30E, P+20E, P+10E. Inaltimea de nivel a fost considerat 3m. Forma in plan a structurii este dreptunghiulara.

Pentru a minimiza numarul variabilelor si a evidenţia mai bine folosirea TMD-urilor structurile au distanţa dintre axe 5m.

Pe langă încărcările provenite din greutatea proprie a structurii au fost considerate si urmatoarele incarcari:

La nivelul etajelor curente:

- Pardoseala si instalatii – 2kN/m$^2$
- Pereti despartitori – 0.5 kN/m$^2$
- Incarcarea utila – 2 kN/m$^2$

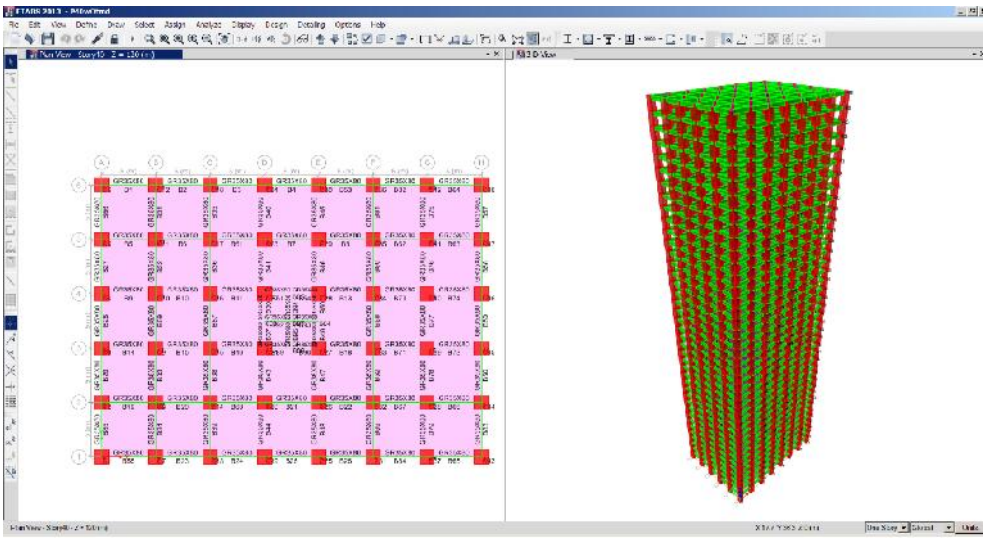

Fig. 25 Structura in cadre cu forma dreptunghiulara P+40E- plan si elevatie

La nivelul ultimului etaj:

- Incarcarea utila 2 kN/m$^2$
- Incarcarea din zapada 2 kN/m$^2$
- Termoizolatia 3 kN/m$^2$
- Instalatii 0.5 kN/m$^2$
- Atic 5 kN/ml – pe grinzile de contur

Clasa betonului este C20/25 cu modulul de elasticitate E=33000 N/mm$^2$

Dimensiunile elementelor sunt urmatoarele:

| Tip Structura | Regim înaltime | Latura Stalpului [cm] | Grinda Longitudinala [cm] | Grinda Transversala [cm] |
|---|---|---|---|---|
| Structura in cadre | P+40E | 130 | 35x80 | 35x80 |
| | P+30E | 130 | 35x80 | 35x80 |
| | P+20E | 100 | 35x65 | 35x65 |
| | P+10E | 80 | 30x60 | 30x60 |

Pentru dimensionarea sistemelor de amortizare cu mase acordate am tinut cont de urmatorii pasi:

- In prima faza se stabileste locatia (pozitia amortizorului) astfel incat aceasta sa coincidă cu punctul de amplitudine maxima al formei modale ce se va controla.

- Masa sistemului primar va fi masa participant pe modul ce se vrea controlata prin intermediul amortizorului.
- Cu cat raportul maselor, $\mu$, este mai mare cu atat raspunsul va fi mai mic (amortizorul va fi mai putin sensibil la acordare). Prin urmare se alege cel mai mare raport posibil.
- Se determina raportuloptim al frecventelor (perioadelor), $f$, din care se calculeaza rigiditatea amortizorului, $k_d = m_d\omega_d^2$.
- Se determina fractiunea optima din amortizarea critica $\zeta_{d,opt}$ cu ajutorul careia se calculeaza amortizarea dispozitivului, $c_{d,opt} = 2\zeta_{d,opt}\omega_d m_d$.

Modelarea sistemului cu masa acordata:

Asa cum s-a stabilit “amortizorul cu masa acordata” trebuie pozitionat in punctual de amplitudine maxima a modului ce se vrea controlat. In cazurile studiate acest punct poate fi orice punct de pe planseul ultimului nivel.

Sistemul TMD se modeleaza cu ajutorul unui isolator de tip “pendul de frecare” (friction pendulum) iar pentru a simula miscarea fizica a TMD-ului, iar pentru partea de amortizare s-a folosit un “link” de tip “amortizor vascos” (Damper). In program se introduc 2 legaturi (link) cu aceste denumiri si cu caracteristicile determinate prin calcul.

La modelare trebuie tinut cont de modul de desenare al legaturilor (de jos in sus) pentru a putea fi definita corect miscarea de amortizare. Pentru o comportare buna, punctul aflat pe planseul de la ultimul nivel va fi situat in centrul acestuia, iar cel liber pe aceeasi verticala situat la distanta egala cu lungimea pendulului.

De asemenea trebuie tinut cont ca punctului liber trebuie sa i se atribuie mase pe directiile principale, mase determinate prin calculul TMD.

$\mu$ - Raportul maselor;

ζ – Fractiune din amortizarea critica;

$m_{mod,1}$ - masa antrenata pe modul 1 de vibratie;

$m_{mod,2}$ - masa antrenata pe modul 2 de vibratie;

$$m_d = \mu \times m_{mod,1}$$

$$f_{opt} = \frac{1}{1+\mu} - (0.241 + 1.7\mu - 2.6\mu^2)\zeta - (1.0 - 1.9\mu + \mu^2)$$

$$\zeta_{d,opt} = \sqrt{\frac{3\mu}{8+(1+\mu)}} + (0.13 + 0.12\mu + 0.4\mu^2)\zeta - (0.01 + 0.9\mu + 3\mu^2)\zeta^2$$

$$f_d = f_{mod,1} \times f_{opt}$$

$$T_d = \frac{1}{f_d}$$

$$\omega^2 = 2\pi f_d$$

$$k_d = m_d\omega_d^2$$

$$c_{d,opt} = 2\zeta_{d,opt}\omega_d m_d$$

$$L_{pendul} = \frac{T_d^{\,2} \times g}{4\pi^2}$$

Pentru structurile analizate caracteristicile TMD-urilor sunt urmoatoarele:

| Tipul structurii | Regim înaltime | Lungimea pendulului [m] | Rigiditatea $k_d$ [kN/m] | Amortizarea dispozitivului $c_d$ [kN/s] | Masa pe modul 1 [kN] | Masa pe modul 2 [kN] |
|---|---|---|---|---|---|---|
| Structura in cadre | P+40E | 2.4 | 21248 | 4032 | 5209 | 5275 |
| | P+30E | 1.1 | 33252 | 4265 | 3276 | 3757 |
| | P+20E | 0.7 | 28376 | 2872 | 1979 | 1987 |
| | P+10E | 0.15 | 49765 | 2540 | 883 | 885 |
| | P+5E | 1.7 | 31128 | 4934 | 5325 | 5390 |

In continuare se va prezenta in paralel comportarea structurilor cu si fara sistemul de amortizare cu masa acordata.

### 6.1. Structura in cadre P+40E

In urma analizei modala cu spectru de raspuns s-au obtinut urmatoarele perioade proprii pentru primele 4 moduri de vibratie:

| Mod | Structura Fara TMD | | | | Structura Cu TMD | | | |
|---|---|---|---|---|---|---|---|---|
| | Perioada | Ux | Uy | Rz | Perioada | Ux | Uy | Rz |
| 1 | 2.769 | 0 | 0.8001 | 0 | 3.398 | 0 | 0.4197 | 0 |
| 2 | 2.62 | 0.8102 | 0 | 0 | 3.312 | 0.3573 | 0 | 0 |
| 3 | 2.333 | 0 | 0 | 0.8274 | 2.457 | 0 | 0.3916 | 0 |
| 4 | 0.895 | 0 | 0.1167 | 0 | 2.384 | 0.4633 | 0 | 0 |

Se observa ca dupa introducerea TMD-ului perioadele s-au marit si repartitia maselor s-a modificat fundamental. Astfel:

- In primul caz (fara TMD) pe modurile 1 si 2 factorul de participare al maselor era 80 %, rezultand forte seismice mari.
- Dupa amplasarea TMD-ului acesti factori de participare ai maselor practic se impart in doua si se distribuie pe cate 2 moduri pe fiecare directive principala. Fenomenul de torsiune generala “coboara” dincolo de modul 4.

Daca analizam din punct de vedere al deplasarilor, se pot observa reduceri ale drift-urilor, in medie cu 20% pe directiile X si Y atat la SLS cat si la SLU, asa cum se evidentiaza in figurile de mai jos:

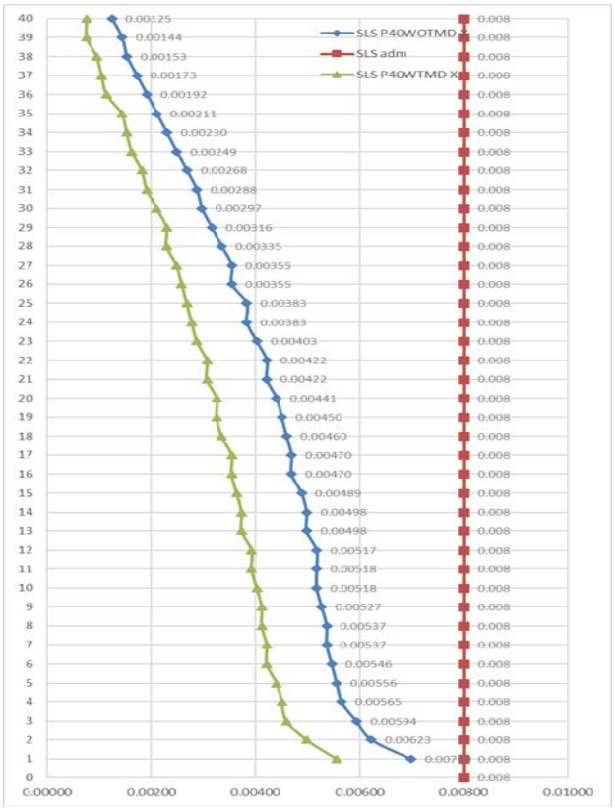


Fig. 26 Deplasari relative pe directia X la SLS

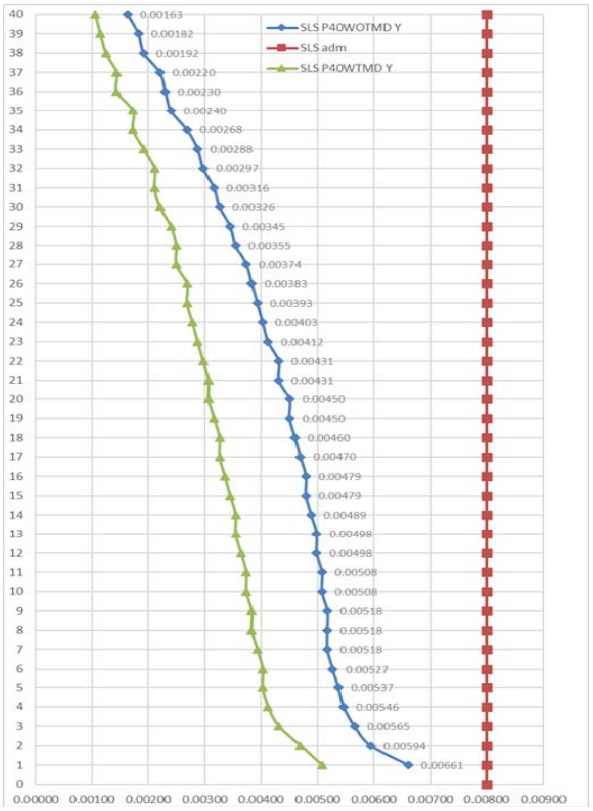


Fig. 27 Deplasari relative pe directia Y la SLS

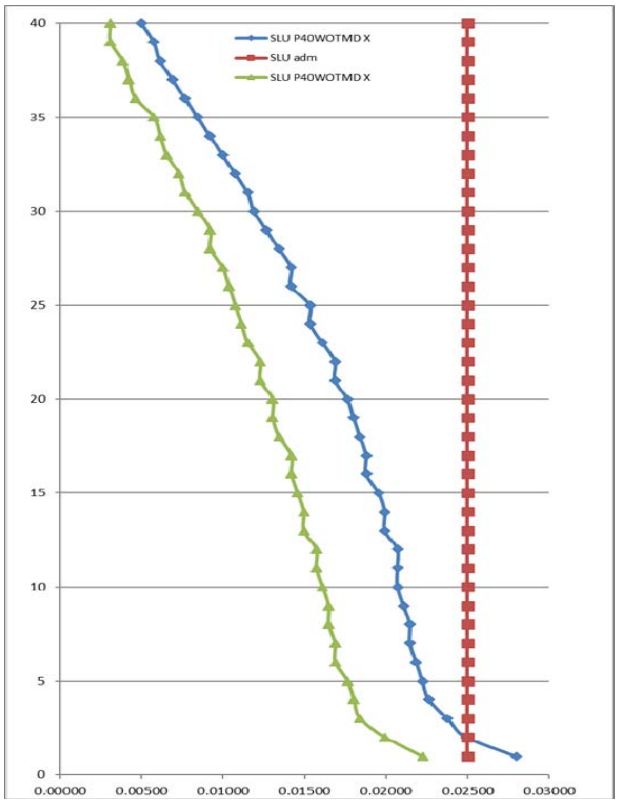


Fig. 28 Deplasari relative pe directia X la SLU

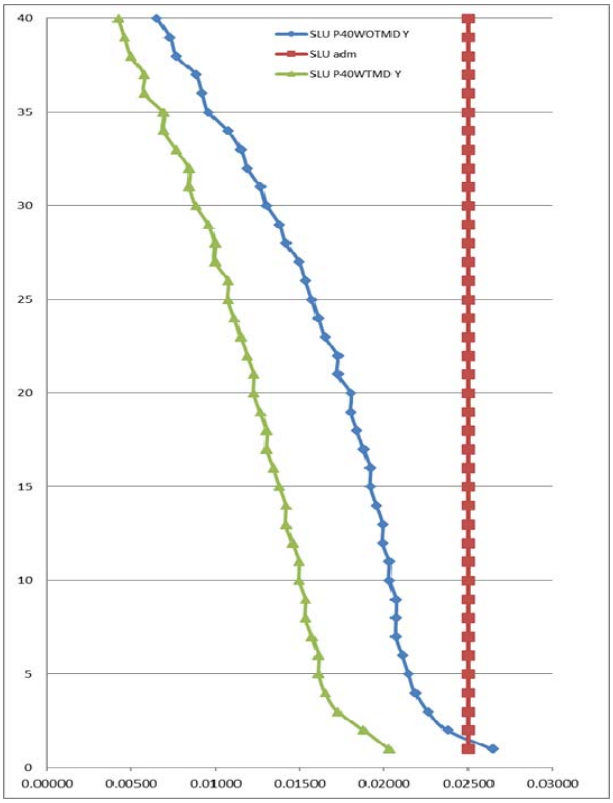


Fig. 29 Deplasari relative pe directia Y la SLU

Pentru a evidentia comportarea TMD-ului in reducerea eforturilor in elemente au fost selectate:

- Un stalp marginal – denumit C19;
- Un stalp interior – denumit C15;
- O grinda – denumita B20;

Se observa o reducere a eforturilor in elementele structurii;

- In stalpul marginal C19 forta axiala a fost redusa in medie cu 5% si o reducere a momentului incovoietor in medie cu 25%.
- In stalpul interior C15 forta axiala a fost redusa in medie cu 8% si o reducere a momentului incovoietor in medie cu 25%.
- In reazemelul din stanga al grinzii B20 momentele incovoietoare au fost reduse in medie cu 25%, iar in reazemul din dreapta o reducere in medie cu 30%.

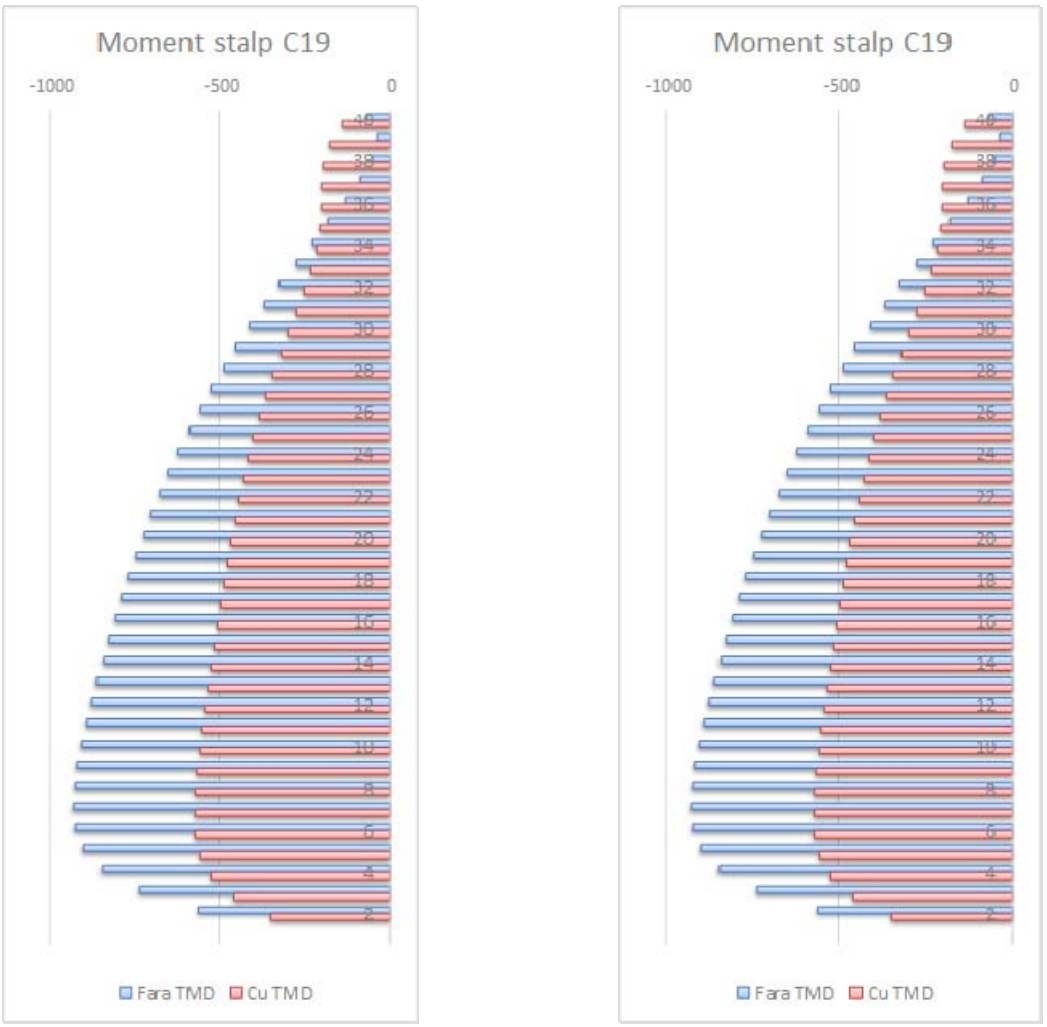


Fig. 30 Forta axiala si momentul incovoietor in stalpul marginal C19

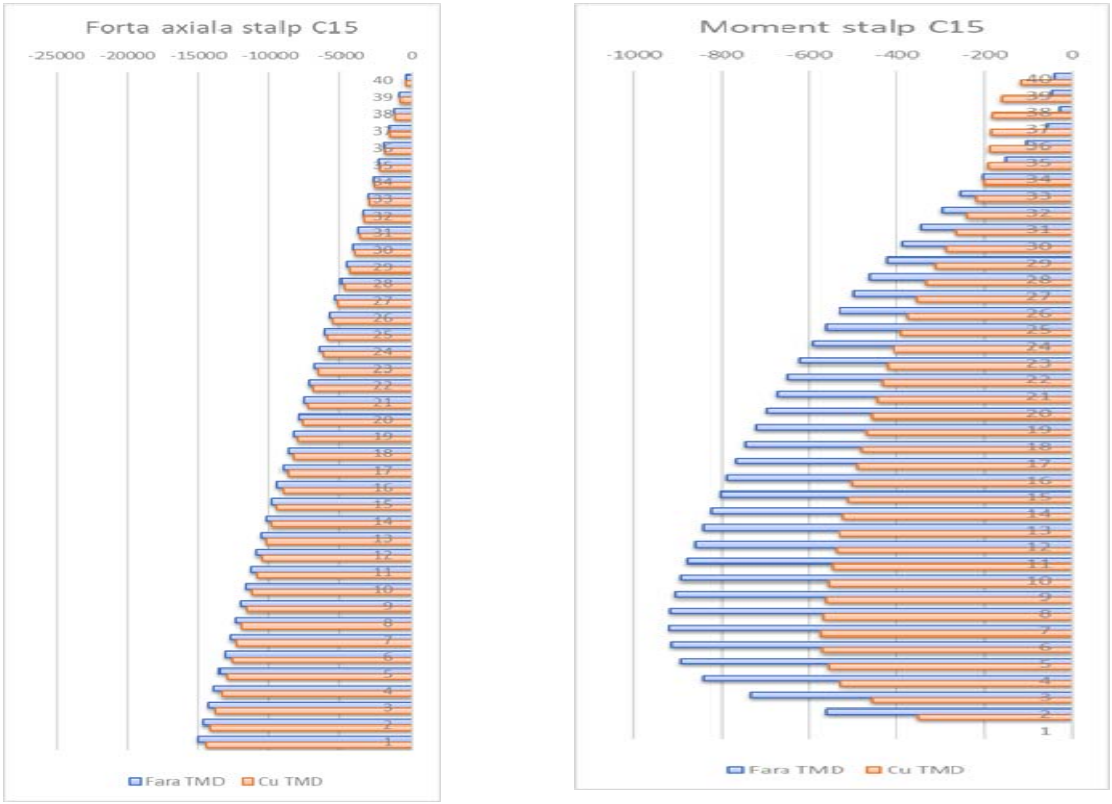


Fig. 31 Forta axiala si momentul incovoietor in stalpul interior C15

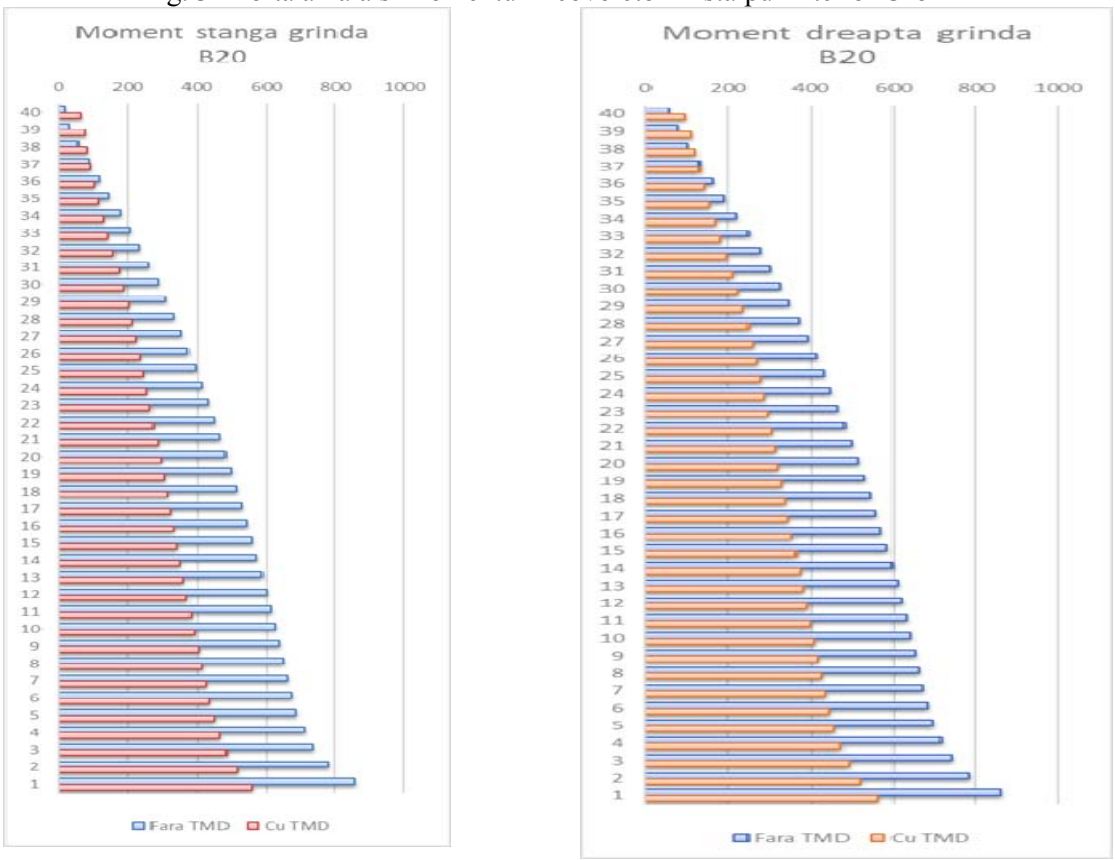


Fig. 32 Momentele din reazemele grinzii B20

## 6.2. Structura in cadre P+30E

In urma analizei modala cu spectru de raspuns s-au obtinut urmatoarele perioade proprii pentru primele 4 moduri de vibratie:

| Mod | Structura Fara TMD | | | | Structura Cu TMD | | | |
|---|---|---|---|---|---|---|---|---|
| | Perioada | Ux | Uy | Rz | Perioada | Ux | Uy | Rz |
| 1 | 1.872 | 0 | 0.7629 | 0 | 2.589 | 0 | 0.4573 | 0 |
| 2 | 1.793 | 0.7693 | 0 | 0 | 2.531 | 0.4279 | 0 | 0 |
| 3 | 1.623 | 0 | 0 | 0.7789 | 1.623 | 0 | 0 | 0.7789 |
| 4 | 0.597 | 0 | 0.1077 | 0 | 1.58 | 0 | 0.3334 | 0 |

Se observa ca dupa introducerea TMD-ului perioadele s-au marit si repartitia maselor s-a modificat fundamental. Astfel:

- In primul caz (fara TMD) pe modul 1 factorul de participare al maselor era 76.29%, iar pe modul 2 factorul de participare al maselor era 76.93%.
- Dupa amplasarea TMD-ului acesti factoride participare ai maselor practic se impart in doua si se distribuie pe cate 2 moduri pe fiecare directive principala. Fenomenul de torsiune generala “coboara” dincolo de modul 4.

Daca analizam din punct de vedere al deplasarilor, se pot observa reduceri ale drift-urilor, in medie cu 20% pe directiile X si Y atat la SLS cat si la SLU, asa cum se evidentiaza in figurile de mai jos:

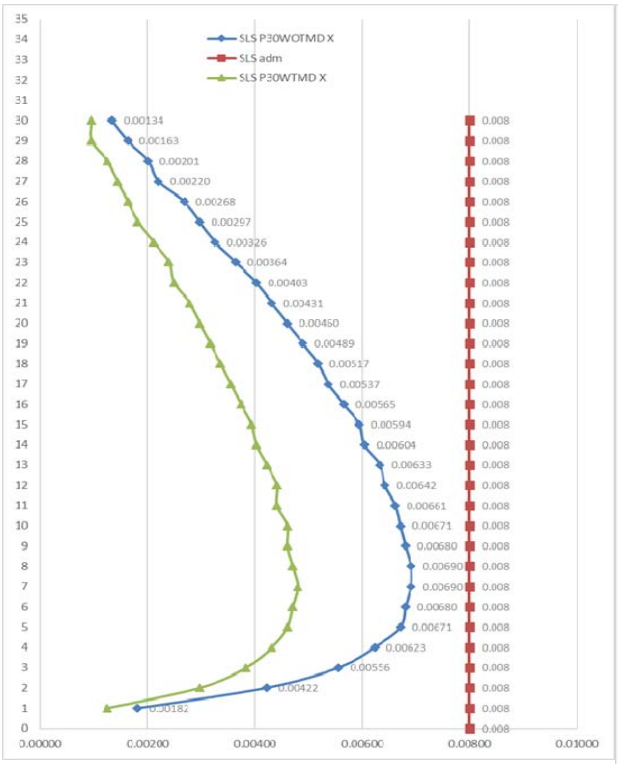


Fig. 33 Deplasari relative pe directia “X” la SLS

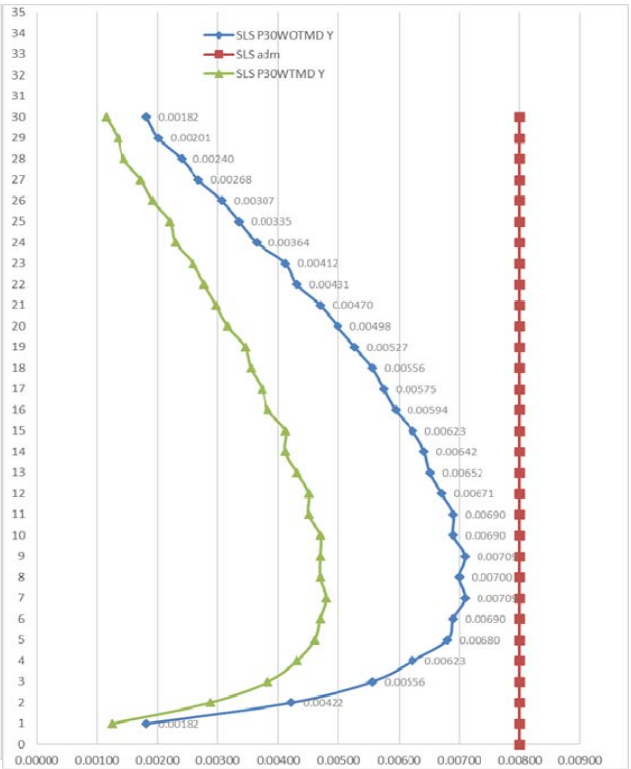


Fig. 34 Deplasari relative pe directia “Y” la SLS

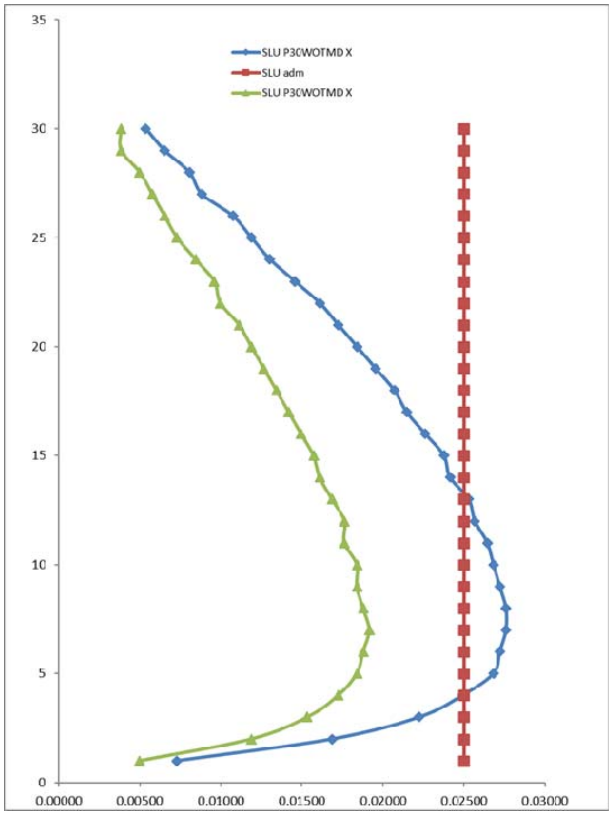


Fig. 35 Deplasari relative pe directia "X" la SLU

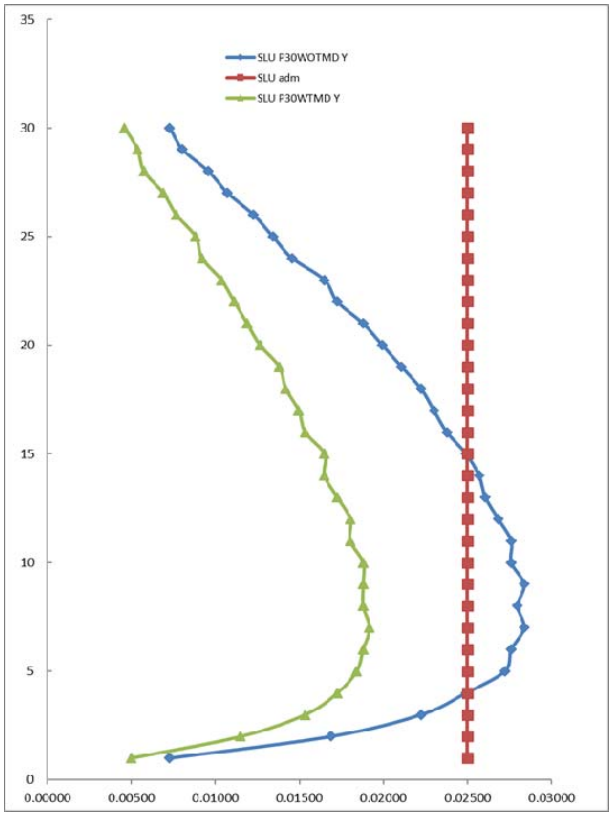


Fig. 6 Deplasari relative pe directia "Y" la SLU

Pentru a evidentia comportarea TMD-ului in reducerea eforturilor in elemente au fost selectate:

- Un stalp de colt – denumit C32;
- Un stalp marginal – denumit C19;
- Un stalp interior – denumit C15;
- O grinda – denumita B20;

Se observa o reducere a eforturilor in elementele structurii;

- In stalpul de colt C32 forta axiala a fost redusa in medie cu 8% si o reducere a momentului incovoietor in medie cu 20%.
- In stalpul marginal C19 forta axiala a fost redusa in medie cu 5% si o reducere a momentului incovoietor in medie cu 25%.
- In stalpul interior C15 forta axiala a fost redusa in medie cu 5% si o reducere a momentului incovoietor in medie cu 18%.
- In reazemele grinzii B20 momentele incovoietoare au fost reduse in medie cu 25%.

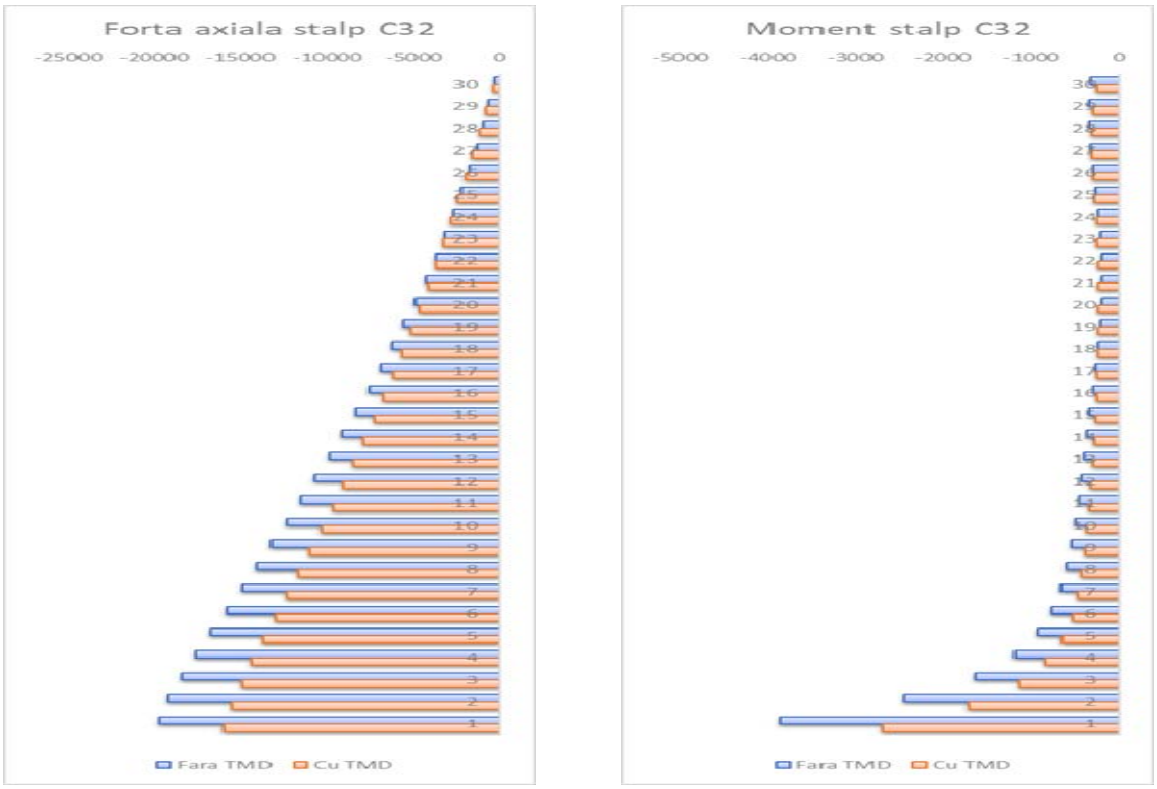


Fig. 37 Forta axiala si momentul incovoietor in stalpul de colt C32

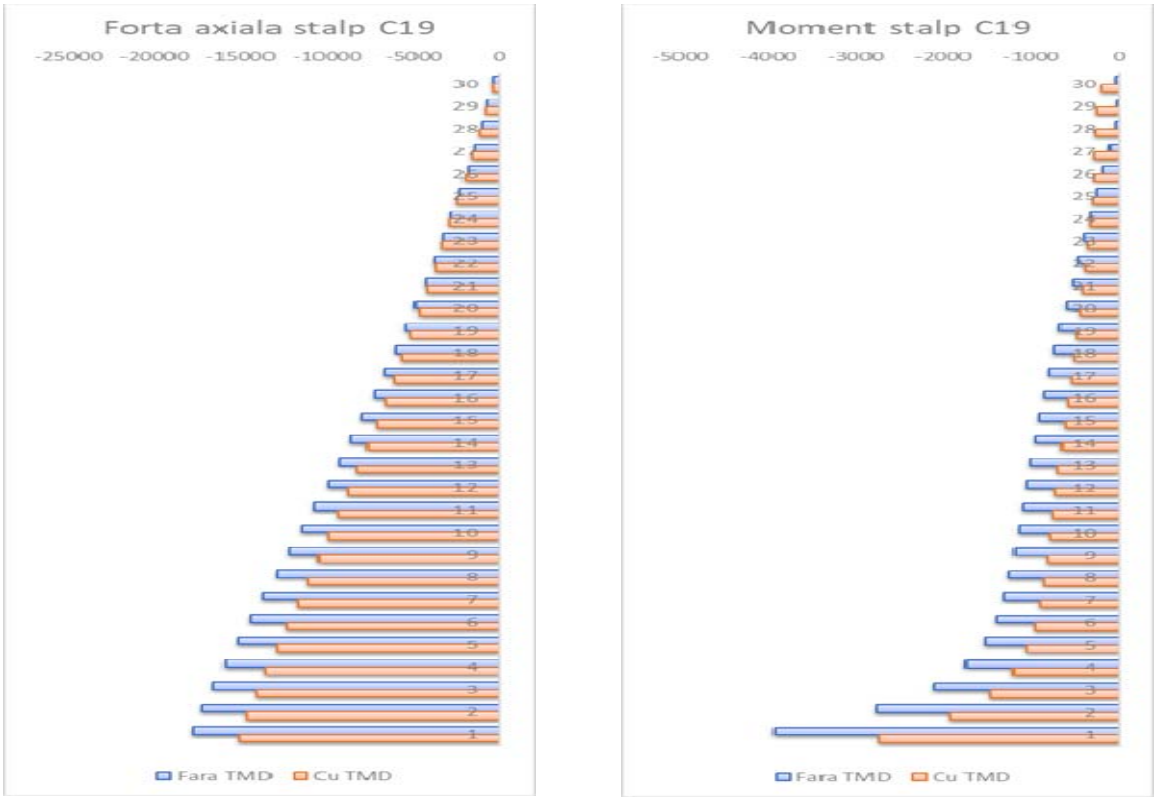


Fig. 38 Forta axiala si momentul incovoietor in stalpul marginal C19

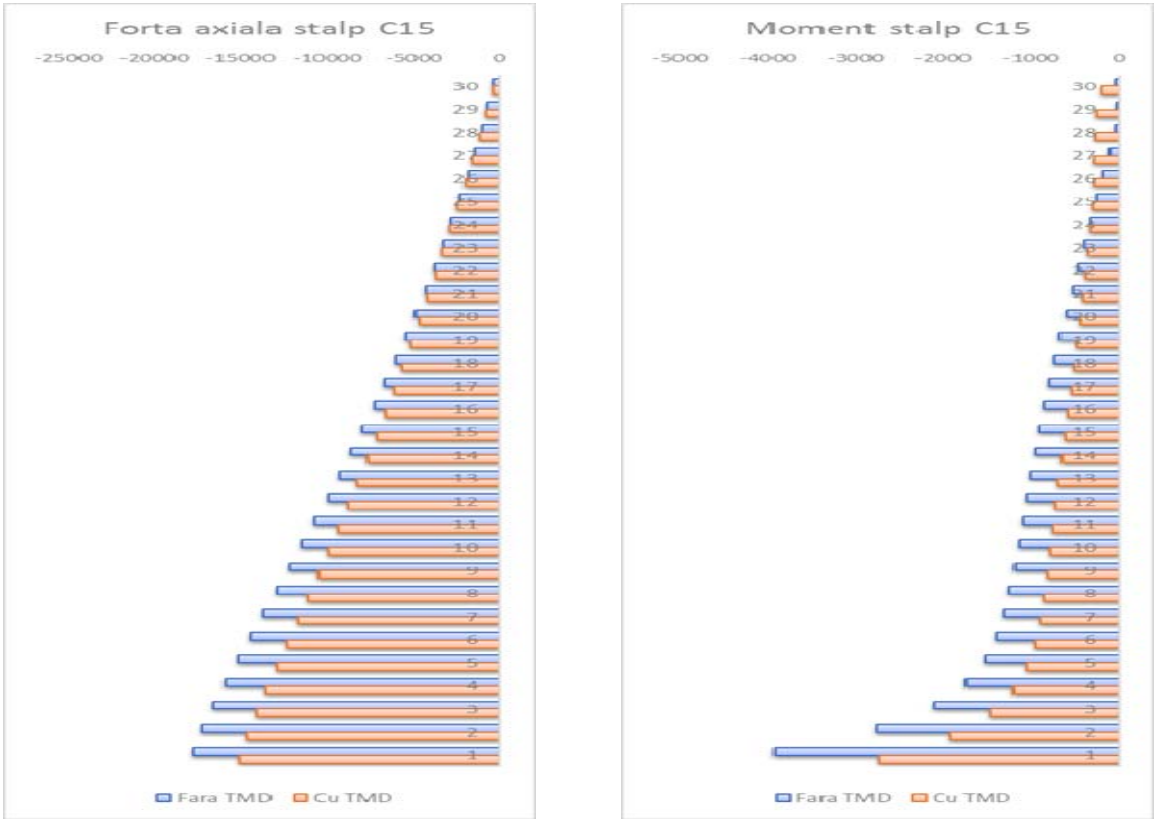


Fig. 39 Forta axiala si momentul incovoietor in stalpul interior C15

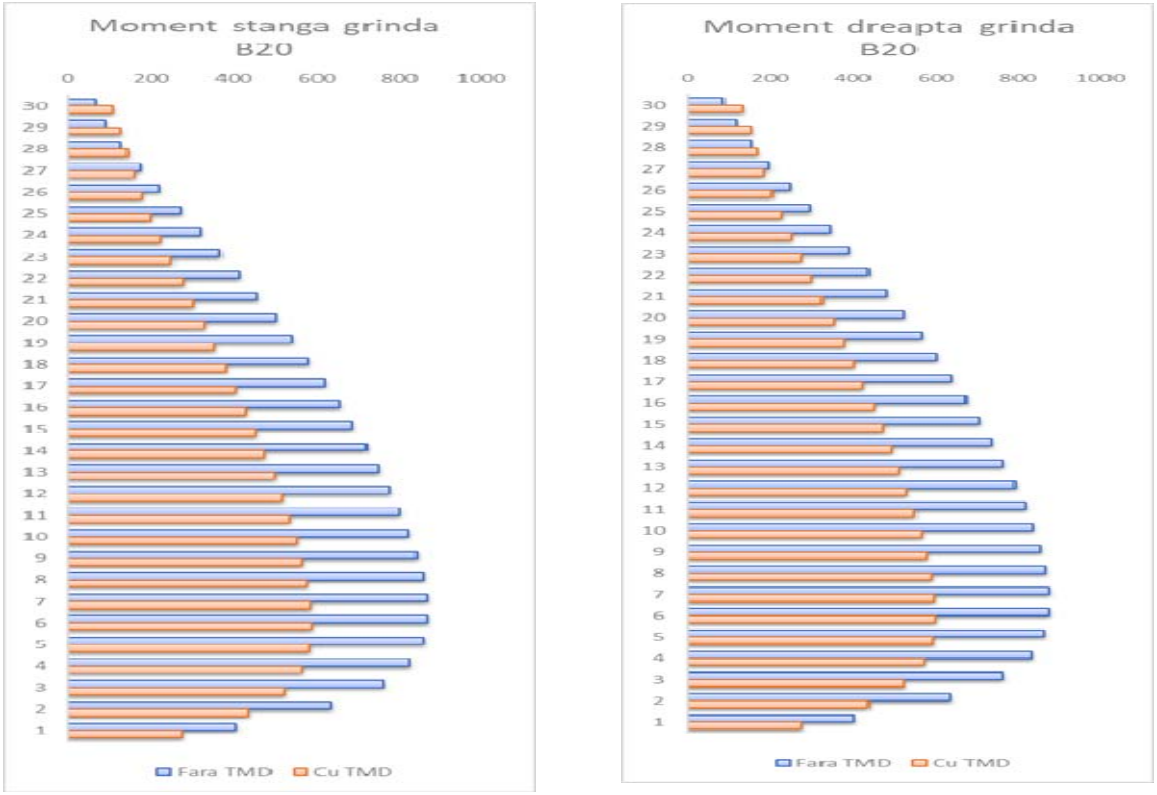


Fig. 40 Momentele din reazemele grinzii B20

### 6.3. Structura in cadre P+20E

In urma analizei modala cu spectru de raspuns s-au obtinut urmatoarele perioade proprii pentru primele 4 moduri de vibratie:

| Mod | Structura Fara TMD | | | | Structura Cu TMD | | | |
|---|---|---|---|---|---|---|---|---|
| | Perioada | Ux | Uy | Rz | Perioada | Ux | Uy | Rz |
| 1 | 1.477 | 0 | 0.7694 | 0 | 2.05 | 0 | 0.4768 | 0 |
| 2 | 1.434 | 0.7726 | 0 | 0 | 2.018 | 0.457 | 0 | 0 |
| 3 | 1.323 | 0 | 0 | 0.7761 | 1.323 | 0 | 0 | 0.7761 |
| 4 | 0.469 | 0 | 0.1009 | 0 | 1.237 | 0 | 0.3217 | 0 |

Se observa ca dupa introducerea TMD-ului perioadele s-au marit si repartitia maselor s-a modificat fundamental. Astfel:

- In primul caz (fara TMD) pe modurile 1 si 2 factorii de participare ai maselor erau 76.94% si 77.26%, rezultand forte seismice mari.
- Dupa amplasarea TMD-ului acesti factori de participare ai maselor practic se impart in doua si se distribuie pe cate 2 moduri pe fiecare directive principala. Fenomenul de torsiune generala “coboara” dincolo de modul 4.

Daca analizam din punct de vedere al deplasarilor, se pot observa reduceri ale drift-urilor, in medie cu 25% pe directiile X si Y atat la SLS cat si la SLU, asa cum se evidentiaza in figurile de mai jos:

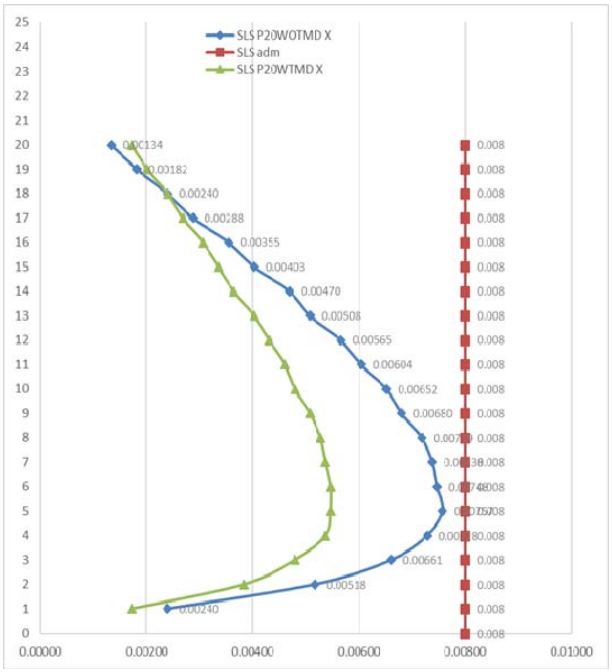


Fig. 41 Deplasari relative pe directia “X” la SLS

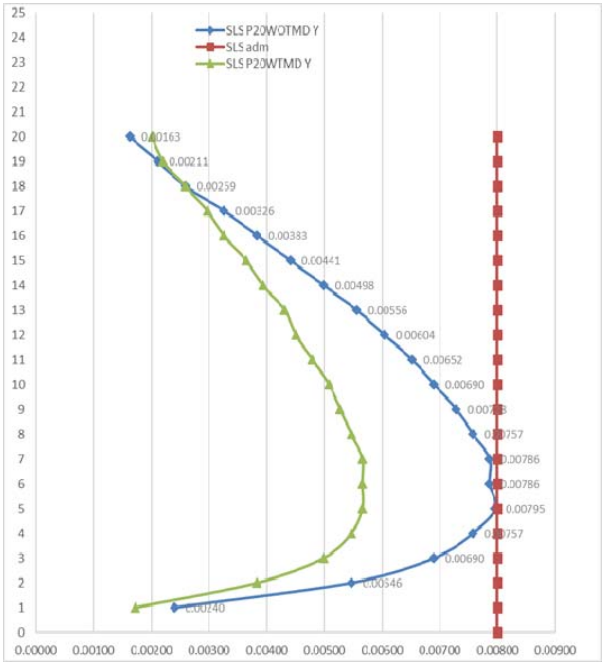


Fig. 42 Deplasari relative pe directia “Y” la SLS

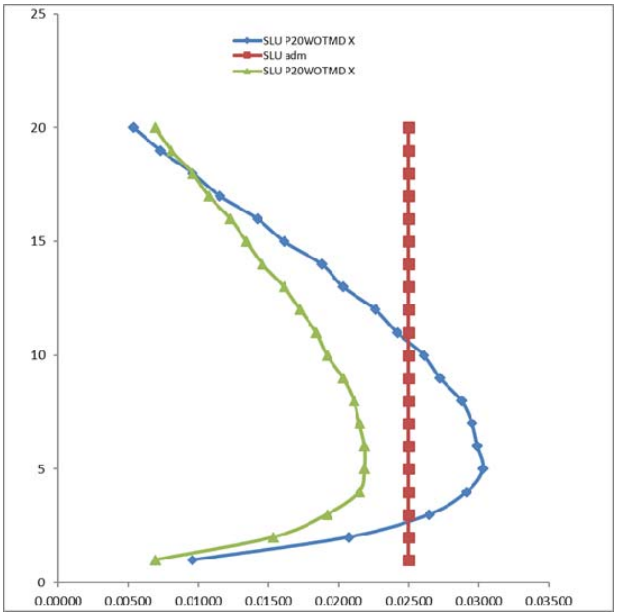


Fig. 43 Deplasari relative pe directia "X" la SLU

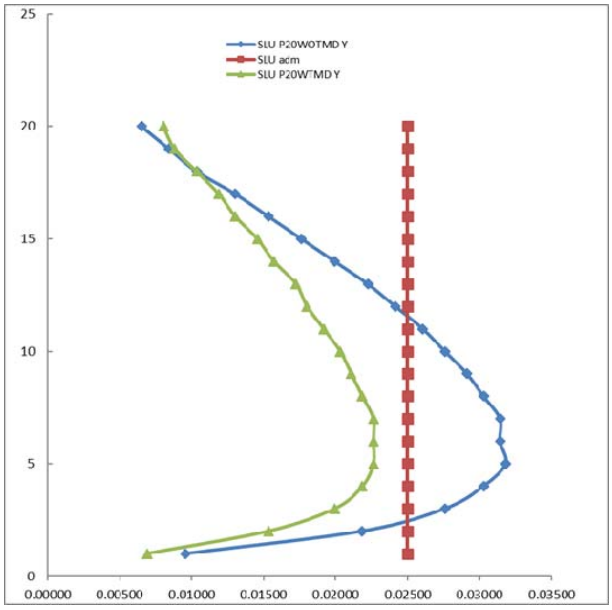


Fig. 44 Deplasari relative pe directia "Y" la SLU

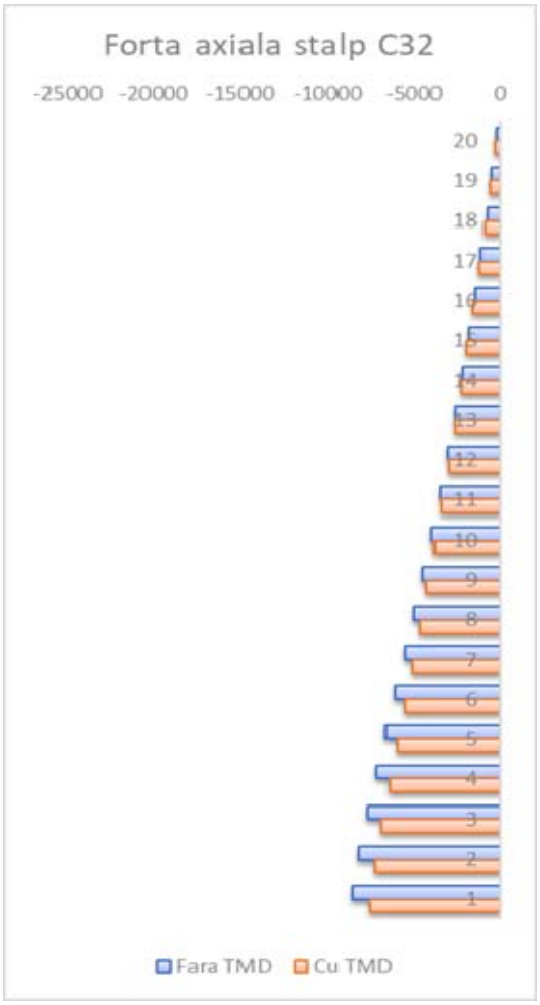


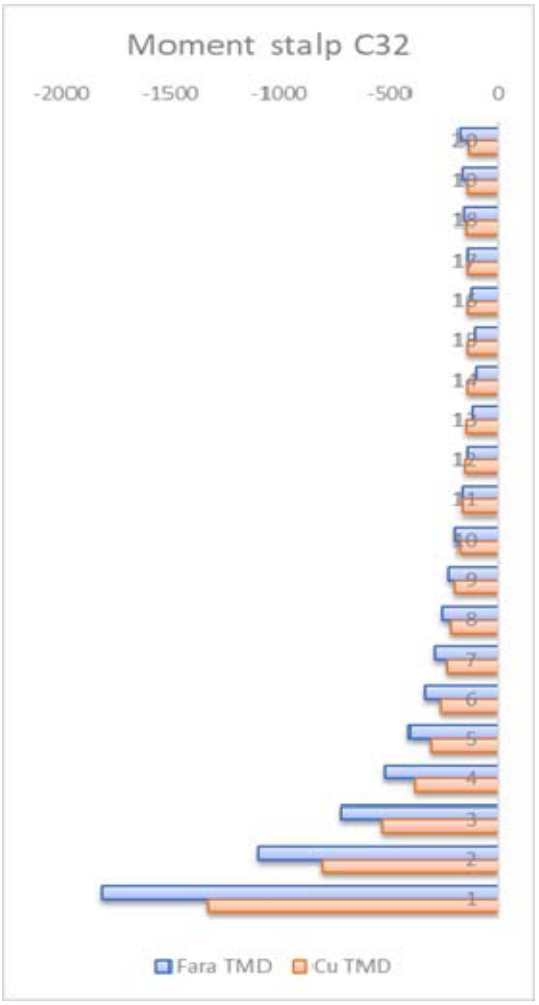


Fig. 45 Forta axiala si momentul incovoietor in stalpul de colt C32

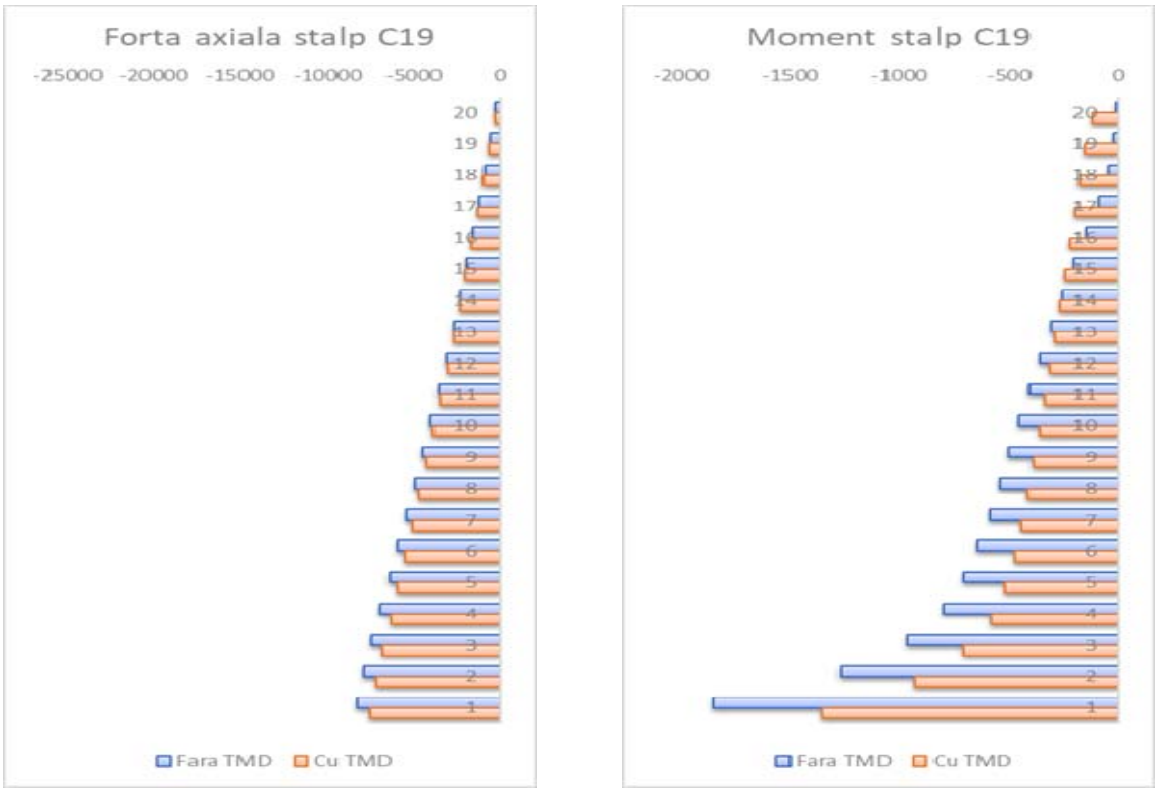


Fig. 46 Forta axiala si momentul incovoietor in stalpul marginal C19

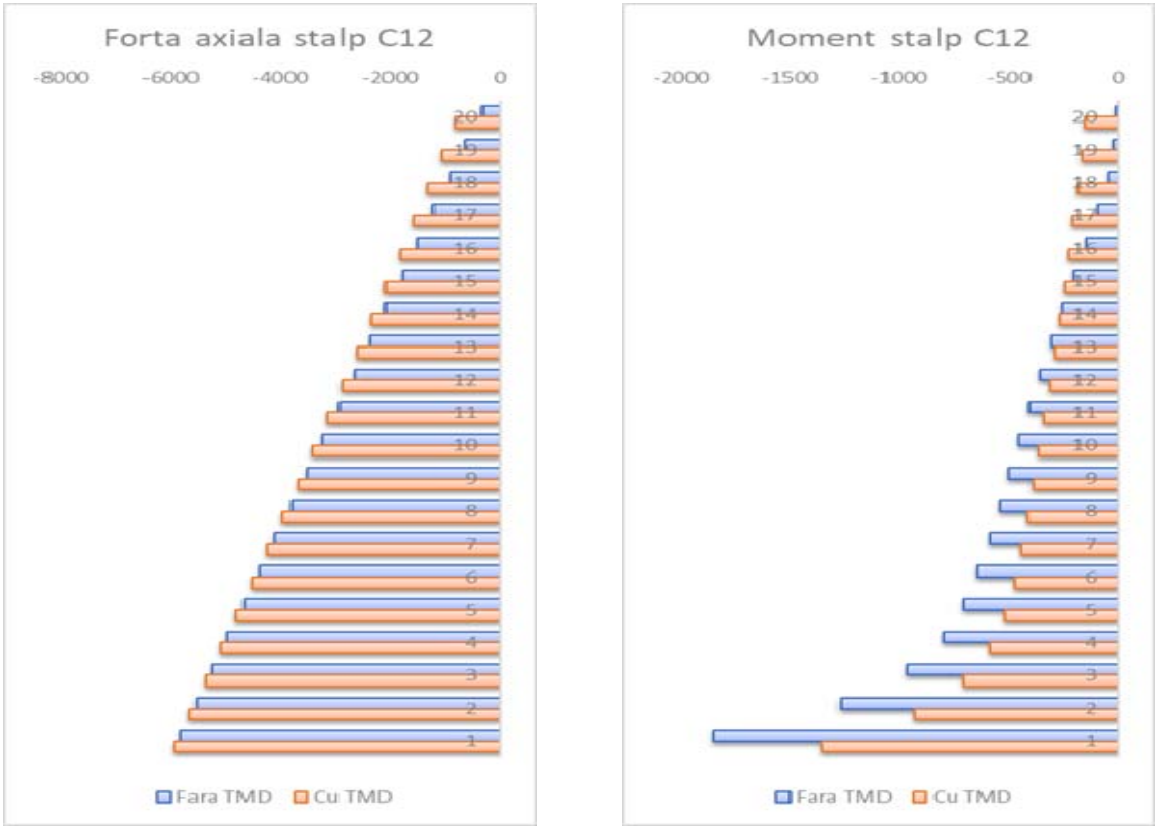


Fig. 47 Forta axiala si momentul incovoietor in stalpul interior C12

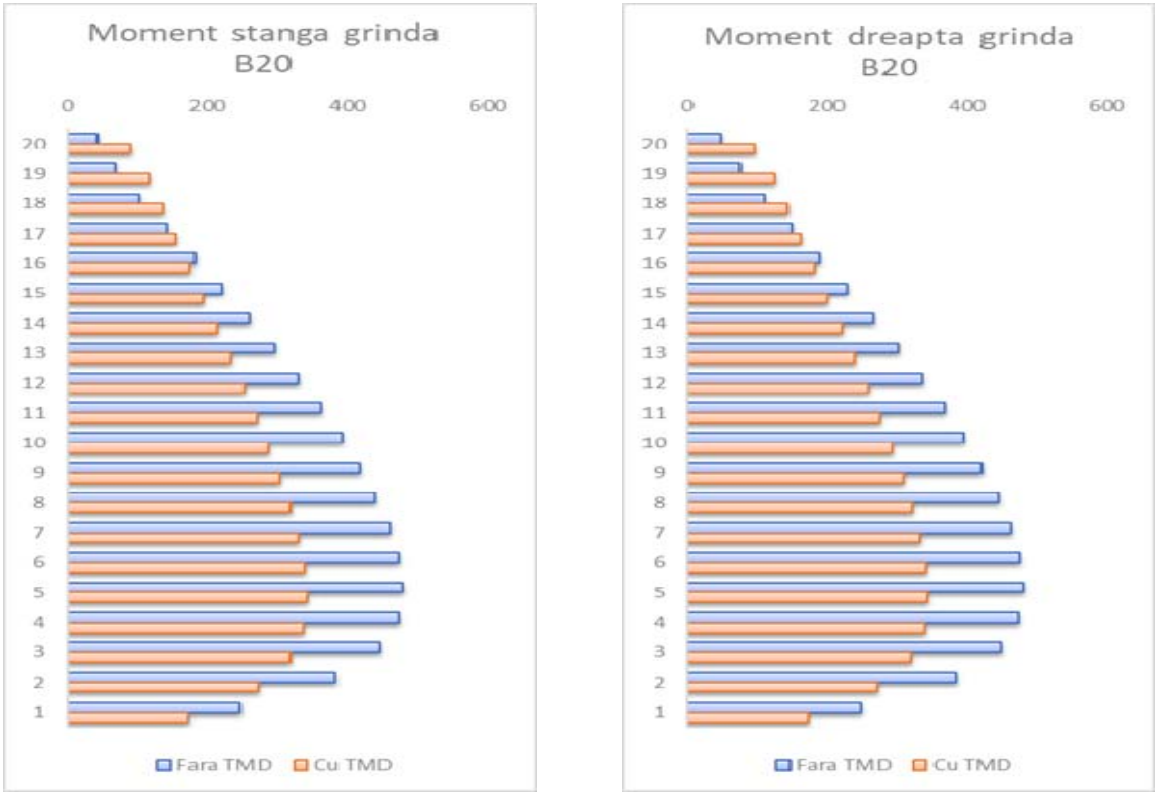


Fig. 48 Momentele din reazemele grinzii B20

Pentru a evidentia comportarea TMD-ului in reducerea eforturilor in elemente au fost selectate:

- Un stalp de colt – denumit C32;
- Un stalp marginal – denumit C19;
- Un stalp interior – denumit C12;
- O grinda – denumita B20;

Se observa o reducere a eforturilor in elementele structurii;

- In stalpul de colt C32 forta axiala a fost redusa in medie cu 7% si o reducere a momentului incovoietor in medie cu 10%.
- In stalpul marginal C19 forta axiala a fost redusa in medie cu 6% si o reducere a momentului incovoietor in medie cu 20%.
- In stalpul interior C12 forta axiala a fost redusa in medie cu 4% si o reducere a momentului incovoietor in medie cu 15%.
- In reazemele grinzii B20 momentele incovoietoare au fost reduse in medie cu 10%.

## 6.4. Structura in cadre P+10E

In urma analizei modala cu spectru de raspuns s-au obtinut urmatoarele perioade proprii pentru primele 4 moduri de vibratie:

| Mod | Structura Fara TMD | | | | Structura Cu TMD | | | |
|---|---|---|---|---|---|---|---|---|
| | Perioada | Ux | Uy | Rz | Perioada | Ux | Uy | Rz |
| 1 | 0.745 | 0 | 0.7748 | 0 | 1.033 | 0 | 0.5006 | 0 |
| 2 | 0.728 | 0.7769 | 0 | 0 | 1.021 | 0.4859 | 0 | 0 |
| 3 | 0.678 | 0 | 0 | 71.0368 | 0.678 | 0 | 0 | 0 |
| 4 | 0.23 | 0 | 0.1036 | 0 | 0.615 | 0 | 0.3046 | 0 |

Se observa ca dupa introducerea TMD-ului perioadele s-au marit si repartitia maselor s-a modificat fundamental. Astfel:

- In primul caz (fara TMD) pe modurile 1 si 2 factorul de participare al maselor era 77.48%, respectiv 77.69% rezultand forte seismice mari.
- Dupa amplasarea TMD-ului acesti factori de participare ai maselor practic se impart in doua si se distribuie pe cate 2 moduri pe fiecare directive principala. Fenomenul de torsiune generala "coboara" dincolo de modul 4.

Daca analizam din punct de vedere al deplasarilor, se pot observa reduceri ale drift-urilor, in medie cu 2% pe directiile X si Y la SLS si 1.5% la SLU, asa cum se evidentiaza in figurile de mai jos.

Din punct de vedere al reducerii deplasarilor pentru structura analizata P+10 E nu se justifica utilizarea TMD considerind ca este o solutie nefezabila.

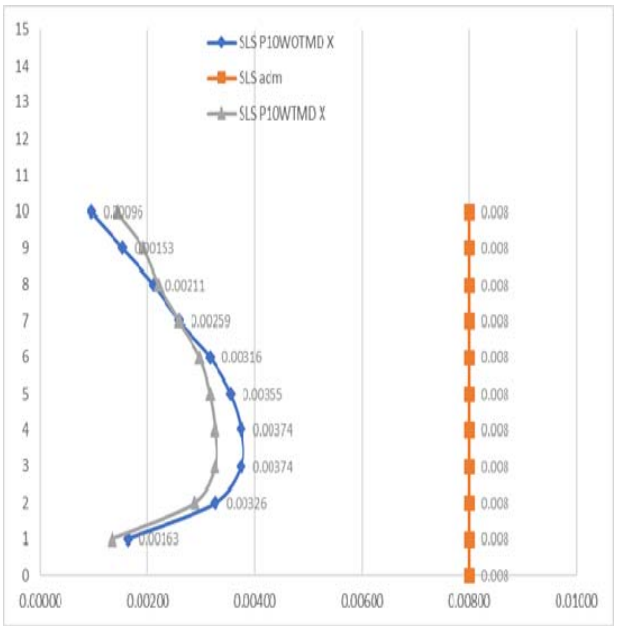


Fig. 49 Deplasari relative pe directia "X" la SLS

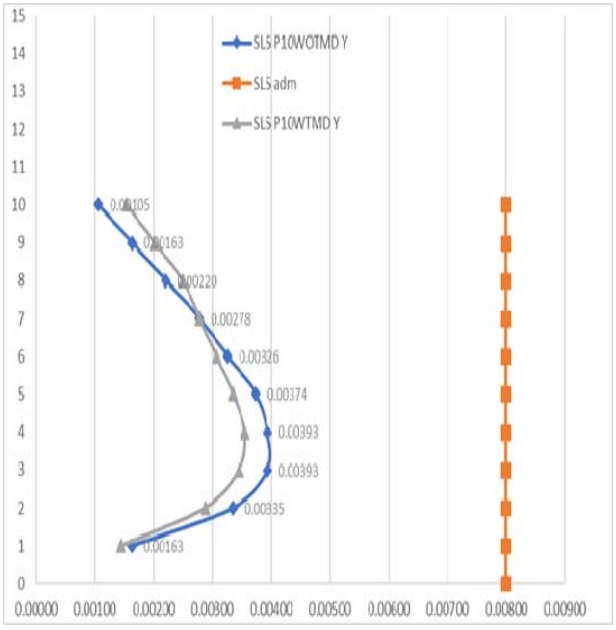


Fig. 50 Deplasari relative pe directia "Y" la SLS

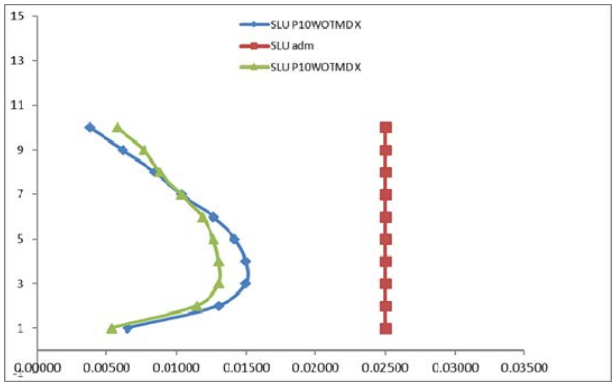


Fig. 51 Deplasari relative pe directia "X" la SLU

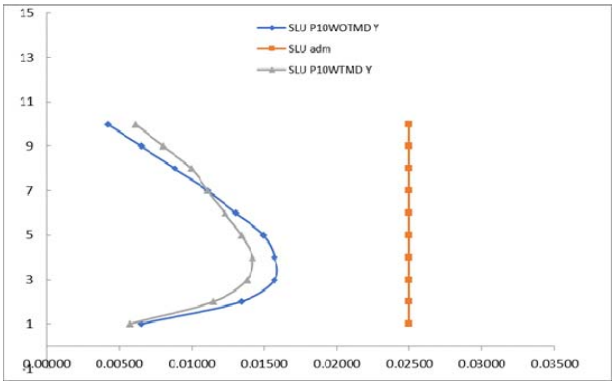


Fig. 52 Deplasari relative pe directia "Y" la SLU

Pentru a evidentia comportarea TMD-ului in reducerea eforturilor in elemente au fost selectate:

- Un stalp de colt – denumit C32;
- Un stalp marginal – denumit C19;
- Un stalp interior – denumit C12;
- O grinda – denumita B20;

Se observa o reducere a eforturilor in elementele structurii;

- In stalpul de colt C32 forta axiala a fost redusa in medie cu 1% si o reducere a momentului incovoietor in medie cu 2%.
- In stalpul marginal C19 forta axiala a fost redusa in medie cu 1% si o reducere a momentului incovoietor in medie cu 2%.
- In stalpul interior C12 forta axiala a fost redusa in medie cu 2% si o reducere a momentului incovoietor in medie cu 4%.
- In reazemele grinzii B20 momentele incovoietoare au fost reduse in medie cu 10%.


Fig. 53 Forta axiala si momentul incovoietor in stalpul de colt C32

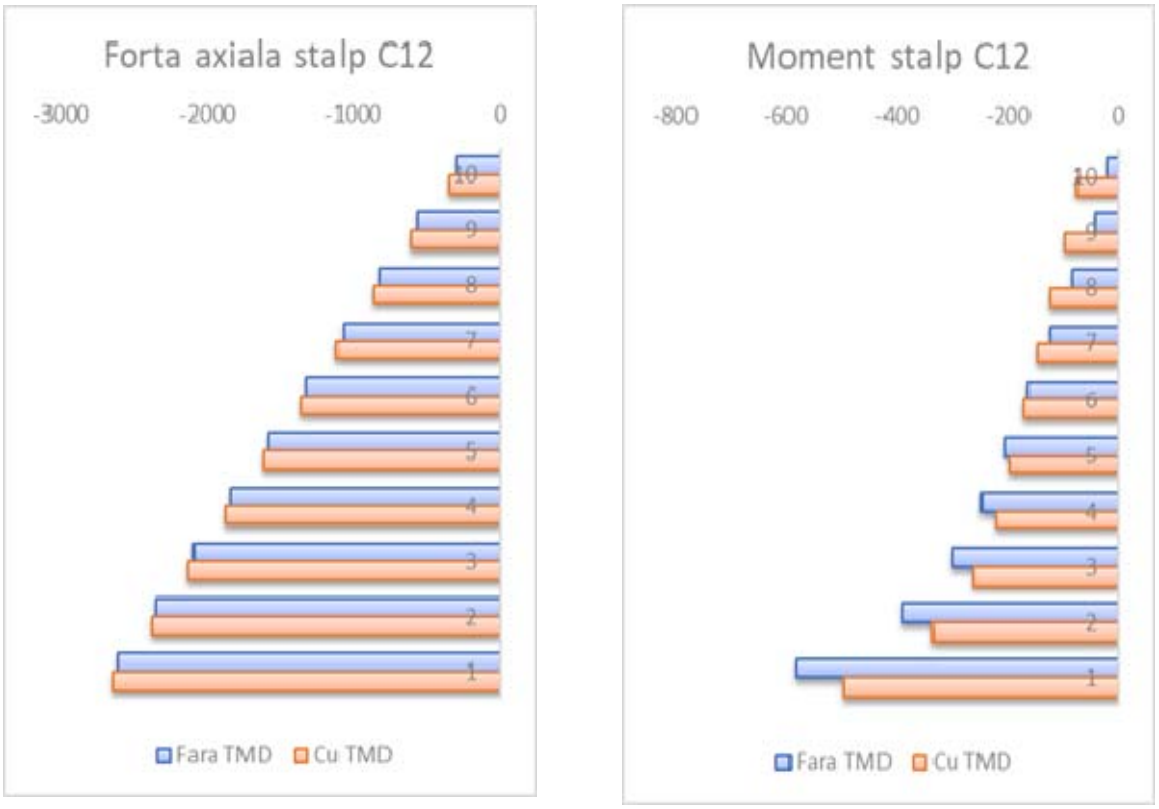


Fig. 54 Forta axiala si momentul incovoietor in stalpul interior C12

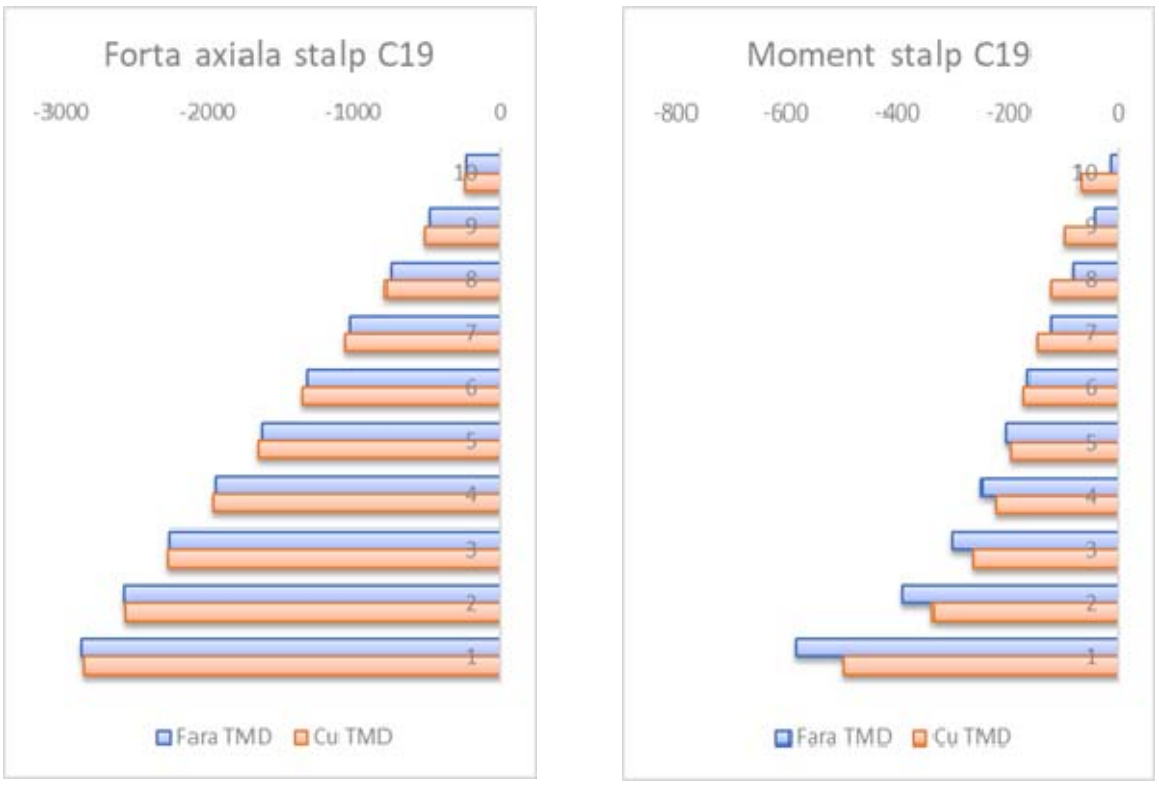


Fig. 55 Forta axiala si momentul incovoietor in stalpul marginal C19

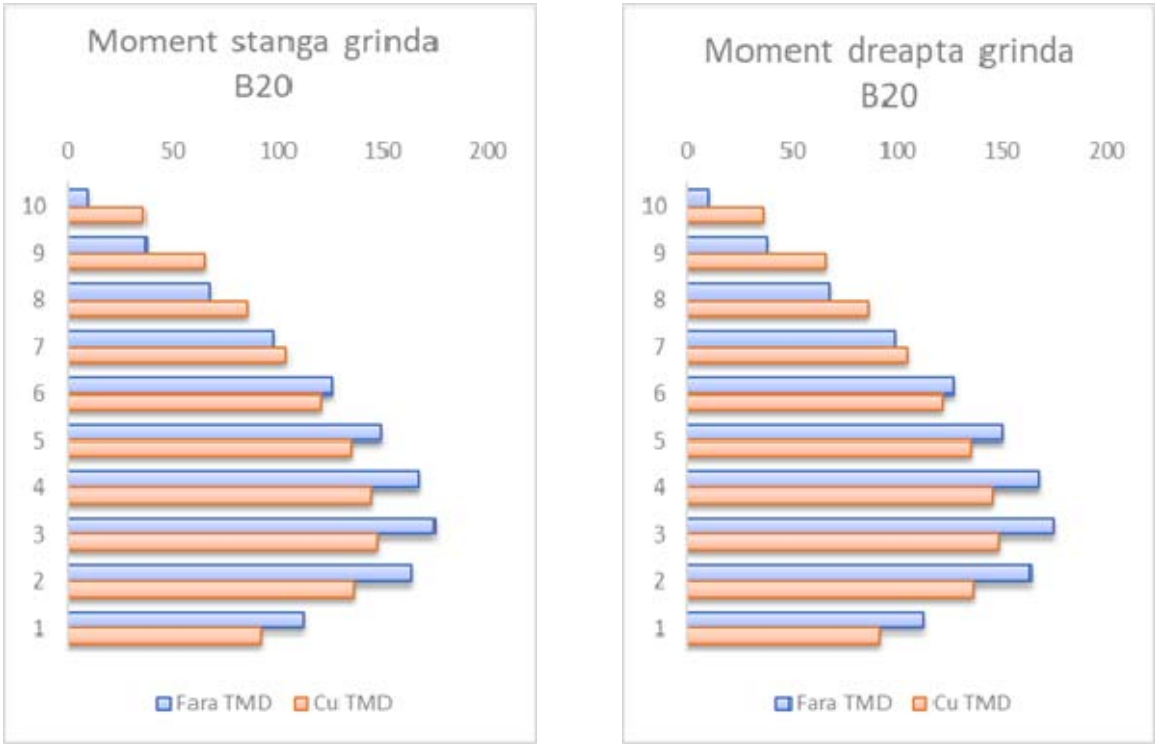


Fig. 56 Momentele din reazemele grinzii B20

## 7. Concluzii

Se constata ca la adaugarea TMD-urilor factorii de participare initiali de circa 75%, pentru translatia pe x (mod 1), translatia pe y (mod 2)si torsiune (mod 3) se modifica simtitor, in sensul ca atat modul 1 cat si modul 3 devin translatii pe x cu factorii de participare masica 37.5%, modurile 2 si 4 translatii pe y cu factorii de participare masica 37.5% respectiv (toate sunt translatii pure, fara torsiune) iar modurile 5 si 6 devin moduri de torsiune cu factorii de participare masica 37.5%.

De asemenea, pentru modurile fundamentale de vibratie se constata o marire a perioadelor de vibratie de 1.4 ori.

In urma analizei dinamice liniare cu spectru de raspuns a tuturor structurilor in cele doua situatii se pot formula urmatoarele concluzii cu caracter de generalitate, expuse sub forma de avantaje si dezavantaje:

**Avantaje:**

- Mecanism relative simplu si usor de realizat;
- Fiabilitate crescuta data desimplitatea mecanismului;
- Reducerile deplasarilor relative de nivel in medie cu circa 25%;
- Reduceri ale fortelor axiale in stalpi si/sau peretii structurali din b.a. cu circa 5%;
- Reduceri ale momentelor incovoietoare din stalpi cu circa 20%;
- Reducerea momentelor incovoietoare la nivelul peretilor structurali din b.a. cu circa 10%;

- Reduceri ale momentelor incovoietoare din reazemele grinzilor cu circa 25%;
- Cresterea amortizarii oscilatiilor sistemului structural
- Simplitatea calculului caracteristicilor sistemului de amortizare cu masa acordata (TMD);
- Sunt in general eficiente la cladiri cu regim mediu si mare de inaltime.

**Dezavantaje:**

- Incarca local elementele structurii cu forte gravitationale importante;
- Sistemul de prindere de structura trebuie gandit astfel incat sa distribuie incarcarea la cat mai multe elemente structurale, pentru a nu exista efecte locale, concentrate, importante;
- Apar problem atunci cand lungimea pendulului este mai mare decat inaltimea de nivel, si cand trebuie prevazut un gol suficient de mare pentru ca acesta sa oscileze;
- Nu sunt eficente la cladiri cu regim mic de inaltime.

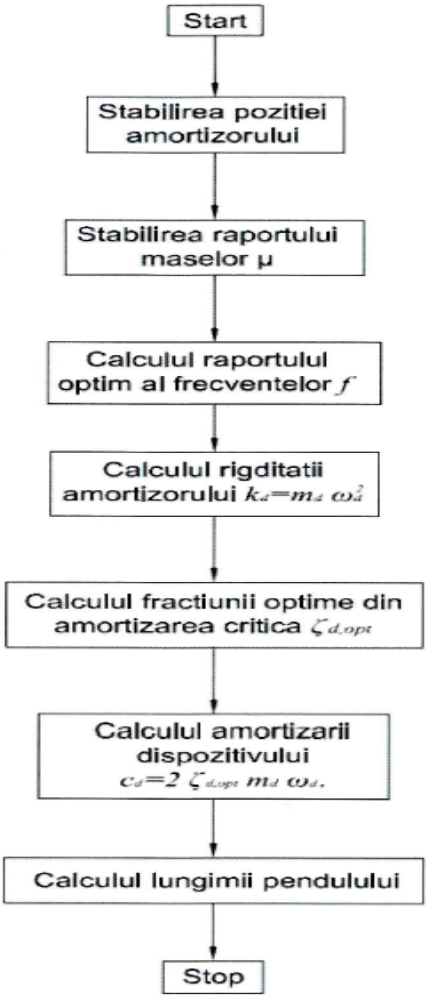


Fig. 57 Schema logica pentru calculul unui amortizor cu masa acordata

## Referinţe


[1] Chopra, A.K. (2007). Dynamics of Structures. Theory and Applications to Earthquake Engineering, Pearson, Prentice Hall, NJ.

[2] P100-1/2006 - Cod de Proiectare Seismica - Partea I - Prevederi de proiectare pentru cladiri, Bucuresti, 2006

[3] Anil K. Chopra - Dynamics of Structures - Theory and Applications to Earthquake Engineering, New Jersey, 1995

[4] "Dinamic of structures" – R.W.Clough, J. Prezien (1993)

[5] "Application of tuned mass damper for vibration control of frame structures under seismic excitation" – Rasmi Mishra (2011)

[6] "The effect of tuned-mass dampers on the seismic response of base-isolated structures" – Hsiang-Chuan Tsai (1993)

[7] "Optimal design theories and applications of tuned mass dampers" - Chien-Liang Leea, Yung-Tsang Chen (2006)

[8] D. Cretu; E. Tulei; C. Ghindea; R. Cruciat - Eficienta dispozitivelor pasive de control la reabilitarea seismica a unei cladiri din Bucuresti

[9] "Studii privind utilizarea dispozitivelor disipatoare cu masa acordata (TMD) la reducerea vulnerabilitatilor seismice ale cladirilor existente cu structura din b.a." – Adrian Ivan – Disertatie 2013

[10] Tulei E., Cretu D., Ghindea C. (2008), Seismic rehabilitation of a reinforced concrete framed structure by the use of tuned mass dampers and viscous dampers, Proceedings of the International Conference Constructions 2008, 9-10 may 2008, Cluj-Napoca, Romania, Vol.1, p.283-290

[11] Tulei E., Cretu D., Lungu D. (2009), Study on seismic upgrade of 5 storey reinforced concrete building by Tuned Mass Damper, Proceedings of the International Conference on Protection of Historical Buildings, Prohitech 09, Rome, Italy, 21-24 june 2009, Vol.1, p.563-568

[12] STUDIUL UNOR METODE DE ATENUARE A ACTIUNII SEISMICE ASUPRA CONSTRUCTIILOR - C. Ghindea – Teza de doctorat – UTCB 2008

[13] P100-3:2008 Cod de evaluare şi proiectare a lucrărilor de consolidare la clădiri existente, vulnerabile seismic

[14] P100-1:2013 Prevederi de proiectare pentru clădiri

[15] SR EN 1993-1-1 Eurocod 3: Proiectarea structurilor de oţel. Partea 1-1: Reguli generale şi reguli pentru clădiri

[16] CR0-2005. (2005). Cod de proiectare. Bazele proiectării structurilor in construcți.

[17] CSI. (fără an). ETABS Nonlinear V 9.7.4-User manual.

[18] P100-1/2013 COD DE PROIECTARE SEISMICA PARTEA I - PREVEDERI DE PROIECTARE PENTRU CLĂDIRI.

# Experimental study on the phenomenon of cracking of a reinforced element in sand concrete

BOUSSERHANE Slimane [1], HAMOUINE Abdelmadjid [2]

[1] ARCHI PEL Laboratory, University Tahri Mohamed of BÉCHAR, Algeria
*bousserhane_sli@yahoo.fr*
[2] ARCHI PEL Laboratory, University Tahri Mohamed of BÉCHAR, Algeria
*ahamouine@yahoo.fr*

DOI: 10.37789/rjce.2021.12.1.13

**Abstract.** *With the diversity of concrete quality, sand has taken a big place in the composition of sand concrete. However, reinforced concrete based on sand is undergoing experimental tests and validation tests, and its cracking in this concept has become a very paramount parameter when sizing this material. In this context, this work of an experimental nature, has for main objective to study the cracking of an element of reinforced concrete based on sand by the variation of the spacings of cracks using a reduced model in reinforced concrete.*

**Key words:** sand concrete - Cracking - tensile test - average crack spacing.

## 1. Introduction

Sand concrete is an artificial agglomerate of sand, cement, water and possibly fines added from fillers. Sand concrete by its current design, are newly created materials, to replace conventional concrete [1].

Indeed, the abundance of sand in our country of Algeria requires more and more to use more to build civil engineering works, especially since the sand concrete being a special concrete in absolute majority is composed of sand [2]. In this context, our interest was concentrated in this new old material, since its creation dates from the 18th century and scientific research became involved in a multi-disciplinary interest just towards the end of the 19th century [3].

Note that the research that has been carried out on the cracking of materials can only concern limited cases and precise problems, hence the fairly wide field of the study of cracking and the large number of researches [4, 5, 6]. To know more about the behavior of cracks in the traction zone below the horizontal axis, This transition zone has an impact on the properties of the crack and is directly influenced by the steel-concrete interface [7, 8].

To this end, our experimental work consists in studying the cracking of concrete in the sand, (pulling case subjected to traction), this element will be made from local materials. In this problem, we took part in the study of this type of concrete in order to know its behavior to cracking when it is provided with reinforcements of steels. (I.e. towards qualification as much as reinforced concrete). And to start this study, We have

developed another experimental program with pulling tests allowing the detection of the network of cracks in a clearer way compared to the bending tests. To do this, we created an experiment on small samples of dimensions (7X7X28) We also reduced the model to adapt it to the nature of the cracks closest to this targeted area [2, 9]. The pulling test is specially chosen to represent the stretched part in the area of constant moments of the four-point bending test.

## 2. Expérimental procédure

### 2.1. Used materials

As part of this experimental program, we used three types of sand of different nature and size. These are coarse ($S_g$), medium ($S_m$) and fine sand ($S_f$). Their physico-chemical characteristics are summarized in the table1.

**Table 1. Physical characteristics of sand**

| Sand type | Units | Coarse sand | Medium sand | Fine sand |
|---|---|---|---|---|
| Absolute volumetric mass $M_{ab}$ | $g/cm^3$ | 2.5 | 2.6 | 2.7 |
| Apparent volumetric mass $M_{app}$ | $g/cm^3$ | 1.71 | 1.57 | 1.51 |
| Equivalent of Sand $E_s$ | % | 72.12 | 91.10 | 95.96 |
| porosity | % | 28.99 | 27.68 | 26.54 |
| compacity | % | 71.01 | 72.32 | 73.46 |
| Fineness module $M_f$ | % | 2,06 | 1.19 | 0.51 |
| Coefficient of uniformity $C_u$ | / | 5 | 2.8 | 2.11 |
| Curvature coefficient Cc | / | 0 .66 | 1.15 | 0.98 |
| Color | / | Yellowish | Yellowish | yellowish red |
| Nature | / | Siliceous | Siliceous | Siliceous |
| form | / | crushed | rolled | rolled |

The particle size curves, expressing the cumulative percentages by weight of the pass as a function of the size of the sieves. The results of particle size analysis of the three types of sand are shown in Figure 1. From this figure, we can observe that the grain size curve for the two sands (coarse and fine) gives a similar character. On the other hand, it badly graduated, and giving a well graduated and spread curve for the medium sand which was a crushed sand presented a well graduated but spread curve.

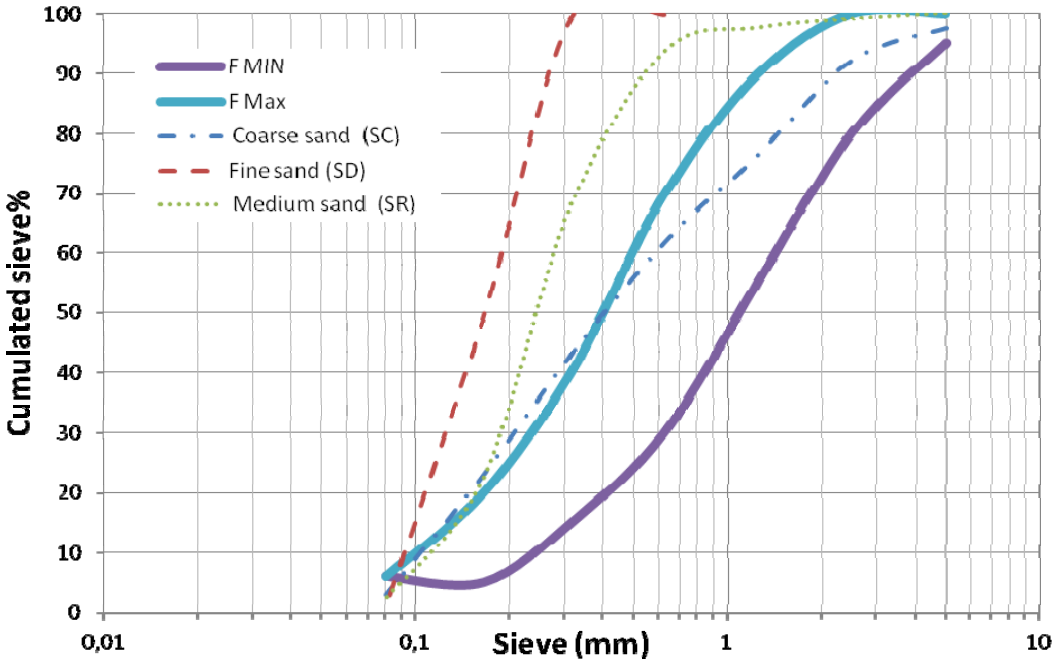


Figure.1 Particle size curve of the three sands used

Analysis of these curves, we can cite the following observations:

- ✓ Fine sand (SD) has a discontinuous particle size distribution; grains with a diameter between 0.63 and 0.5 mm are missing, so this sand is characterized by a dense particle size distribution.
- ✓ Coarse sand (SC) with a fineness module 2.06. Is at a position between two zones Min and Max, and that for the coarse elements, and the lower part confused with the zone Max.
- ✓ Medium sand (SR) is a sand rich in fine elements, due to the fact that the particle size curve below the maximum time zone.

A single type of cement was used for the preparation of all of the elaborate sand concrete compositions. It is CPJ-CEM II/B 42.5N cement which conforms to the standard (NFP 15-301/9). The physico-mechanical characteristics are summarized in Table 2.

**Table 2. Physical characteristics of cement**

| characteristics | Absolute volumetric mass ($g/cm^3$) | Apparent volumetric mass ($g/cm^3$) | Normal consistency (%) | Beginning of setting (h/min) | Fineness of grind | compressive strength at 28 days (MPa) | tensile strength at 28 days (MPa) |
|---|---|---|---|---|---|---|---|
| Values | 1,057 | 3,20 | 29 | 2h34min | 9,60 | 39 | 07 |

Only one adjuvant was used as a super water-reducing super plasticizer. This is MEDAPLASTE SP40 brown in color, their density is equal to 1.2 g / cm3, and with a PH = 8.2. In contrast, the addition of MEDAPLAST HP was used as a powder addition, it is characterized by a density of 0.5 g / cm3, a mass area greater than 15 (m2 / gr), a humidity per oven at 105 ° C of less than 1%; with a particle size of less than 0.1 microns. Its chemical composition shows the percentages of: SiO2> 8.5 (%); SO3 <2.5 (%); Cl <0.2 (%).

Two types of stell bar were used in the manufacture of reinforced sand concrete specimens. These are high-adhesion and smooth round frames, chosen according to four diameters respectively (10mm, 12mm, 14mm and 8mm). The mechanical characterization of the different steels used is shown in Table 3. It should be noted that the presented values of the elastic limit, the breaking stress and the modulus of elasticity are obtained with the average of three measurements. It is interesting to mention that we cannot exceed 14mm because the test device does not allow for larger diameters.

**Table 3. Mechanical characteristics of the steels used**

| Ø [mm] | Type | Tensile stress on steel [MPA] | | $E_s$ [MPa] |
|---|---|---|---|---|
| | | Elastic limit fe | Break fr | |
| 10 | HA | 564 | 623 | 210200 |
| 12 | HA | 612 | 667 | 210000 |
| 14 | HA | 610 | 729 | 197300 |
| 8 | RL | 293 | 413 | 210530 |

## 2.2. Formulation and implementation of elaborate concrete

The composition method used in this sand concrete study is the so-called experimental one. where the water dosage is developed by setting the cement dosage with the W / C ratio, and we vary the dosage of sand in such a way as to obtain a workable concrete to finally reduce this quantity to the estimated workability. After mixing, it is possible to obtain a dry confection, We seek for each mixture the quantity of water necessary to ensure a maneuverability fixed beforehand, because the W / C ratio is increased until a more manageable sand concrete is obtained [2, 10].

Table 4 brings together the different compositions.

**Table 4: Different composition of sand concrete**

| reference | W/C | Cement ($kg/m^3$) | Water (l) | Adjuvante (l) | Silica fume ($kg/m^3$) | Coarse sand ($kg/m^3$) | Medium sand ($kg/m^3$) | Fine sand (kg/m3) |
|---|---|---|---|---|---|---|---|---|
| BSC | 0.9 | 350 | 315 | 8.75 | 20 | 1328.67 | - | - |
| BSR | 0.9 | 350 | 315 | 8.75 | 20 | - | 1434.98 | - |
| BSD | 0.9 | 350 | 315 | 8.75 | 20 | - | - | 1381.82 |

## 2.3. Experimental characterization procedure

The pulling specimen taken here to study the crack spacing, is a simulation of the cracked part of any beam between its two supports, the main reinforcement is therefore at the low level of the beam, where the concrete also is stressed by traction which by reaching its limit of tensile strength will crack in this area.

The specimen has the dimension (7x7x28 cm3) in concrete prism, of reinforcement coated in this prism having a total length of 40 cm, because with the 6 cm of steel extended beyond the longitudinal end of the prisms, have to hold the test piece at press level during the tensile test (fig.2). The specimen is held by its two symmetrical steel ends, to calibrate the tensile load.

The loading is carried out by an automatic piloting of the press (fig.2) with a low loading speed; corresponding to the same speed of the concrete compression test. The test piece in this test was stressed until the steel bar broke, reading the crack spacing is easily acquired on the crack network. The completion of the test was started at the time of the plasticity of the steel, where the crack network is already stabilized and the recovery of the tensile load is almost entirely taken up by the reinforcement.

The measurement of the spacing of the consecutive cracks is carried out after stability of the network of cracks it can be evaluated on the four lateral faces of the test-tube. The distance between the free edge and the first crack is not taken into account, because the edge effects introduced by the free surface completely modify the value of this spacing (fig. 2)

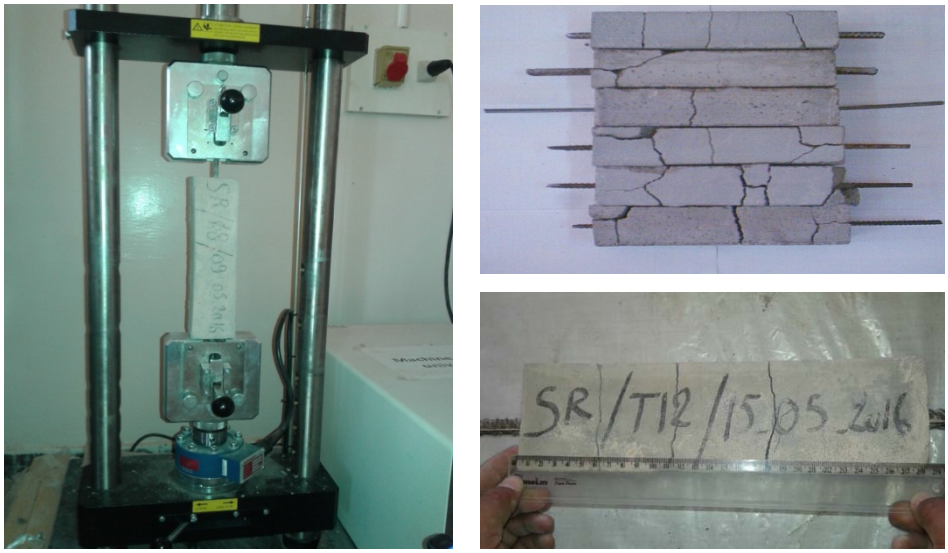


a) (c)

Figure.2 (a) Universal testing machine device assembly of test pieces after test (b) network of cracks. (c) measurement of crack spacing)

## 3. Experimental results and analyzes

The measurement of the total elongation of the tie rod was exploited as the traction loading was carried out by the simultaneous recording of the overall elongation of the test specimen with the increase in the load. To this end, the experimental results are shown in Figure 3.

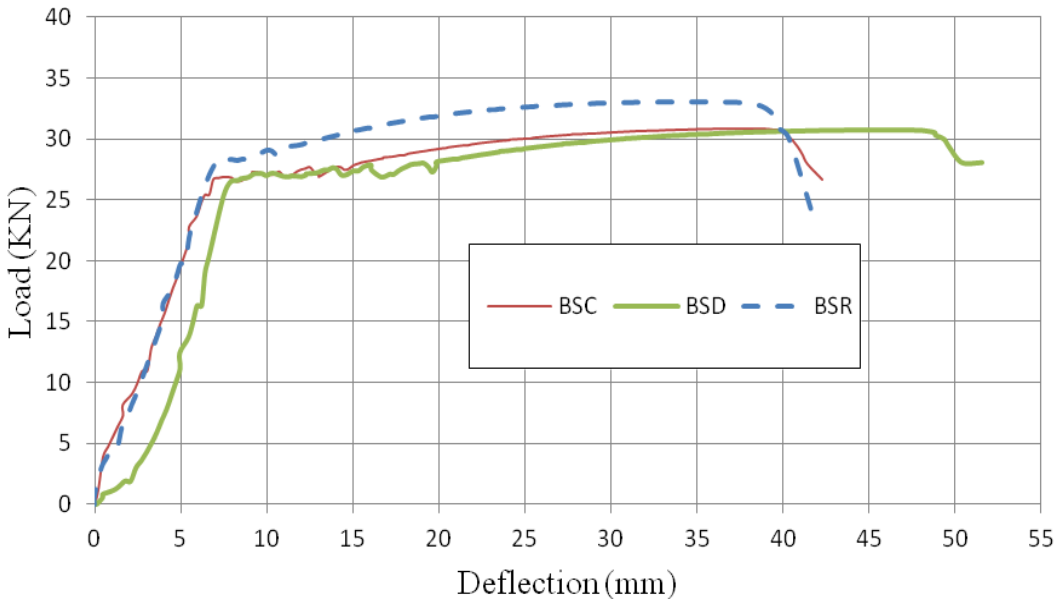


Figure 3 Extension of the Ø8 tie rod under tensile stress
«Case of three types of sand BSC; BSD; BSR »

From this figure, we can observe that the evolution of the overall deformation of the pulling specimen begins at the beginning with an almost linear behavior (elastic phase). Thus, the behavior of the tie rod goes through several symptomatic phases [9,11,12].

a) **Non-cracked phase**: In this phase the element behaves in a pseudo-linear elastic homogeneous fashion and does not crack, as long as the concrete has not yet reached its tensile strength. The appearance of the first crack corresponding to the tensile strength of the concrete.
b) **Crack formation phase**: this phase is mentioned by a gradual decrease in the rigidity of the element as new successive cracks appear and by the low rate of increase in normal force.
c) **Stabilized cracking phase**: In this last phase, the normal force increases more sharply than before, and no new crack develops. This phase will result in the rupture of the element where the relative elongation of the reinforcement exceeds the value corresponding to the flow limit of the steel used.

In order to determine the influence of the diameter of the bars on the cracking, we gathered on (figure 4) the evolution of nominal diameter of the bars (HA8, HA10, HA12 and HA14) according to the average spacing of the cracks for the three elaborate sand concretes.

From this figure, we can mainly observe that all the spacings are reduced with the increase in the diameter of the bars, only the diameter (HA14) presents a very strong increase for the three concretes. this is mainly linked to the diametral pressure which causes the encasing concrete to burst and largely detach it from the reinforcement, otherwise the three types of concrete are refined in spacing value, especially when it acts of (HA10 and HA12).

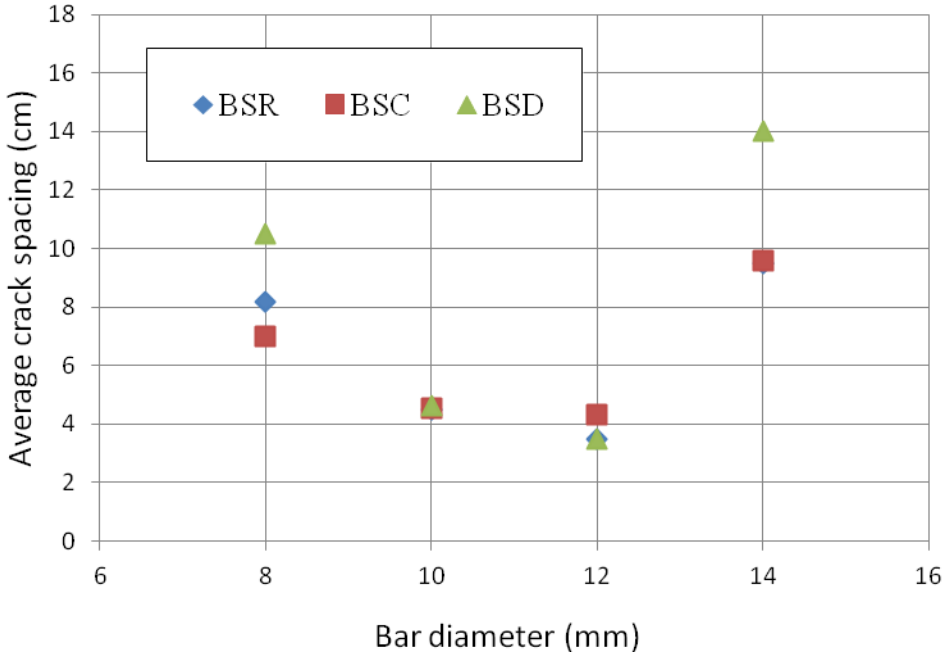


Figure 4 Influence of diameter on the mean crack spacing.

To determine the influence of the geometric percentage of reinforcement, we grouped the variations of the average crack spacing according to the percentage of reinforcements used, for the different types of sand concrete used, on figure 5 ci below. From this last, we can note that the increase in the geometrical percentage of reinforcements in the section involves a reduction in the average spacing between the cracks except in the case (HA14) of strong percentge ($\rho$ = 0,03% ), which confirms that the concrete resistance has only a very weak influence on the cracking network especially for the tie rods of average diameter (Ø10 and Ø12 mm).

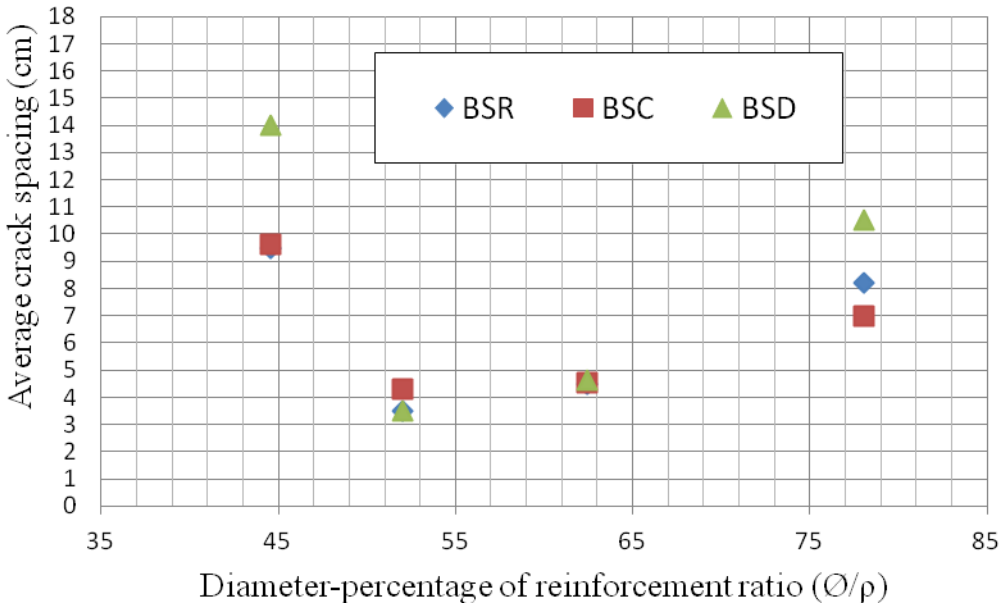


Figure 5 Influence of the diameter-percentage ratio of reinforcements (Ø / ρ)

## 5. Conclusions

The experimental set-up reserved for the test having successfully completed the task intended for the study of crack spacing, we carried out for this purpose compositions of sand concrete making it possible to concretize the crack spacing parameter. These tests carried out in this experimental program were followed by a simultaneous recording of the total elongation of the tie as a function of the tensile load, which also makes it possible to detect the appearance of cracks and the corresponding loads. Analysis of the experimental results allows us to draw the following conclusions:

- ✓ Increasing the reinforcement rate in the section reduces the average crack spacing.
- ✓ The variation of the different types of sand concrete has little influence on the crack behavior of the tie rod because the spacings obtained after the network stability merge for the different types of concrete.
- ✓ The effect of diametrical pressure only has an effect from reinforcement diameters exceeding 14 mm, otherwise the spacing of the cracks, in terms of growth, corresponds to the inverse of the diameter [13].
- ✓ This study made it possible to open up very broad perspectives for the use of sand concrete, as much as reinforced concrete, still remains the elaboration of studies concerning the main elements made of sand concrete.

## References

[1] Sablocrete "sand concrete: characteristics and practices of use", presses of the national school of bridges and roads (France), 1994.

[2] BOUSSERHANE.S, HAMOUINE. A, "Study of the cracking of scale models in reinforced sand reinforced concrete case", 2nd International Seminar of civil engineering CIGCB, BECHAR, 27-28 October 2015

[3] BOUSSERHANE.S "Contribution towards the qualification of use of sand concrete in reinforced concrete ″ cracking phenomenon ″" Master thesis specializing in civil engineering, Béchar University, June 2006.

[4] FAVRE.R, JACCOUD. J.-P., BURDET. O and CHARIF. H "Sizing of concrete structures" Civil Engineering Treaty, volume 8, 3rd edition, 2004.

[5] FARRA. B; JACCOUD. J "cracking of BHP instant tests on reinforced concrete tie rods" contribution to the RILEM HIGH PERFORMANCE CONCRETE seminar Casablanca, April 19-21, 1992.

[6] FARRA. B "Influence of the resistance of concrete and its adhesion with reinforcement on cracking". Thesis of the Federal Polytechnic School of Lausanne, year 1995.

[7] Eurocode 2. Calculation of concrete structures, NF-EN-1992; 2007.

[8] CHARIF, JACCOUD. "Reduction of deformations and improvement of the quality of concrete slabs", IBAP publication N ° 126 MAY 88, EPFL.

[9] HAMOUINE. A "Contribution to the study of high performance steel-concrete adhesion". Doctoral thesis specializing in civil engineering, INSA Toulouse, May 1996.

[10] RIKIOUI.T "Concrete in the laboratory, unit of bechar-1999".

[11] FAVRE.R "Service Suitability and Elements of Structures", Editions Presses Polytechniques et Universitaires Romandes, pp 591, 1997.

[12] JACCOUD. J P "Minimum reinforcement for cracking control of concrete structures". Doctoral thesis EPF Lausanne 1987.

[13] GOTO.Y. «Cracks formed in concrete around deformed tension bars», ACI journal no 68-26, April 1971.

# Experimental and numerical study on the performance of different fire ventilation systems

Marius Dorin Lulea[1]

[1] doctoral Candidate at the Technical University of Civil Engineering Bucharest, Faculty of Building Services Engineering, street bdul. Pache Protopopescu, no. 66, Bucharest, zip code 021414, Romania phone 0040 764 701 500,
*E-mail: luleamariusdorin@gmail.com*

DOI: 10.37789/rjce.2021.12.1.14

**Abstract.** *In the fire safety design of buildings, it is common practice to consider a smoke and heat exhaust ventilation system. The choice is made between either natural ventilation or a mechanical ventilation system. In case of a fire, the main requirement for building designers is to save users. For the safety of users during a fire, low temperatures, high oxygen concentration and good visibility for a certain period must be ensured.*
*Three different cases of ventilation in case of fire were analyzed in this study: mechanical ventilation (CASE1) and natural ventilation (CASE2- wall hatches and CASE3- roof hatches). The results of an experimental study were used to validate a numerical model (CASE0- no ventilation system) using FDS software. The action of the fire in a room with an area of 18(m2) has been studied.*
*Indoor temperatures, oxygen concentration and visibility are determined and used to establish the performance of different ventilation system. The three parameters play an important role in assessing the environmental conditions necessary to save users.*
*The study shows that natural or mechanical ventilation in case of fire considerably improves the evacuation conditions, saving users' lives. Both types of ventilation ensure good performance in the situation of a correct dimensioning and designs.*

***Key words:*** *CFD, FDS, fire, real- scale fire tests, ventilation*

## 1. Introduction

Design of buildings for fire action has become a common concern. Designing buildings for fire action involves identifying the best solutions that allow saving users, ensuring firefighters' intervention, preventing the collapse of buildings, limiting the spread of fire, limiting the damage of a fire [1].

Globally, the number of victims resulting from the action of the fire exceeds any other risk to which a building is subjected during its lifetime [2]. Most victims of a fire occur because of intoxication with smoke, hot gases, and pollutants [3].

The main parameter used to define the action of a fire is the indoor temperature. The concentration of oxygen, the concentration of toxic gases and the visibility are also important.

Modeling the action of fires on constructions can be done by simple mathematical models, zonal models, or complex field models [4]. Mathematical models are the most used due to the low computational resources required. As the computational technique develops, the use of complex field models in fire modeling becomes relevant. Field models allow to simulate the action of fires close to reality but require high computing resources.

Ventilation is a method of protecting the space in case of fire. The purpose of ventilation is to maintain optimal conditions for the survival of users for a certain period (low temperatures, high oxygen concentration, low harmful gases concentration and good visibility).

Ventilation in case of fire can be mechanical ventilation or natural ventilation. Natural ventilation involves the automatic and manual opening of the windows/hatches from the burned space to evacuate the defective air. Mechanical ventilation involves the use of an electric fan to extract foul air.

In this study, three cases have been simulated with different smoke and hot air ventilation system. Predictions of temperature, visibility and oxygen concentration are presented. The fire dynamics simulator (FDS) code, based on the concept of large eddy simulation, is adopted in the present simulation for good the fire modeling performance [5] [6]. No ventilation in room is used as a benchmark.

## 2. Materials and Methods

The test results are designated as reference for calculation models validation [7].

A real-scale experimental stand bas been used in the present research. The fire action was simulated with the help of a burner that uses LPG gas as a fuel.

The interior temperatures were recorded during the experiment.

The main components of the experimental stand are the construction, the combustion plant of the fuel, the installation of the exhaust air, the slit that provides the fresh air supply and the temperature sensor.

### 2.1. Experimental device

The experimental stand is a realistic room with an area of *18 ($m^2$)* (**Fig. 1**). The interior dimensions are *3 (m) x 6 (m)* ground surface, with a ceiling height of *2.7 (m).*

The test room consists in four exterior walls made of mineral wool panels which have a thickness of *0.10 (m)*.

In the exterior walls there was provided a door (*0.9 (m) x 2.1 (m)*), a window with an incombustible metal frame (*0.6 (m) x 1.2 (m)*), air outlet (*0.25 (m) x 0.25 (m)*) and an air inlet (*0.4 (m) x 0.1 (m)*).


Fig. 1. Image of the experimental stand.

The experimental stand was made of incombustible materials that provide a fire resistance of *180 (min)* for walls, floor, and roof and *90 (min)* for the door.

### 2.2. Burner

LPG gas was used as a fuel to simulate the fire. Gas was used because the combustion is controlled, unlike if solid or liquid fuels were used.

The installation consists of a burner, a metal supply line, and a fuel tank (**Fig. 2**). The combustion installation had two burners with a cumulative area of *0.25 (m) x 0.6 (m)*. The gas supply was made from a *60 (l)* tank mounted outside the experimental stand. With the help of a gas pressure regulator and a service tap, the flue gas flow was adjusted.

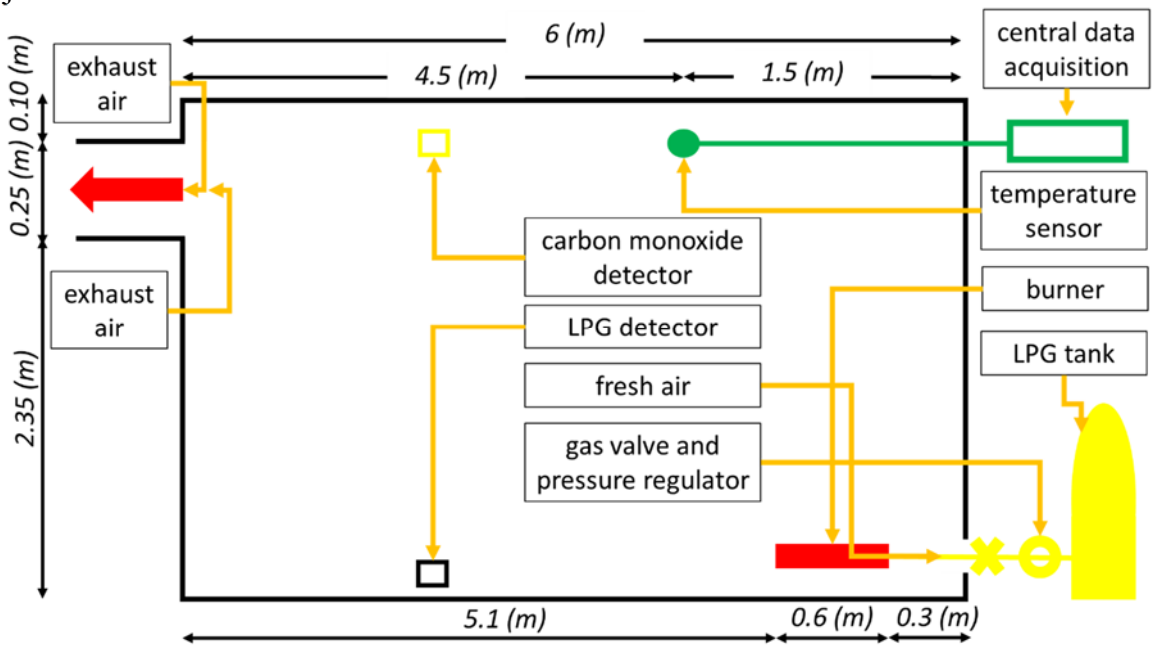


Fig. 2. Experimental stand sketch.

Near the burner was provided the air inlet slot. This slot provides the fresh air charged with the oxygen needed to burn.

At the bottom of the stand there is an LPG detector. It has the role of detecting the unburned gas and is provided for the safety of the experiment. At the top of the stand was provided a carbon monoxide detector for the situation in which the combustion would not be complete.

### 2.3. Measurement of temperature

The only parameter recorded was the indoor air temperature in point S1. One sensor was placed at the centerline of the ceiling (**Fig. 2**).

A thermocouple type K sensor was used. Data recording was done with an *ALMEMO710* data acquisition plant. This type of sensor is recommended for positive temperatures lower than *1000 ($^oC$)*. The measurement error is *0.1 ($^oC$)*.

The duration of the experiment has been *760 (s)*- the tests has been stopped when a *90 (°C)* temperature was reached in the room. The evolution of indoor temperatures throughout the event was recorded. The data recording step was set at *5 (s)*.

For safety, a sensor for detecting unburned LPG was mounted on the bottom of the camera and a sensor for detecting carbon monoxide was mounted on the top of the camera.

## 3. Modelling and calibration

There are three type of methods for modelling the reaction to fire of buildings: simplified mathematical models [8], zonal models who divide the burnt space into two zones characterized by an average temperature [9], computational fluid dynamics (CFD) models that allow the simulation of the fire closer to the reality [4].

Full-scale complementary computational fluid dynamic (CFD) simulations are carried out with fire dynamics simulator FDS. An approximate form of Navier–Stokes equations appropriate for low Mach number applications is used [10]. To handle sub-grid scale convective motion, Large Eddy Simulation (LES) technique is adopted [11].

The numerical model assumes knowledge as input data of the geometrical characteristics of the room, the material characteristics, the way in which the combustion is modeled, the size of the discretization network.

### 3.1. Geometric model and mesh

The dimensions of the room were determined by direct measurement (***Fig. 3***). The room has the interior dimensions of *6x3x2.7 ($m^3$)*. The wall thickness is *0.10 (m)*. The burner (*0.25x0.6 ($m^2$)*), air outlet (*0.25x0.25 ($m^2$)*) and air inlet (*0.4x0.1 ($m^2$)*) are placed in the same position as in the experiment. The dimensions were determined by direct measurements.

Reasonable extension of the computational domain has been proved to be necessary to acquire accurate results. Therefore, some additional computational regions are added near the wall (*0.5m*).

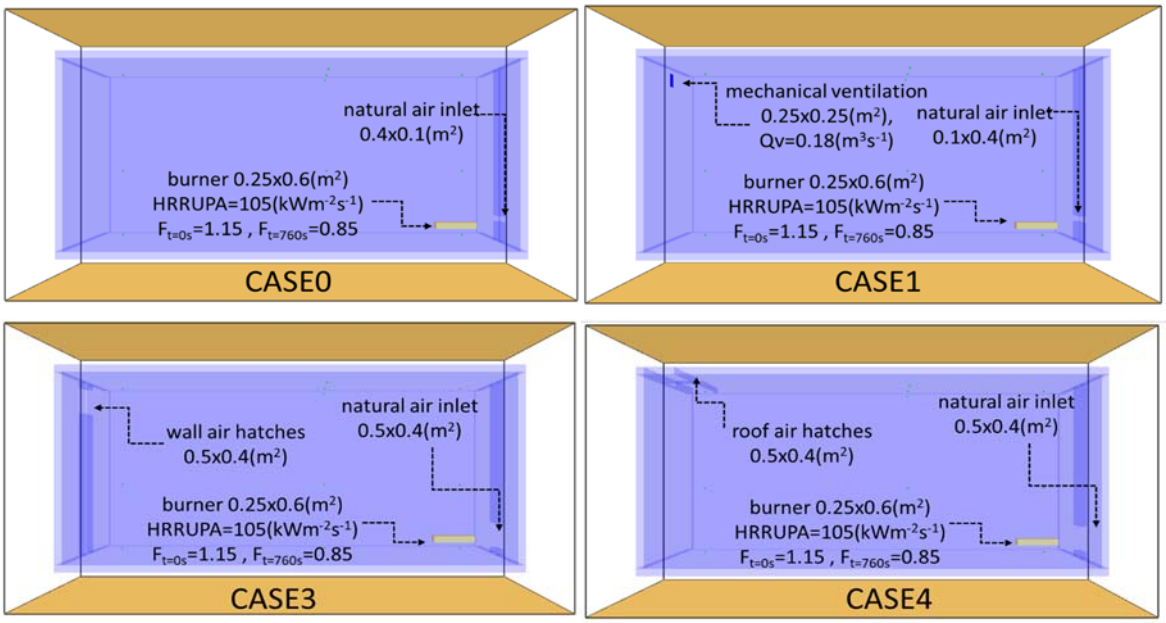


Fig. 3**.** Graphical representation of the model.

Details such as the existence of the door, windows, various interior objects such as the water supply pipe, sprinklers, wires of temperature sensors, joints between the panels were not reproduced.

The grid size is an important factor to be considered. To establish the mesh, several different mesh sizes ranging from *0.025 (m)* to *0.25 (m)* are chosen for comparison. Two criteria were considered to determine the optimal mesh: computation time and standard deviation. **Fig. 4** shows temperature distribution in point S1 of the three simulation with three different dimensions of the discretization network.

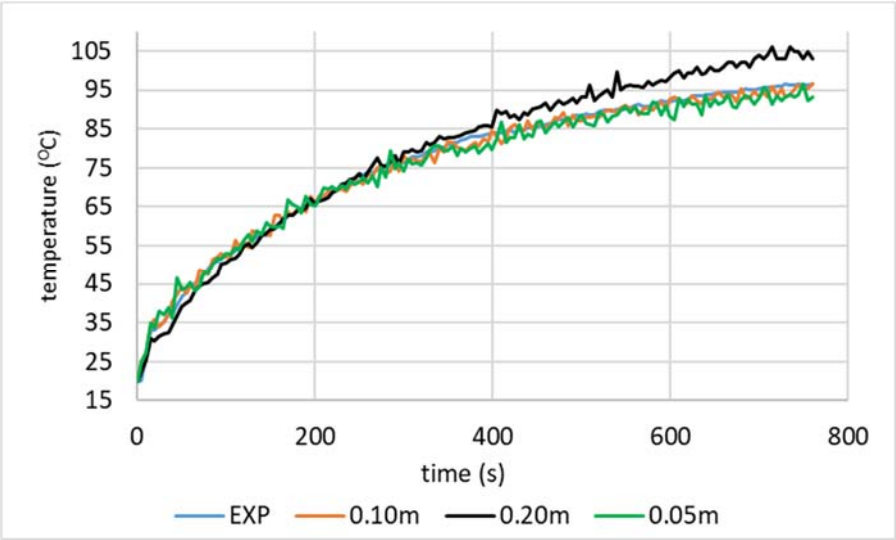


Fig. 4**.** Temperature evolution chart at different mesh, point S1.

The computer could not operate the calculation for network dimensions less than *0.05 (m)*, for *0.05 (m)* a single run lasted about *120 (h)*. A grid size of *0.1 (m)* was chosen and it offers results very close to reality, with an error of only *2.1 (°C)*.

*Table 1.*

**Calculation time and standard mean deviation at different values of mesh dimensions**

| Grid Dimension (m x m x m) | Calculation time (h) | $\sigma_{Err}$ ($^{O}$C) |
|---|---|---|
| 0.25 m x 0.25 m x 0.25 m | 0.5h | 21.0 |
| 0.20 m x 0.20 m x 0.20 m | 1h | 19.8 |
| 0.15 m x 0,15 m x 0,15 m | 2h | 12.8 |
| 0.10 m x 0.10 m x 0.10 m | 7h | 2.1 |
| 0.05 m x 0.05 m x 0.05 m | 120h | 4.8 |

## 3.2. Material characteristics of the walls

The materials from which the walls and floors are made are important for the calculation. The main material characteristics important for numerical analysis are: (a) the density ($\rho$=*120 (kg/m$^3$)*), (b) the thermal conductivity (λeqv (W/m.K)-determined), (c) the lower calorific value (*qi=0 (MJ/kg)*) and (d) the thermal capacity (*cp=0.840 (kJ/kg.K)*).

All characteristics were taken from the product sheet except the thermal conductivity. It was necessary to determine an equivalent thermal conductivity considering the differences between the real situation and the one in the model (the window and the door are not found in the calculation model) as well as the need to correct the value in the data sheet with the losses through the thermal bridges (intensified heat losses through the joints of the panels, in the area of the door and window, the joint between the walls and floors).

Several calculations were iterated at different values of thermal conductivity. The value of the thermal conductivity that showed the minimum average deviation ($\sigma_{Err}$ *(°C)*) was chosen.

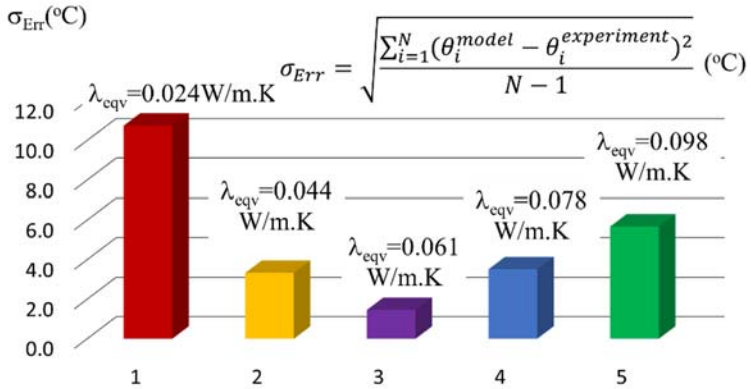


Fig. 5. $\sigma_{Err}$ *(°C)* for different values of *λeqv (W/m.K)*

The equivalent thermal conductivity of the walls and floors has been set at $\lambda eqv = 0.061(^oC)$ with $\sigma_{Err} = 1.5\ (^oC)$.

### 3.3. Burner modeling

The correct modeling of the fire source is necessary because this influences the obtained results [12].

A fire source is placed at *0.3(m)* from the outer wall. Its heat release rate is determined by the fire source area and heat release rate per unit area.

LPG gas from the cylinder was used during the experiment. Gas has the advantage of controlled combustion over solid fuels, with clear chemical and physical equations that are easy to model.

The total amount of gas consumed by combustion was determined by measuring the weight of the cylinder before and after the experiment: $M_i = 0.315\ (kg)$.

Knowing the lower calorific value of the LPG gas, $Qi(MJkg^{-1})$, it was possible to determine the total amount of heat resulting from combustion [13], according to the equation $HRR=Q_iM_i(MJ)$ (1) :

$$HRR = Q_iM_i(MJ) \quad (1)$$

FDS allows fire modeling using HRRPUA (heat release rate per unit area). The surface of the burner is the same as in the experiment: $0.25 \times 0.60\ (m^2)$.

The amount of fuel burned is not constant during the experiment because of the decrease of pressure in cylinder: $HRRPUA=105\ (kWm^{-2}s^{-1})$, $F_{t=0(s)}=1.15$, $F_{t=760(s)}=0.85$. The decrease curve was determined by repeated simulations.

### 4. Results and discussion

This study analyzes three possible cases of ventilation(*CASE1, CASE2, CASE3*) and compares them with the situation in which the space does not have any ventilation system in case of fire(*CASE0*):

*CASE0*: the room does not have a mechanical or natural ventilation system in case of fire;

*CASE1*: the room has a mechanical ventilation system for extracting hot air; the hot air extraction flow is $Q_v = 0.18(m^3/s)$; the air supply for compensation is made naturally through a slit located at the bottom of the outer wall: *0.10(m) x (0.40(m)*;

*CASE2:* the hot air is natural evacuated through a wall smoke hatches: *0.5(m) x 0.4(m);* the air supply for compensation is made naturally through a slit located at the bottom of the outer wall: *0.50(m) x 0.40(m);*

*CASE3:* the evacuation of hot air is done natural through roof smoke hatches: *0.5(m) x 0.4(m).*

The three cases take into account the recommendations of the current technical regulations [14].

Through this study we try to analyze which ventilation system has a higher performance.

Three main parameters will be followed: indoor temperature, visibility and oxygen concentration at point S1.

### 4.1. Temperature distribution

In the temperature evolution chart (***Fig. 6***) it can be observed that all three situation smoke and hot air ventilation systems have similar performance. Indoor temperatures drop at point *S1* from almost *100(°C)-CASE0* to about *60(°C)-CASE1*, *CASE2*, *CASE3*, proving that the performance of the ventilation system is high in all three cases.

Mechanical smoke and hot air ventilation lead to better ventilation in the initial stages of the fire *(CASE1)*, when hot air velocities are low due to low temperatures for *CASE2* and *CASE3*. As the fire continues, indoor temperatures rise and air velocity increases through the wall or roof smoke hatches *(CASE2*, *CASE3)* and natural ventilation was done at a flow rates almost equal to mechanical ventilation.

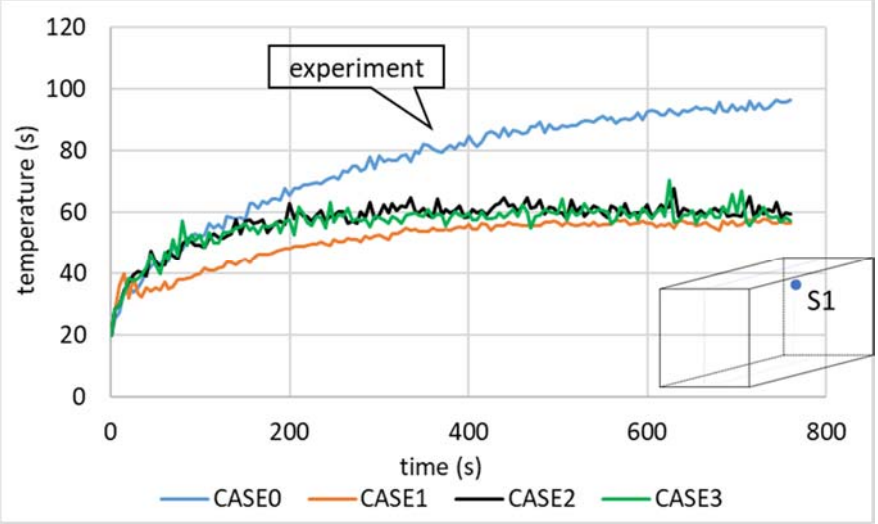


Fig. 6. Temperature evolution chart, point S1.

**Fig. 6** shows a rapid stabilization of the temperature curve close to *60 (°C)*. This is because a balance is struck between the amount of heat introduced into the room by the burning of gas and the loss of energy through the walls and the ventilation system.

The current regulations establish a correlation between the flow of hot exhaust air and the surface of the fan-protected space. It follows from the chart below that a correlation between the extraction flow and the thermal load, i.e. the amount of heat resulting from the combustion of combustible materials in the room, would be more appropriate.

**Fig. 7** shows that in all cases the hot air rises to the top of the room from where it is evacuated to the outside through the mechanical ventilation system or through wall or roof hatches. In the case of mechanical ventilation, a destratification of the air can be observed and the hot air has a controlled circulation. It can be seen that cold air enters

through the slit situated at the bottom of the outer wall. As shown in the figure, temperatures near the fire source are much high.

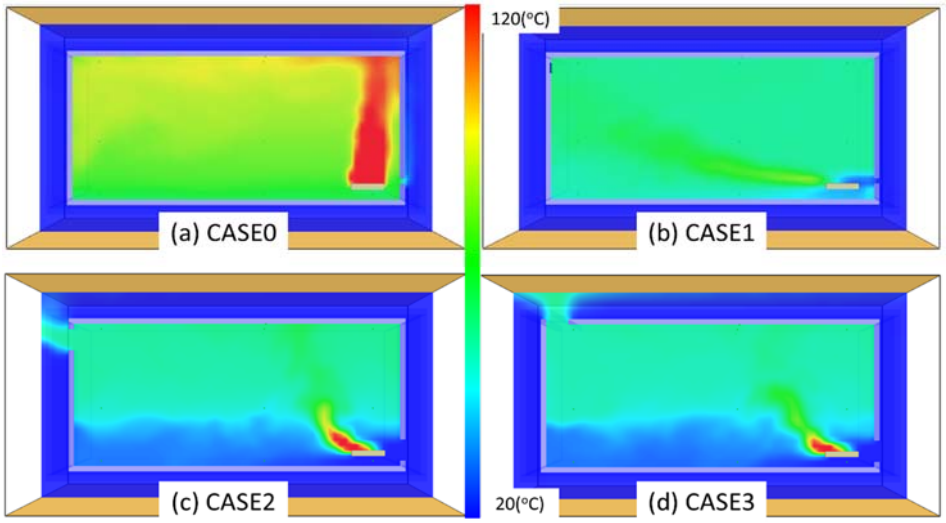


**Fig. 7** Temperature at t=760(s), y=2.1(m)

It can be seen that the temperatures at different points in the same horizontal plane are approximately equal and decrease as the horizontal plane is closer to the floor.

The cold air introduced from outside mixes with the hot air in the room and causes a considerable drop in indoor temperatures.

We conclude that in all three cases the ventilation affects indoor temperatures.

### 4.2. Visibility distribution

One of the most important parameters for evacuation in room fires is visibility. According to fire performance-based criterion, a minimum visibility of *10 (m)* at one person's head must be maintained for evacuating and ensure the possibility for the fire fighters to put out the fire [15].

In the next figure (***Fig. 8***) the visibility decreases in the experiment *(CASE1)* below *2(m)*. In this situation, conditions for the evacuation of users can no longer be ensured. When the ventilation systems work *(CASE1, CASE2, CASE3)*, the visibility increases at almost *5(m):* evacuation conditions are provided even if in difficult conditions.

On average, the three fire ventilation systems offer similar performance. In the initial phase, mechanical ventilation offers better performance because the speed of natural circulation of hot air is slow at low temperatures.

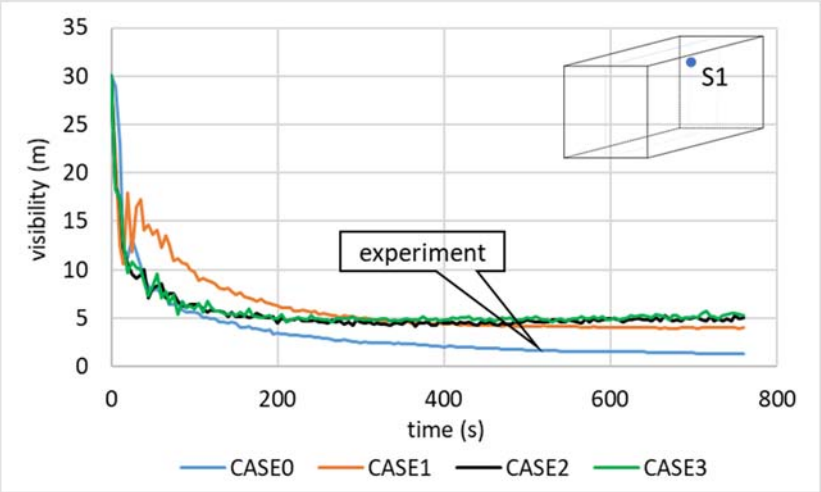


***Fig. 8*** Visibility evolution chart, point S1.

**Fig. 9** shows that mechanical ventilation and natural ventilation considerably increase the visibility. No significant differences are observed in terms of natural ventilation performance between the two situations studied: *CASE2*- wall hatches and *CASE3*- roof hatches.

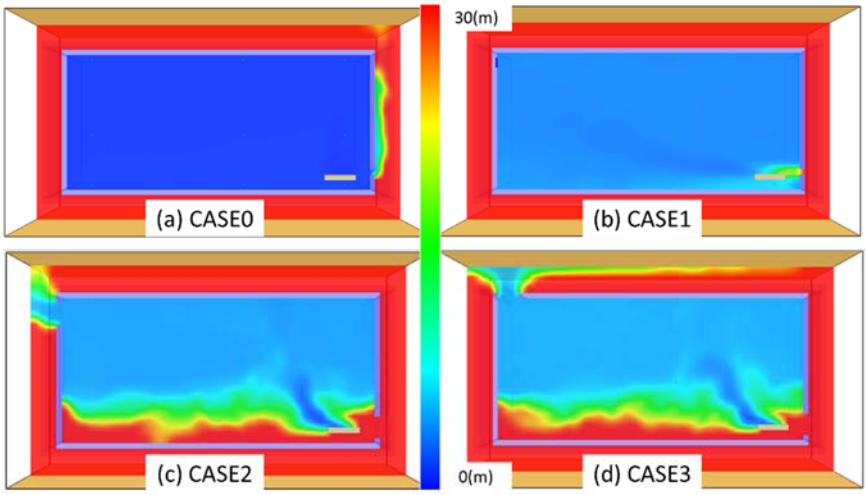


Fig. 9 Visibility at t=760(s), y=2.1(m)

Visibility is higher at the bottom of the camera. When there is no ventilation system at the end of the experiment the visibility decreases to almost zero. When there is a ventilation system the visibility is maintained at approximately *5(m)* which means that parameters for evacuation are maintained but in difficult conditions.

### 4.3. Oxygen concentration distribution

The concentration of oxygen in the air is important because oxygen is indispensable for human survival, low oxygen concentrations leading to loss of consciousness and eventually death. During a fire, oxygen is used in the combustion

process resulting in carbon dioxide and other harmful gases depending on the type of fuel used.

LPG is a mixture of propane and butane. The chemical equations of combustion are given below [16]:

chemical propane combustion equation: $C_3 H_8+5O_2 \rightarrow 3CO_2+4H_2O$ ( 2 )

chemical butane combustion equation: $4C_4 H_{10}+9O_2 \rightarrow 8CO_2+10H_2O$ ( 3 )

When no ventilation system is operating oxygen, concentration decreases rapidly ( **Fig. 10** ) under the value of *0.19(mol/mol)*. When the ventilation systems are working, the oxygen concentration is set at values higher than *0.202(mol/mol)*.

Mechanical ventilation provides better oxygen concentrations in the initial stages of the fire.

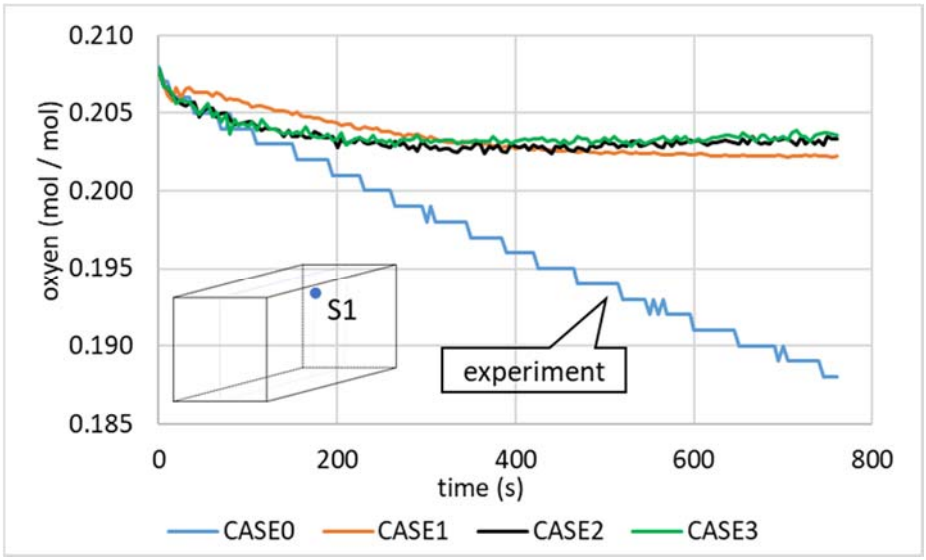


Fig. 10. Oxygen concentration evolution chart, point S1.

**Fig. 11** shows that natural ventilation produces similar results in both cases studied (*CASE2*- wall hatches and *CASE3*- roof hatches). Mechanical ventilation produces greater agitation of the air and destratifies the air. At the bottom of the room the oxygen concentration is higher in all cases.

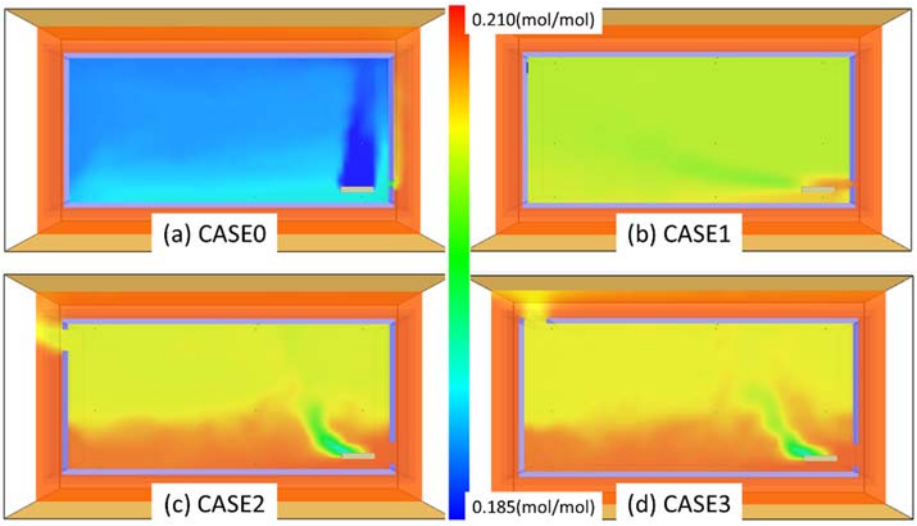


**Fig. 11.** *Oxygen concentration at t=760(s), y=2.10(m)*

Analyzing the three parameters it can be concluded that a correct sizing makes both mechanical ventilation and natural ventilation to have close performance.

## 5. Conclusions

In this research, the performance of three ventilation system for the evacuation of smoke and hot air was compared.

A real-scale fire test has been performed on instrumented single room. During these test, temperatures have been recorded in sensor S1. This test have been used as reference test to validate fire-modeling tools. Mathematical modeling of the fire was performed using FDS.

The results obtained were compared with the experimental results recorded for the situation when there is no mechanical or natural ventilation system.

Three fire ventilation systems have been proposed and studied: mechanical ventilation *(CASE1)* and natural ventilation (*CASE2*- wall hatches and *CASE3*- roof hatches).

Based on the analysis of the temperature distribution, visibility distribution and oxygen concentration distribution, it can be concluded qualitatively that:

1. mechanical ventilation provides better performance in the early stages of the fire.
2. the stratification of hot air is more pronounced in the case of natural ventilation.
3. the increase in indoor temperature leads to an increase in the flow of hot air and smoke.
4. fire ventilation systems maintain low temperatures, good visibility, and high oxygen concentration, ensuring optimal conditions for the survival and evacuation of users.
5. FDS provides good results in fire modeling.

6. natural or mechanical ventilation protects the building elements by cooling the air.

The main conclusion is that a well-sized ventilation system provides similar results regardless of whether it is mechanical or natural ventilation for the evacuation of smoke and hot air.

**Acknowledgment**

Author would like to thank Dr. Vlad Iordache for his valuable support and advice, Dr. Ilinca Năstase and all the technical staff of Department of Thermohydraulic Systems and for Atmoshere Protection involved in construction, instrumentation, and realization of the tests.

**References**

[1] *Law 307/2006 on fire protection, Romania,* 2006.

[2] P. Carlotti, D. Parisse, N. Rislera, *Statistical analysis of intervention reports for fires resulting in casualties deceased on the spot in Paris area,* Fire Safety Journal, 2017.

[3] H. Gormsen, N. Jeppesen, A. Lund, *The causes of death in fire victims,* 1984: Forensic Science International.

[4] S. Tavelli, R. Rota, M. Derudi, *A Critical Comparison Between CFD and Zone Models for the Consequence Analysis of Fires in Congested Environments,* Chemical Engineering Transactions, vol. 36, 2014.

[5] Kevin McGrattan, Bryan Klein, Simo Hostikka, Jason Floyd, *Fire dynamics simulator 5 user guide,* National Institute of Standards, 2019.

[6] R. Luiz, F. Oliveira, G. Doubek, S. S. V. Vianna, *On the behaviour of the temperature field around pool fires in controlled experiment and numerical modelling,* Process Safety and Environmental Protection, 2019.

[7] E. Guillaume, F. Didieux, A. Thiry, A. Bellivier, *Real-scale fire tests of one bedroom apartments with regard to tenability assessment,* Fire Safety Journal, 2014.

[8] *EN 1991-1-2: Eurocode 1: Actions onstructures - Part 1-2: General actions - Actions onstructures exposed to fire,* 2002.

[9] A. M. Salem, *Parametric analysis of a cabin fire using a zone fire model,* Alexandria Engineering Journal, 2013.

[10] Z. Xu, X.Z. Lu, H. Guan, C. Chen, A.Z. Ren, *A virtual reality based fire training simulator with smoke hazard assessment capacity,* Advances in Engineering Software, 2013.

[11] Y. Huang , E. Wang , Y. Bie, *Simulation investigation on the smoke spread process in the large-space building with various height,* Case Studies in Thermal Engineering, 2020.

[12] M. Lulea, V. Iordache, I. Năstase, *Fire simulation by using three methods of introducing HRR (Heat Release Rate),* Bucharest: Romanian Civil Engineering Magazine, 2019.

[13] *SR 10903-2, Fire protection measures. Determination of the thermal load in constructions, ASRO,* 2016.

[14] *P118-Romanian building fire safety regulation,* 1999.

[15] Yuang Jiang-Ping, Fang Zheng, Tang Zhi, Sun Jia-yun, *Numerical simulations on sprinkler system and impulse ventilation in a underground car park,* Wuhan: Engineering Procedia, 2011.

[16] B. Horbaniuc, G. Dumitraşcu, *Procese de ardere,* Editura POLITEHNIUM, 2008.